



UNIVERSITÀ  
DEGLI STUDI  
DI PADOVA

Sede Amministrativa: Università degli Studi di Padova

Dipartimento di *Ingegneria Industriale*

---

SCUOLA DI DOTTORATO DI RICERCA IN: INGEGNERIA INDUSTRIALE  
INDIRIZZO: PROGETTAZIONE E DINAMICA DEI SISTEMI MECCANICI  
CICLO XXI

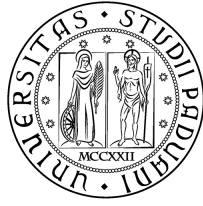
**DEVELOPMENT OF INTEGRATED METHODS FOR THE ENGINEERING  
CHARACTERIZATION OF BICYCLE COMPONENTS**

**Direttore della Scuola:** Ch.mo Prof. Paolo Colombo

**Coordinatore d'indirizzo:** Ch.mo Prof. Alberto Doria

**Supervisore:** Ch.mo Prof. Nicola Petrone

**Dottorando:** Federico Giubilato



**UNIVERSITÀ DEGLI STUDI DI PADOVA**

**Department of Industrial Engineering**

PhD Thesis

**DEVELOPMENT OF INTEGRATED METHODS FOR THE  
ENGINEERING CHARACTERIZATION OF BICYCLE  
COMPONENTS**

PhD Candidate: **Federico Giubilato**

Academic supervisor: Prof. Nicola Petrone

Company supervisor: Eng. Valentino Franch

January 2014



# Contents

|  |           |
|--|-----------|
| <b>Abstract</b>  | <b>1</b>  |
| <br>   |           |
| <b>Part 1 - Introduction</b>   |           |
| <br>   |           |
| <b>1. Introduction</b>   | <b>7</b>  |
| 1.1 Background   | 7         |
| 1.2 Thesis overview  | 7         |
| 1.3 Work stages  | 10        |
| 1.4 Literature review and innovative features of the thesis  | 12        |
| <br>   |           |
| <b>2. Integrated approach for the engineering characterization of bicycle wheels</b>                   | <b>15</b> |
| 2.1 Introduction   | 15        |
| 2.2 Work phases  | 16        |
| <br>   |           |
| <b>Part 2 - Development of test methods for the engineering characterization of bicycle components</b> |           |
| <br>   |           |
| <b>3. Comfort properties of bicycle components</b>   | <b>23</b> |
| 3.1 Comfort definition   | 23        |
| 3.2 Review of the literature on comfort analysis   | 25        |
| <br>   |           |
| <b>4. Radial structural behaviour of wheels</b>  | <b>29</b> |
| 4.1 Introduction   | 29        |
| 4.2 Adopted model  | 29        |
| 4.3 Test methods developed in the University laboratories  | 30        |
| 4.3.1 Test bench setup   | 30        |

|           |   |           |
|-----------|---|-----------|
| 4.3.2     | Wheels considered for the tests                             | 31        |
| 4.3.3     | Testing protocols   | 32        |
| 4.3.4     | Data analysis   | 34        |
| 4.3.5     | Results   | 37        |
| 4.3.6     | Tire behaviour and methods validation                       | 49        |
| 4.4       | Test methods implemented in Campagnolo testing laboratories | 52        |
| 4.4.1     | Test bench setup  | 52        |
| 4.4.2     | Measuring system  | 53        |
| 4.4.3     | Testing protocol  | 54        |
| 4.4.4     | Data analysis   | 55        |
| 4.5       | Conclusions and possible further developments               | 58        |
| <b>5.</b> | <b>Wheels vibration transmissibility</b>                    | <b>59</b> |
| 5.1       | Introduction  | 59        |
| 5.2       | Full bicycle laboratory test method (University lab.)       | 60        |
| 5.2.1     | Adopted model   | 60        |
| 5.2.2     | Test bench setup  | 60        |
| 5.2.3     | Measuring system  | 62        |
| 5.2.4     | Wheels considered for the tests                             | 62        |
| 5.2.5     | Testing protocol  | 63        |
| 5.2.6     | Data analysis   | 64        |
| 5.2.7     | Results   | 65        |
| 5.3       | Swinging arm laboratory test method (Campagnolo lab.)       | 70        |
| 5.3.1     | Adopted model   | 70        |
| 5.3.2     | Test bench setup  | 70        |
| 5.3.3     | Measuring system  | 71        |
| 5.3.4     | Testing protocol  | 72        |
| 5.3.5     | Data analysis   | 74        |
| 5.3.6     | Results   | 74        |
| 5.4       | Conclusions and possible further developments               | 76        |
| <b>6.</b> | <b>Saddles vibration transmissibility</b>                   | <b>79</b> |
| 6.1       | Introduction  | 79        |
| 6.2       | Adopted model   | 79        |
| 6.3       | Test bench setup  | 80        |
| 6.3.1     | Saddle and wooden dummy bottom positioning                  | 81        |
| 6.4       | Measuring system  | 85        |
| 6.5       | Saddles considered for the tests                            | 85        |
| 6.6       | Testing protocol  | 87        |

|   |            |
|---|------------|
| 6.7 Data analysis   | 87         |
| 6.8 Results   | 91         |
| 6.9 Conclusions   | 95         |
| <br>  |            |
| <b>Part 3 - Correlation between the user quality requirements and the engineering parameters of racing bicycle wheels</b> |            |
| <br>  |            |
| <b>7. Introduction to the analysis of the user requirements</b>   | <b>99</b>  |
| 7.1 Background  | 99         |
| 7.2 Literature review   | 99         |
| 7.3 Approach adopted in this thesis   | 101        |
| <br>  |            |
| <b>8. Identification and organization of wheels quality requirements</b>  | <b>103</b> |
| 8.1 Introduction  | 103        |
| 8.2 Introduction of ODI   | 103        |
| 8.3 Method developed in this work   | 107        |
| 8.4 Results   | 110        |
| <br>  |            |
| <b>9. Subjective evaluation tests</b>   | <b>115</b> |
| 9.1 Introduction  | 115        |
| 9.2 Selection of the wheelsets  | 115        |
| 9.3 Selection of the testers  | 119        |
| 9.4 Construction of the questionnaire   | 119        |
| 9.5 Selection of the testing road path  | 121        |
| 9.6 Execution of the test session   | 122        |
| 9.7 Data analysis   | 123        |
| 9.8 Results   | 125        |
| 9.9 Conclusions   | 127        |
| <br>  |            |
| <b>Appendix A – Questionnaire used during the subjective evaluation tests</b>   | <b>129</b> |
| <br>  |            |
| <b>10. Correlation between the user quality requirements and the engineering parameters of wheels</b>                     | <b>141</b> |
| 10.1 Introduction   | 141        |
| 10.2 Correlation method according to standard QFD   | 141        |

|  |     |
|--|-----|
| 10.3 Correlation method adopted in this work | 142 |
| 10.4 Results                                 | 144 |
| 10.5 Conclusions                             | 146 |

## **Part 4 - Development of engineering complex indexes of racing bicycle wheels**

|   |            |
|---|------------|
| <b>11. Engineering complex indexes</b>  | <b>149</b> |
| 11.1 Introduction   | 149        |
| 11.2 General approach for the development and validation of a complex index       | 149        |
| 11.3 Developed Indexes and their definition                                       | 151        |
| 11.4 Literature review  | 151        |
| <b>12. Reactivity Index</b>   | <b>153</b> |
| 12.1 Introduction   | 153        |
| 12.2 Approach   | 153        |
| 12.3 Energy absorbed by a wheel during a sprint                                   | 154        |
| 12.4 Reactivity index computation   | 159        |
| 12.5 Data considered for the index computation                                    | 160        |
| 12.5.1 Analysis of the data acquired during the field tests                       | 160        |
| 12.5.2 Summary of the data considered for the computation of the Reactivity Index | 164        |
| 12.6 Index validation and discussion  | 165        |
| <b>13. Handling and Road Holding Index</b>  | <b>167</b> |
| 13.1 Introduction   | 167        |
| 13.2 Handling Index   | 167        |
| 13.2.1 Approach   | 167        |
| 13.2.2 Energy absorbed by a wheel during a change of direction                    | 168        |
| 13.2.3 Handling Index formulation   | 172        |
| 13.2.4 Data considered for Handling Index computation                             | 173        |
| 13.2.5 Handling Index validation  | 179        |
| 13.3 Road Holding Index   | 179        |
| 13.3.1 Approach and formulation   | 179        |
| 13.3.2 Data considered for Road Holding Index computation                         | 181        |
| 13.3.3 Road Holding Index validation  | 185        |

|  |            |
|--|------------|
| <b>14. Impulsive Comfort Index</b>   | <b>187</b> |
| 14.1 Introduction  | 187        |
| 14.2 Impulsive Comfort Index formulation   | 188        |
| 14.2 Validation of Impulsive Comfort Index and discussion                                  | 189        |
| <br>   |            |
| <b>15. Index of Forward Rolling Efficiency and Index of Stability to Crosswind</b>         | <b>191</b> |
| 15.1 Introduction  | 191        |
| 15.2 Aerodynamic loads acting on wheels  | 191        |
| 15.3 Review of the literature on aerodynamics of bicycle and wheels                        | 193        |
| 15.4 Index of Forward Rolling Efficiency   | 195        |
| 15.4.1 Index formulation   | 195        |
| 15.4.2 Data considered for the index computation   | 196        |
| 15.4.3 Index validation  | 199        |
| 15.5 Index of Stability to Crosswind   | 200        |
| 15.5.1 Index formulation   | 200        |
| 15.5.2 Data considered for the index computation   | 201        |
| 15.5.3 Index validation  | 202        |
| <br>   |            |
| <b>16. Conclusions on the engineering complex indexes</b>                                  | <b>205</b> |
| 16.1 Engineering complex indexes calculated for all Campagnolo wheelsets                   | 205        |
| 16.2 Indexes of destination of use   | 206        |
| 16.3 Correlation between the engineering complex indexes and the user quality requirements | 207        |
| 16.4 Discussion about the developed indexes  | 209        |
| <br>   |            |
| <b>Part 5 - Development of an instrumented racing bicycle</b>                              |            |
| <br>   |            |
| <b>17. Development of the instrumented racing bicycle</b>                                  | <b>213</b> |
| 17.1 Introduction  | 213        |
| 17.2 Characteristics of the instrumented bicycle   | 213        |
| 17.3 Setup of the data acquisition system  | 217        |
| 17.4 Instrumented brake levers   | 218        |
| 17.4.1 Application of the strain gauges and positioning of the potentiometers              | 218        |
| 17.4.2 Calibration of the strain gauge channels  | 218        |
| 17.4.3 Calibration of the rotational potentiometers  | 220        |



|   |            |
|---|------------|
| 17.5 Calibration of the instrumented spider arm of the crankset | 221        |
| 17.6 Description of the field tests                             | 223        |
| 17.6.1 Preparation of the equipment                             | 223        |
| 17.6.2 Testers and workgroup                                    | 224        |
| 17.6.3 Characteristics of the performed tests                   | 225        |
| <b>18. Analysis of the road downhill field tests</b>            | <b>227</b> |
| 18.1 Introduction   | 227        |
| 18.2 Data analysis  | 227        |
| 18.2.1 Signals processing                                       | 228        |
| 18.2.2 Parameters computations                                  | 230        |
| 18.3 Results  | 233        |
| 18.3.1 Analysis of a reference braking action                   | 235        |
| 18.4 Conclusions  | 238        |
| <br>  |            |
| <b>Part 6</b>   |            |
| <br>  |            |
| <b>19. Conclusions</b>  | <b>241</b> |
| <br>  |            |
| <b>References</b>   | <b>245</b> |
| <br>  |            |
| <b>List of publications</b>                                     | <b>251</b> |
| <br>  |            |
| <b>Acknowledgements</b>   | <b>253</b> |





# Abstract

## English

Aim of this work was the development of integrated methods for the engineering characterization of the bicycle components, following a user-centred approach. The overall methodology was developed through five main stages. The first stage concerned the development of laboratory testing methods for the evaluation of the basic engineering characteristics of the bicycle components. The regarding activities were focused on the study of the vibrational and impulsive comfort properties of bicycle wheels and saddles. New laboratory testing methods were therefore developed for the evaluation of the wheels radial structural behaviour, and for the measurement of the vibration transmissibility of wheels and saddles. The testing methods developed for the evaluation of the radial stiffness and the vibration transmissibility of the wheels were developed in the University laboratory, and then implemented in Campagnolo srl. The second stage of the work regarded the development of a structured and objective method for the identification and organization of wheels quality requirements, evaluated by the cyclists during road cycling. A dedicated subjective evaluation tests session was performed in order to collect the assessment of 33 cyclists among the quality requirements of three different wheelsets. The correlation between them and the basic engineering characteristics of the wheels was then calculated through the adoption of a mathematic method. The adoption of a mathematic method for the computation of the correlation coefficients, represents a significant improvement of the arbitrary method proposed by the widely used QFD [16]. The high differences obtained among the evaluated quality requirements of three different tested wheelsets suggested the development of the engineering complex indexes. Six engineering complex indexes were formulated in the fourth stage with the aim to express a technical measurement of the user quality requirements. The engineering complex indexes were developed through a scientific and rigorous approach, in which the analysis of the subjective evaluation of the cyclists and of the bicycle dynamics is combined. In the fifth stage, an instrumented racing bicycle was developed for measuring, through dedicated field tests, the parameters needed for the computation of the indexes, and for characterizing the braking actions performed by the cyclists during road downhill riding. The engineering complex indexes are the final outcome of the overall method developed. Since they give a technical measurement of the cyclist feelings, they represent the integrated engineering characterization of the wheels. They can assist the product development based on a user-centred approach, the management of the products range, and the definition of the target characteristics of new products. They can also represent a reliable guideline for customers in the product choice, or for marketing communication messages.

So, an innovative structured approach for the user-centred characterization of sports equipment is presented in this thesis. The overall methodology was developed mainly considering racing bicycle wheels, but it is suitable also for the characterization of other bicycle components, or other sports equipment.

## **Italian**

Lo sviluppo di metodi integrati per la caratterizzazione ingegneristica di componenti ciclistici rappresenta lo scopo di questo lavoro. La metodologia complessiva è stata sviluppata attraverso cinque fasi. Nella prima fase sono stati sviluppati dei metodi di prova di laboratorio per la caratterizzazione dei parametri ingegneristici base dei componenti ciclistici. Tale fase ha riguardato principalmente lo studio delle proprietà di comfort vibrazionale e impulsivo. Nello specifico, sono stati sviluppati dei nuovi metodi di prova di laboratorio dedicati alla valutazione delle caratteristiche strutturali radiali delle ruote e della trasmissibilità delle vibrazioni di ruote e selle ciclistiche. I metodi di prova riguardanti la misurazione della rigidità radiale e della trasmissibilità delle vibrazioni delle ruote sono stati inoltre implementati nel centro prove della ditta Campagnolo srl. La seconda fase del lavoro ha riguardato lo sviluppo di un metodo strutturato e oggettivo per la ricerca e l'organizzazione dei requisiti di qualità delle ruote, valutati dai ciclisti durante l'utilizzo della bicicletta da corsa. È stata dunque condotta una sessione di test di valutazione soggettiva per ricavare il giudizio di 33 ciclisti relativamente ai requisiti di qualità di tre differenti coppie di ruote. La correlazione tra i requisiti di qualità dei ciclisti e i parametri ingegneristici delle ruote è stata ottenuta attraverso l'applicazione di un metodo matematico. L'adozione di un metodo matematico per il calcolo dei coefficienti di correlazione rappresenta un significativo miglioramento della metodologia arbitraria proposta dal diffuso metodo QFD [16]. Le elevate differenze riscontrate tra i giudizi dei tester relativi alle diverse coppie di ruote provate hanno suggerito lo sviluppo di un set di indici ingegneristici complessi, il cui fine è stato fornire una misura tecnica dei requisiti di qualità valutati dal ciclista. Sei indici sono stati dunque formulati adottando un approccio scientifico rigoroso, nel quale i risultati dell'analisi delle valutazioni soggettive vengono combinati con l'analisi della dinamica della bicicletta. La quinta fase del lavoro ha riguardato lo sviluppo di una bicicletta strumentata con un duplice scopo: misurare, mediante prove sul campo, i parametri necessari al calcolo degli indici ingegneristici e caratterizzare l'azione frenante svolta durante l'utilizzo in discesa della bicicletta da corsa.

Gli indici ingegneristici complessi rappresentano il risultato finale della metodologia complessiva sviluppata. Dal momento che essi forniscono una misurazione tecnica delle sensazioni del ciclista, rappresentano la caratterizzazione ingegneristica integrata delle ruote. Tali indici risultano utili per lo sviluppo del prodotto, svolto adottando un approccio user-centred, per la gestione della linea di prodotti e per la definizione delle caratteristiche-obiettivo di nuovi prodotti. Possono essere inoltre impiegati come linee guida che assistono il cliente nella scelta del prodotto, o come strumenti per la comunicazione marketing.

In questa tesi viene dunque presentato un approccio user-centred innovativo per la caratterizzazione ingegneristica dell'attrezzo sportivo. Il metodo complessivo è stato sviluppato prendendo in considerazione le ruote per biciclette da corsa, anche se la metodologia risulta comunque adatta per la caratterizzazione di altri componenti ciclistici o di diversa attrezzatura sportiva.



# ***Part 1***

## **Introduction**





# ***Chapter 1***

## **Introduction**

### **1.1 Background**

The bicycle market is characterized by a huge variety of products. The different models offered by the bicycles producers for different destinations of use can be grouped into eight main product families, of which the e-bikes and the city bikes are made for the urban context, the mountain, the trekking and the racing bikes are related to a sports use, the other three families are represented by the fixed gear/single speed bikes, the vintage and the junior bikes. If we consider the three families connected to the sports use of the bicycle, we can observe that each family can be divided into other sub-categories, depending on the specific use of the bicycle. In some cases these sub-categories are continuously changing, new kind of bicycles with new specifications for new fields of use are produced every season. In this context the user, often driven by misleading marketing campaigns and empirical technical guides, has some difficulties in the choice of the bicycle or of the component which could meet its needs. The adoption by the designer of the common trial and error approach could outcome in a long time product development or in a product which is not compliant with its destination of use.

An engineering characterization of the bicycle components obtained from an integrated approach, which combines the technical analysis of the engineering properties with the study of the user quality requirements is needed in order to obtain a set of guidelines useful for the designer in the product development, for the user in the product choice, for the marketing department in the formulation of consistent communication messages.

Aim of this work is the development of methods for the engineering characterization of cycling components following an integrated approach which relates the technical analysis of the engineering characteristics to the user quality requirements.

The PhD research activities have been supported by the Campagnolo srl company which is one of the world main producers of high end components for racing bicycles. All the activities were conducted in collaboration with the test department of Campagnolo srl and with the laboratory of Machine Design, Department of Industrial Engineering, University of Padova, which, between all the research activities regarding the sport engineering, is involved in the structural analysis of bicycle components for the safety standard definition.

### **1.2 Thesis overview**

The racing bicycle wheels, the bicycle saddles and the braking systems for racing bicycle are the components considered in the PhD study. The research activities related to each cycling

component are briefly described in the following points.

- **Racing bicycle wheels**

The main activities were conducted for the characterization of the wheels, which have been considered in the development of the integrated characterization method. This method was obtained through four stages. The first stage concerned the development of new measurement methods for the wheels engineering characteristics which were not yet measured before. The methods developed were focused on the engineering parameters directly correlated with the comfort behaviour such as the radial stiffness and the vibration transmissibility, a topic which was formerly studied in my M.Sc. thesis [8]. In the second stage the study was focused on the collection and organization of the wheels perceived quality requirements evaluated by the cyclists. In the third stage a method for the quantitative correlation between the user quality requirements and the engineering measurable parameters was developed. As we can see in the dedicated chapter, the achievement of the correlation coefficients through a mathematical method represents a significant improvement of the arbitrary behaviour that the classic QFD method (Quality Function Deployment) has in this field. The fourth stage concerned the development of computation methods for the engineering complex indexes which represent a technical measurement of the cyclists perceived performance requirements. The engineering complex indexes are the final result of the overall method developed. Since they give a technical measurement of the cyclist feelings, they represent the integrated engineering characterization of the wheels.

- **Bicycle saddles**

The bicycle saddles were analysed with respect to their engineering characteristics. On the basis of the experiences applied to the study of the wheels comfort behaviour, a new laboratory test method was developed for measuring the saddle vibration transmissibility with the aim of comparing the comfort properties of bicycle saddles without any influence of the full bicycle frame, using a quantitative approach. The saddles were so studied considering an engineering parameter which was supposed to be directly correlated to the vibrational comfort perceived by the user.

- **Braking systems for racing bicycle**

A racing bicycle was instrumented in order to characterize the phases of the braking actions performed during the real use of the racing bicycle. The brake levers were instrumented with strain gauges for measuring the cyclist command force, a rotational potentiometer was used for the measurement of the lever rotation angle. The bicycle was also equipped with an inertial measurement unit provided with a GPS, with a crankarm drive torque sensor and with a speed meter.

The data collected with the instrumented bicycle were useful also for the computation of the

wheels engineering complex indexes.

The thesis is divided into the following 6 parts:

- PART 1: INTRODUCTION

- PART 2: DEVELOPMENT OF TEST METHODS FOR THE ENGINEERING CHARACTERIZATION OF BICYCLE COMPONENTS.

In this part the laboratory test methods developed for the wheels radial stiffness, the wheels and the saddles vibration transmissibility are showed in detail together with the respective results.



Fig. 1.1 Images of the test bench developed.

- PART 3: CORRELATION BETWEEN THE USER QUALITY REQUIREMENTS AND THE ENGINEERING PARAMETERS OF RACING BICYCLE WHEELS

The method developed for identifying and organizing the perceived quality requirements of racing wheels evaluated by the cyclists, the subjective evaluation tests performed for collecting the cyclists evaluation on three different wheelset and the method adopted for computing the correlation coefficients between the user quality requirements and the engineering parameters are presented in part 3.

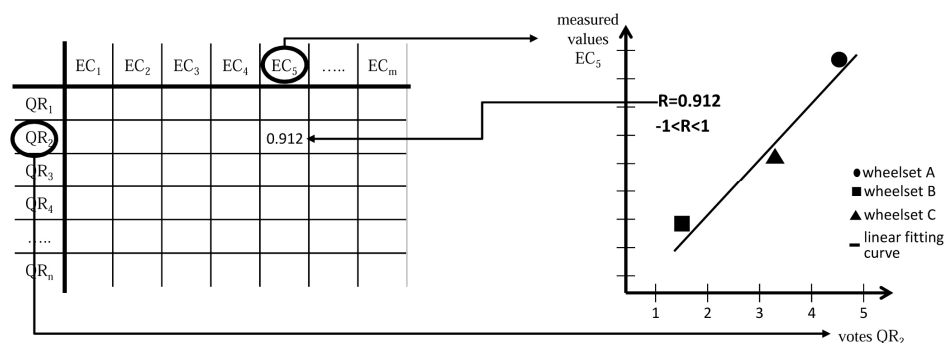


Fig. 1.2 Schematics of the method developed for the correlation coefficients computation.

- PART 4: DEVELOPMENT OF ENGINEERING COMPLEX INDEXES OF RACING BICYCLE WHEELS

In this part the computation methods developed for the wheels engineering complex indexes are exposed.

- PART 5: DEVELOPMENT OF AN INSTRUMENTED RACING BICYCLE

An instrumented racing bicycle was developed for the study of the braking action and for acquiring data useful for the wheels complex indexes computation



*Fig. 1.3 Instrumented bicycle and tester in action during the field test session.*

- PART 6: CONCLUSIONS

The next chapter presents an overview or the integrated method developed considering the racing bicycle wheels. The overall approach is suitable for the characterization of different cycling components and of other sports equipment.

### 1.3 Work stages

The figure 1.4 shows a schematic of the work stages which highlights the logical connection between each stage and the relative outputs. The colour of each stage block identifies the thesis part in which the activity is presented. The integrated approach developed considering the wheels is clearly recognizable. It presented in details in the chapter 2. The results of the saddle vibration transmissibility laboratory test and the results of the road downhill field tests can represent the starting point for a further development of this work.

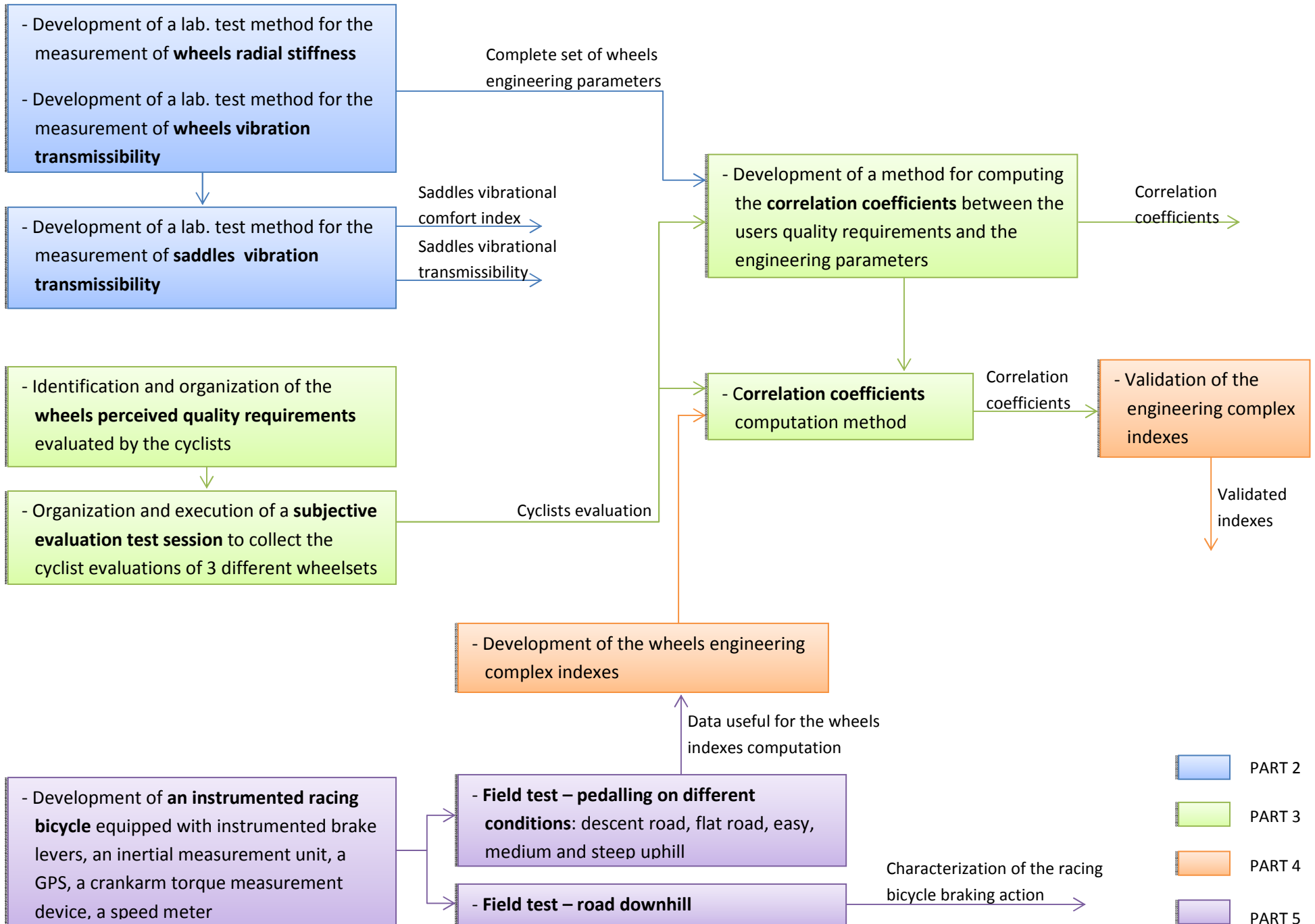


Fig. 1.4 Schematic of the work stages concerning the PhD research activity carried out.

## 1.4 Literature review and innovative features of the thesis

A brief review of the literature is presented below. A detailed review can be found in the introductory chapters of each Part.

An integrated approach which started from the investigation of the user requirements in order to define a user-centred design process was adopted by Clifton in his PhD thesis [20] considering the snowboard as object of the study. In this thesis Clifton has collected the snowboard user requirements, has performed a technical analysis of the snowboard design parameters and has matched the design parameters with the user requirements, applying the standard QFD method in order to define a user centred design process. In literature there are not works which correlates the analysis of the user requirements with the analysis of the technical characteristics of bicycle or of bicycle components.

Several works were focused on the structural analysis of bicycle components for the safety standard definition (Petroni *et al.* [36, 37, 38]) and for the fatigue design (Callens & Bignonnet [40]). The bicycle wheels were considered in studies concerning the loads measurement (Drouet & Champoux [43]), the fatigue (Redfield & Sutela [45]) and the aerodynamic [48-53] analysis.

Previous studies on the comfort analysis were focusing mainly on the modal analysis of the bicycle and its components [2, 9, 10], or on the study of the vibrational comfort through field tests [3, 5, 7, 8]. There are no studies analysing the structural radial behaviour and the vibration transmissibility of bicycle wheels and saddles and their correlation with the cyclist comfort.

The correlation between the user quality requirements and the product characteristics of sports equipment was investigated in previous studies (J.Darques *et al.* [19], P. Clifton [20], P. Clifton *et al.* [21], Usma-Alvarez *et al.* [26]) and, for this purpose, the QFD approach was adopted. The arbitrary behaviour of the correlation coefficients so obtained represents a limitation of these works, limitation that I have tried to overcome with the method proposed in this thesis.

The bicycle braking systems were considered in few studies. Nakae *et al.* [54] have performed a laboratory analysis of disk brakes vibrations and noise phenomena, Lie & Sung [55] did a theoretical analysis of the bicycle braking action, Oertel *et al.* [56] developed a test bench for bicycle brakes. No studies have analysed the braking action during the road downhill use of the racing bicycle.

The innovative features of this PhD thesis are summarized in the following points:

- adoption of an integrated approach for the engineering evaluation of bicycle components;
- development of new laboratory test methods for evaluating the comfort properties of bicycle wheels and saddles which can be applied also to other components;
- proposal of new structured methods for the collection of the user quality requirements of sports equipment and for the mathematical computation of the correlation coefficients with the technical characteristics;
- development of a set of engineering complex indexes which express a technical measurement

- of the cyclists perceived performance requirements;
- characterization of the racing bicycle braking action.





# Chapter 2

## Integrated approach for the engineering characterization of bicycle wheels

### 2.1 Introduction

Each sports equipment is evaluated by the user and by the R&D team from two different points of view (fig. 2.1). The **user** considers different **quality requirements** which can be divided into the following five macro-categories: usability, comfort, performance, safety, and aesthetic/emotional requirements. The **R&D team** refers to the **product characteristics** such as the architectural characteristics and the technological characteristics, and the engineering parameters measurable by means of laboratory tests. Quality requirements and product characteristics are mutually correlated. The analysis of the user quality requirements, the technical product characterization and a method for computing the correlation coefficients are therefore needed in order to obtain a quantitative correlation between these two worlds.

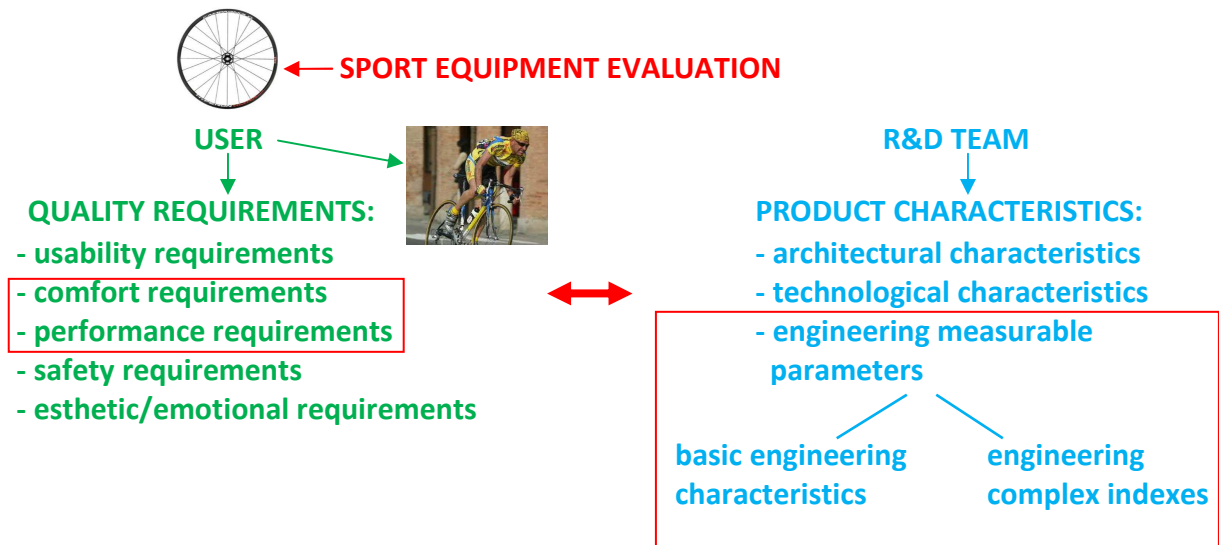


Fig. 2.1 Schematic of the evaluation parameters adopted by the user and by the R&D team for the assessment of sports equipment.

The overall method was developed considering the racing bicycle wheels and focusing on their comfort and performance requirements perceived by the cyclists during road cycling, and on the engineering parameters measured by means of laboratory tests. The engineering parameters are represented by the **basic engineering characteristics**, such as mass, the inertial, stiffness and

damping properties, and by the **engineering complex indexes** which, resulted from a scientific processing of the basic characteristics, give a technical measurement of the cyclist perceived quality requirements perceived by the cyclist.

## 2.2 Work phases

The “House of Quality” matrix (fig. 2.2) used in the QFD (Quality Function Deployment) method [16] was adopted in this study for representing the correlation between the user perceived requirements and the wheels engineering characteristics. The user requirements and the engineering characteristics are, respectively, the rows and the columns headers, whereas the matrix is filled with the correlation coefficients.

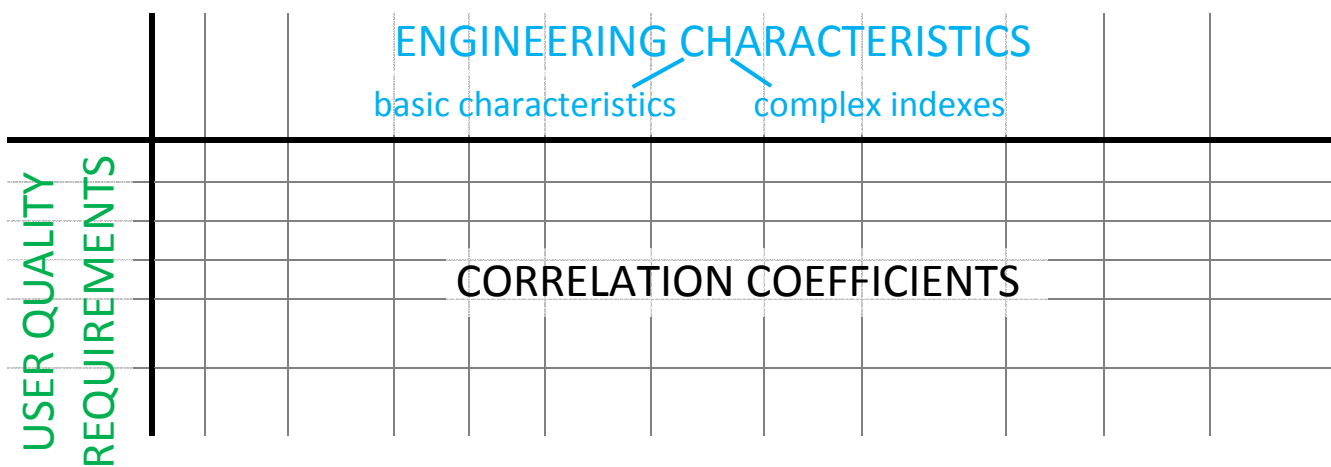


Fig. 2.2 Structure of the “House of Quality” matrix.

At the beginning of this work, only four basic engineering characteristics were considered for the wheels characterization (fig. 2.3): since there was a lack of data for what regards both the engineering characteristics and the user requirements, their correlation was estimated by empirical considerations.

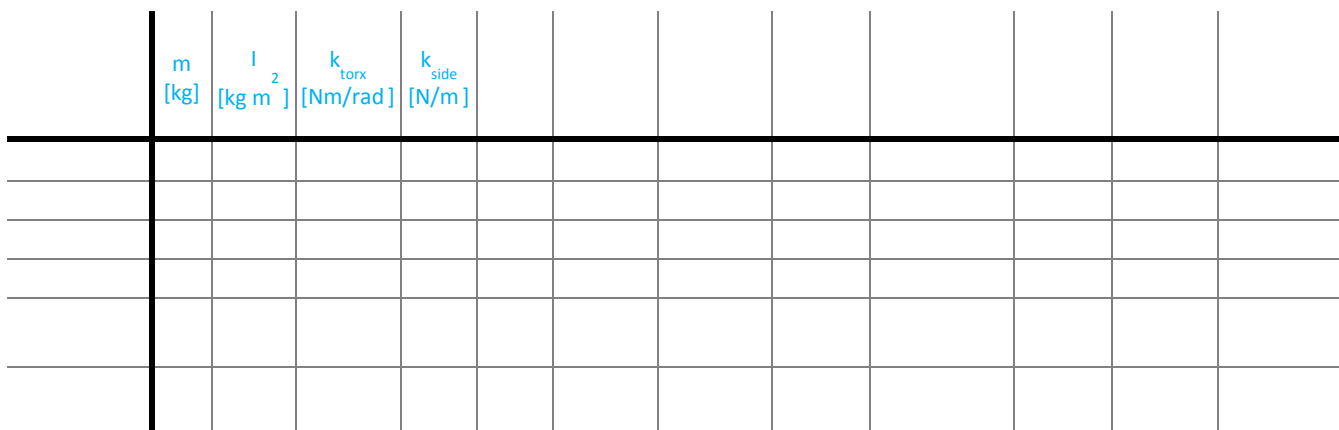


Fig. 2.3 Data available for the House of Quality matrix at the beginning of the work.

The work phases were therefore organized as it follows.

**1) Development of additional laboratory test methods for the measurement of the wheels basic engineering characteristics (fig. 2.4).**

In this phase the laboratory test methods for the measurement of the wheels radial stiffness and of the wheels vibration transmissibility were developed.

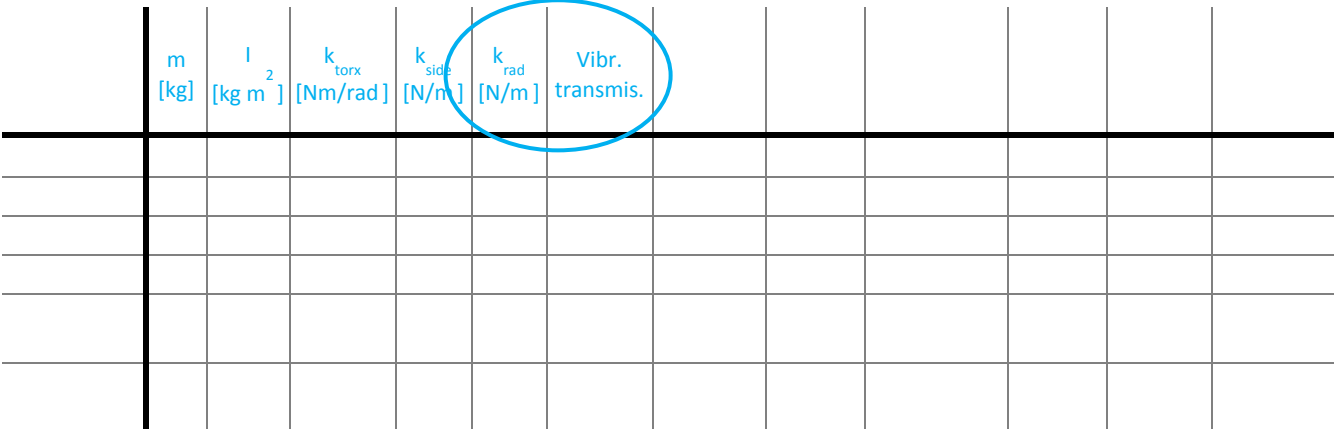


Fig. 2.4 Upgrade of the basic engineering characteristics.

**2) Development of a structured method for identifying and organizing the wheels quality requirements evaluated by the cyclists during road riding (fig. 2.5).**

The theory and the corresponding structured method proposed in ODI (Outcome Driven Innovation) [17] for discovering the customers’ needs with respect to a considered product was conveniently adapted for the purpose of this work phase.

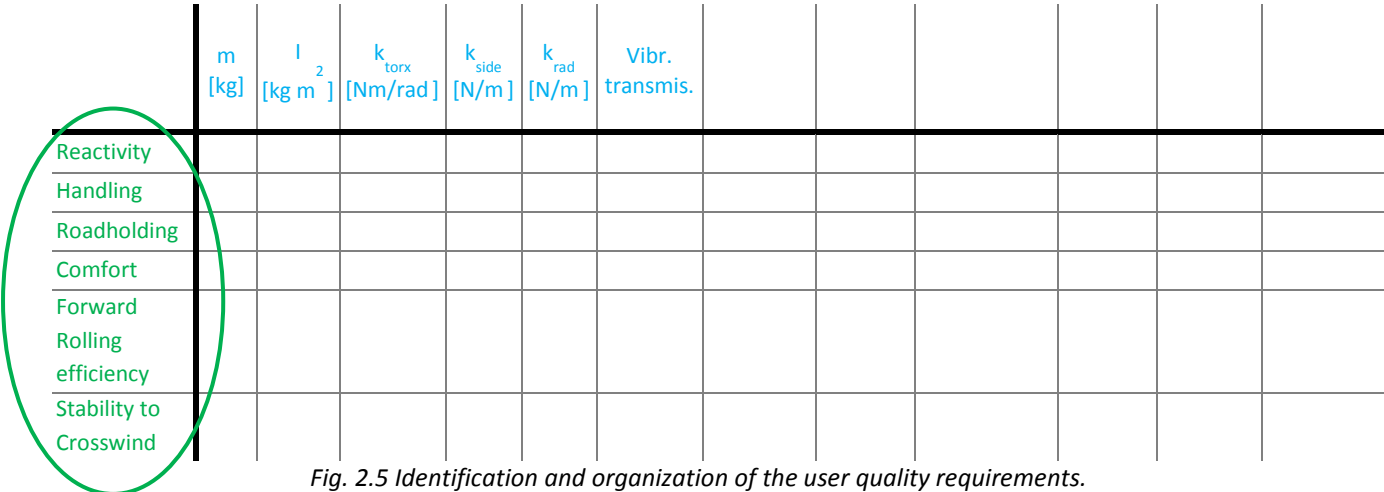


Fig. 2.5 Identification and organization of the user quality requirements.

**3) Organization and execution of subjective evaluation tests.**

A subjective evaluation test session was organized and carried out in order to collect the cyclist evaluations on the perceived quality requirements of three different wheelsets conveniently

selected.

**4) Development of a mathematical method for computing the correlation coefficients between each quality requirement and each engineering characteristic (fig. 2.6).**

The QFD involves a method and some tools for the estimation of the correlation coefficients obtained from arbitrary judgments based on an empirical approach. This represents a limitation of the QFD which was overcome through the mathematical approach chosen in this thesis.

|                            | m<br>[kg] | $I_2$<br>[kg m <sup>2</sup> ] | $k_{torx}$<br>[Nm/rad] | $k_{side}$<br>[N/m] | $k_{rad}$<br>[N/m] | Vibr.<br>transmis. |  |  |  |  |  |
|----------------------------|-----------|-------------------------------|------------------------|---------------------|--------------------|--------------------|--|--|--|--|--|
| Reactivity                 | -0.88     | -0.94                         | -0.30                  | -0.64               | -0.80              | 0.81               |  |  |  |  |  |
| Handling                   | -0.99     | -0.994                        | 0.12                   | -0.69               | -0.98              | 0.82               |  |  |  |  |  |
| Roadholding                | -0.98     | -0.938                        | 0.36                   | -0.65               | -0.99              | 0.80               |  |  |  |  |  |
| Comfort                    | -0.96     | -0.991                        | -0.10                  | -0.68               | -0.91              | 0.90               |  |  |  |  |  |
| Forward Rolling efficiency | -0.94     | -0.886                        | 0.48                   | -0.62               | -0.98              | 0.75               |  |  |  |  |  |
| Stability to Crosswind     | 0.75      | 0.649                         | -0.77                  | 0.46                | 0.83               | -0.72              |  |  |  |  |  |

Fig. 2.6 Correlation coefficients calculated between each quality requirement and each basic engineering characteristic.

**5) Formulation of engineering complex indexes representing a technical measurement of the cyclists perceived quality requirements (fig. 2.7).**

The development of the engineering complex indexes started from the results of the subjective evaluation tests (phase 3), which highlighted that high differences were perceived by the cyclists between the different tested wheelsets among all the user requirements individuated in the phase 2. The indexes formulation comes from a dynamic analysis of the bicycle action in which the user requirement, expressed by the index, is evaluated by the cyclist. The data used for the index computation were acquired during the field test session performed with the instrumented bicycle realized for this purpose.

|                            | m<br>[kg] | $I_2$<br>[kg m <sup>2</sup> ] | $k_{torx}$<br>[Nm/rad] | $k_{side}$<br>[N/m] | $k_{rad}$<br>[N/m] | Vibr.<br>transmis. | Reactivity Index<br>[1/J] | Handling Index<br>[1/J] | Road Holding Index<br>[1/J] | Comfort Index<br>[mm/N] | Index of Forward Rolling efficiency<br>[1/W] | Index of Stability to crosswind<br>[1/N] |
|----------------------------|-----------|-------------------------------|------------------------|---------------------|--------------------|--------------------|---------------------------|-------------------------|-----------------------------|-------------------------|--|--|
| Reactivity                 | -0.88     | -0.94                         | -0.30                  | -0.64               | -0.80              | 0.81               |                           |                         |                             |                         |  |  |
| Handling                   | -0.99     | -0.994                        | 0.12                   | -0.69               | -0.98              | 0.82               |                           |                         |                             |                         |  |  |
| Roadholding                | -0.98     | -0.938                        | 0.36                   | -0.65               | -0.99              | 0.80               |                           |                         |                             |                         |  |  |
| Comfort                    | -0.96     | -0.991                        | -0.10                  | -0.68               | -0.91              | 0.90               |                           |                         |                             |                         |  |  |
| Forward Rolling efficiency | -0.94     | -0.886                        | 0.48                   | -0.62               | -0.98              | 0.75               |                           |                         |                             |                         |  |  |
| Stability to Crosswind     | 0.75      | 0.649                         | -0.77                  | 0.46                | 0.83               | -0.72              |                           |                         |                             |                         |  |  |

Fig. 2.7 Developed engineering complex indexes.

## 6) Validation of the engineering complex indexes (fig. 2.8).

The high correlation coefficients (greater than 0.9) obtained between the engineering complex indexes, calculated for three different wheelsets, and the corresponding quality requirements, evaluated by the cyclists about the same wheels, was considered as a validation of the indexes formulations.

|                                  | $m$<br>[kg] | $I$<br>[kg m <sup>2</sup> ] | $k_{\text{torx}}$<br>[Nm/rad] | $k_{\text{side}}$<br>[N/m] | $k_{\text{rad}}$<br>[N/m] | Vibr.<br>transmis. | Reactivity<br>index<br>[1/J] | Handling<br>index<br>[1/J] | Roadholding<br>index<br>[1/J] | Comfort<br>index<br>[mm/N] | Rolling<br>efficiency<br>index<br>[1/W] | Index of<br>sensibility<br>to lateral<br>wind [1/N] |
|----------------------------------|-------------|-----------------------------|-------------------------------|----------------------------|---------------------------|--------------------|------------------------------|----------------------------|-------------------------------|----------------------------|---|---|
| Reactivity                       | -0.88       | -0.94                       | -0.30                         | -0.64                      | -0.80                     | 0.81               | 0.92                         |                            |                               |                            |   |   |
| Handling                         | -0.99       | -0.994                      | 0.12                          | -0.69                      | -0.98                     | 0.82               |                              | 0.99                       |                               |                            |   |   |
| Roadholding                      | -0.98       | -0.938                      | 0.36                          | -0.65                      | -0.99                     | 0.80               |                              |                            | 0.91                          |                            |   |   |
| Comfort                          | -0.96       | -0.991                      | -0.10                         | -0.68                      | -0.91                     | 0.90               |                              |                            |                               | 0.96                       |   |   |
| Forward<br>Rolling<br>efficiency | -0.94       | -0.886                      | 0.48                          | -0.62                      | -0.98                     | 0.75               |                              |                            |                               |                            | 0.97                                    |   |
| Stability to<br>Crosswind        | 0.75        | 0.649                       | -0.77                         | 0.46                       | 0.83                      | -0.72              |                              |                            |                               |                            |   | 0.96  |

Fig. 2.7 Highlight of the correlation coefficients considered for the engineering complex indexes validation.

The engineering complex indexes represent the outcome and the most innovative feature of the overall method, because they combine the outcomes of the technical analysis and with the results of the user requirements analysis.



## ***Part 2***

**Development of test methods for the engineering  
characterization of bicycle components**





# Chapter 3

## Comfort properties of bicycle components

### 3.1 Comfort definition

Comfort is one of the main parameters perceived by the cyclist during bicycle riding. It involves multiple aspects related to the different physical, thermodynamic and physiological quantities perceived such as force, friction, acceleration, pressure, thermal transmission, and perspiration. If we do not consider the thermodynamic and physiological quantities, comfort can be divided into five macro categories: the vibrational comfort, the impulsive comfort, the contact pressure comfort, and the posture comfort. For a complete analysis of comfort, a multi-disciplinary approach is therefore needed.

- The **vibrational comfort** is related to the vibrations perceived by the cyclists at the three body/bicycle interfaces due to the uneven road surface.
- The **impulsive comfort** concerns the impulsive loads transmitted to the cyclists due to the impacts or jolts that occurs during bicycle riding. The typical jolts related to the racing bicycle riding are the overcoming of potholes, asphalt holes, bumps, and asphalt patches. The magnitude of the impulsive loads transmitted to the cyclist, affects the entity of the body stress perceived.
- The **contact pressure comfort** is related to the pressure distribution at the body/bicycle interfaces, such as the saddle, the grips, and the pedals.
- The **posture comfort** involves all aspects concerning the cyclist posture, and the interaction between the bicycle and the movements performed by the cyclist on it.

In this thesis, the vibrational and the impulsive comfort were considered. They are related to the in-plane vertical dynamics of the bicycle, higher vibrations and higher body stress due to shock events mean an increase of muscle fatigue of arms, legs and lumbar area that affects the athletic performance of the cyclist. The entity of the vibrations and of the impulsive loads transmitted by the bicycle depends on its geometry and mass, inertia, and on the structural characteristics of its components. The global system represented by the bicycle and the cyclist can be divided into subsystems (fig. 3.1), in order to evaluate the contribution of each component to the global vibration or to the impulsive loads transmissibility. The global system can therefore be

qualitatively represented in the blocks diagram showed in figure 3.2, in which the input is represented by the irregularities of the road surface.

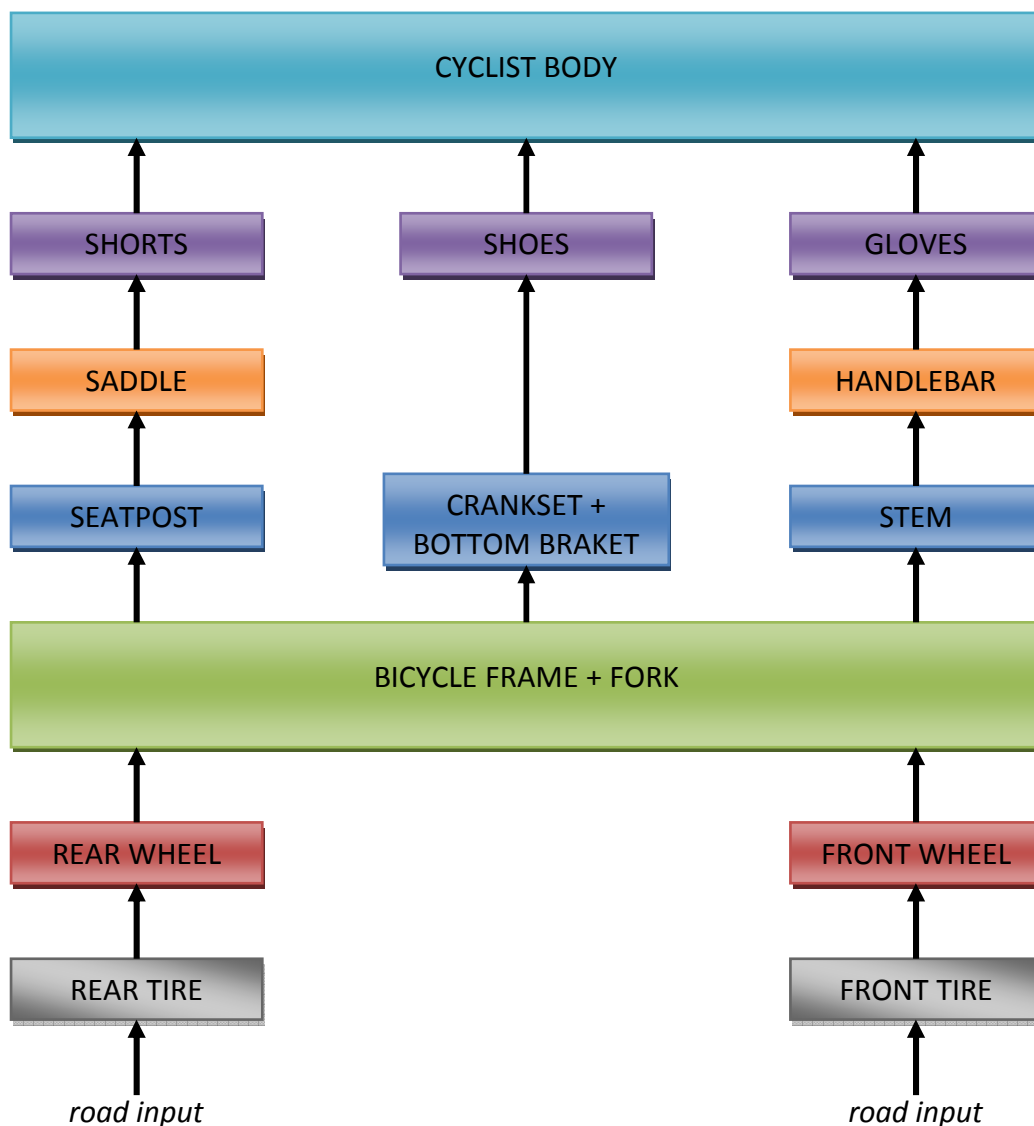


Fig. 3.2 Blocks diagram of the global bicycle + cyclist system.

The standard ISO 13473 [14] establishes the methods for the characterization of the road pavement and gives the following definitions (fig. 3.3):

- **pavement texture**: the deviation of a pavement surface from a true planar surface;
- **profile**: a two-dimensional representation of a surface;
- **texture wavelength**: the minimum distance between periodically repeated parts of the curve.

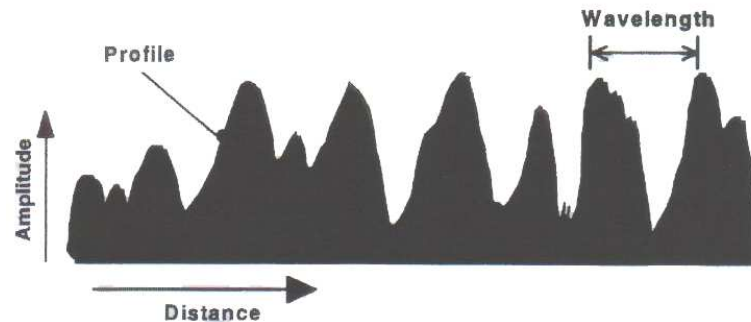


Fig. 3.3 Illustration of the quantities that describes the pavement surface characteristics accordingly to ISO 13473 [14].

The normative establishes also a classification of the pavement texture based on the range of the wavelength (fig. 3.4).

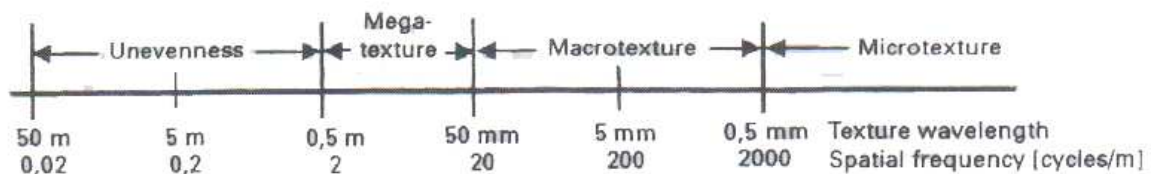


Fig. 3.3 Pavement texture classification proposed by ISO 13473-1.

Different road textures produce different road inputs which cause noise, vibrations or shock events.

For the approach adopted, the complete analysis of the bicycle comfort properties needs a characterization of each subsystem for evaluating its contribution to the transmission of vibrations and impulsive loads.

The following chapters show the laboratory test methods developed for the analysis of the wheels radial structural behaviour, which were found to be correlated to the wheels comfort properties in terms of shock absorption, and the analysis of the wheels and the saddles vibration transmissibility.

### 3.2 Review of the literature on comfort analysis

The interest in the bicycle comfort properties has increased in the last years.

The effect of frame materials on the vibrations transmitted to the cyclists was analysed by Hastings *et al.* [1]. The authors of this work have developed a treadmill with a cylindrical bump to induce vibrations to the bicycle. During the tests, performed with frames made of three different

materials (steel, aluminium, carbon fibre), the acceleration at the seat post, the cyclist power and the cyclist oxygen cost ( $\text{VO}_2$ ) were measured for evaluating the influence of the frame material on the vibrations transmitted and on the cyclists performance. The results showed that the steel frame was the most comfortable in terms of vibrations transmitted, followed by the carbon fibre and the aluminium frames. Since the tests were performed with only one tester, the results regarding the influence of vibrations transmitted on the athlete performance cannot be generalized.

The modal analysis of the bicycle and its components was performed in the works of Doria & Taraborelli [9], of Wojtowicki *et al.* [10] and of Richard & Champoux [2].

Doria & Taraborelli [9] performed the modal analysis for identifying the out-of-plane modes of bicycles with similar geometric properties and different destination of use (city and racing bicycle), and of racing bicycles with different frame materials. The test results showed that in the range 10-125 Hz all the tested bicycles have some typical modes (e.g.: torsion mode, frame bending); the possible correlations between the bicycle modal behaviour and its stability were also discussed.

Wojtowicki *et al.* [10] have carried out a modal analysis of a racing bicycles in a freely supported configuration and with a cyclist on the bicycle in the riding conditions. They performed also a road track test session for measuring the impulse response between the front wheel and the handlebar while overcoming an obstacle on a flat surface. No correlations were found between the results of the free-conditions modal analysis and the same analysis carried out with the cyclist positioned on the bicycle. Road tests results showed that the vibration levels on the handlebar cannot be associated to a particular strong mode, whereas the track roughness is the principal factor.

The same research group have done a modal analysis of the front part of a racing bicycle, in both the presence and the absence of the cyclist (Richard & Champoux [2]). In this work, the authors have done the modal analysis of the fork in free-free boundary conditions and of the bike's forepart with and without the cyclist. Three forks with different materials showed a similar dynamic behaviour in free-free boundary conditions. These forks showed different behaviour in the modal analysis of the forepart of the bicycle, in both the presence and absence of the rider, due to a change of the boundary conditions.

Many works concerning the analysis, through field tests, of the factors which affect the vibrational comfort, were presented during the last conferences on sports engineering.

In my paper (Giubilato & Petrone [7]), arisen from the research carried out during the M.Sc. thesis [6], the effects of the road roughness, of the cruising speed and of the wheels characteristics on the vibrations transmitted by the wheels during road cycling, were studied. The frequency analysis of acceleration signals, measured at the rear wheel axis and at the seat post clamp, was performed using random signal analysis methods. The results have showed that the ranking of four different wheels in respect to the vibrational response varied with the road pavement macrotexture and with the cruising speed. The spectra and the calculated comfort indexes have showed that higher cruising speed and higher road macrotexture resulted in an increase of the vibrations transmitted by the wheels.

The same results relating to the effects of the road surface and of the speed were found by

Olieman *et al.* [3]. In this work the authors have also investigated how the wheels and the tire pressure affected the vibrations induced to the frame and fork. The ISO 2631-1 was considered for the analysis of the acceleration signals acquired during the field tests. An increase of tire pressure produced an increase of vibrations, whereas no significant differences were observed in respect to different wheelsets.

The analysis following the ISO 2631-1 standard was also performed by Hölzel *et al.* [8] in the evaluation of the influence of speed and road roughness on the vibrations transmitted to the cyclist. The results of this work were consistent with the results of the works briefly presented above.

A different approach for evaluating the vibrations was adopted in the work of Vanwalleghem *et al.* [5]. The authors of this work have compared the results of the vibrational analysis performed following the ISO 2631-1 standard with the results obtained through an analysis based on the absorbed power computation at the rider/bicycle interfaces.

From the literature analysis, the approach adopted in this thesis, in which the bicycle/cyclist global system is divided into subsystems for evaluating their single influence on the bicycle comfort through laboratory tests reproducing real road conditions, appears new. The methods developed for evaluating the wheels radial structural behaviour, the wheels and the saddles vibration transmissibility do not have any correspondences in previous works. The inclusion of these laboratory test methods in an integrated approach, which correlates them with the subjective evaluation of the cyclist, overcomes most of the limitations of the works here analysed.



# Chapter 4

## Radial structural behaviour of wheels

### 4.1 Introduction

The aim of this phase of the work was the development of a standard test method for the quantitative analysis of racing wheels in terms of static and dynamic radial behaviour. The influence of the load level on the wheels radial stiffness and the energy absorbed by the wheels were respectively evaluated by means of static, dynamic, and impact radial tests, performed at different load levels and rates. The test methods were developed in the Laboratory of Machine Design of University of Padova. The pilot tests were performed considering four different wheelsets. The static test method was implemented at a later stage in Campagnolo testing laboratories.

The test methods developed in the laboratory of University together with the results are presented in the first part of this chapter. The second part describes the standard test method defined for Campagnolo laboratories.

### 4.2 Adopted model

The Wheel assembly was considered as the combination of two subsystems (fig. 4.1). One main system and two subsystems were therefore considered:

- **Wheel** system: system composed by tire, rim, spokes and hub;
- **Rim** subsystem: system composed by rim, spokes and hub;
- **Tire** subsystem: system composed by the tire.

The Wheel system was modelled by a lumped parameters model (fig. 4.1.b) composed by 2 subsystems in series (spring-damper parallel elements), representing respectively the Rim and Tire subsystems.

The displacements of the Wheel and of the Rim systems were directly measured. The stiffness of the Wheel, Rim and Tire systems were computed as it follows:

$$K_W = \frac{F}{x_W} \quad (1)$$

$$K_R = \frac{F}{x_R} \quad (2)$$

$$K_T = \left( \frac{1}{K_W} - \frac{1}{K_R} \right)^{-1} \quad (3)$$



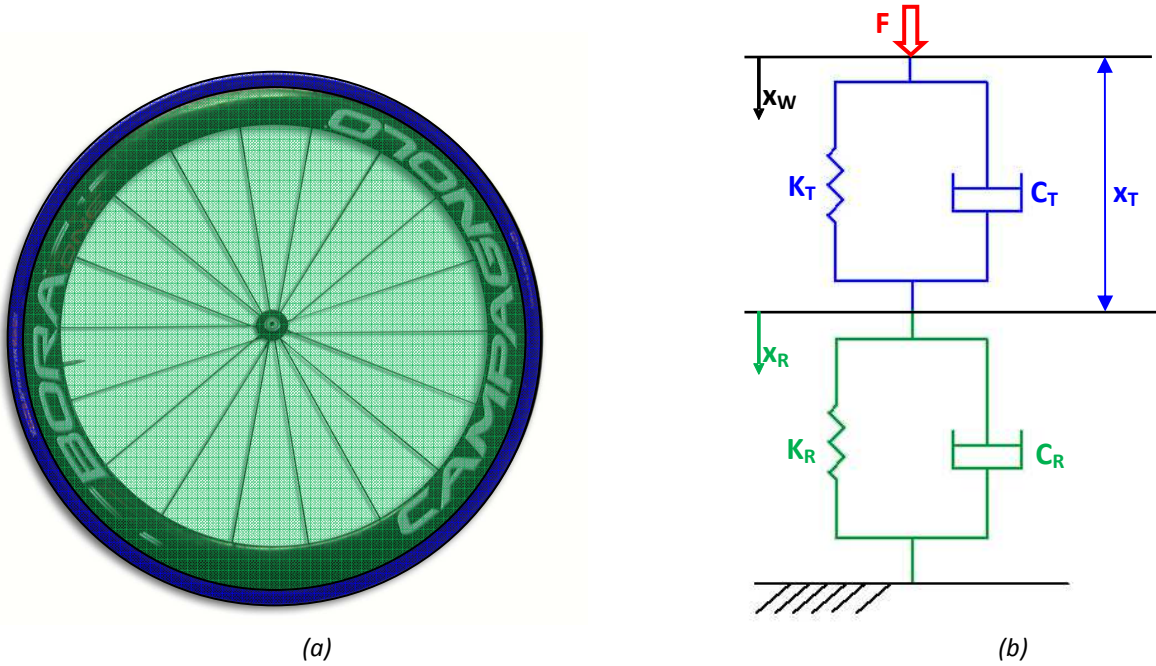


Fig. 4.1 (a) Schematic of the subsystems considered for the wheel assembly; (b) Wheel lumped parameters model.

### 4.3 Test methods developed in the University laboratories

#### 4.3.1 Test bench setup

The wheels were rigidly supported at the hub axis as shown in figure 4.2.a. A servohydraulic MTS 242 cylinder with a 15 kN load cell was used to load the wheels in the radial direction by means of a stiff aluminium plate (fig. 4.2.b). The load was applied to the tire and the radial displacement of the Wheel system  $x_W$  was measured by the cylinder internal LVDT. An additional LVDT ( $\pm 5\text{mm}$ ) was placed internally on the rim to measure the rim radial displacement  $x_R$ ; the tire radial compression  $x_T$  was calculated as the difference between the wheel and the rim displacements:

$$x_T = x_W - x_R \quad (4)$$

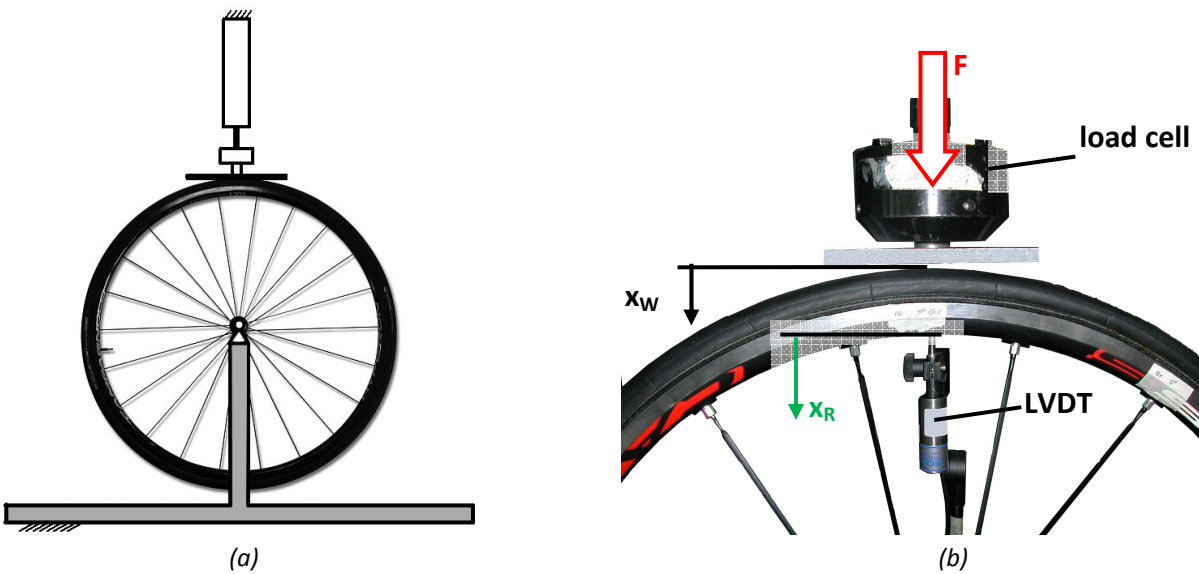


Fig. 4.2 (a) Schematic of the test bench; (b) measuring system.

The force and the two displacement signals were simultaneously recorded by means of the MTS control system at a sampling frequency of 2 kHz.

The vertical load was applied at a point between two consecutive spokes, and the wheel was oriented in order that the tube, or tubular valve, resulted parallel to the horizontal plane.

#### 4.3.2 Wheels considered for the tests

Four wheelsets for racing bicycle (named A, B, C, D, fig. 4.3) were selected for the study. Wheels were all equipped with the same tubular tire, the Continental “Sprinter” 700x23 inflated at 8 bar, but they were all different for material, rim profile, spokes number and disposition, as summarized in tables 4.1 and 4.2. Each wheel was identified by two letters, of which the first indicates the wheel model (A, B, C, D), the second indicates if it is a front (F) or a rear (R) wheel (e.g. BR indicates rear wheel of the model B).



*A: Campagnolo Hyperon Ultra Two*



*B: Campagnolo Bora One*



*C: Lightweight standard*



*D: Campagnolo Shamal Ultra*

*Fig. 4.3 Photos of the wheel models selected for the study.*

| Wheel | Rim profile       | Rim material | Hub material | Spokes Nr. | Spokes Pattern | Spokes material | Mass* |
|-------|-------------------|--------------|--------------|------------|----------------|-----------------|-------|
| AF    | Low<br>H 20 mm    | Composite    | Composite    | 22         | Radial         | Steel           | 850 g |
| BF    | High<br>H 50 mm   | Aluminium    | Aluminium    | 18         | Radial         | Steel           | 900 g |
| CF    | Medium H<br>30 mm | Composite    | Composite    | 20         | 2x             | Composite       | 760 g |
| DF    | Medium H<br>30 mm | Aluminium    | Aluminium    | 16         | Radial         | Steel           | 930 g |

Tab 4.1. Tested front wheels characteristics (\* mass including tire).

| Wheel | Rim profile       | Rim material | Hub material | Spokes Nr. | Spokes Pattern                        | Spokes material | Mass*  |
|-------|-------------------|--------------|--------------|------------|---------------------------------------|-----------------|--------|
| AR    | Low<br>H 20 mm    | Composite    | Composite    | 24         | Radial left side<br>2x sprockets side | Steel           | 1320 g |
| BR    | High<br>H 50 mm   | Composite    | Aluminium    | 21         | Triplets                              | Steel           | 1340 g |
| CR    | Medium<br>H 30 mm | Composite    | Composite    | 24         | 2x                                    | Composite       | 1190 g |
| DR    | Medium<br>H 30 mm | Aluminium    | Aluminium    | 21         | Triplets                              | Steel           | 1420 g |

Tab. 4.2 Tested rear wheels characteristics (\* mass including tire and sprockets).

### 4.3.3 Testing protocols

Three types of radial tests were developed, having different maximum load levels and different loading rates: Static, Cyclic and Bump tests.

#### Static radial test

In the Static radial test the maximum load of 2000 N was reached at a loading rate of 200 N/s: the rationale of this test was the simulation of a quasi-static radial overload on the wheel. The load function (fig. 4.5) is represented by an increasing and a consecutive decreasing linear ramp.

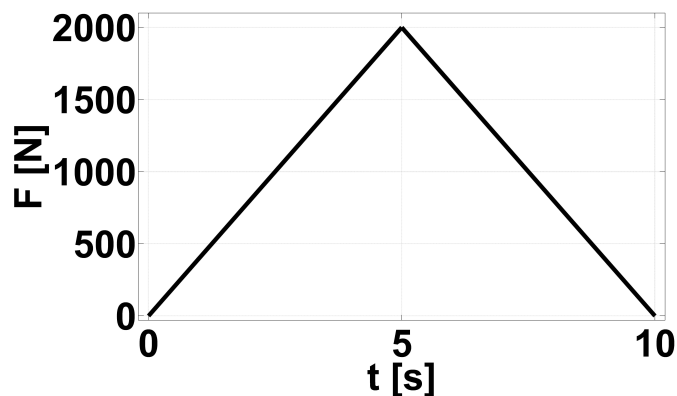


Fig. 4.4 Load function applied during static tests.

### Cyclic radial test

The Cyclic radial test was developed in order to simulate the load acting on the wheel during its rolling over a flat and smooth surface at a speed of 30 km/h. It consisted in the repeated application at 4 Hz frequency of the load cycle shown in figure 4.5, composed by a half sine load reaching the peak of 1000 N and a zero load plateau of the same duration. The maximum load rate was about 14800 N/s.

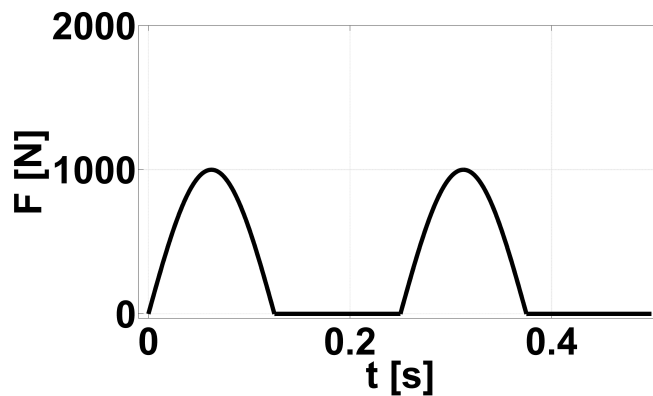


Fig. 4.5 Cycle repeated during cyclic tests.

### Bump radial test

The Bump test was introduced to simulate the case when the wheel hits a common obstacle like a road bump. The maximum load of 1500 N was linearly reached at a constant loading rate of 22200 N/s (fig. 4.6).

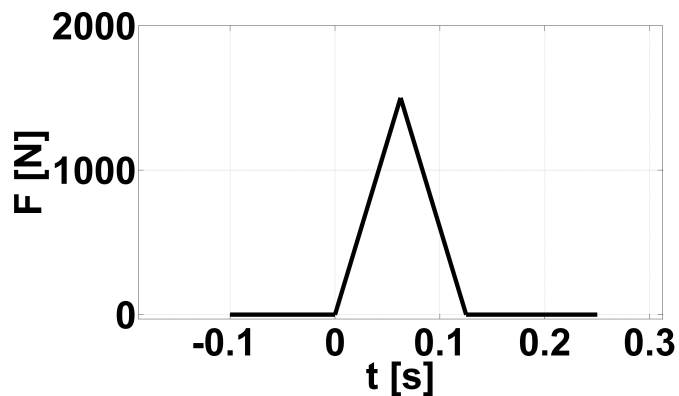


Fig. 4.6 Load function applied during bump tests.

All tests were performed with the same tubular tires inflated at 8 bar and controlled by a precision pressure gauge (fig. 4.7). Spokes pre-tension levels were not measured, nor the spokes tension throughout the tests.



Fig. 4.7 Pressure gauge SKS Airchecker.

The effect of tire pressure was investigated by performing pilot static tests on the same front wheel AF with the tubular inflated at 7, 8 and 9 bar.

The table 4.3 shows the main feature of the three radial tests developed.

| Radial test | Load function | Maximum load | Load rate | Load condition simulated                                |
|-------------|---------------|--------------|-----------|---|
| Static      | Ramp          | 2000 N       | 200 N/s   | quasi-static radial overload on the wheel               |
| Cyclic      | Half sine     | 1000 N       | 14800 N/s | cyclic load due to wheels rolling at a speed of 30 km/h |
| Bump        | Ramp          | 1500 N       | 22200 N/s | load due to a bump obstacle                             |

Tab. 4.3 Characteristics of the radial tests.

#### 4.3.4 Data analysis

Different parameters relating to the stiffness or the damping behaviour of the wheels were calculated in the data analysis. The computation method developed for each parameter is presented in details in the following paragraphs. The list of the parameters calculated for each test method is summarized in table 4.4.

##### Stiffness

The Load-Displacement curves (fig. 4.8.a) obtained during all the three types of tests were analysed in order to calculate meaningful values of the stiffness  $K$  (N/mm), defined as the local tangent slope to the Load-Displacement curves. The stiffness  $K$  was evaluated for Wheel ( $K_W$ ), Rim ( $K_R$ ) and Tire ( $K_T$ ): due to the nonlinearity of the wheel assembly behaviour, the stiffness values varied with the load level and were plotted as a function of the applied load  $F$ . For each system, the calculation of stiffness  $K$  was performed at load steps of 100 N, based only on the raising part of the load cycle as represented in the load-displacement diagram (fig. 4.8.b). A second letter in the subscript was introduced to distinguish among Static (S), Cyclic (C) and Bump (B) test results.

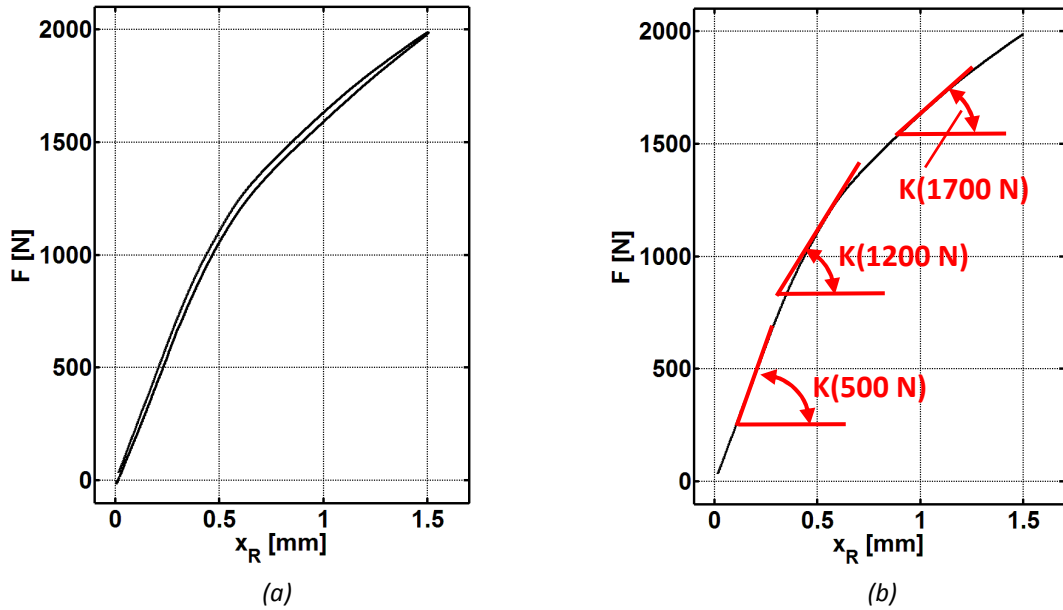


Fig. 4.8 (a) Example of a Load-Displacement curve measured for the Rim system during a static test; (b) example of a Load-Displacement curve raising part and calculation of local stiffness  $K$  as a function of load level.

### Gross stiffness

A linear least squares fitting of the complete Load-Displacement cycle was performed in order to calculate the overall gross stiffness value  $K^G$  (fig. 4.9). The divergence from a linear behaviour of the curve, which corresponds to a stiffness variation, is expressed by the  $R^2$  parameter. These two parameters, calculated for all the three tests, summarize the trend of the Load-Displacement curve:  $K^G$  is the measurement of the average stiffness from 0 to  $F_{\max}$ , low values of  $R^2$  express a stiffness drop or a progressive stiffness variation.

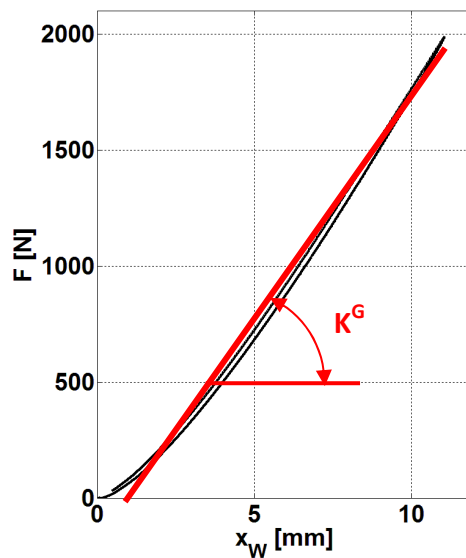


Fig. 4.9 Calculation of the stiffness parameter  $K^G$ .

Critical load

From the static tests data, a critical load  $P_{cr}$  of the wheel was also calculated in the cases showing sudden rim stiffness  $K_{RS}$  decrease greater than 20%. The spokes that are fixed to the rim nearby the load application point are subjected to a compressive force. As the force increases, their tensile stress decreases. At a certain force level (named  $P_{cr}$ ), the spokes axial stress changes from traction to compression causing a stiffness drop of the Rim system.

Energy dissipated

With respect to Cyclic and Bump tests, the energy  $E$  dissipated by the three systems was calculated as the area enclosed between the increasing and decreasing load branches of the load cycle, after the introduction of a minimum threshold of 50 N - cyclic tests - or 200 N - bump tests (fig. 4.10). The energy dissipated is a parameter directly correlated to the damping behaviour of the three systems.

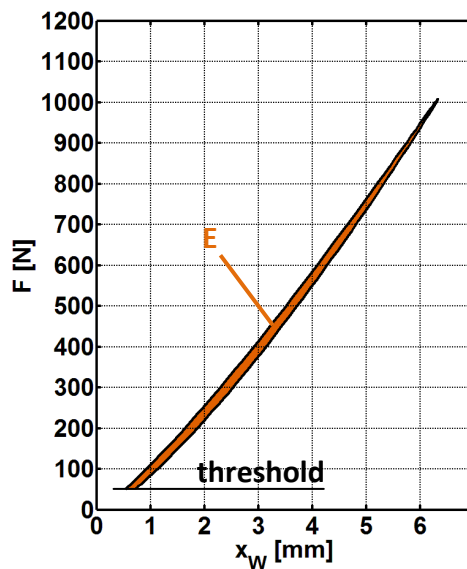


Fig. 4.10 Representation of the cyclic dissipated energy  $E$  of the Wheel system.

|                             | Static test | Cyclic test | Bump test |
|-----------------------------|-------------|-------------|-----------|
| Stiffness $K_W$ $K_R$ $K_T$ | X           | X           | X         |
| Cycle stiffness $K^C$       | X           | X           | X         |
| Critical load $P_{cr}$      | X           |             |           |
| Dissipated energy $E$       |             | X           | X         |

Tab 4.4 List of the parameters calculated for each radial test.

### 4.3.5 Results

#### Stiffness curves

The stiffness curves as a function of load, obtained for the Wheel and Rim systems of the front and rear wheels, are respectively reported on figures 11-12 and on figures 13-14.

Despite the rim stiffness resulted to differ of more than a factor of two within the front and the rear tested wheels, the wheel assembly behaviour resulted to be very similar.

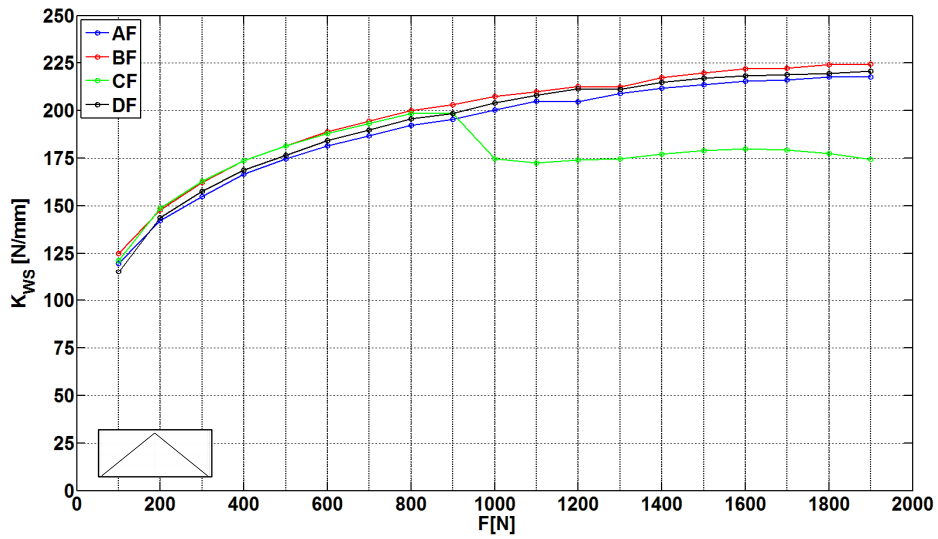
The stiffness values of the Rim during static tests (fig. 4.12.a and 4.14.a) tended to be constant with increasing loads, except for rim CF that revealed an evident unstable behaviour of spokes at loads greater than 1000 N, losing almost the 68% of its stiffness, and for rim CR that shows a progressive stiffness loss for loads greater than 600 N. This instability, which is visible also in the Wheels stiffness diagrams, is related to spokes axial stress changing from traction to compression at  $P_{cr}$ , and it is possibly due to low pre-tensioning levels, as showed by video images. The spokes pre-tension determines the overall load at which critical spokes can change from tensile to compression stress, therefore causing a global unstable behaviour.

The flatness of Rim stiffness curves up to the critical load  $P_{cr}$  suggests that Rim stiffness is not influenced by spokes pre-tension levels: this fact may need further confirmation by tests measuring also spokes tension.

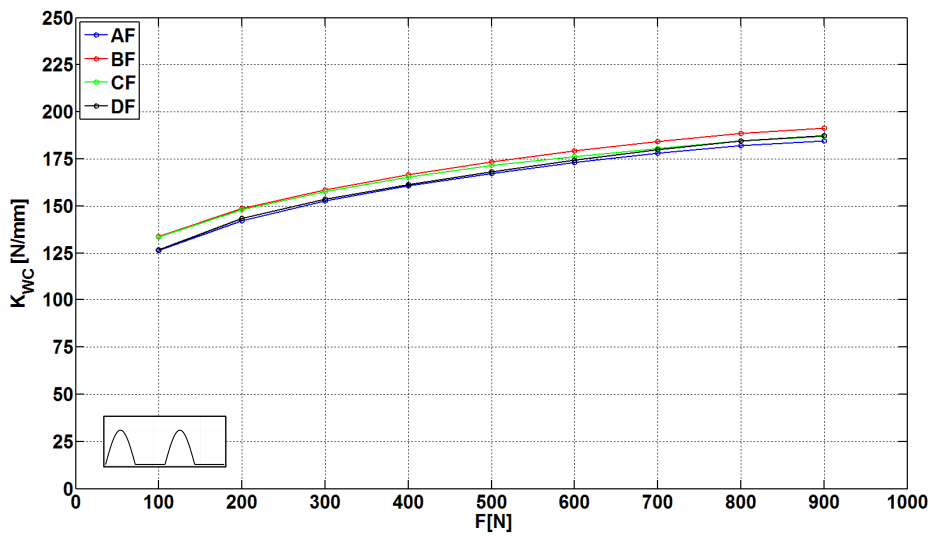
The curve trend of Rim stiffness obtained for the front wheels after the cyclic test (fig. 4.12.b) agrees with the static results. The application of a vertical force on a rear wheel produces a radial and a lateral deformation component, which can be optically observed. The lateral deformation, which is due to the different pre-tension level of the right and left side spokes, probably affects, during the cyclic tests, the dynamic measurement of the Rim radial deformation. For this reason, the  $K_{RC}$  curves obtained for the rear wheels show an irregular trend (fig. 4.14.b). A non-constant trend of the Rim stiffness curves is also obtained after Bump tests for both the front and the rear wheels (fig. 4.12.c, 4.14.c). This suggests a more detailed analysis of this phenomenon.

Linearity of rim stiffness static curves induced to attribute the nonlinear shape of Wheel stiffness curves mostly to tires. The Wheel stiffness curves obtained for the static and the cyclic tests (fig. 4.11.a-b, 4.13.a-b) shows an asymptotic increasing trend. A different trend was obtained for the stiffness curve during bump tests, which was non-monotonic, showing a relative peak around 1000 N. This is due to the dependence of the tire response on the load rate.

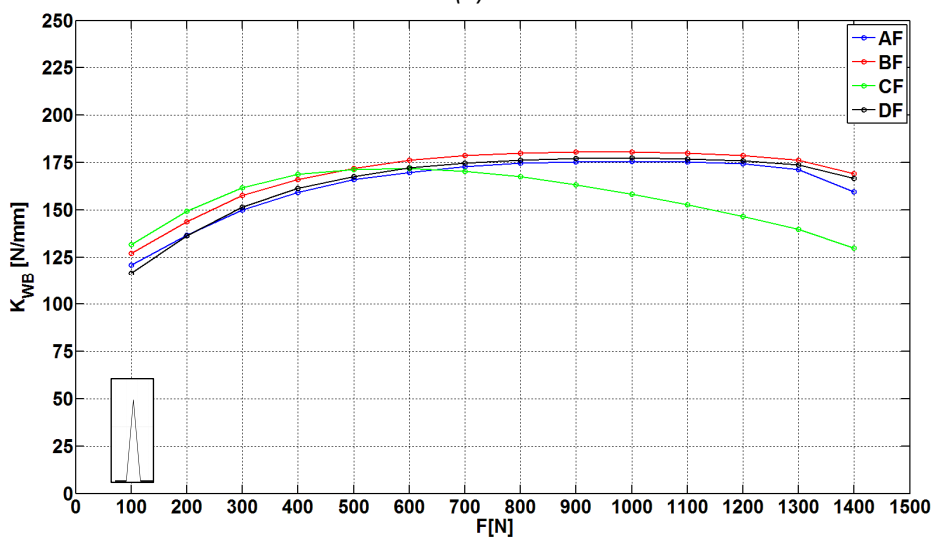




(a)



(b)



(c)

Fig. 4.11 Stiffness curve of the Wheel system calculated for the front wheels after the static (a), cyclic (b) and bump (c) tests.

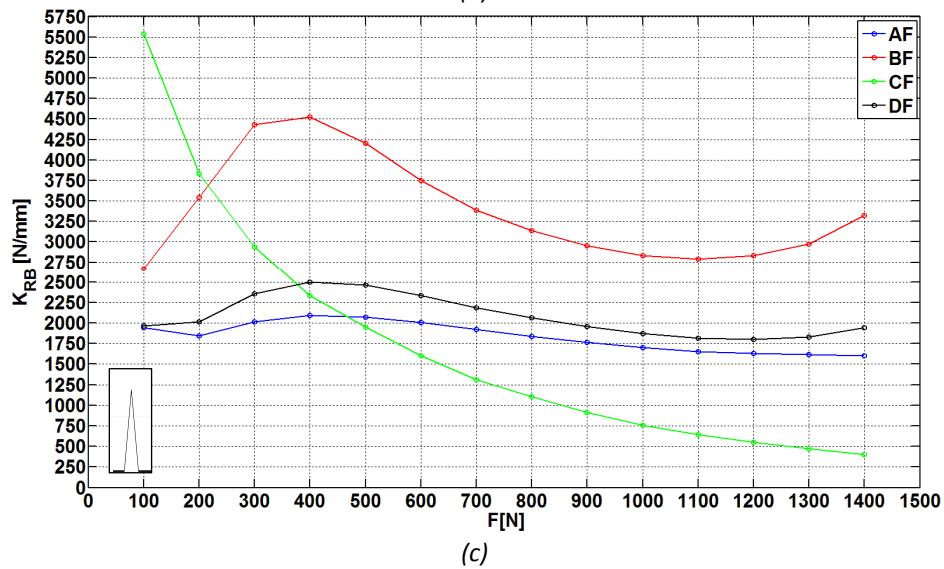
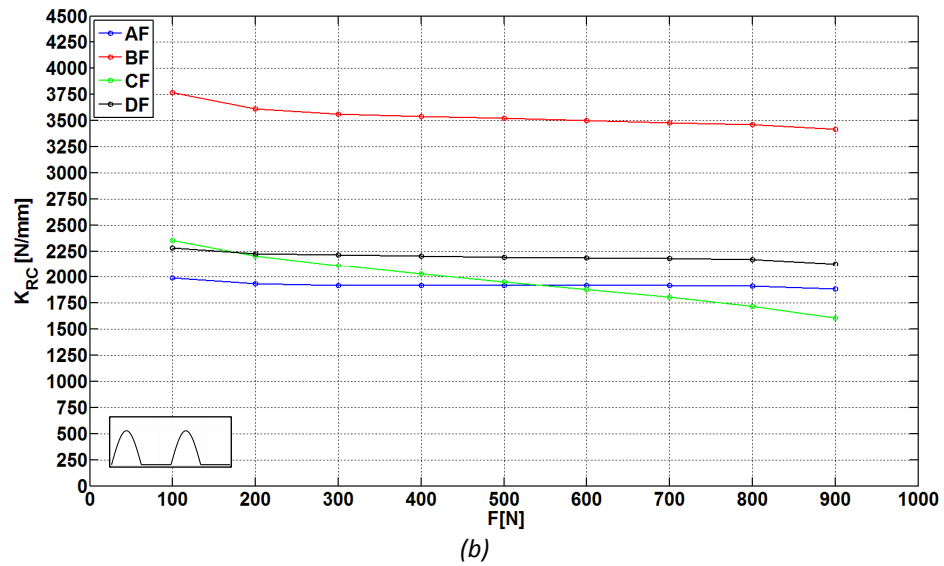
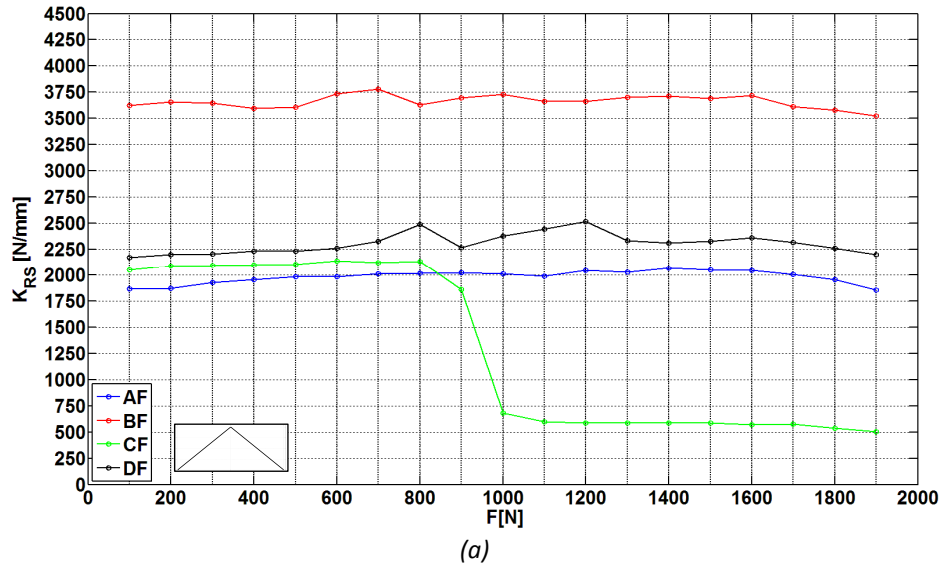
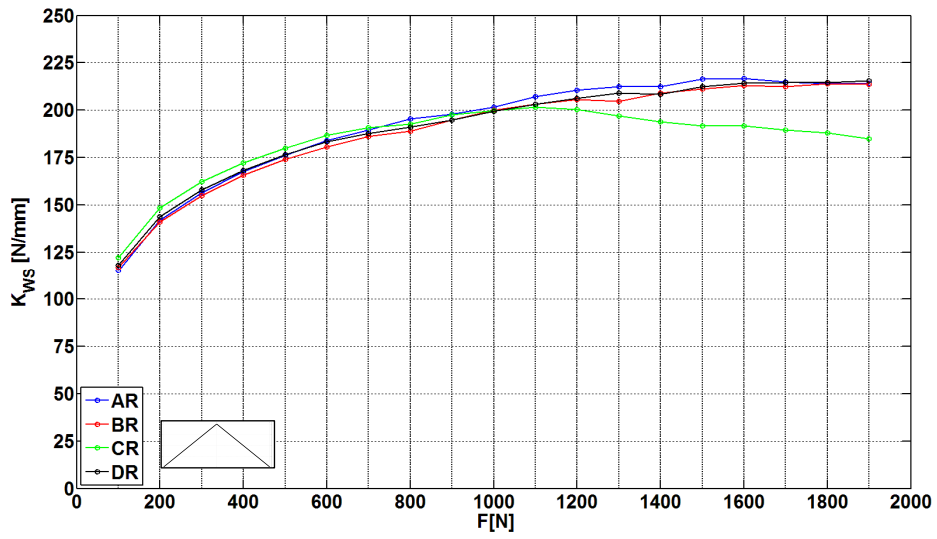
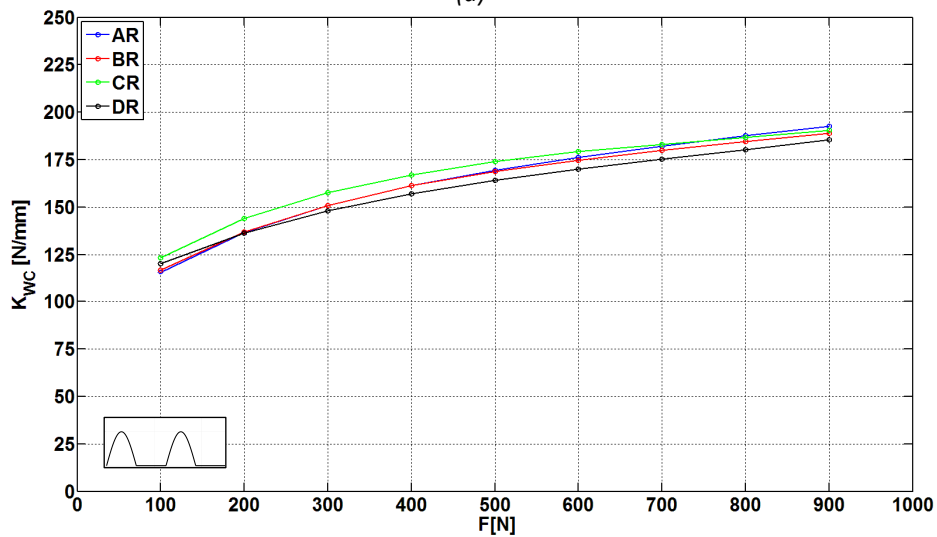


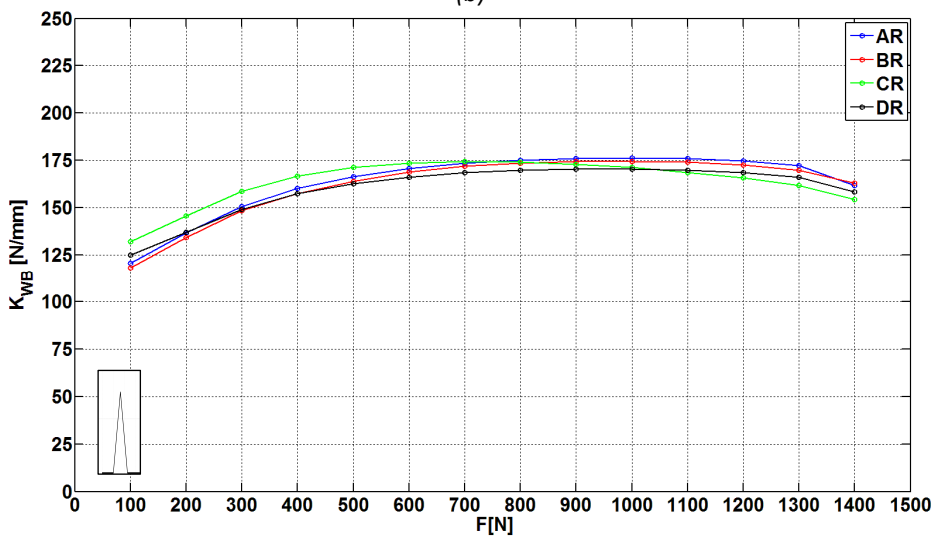
Fig. 4.12 Stiffness curve of the Rim system calculated for the front wheels after the static (a), cyclic (b) and bump (c) tests.



(a)



(b)



(c)

Fig. 4.13 Stiffness curve of the Wheel system calculated for the rear wheels after the static (a), cyclic (b) and bump (c) tests.

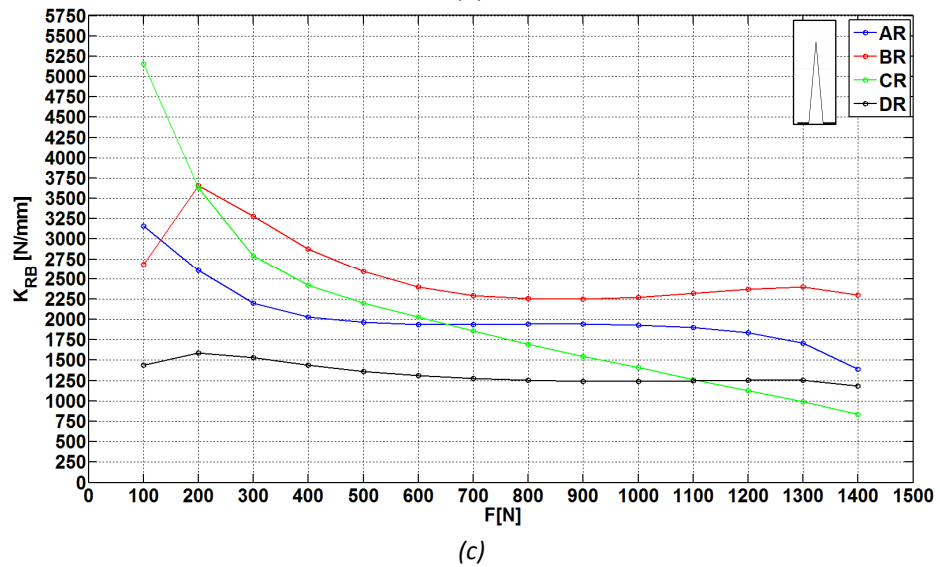
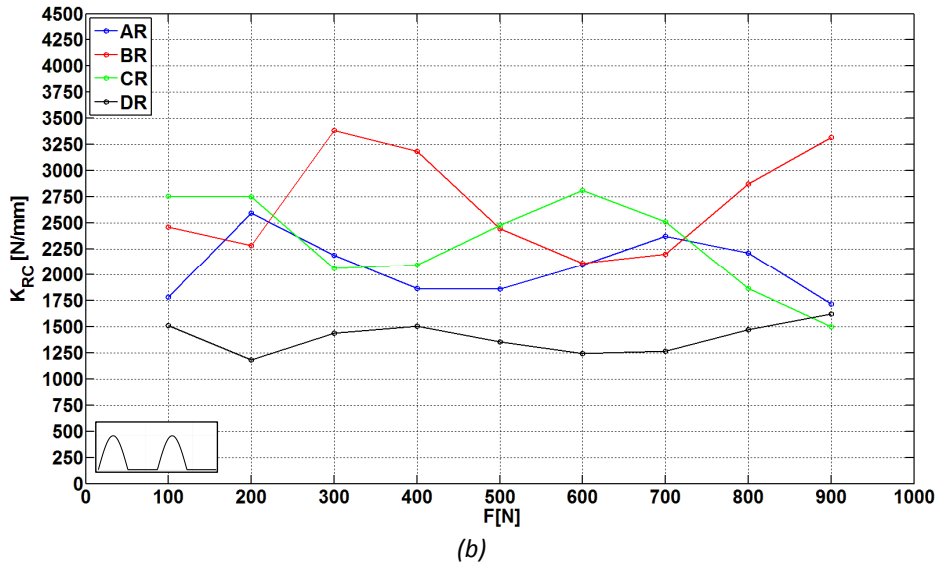
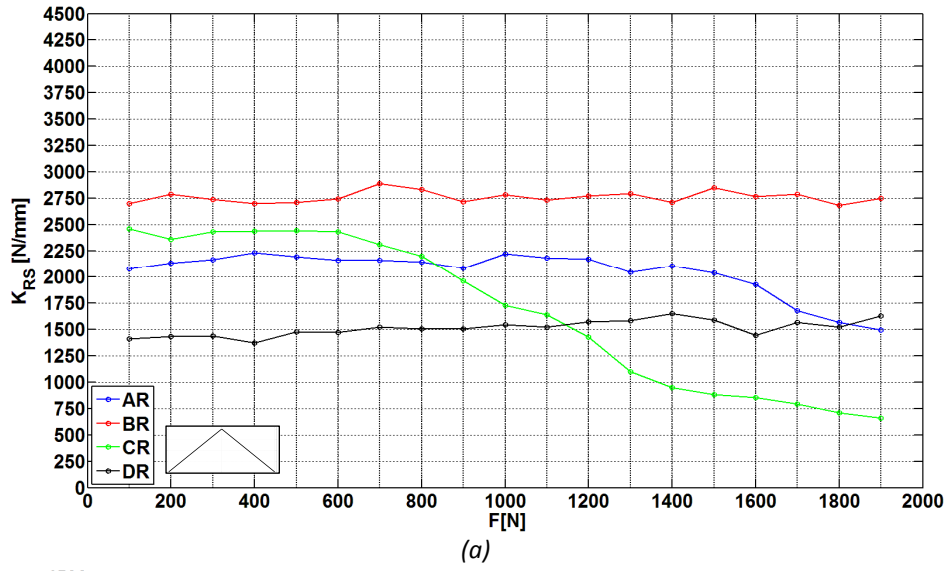


Fig. 4.14 Stiffness curve of the Rim system calculated for the rear wheels after the static (a), cyclic (b) and bump (c) tests.

### Gross Stiffness $K^G$ and $R^2$

The Gross Stiffness  $K^G$  values calculated for the Wheel and Rim systems of the front and rear wheels are represented in the histograms of figure 4.15 and 4.16. At the top of each histogram the respective  $R^2$  value is reported.

High differences between the four wheel models are clearly visible if we consider the Rim system (red histograms) of both the front and the rear wheels. Negligible differences can be observed considering the Wheel systems. The ranking between the four tested wheel models resulting from the static, cyclic and bump test is the same.

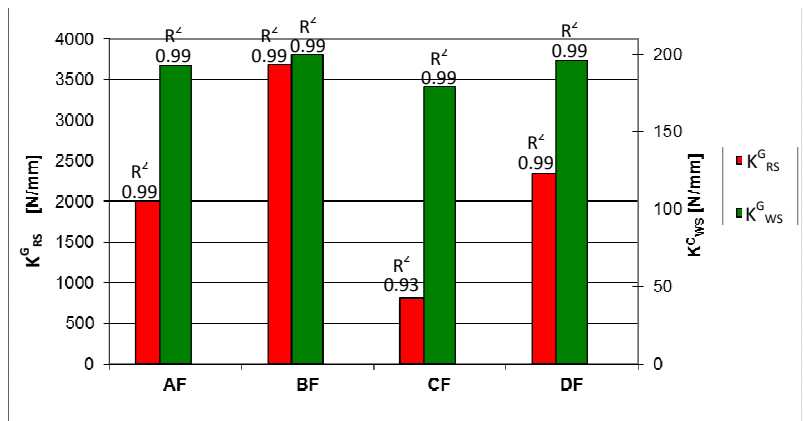
The instability phenomena of the CF and CR wheels are proved by the low values of  $K^G_R$  and of the corresponding  $R^2$  (fig. 4.15.a-c, 4.16.a-c).

The maximum values of  $K^G_W$  were obtained during the static tests due to the higher maximum load reached during this test.

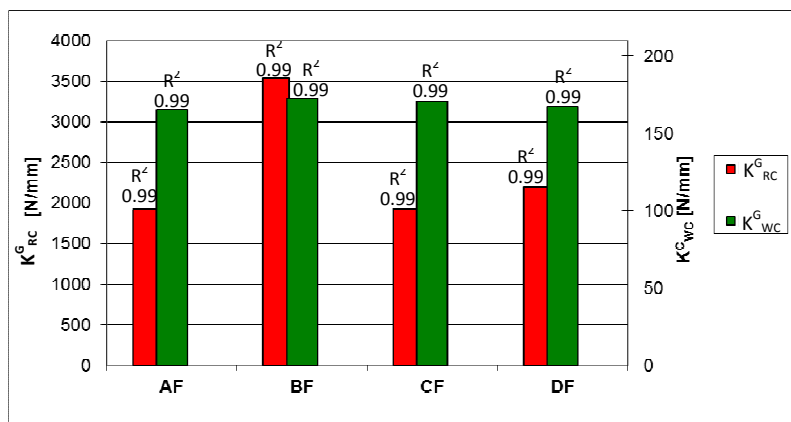
If we consider the values of  $K^G_R$  obtained for each tested wheel after the three tests performed, we can observe that as the load rate increases, the Rim Cycle Stiffness decreases. A further more detailed analysis is needed to better understand this aspect.

### Critical Load $P_{cr}$

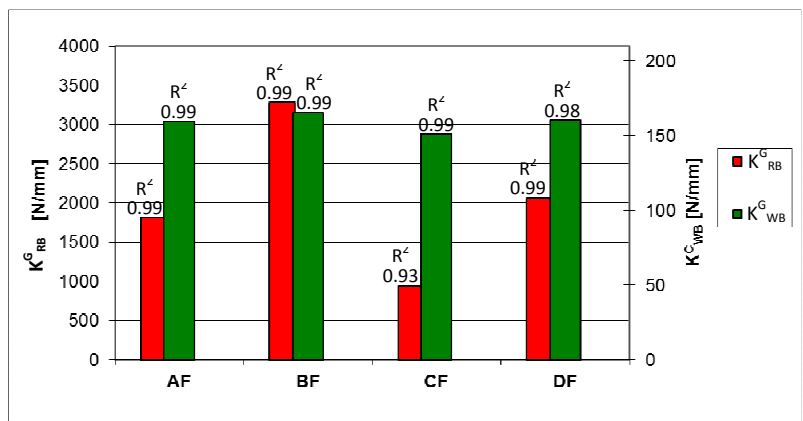
The wheels CF, CR and AR presented a  $P_{cr}$  lower than the maximum static load applied (2000 N) (tab. 4.5, 4.8). The critical load measured for the CF and CR wheels is equal to 1000 N in correspondence of which they respectively presented a stiffness drop of 68% and 30%. The wheel AR showed an unstable behaviour for loads greater than 1700 N, presenting at this load level a decrease of stiffness equal to 23%. The unstable behaviour of the CF and CR wheels was due to their constructive characteristics: since their spokes in composite material are glued at the hub and at the rim, they resulted in a low pre-tension level.



(a)

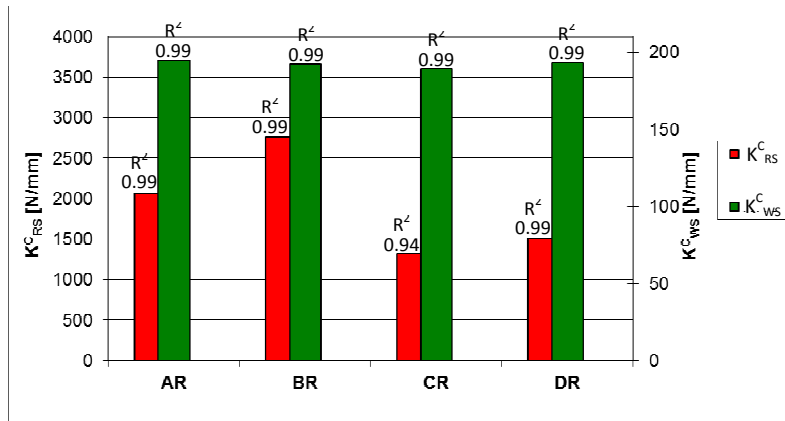


(b)

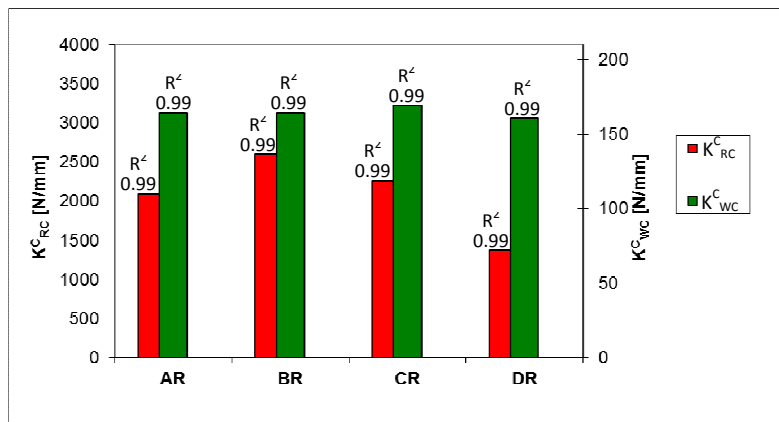


(c)

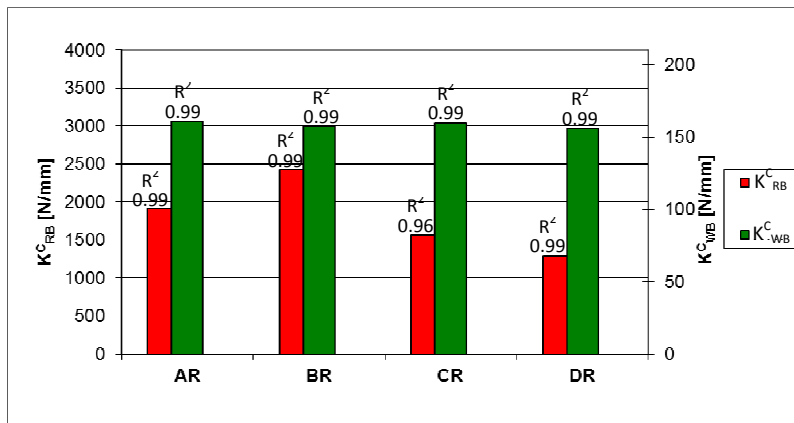
Fig. 4.15 Gross Stiffness  $K^G$  of the Wheel and Rim system and  $R^2$  calculated for the front wheels after the static (a), cyclic (b) and bump (c) tests.



(a)



(b)



(c)

Fig. 4.16 Cyclic Stiffness  $K^C$  of the Wheel and Rim system and  $R^2$  calculated for the rear wheels after the static (a), cyclic (b) and bump (c) tests.

### Dissipated Energy

The energy  $E$  dissipated by the Wheel and Rim systems of the front and rear wheels are represented in the histograms of figure 4.17 and 4.18.

The energy dissipated by the Wheel system was approximately ten times the energy dissipated by the Rim system. The differences between the Rim system of different rear or front wheels cannot be observed considering the Wheel system. The higher amount of energy was therefore dissipated by the Tire which can mask the Rim differences. The Rim dissipated the 6÷10% and the 3÷6% of the total energy respectively during the Cyclic and Bump tests. The energy dissipated by the Wheel and Rim systems of the front and rear wheels were of the same order of magnitude.

The energy absorbed by the Rim system was inversely proportional to the Rim stiffness: the stiffer wheel dissipated less energy in both the tests (wheels BF and BR). Among the front wheels, the wheel CF, which showed an elevated unstable behaviour during the static and bump tests, presents the highest values of dissipated energy for both the Wheel and the Rim systems.

Comparing the results obtained for each wheel after the cyclic and the bump tests, we can observe that the energy dissipated by the Rim and the Wheel systems during the Bump test (fig. 4.16.b, 4.17.b) is five times the energy dissipated during the Cyclic test (fig. 4.16.a, 4.17.a) due to the higher load rate and the higher maximum load reached during the bump tests.

| Wheel Type | $E_{RC}$ [ $10^{-3}$ J] | $E_{WC}$ [ $10^{-3}$ J] |
|------------|-------------------------|-------------------------|
| AF         | 12.5                    | 155                     |
| BF         | 7.0                     | 150                     |
| CF         | 15.0                    | 160                     |
| DF         | 10.0                    | 160                     |

(a)

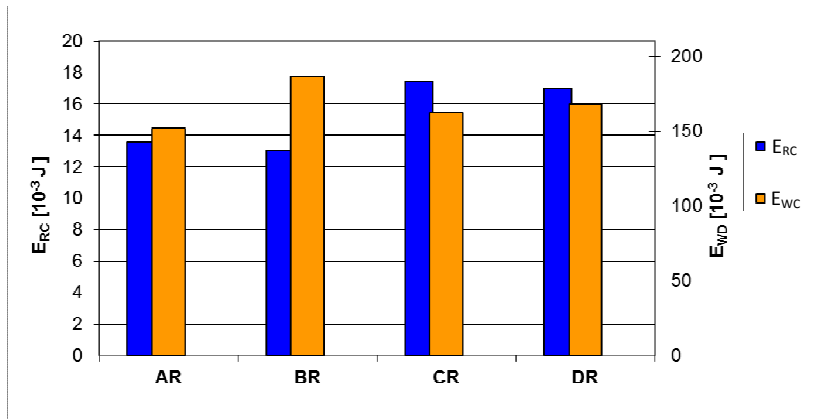
| Wheel Type | $E_{RB}$ [ $10^{-3}$ J] | $E_{WB}$ [ $10^{-3}$ J] |
|------------|-------------------------|-------------------------|
| AF         | 60                      | 500                     |
| BF         | 35                      | 500                     |
| CF         | 180                     | 680                     |
| DF         | 55                      | 500                     |

(b)

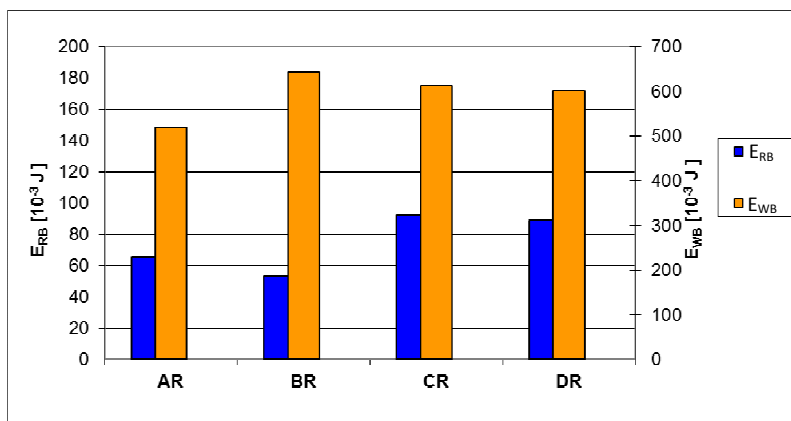
Fig. 4.17 energy dissipated by the Wheel and Rim system of the front wheels after the cyclic (a) and bump (b) tests.

45





(a)



(b)

Fig. 4.18 Energy dissipated by the Wheel and Rim system of the rear wheels after the cyclic (a) and bump (b) tests.

### Effect of tire pressure

The effect of the inflation pressure on the wheel stiffness curve for the Front wheel AF is presented in Figure 4.19. The Rim stiffness is not affected by the tire pressure, whereas the Wheel stiffness is linearly dependent to the Tire pressure by an estimated factor of 14.4.

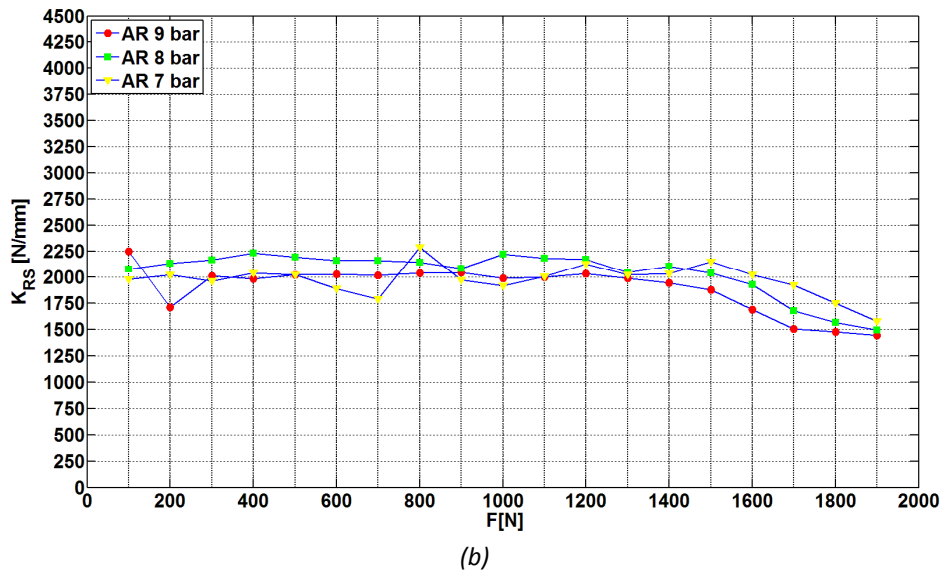
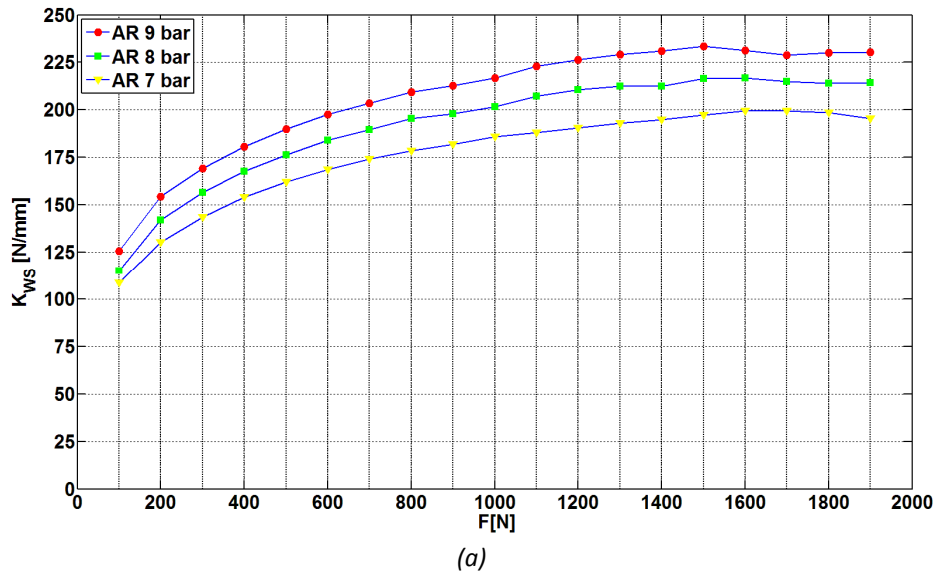


Fig. 4.19 Effect of tire pressure on Wheel (a) and Rim (b) stiffness.

| WHEEL | $K_{ws}^G$ [N/mm] | $R2(K_{ws}^G)$ | $K_{rs}^G$ [N/mm] | $R2(K_{rs}^G)$ | $P_{CR}$ [N] | $\Delta K_{RS}$<br>at $P_{CR}$ [%] |
|-------|-------------------|----------------|-------------------|----------------|--------------|------------------------------------|
| AF    | 193               | 0.9941         | 2007              | 0.9988         | > 2000       |                                    |
| BF    | 200               | 0.9944         | 3681              | 0.9983         | > 2000       |                                    |
| CF    | 179               | 0.9980         | 811               | 0.9327         | 1000         | -68                                |
| DF    | 196               | 0.9936         | 2341              | 0.9980         | > 2000       |                                    |

Tab. 4.5 Results of Front wheels Static tests.

| WHEEL | $K_{wc}^G$ [N/mm] | $R2(K_{wc}^G)$ | $K_{rc}^G$ [N/mm] | $R2(K_{rc}^G)$ | $E_{wc}$ [J] | $E_{rc}$ [J] |
|-------|-------------------|----------------|-------------------|----------------|--------------|--------------|
| AF    | 166               | 0.9948         | 1926              | 0.9987         | 162          | 13           |
| BF    | 173               | 0.9951         | 3544              | 0.9986         | 158          | 7            |
| CF    | 171               | 0.9952         | 1927              | 0.9962         | 168          | 15           |
| DF    | 168               | 0.9945         | 2202              | 0.9990         | 167          | 10           |

Tab. 4.6 Results of Front wheels Cyclic tests.

| WHEEL | $K_{ws}^G$ [N/mm] | $R2(K_{ws}^G)$ | $K_{rs}^G$ [N/mm] | $R2(K_{rs}^G)$ | $E_{ws}$ [J] | $E_{rs}$ [J] |
|-------|-------------------|----------------|-------------------|----------------|--------------|--------------|
| AF    | 159               | 0.9905         | 1811              | 0.9947         | 532          | 61           |
| BF    | 165               | 0.9906         | 3284              | 0.9933         | 543          | 35           |
| CF    | 152               | 0.9910         | 935               | 0.9356         | 681          | 180          |
| DF    | 161               | 0.9896         | 2056              | 0.9946         | 547          | 52           |

Tab. 4.7 Results of Front wheels Bump tests.

| WHEEL | $K_{ws}^G$ [N/mm] | $R2(K_{ws}^G)$ | $K_{rs}^G$ [N/mm] | $R2(K_{rs}^G)$ | $P_{CR}$ [N] | $\Delta K_{RS}$<br>at $P_{CR}$ [%] |
|-------|-------------------|----------------|-------------------|----------------|--------------|------------------------------------|
| AR    | 192.89            | 0.9941         | 2006.78           | 0.9988         | >2000        |                                    |
| BR    | 200.06            | 0.9944         | 3680.95           | 0.9983         | >2000        |                                    |
| CR    | 179.18            | 0.9980         | 810.67            | 0.9327         | 1000         | 68                                 |
| DR    | 196.14            | 0.9936         | 2341.25           | 0.9980         | >2000        |                                    |

Tab. 4.8 Results of Rear wheels Static tests.

| WHEEL | $K_{wc}^G$ [N/mm] | $R2(K_{wc}^G)$ | $K_{rc}^G$ [N/mm] | $R2(K_{rc}^G)$ | $E_{wc}$ [J] | $E_{rc}$ [J] |
|-------|-------------------|----------------|-------------------|----------------|--------------|--------------|
| AR    | 164               | 0.9933         | 2096              | 0.9977         | 152          | 14           |
| BR    | 164               | 0.9929         | 2595              | 0.9960         | 187          | 13           |
| CR    | 169               | 0.9942         | 2253              | 0.9952         | 162          | 17           |
| DR    | 161               | 0.9940         | 1371              | 0.9982         | 168          | 17           |

Tab. 4.9 Results of Rear wheels Cyclic tests.

| WHEEL | $K_{ws}^G$ [N/mm] | $R2(K_{ws}^G)$ | $K_{rs}^G$ [N/mm] | $R2(K_{rs}^G)$ | $E_{ws}$ [J] | $E_{rs}$ [J] |
|-------|-------------------|----------------|-------------------|----------------|--------------|--------------|
| AR    | 161               | 0.9911         | 1915              | 0.9928         | 519          | 66           |
| BR    | 158               | 0.989          | 2427              | 0.9929         | 641          | 53           |
| CR    | 160               | 0.9911         | 1561              | 0.9699         | 614          | 92           |
| DR    | 156               | 0.9902         | 1293              | 0.9946         | 602          | 89           |

Tab. 4.10 Results of Rear wheels Bump tests.

#### 4.3.6 Tire behaviour and methods validation

Front and rear wheels were all equipped with the same tubular tire inflated at the same pressure. The Tire behaviour obtained from the data analysis was therefore expected to be equivalent for different wheels. The percentage standard deviation was computed between the Tire stiffness  $K_T$  and between the energy dissipated by the tire  $E_T$  calculated for the eight tested wheels. The Tire stiffness standard deviation resulted to be in the 2÷4% range for all the tests performed. The same results were obtained for the standard deviation of the absorbed energy  $E_T$  calculated for the front wheels, which is in the 2÷3% range for both the Cyclic and the Bump tests. An higher standard deviation of  $E_T$  was obtained for the rear wheels due to the lateral component of the wheel deformation, which affected the measurement of the Rim displacement during the dynamic tests. The low values obtained for the standard deviations were assumed as a validation of the test method and the overall approach.

The Tire stiffness curves and energy dissipated are respectively showed in the diagrams of figures 4.20-25 and 4.26.

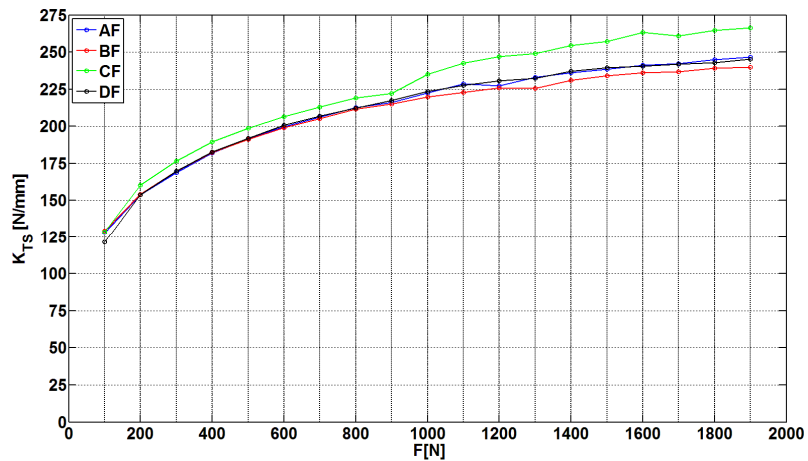


Fig. 4.20 Tire Stiffness curve calculated for the front wheels after the static tests.

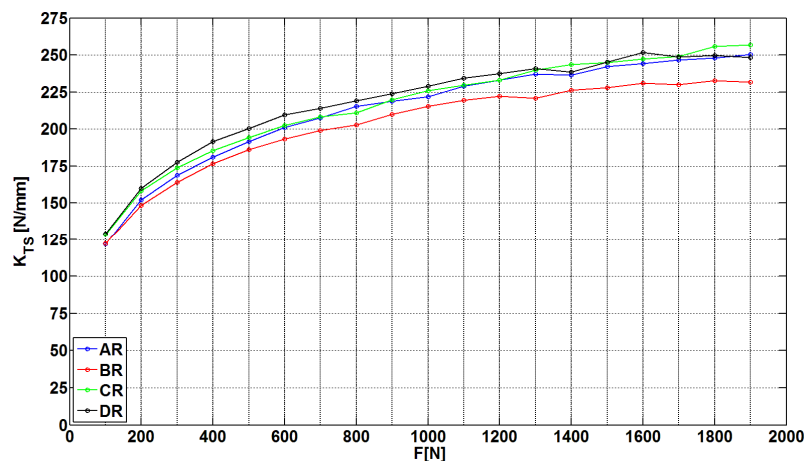


Fig. 4.21 Tire Stiffness curve calculated for the rear wheels after the static tests.

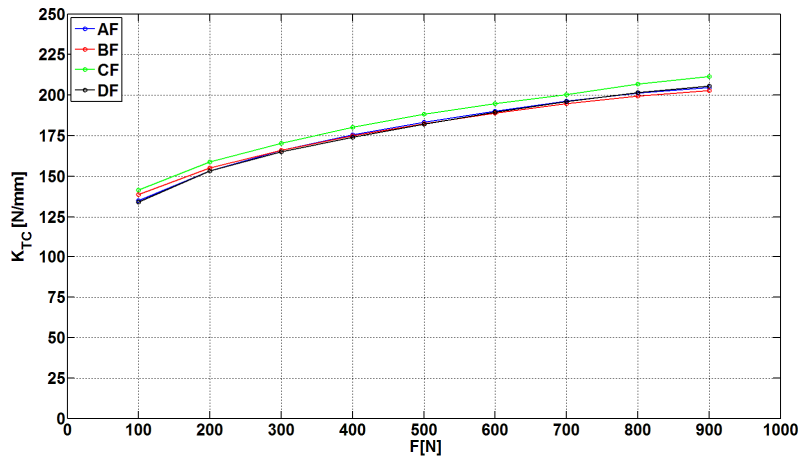


Fig. 4.22 Tire Stiffness curve calculated for the front wheels after the cyclic tests.

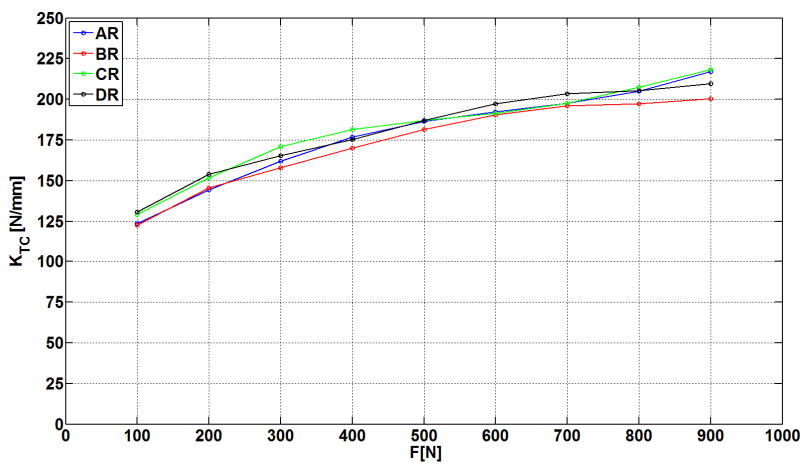


Fig. 4.23 Tire Stiffness curve calculated for the rear wheels after the cyclic tests.

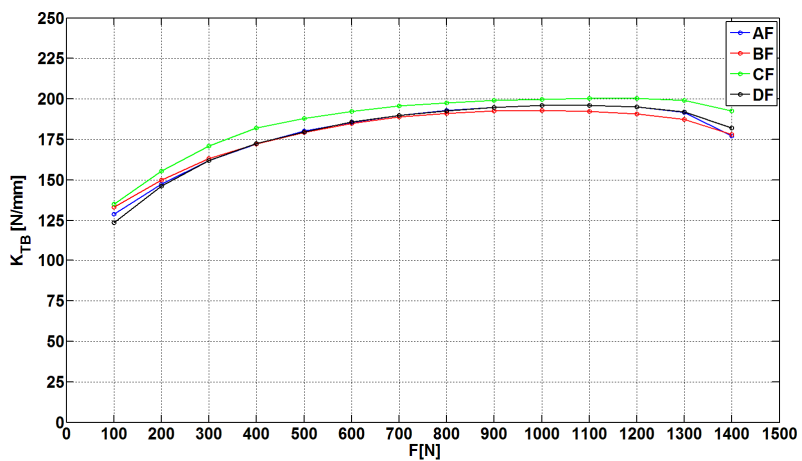


Fig. 4.24 Tire Stiffness curve calculated for the front wheels after the bump tests.

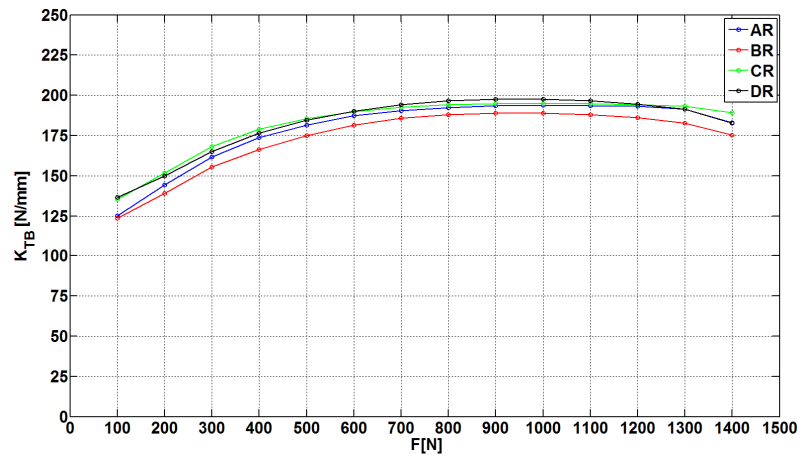
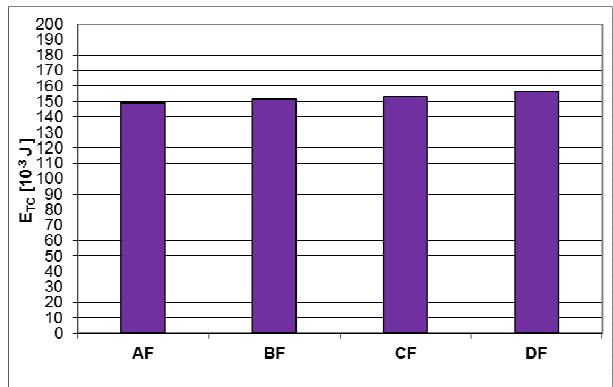
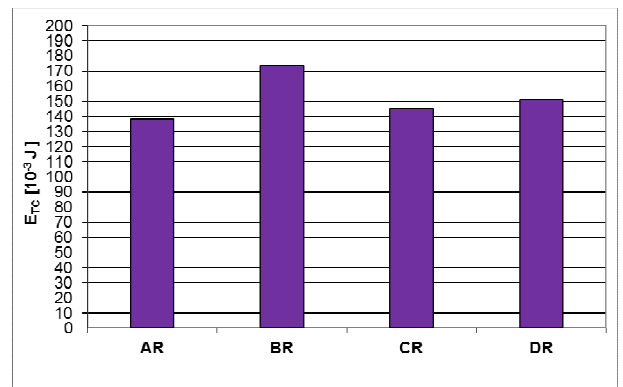


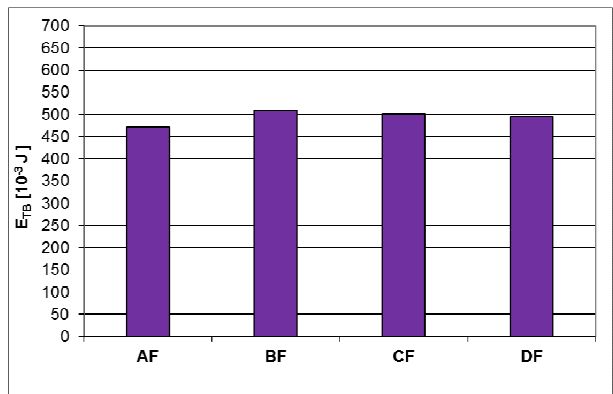
Fig. 4.25 Tire Stiffness curve calculated for the rear wheels after the bump tests.



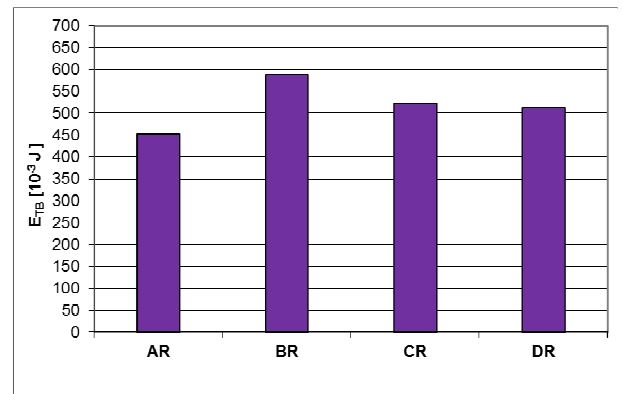
(a)



(b)



(c)



(d)

Fig. 4.26 Tire energy dissipated during the cyclic (a-b) and the bump tests (c-d).

#### 4.4 Test methods implemented in Campagnolo testing laboratories

The Static radial test was implemented in Campagnolo testing laboratories. In the following paragraphs the test bench setup, the testing protocol and the data analysis are presented.

##### 4.4.1 Test bench setup

The test bench developed (fig. 4.27) follows the schematic in figure 4.2.a. An Instron 5966 dual column tabletop universal testing systems, with 10kN load cell and 1256 mm vertical test space, was used for the tests.



*Fig. 4.27 Test bench developed for static radial test.*

The test bench equipment was designed for giving the possibility to test all wheel typologies available in the market, from downhill to racing bicycle wheels.

The wheel support (fig. 4.28.a) is therefore suitable for hubs axle length ranging from 100 to 150 mm and for axle diameters ranging from 10 to 20 mm. The LVDT sensor, internally placed on the rim to measure its radial displacement, is supported by a device which allows the adjustment of its position in the vertical and horizontal directions (fig 4.28.b). The vertical load is applied to the tested wheel through a steel rigid plate (fig. 4.29), fixed at the test bench load cell, appropriate for the mountain bikes and the racing bicycle tires.



(a)



(b)

Fig. 4.28. (a) Wheel adjustable support; (b) adjustable support device for the LVDT sensor.



(a)



(b)

Fig. 4.28. Detail of the rigid plate suitable for the MTB 8a) and racing bicycle (b) tires.

#### 4.4.2 Measuring system

The load is applied to the wheel through the movement of the test bench crossbeam. During the tests the following parameters are measured (fig. 4.29):

- Vertical force  $F$ : measured by means of the 10 kN Instron load cell;
- Wheel total radial displacement  $x_w$ : measured by means of the encoder enclosed in the Instron 5966 test bench, which controls the crossbeam position;



- Rim radial displacement  $x_R$ : measured by means of the external LVDT ( $\pm 5$  mm displacement range, 0-10V output range).

The vertical force  $F$  and the wheel displacement  $x_W$  are acquired simultaneously through the control system of the Instron 5966 test bench. The LVDT signal has to be sampled through an external NI USB-6008 data acquisition system (fig. 4.30) due to the Instron 5966 configuration, which does not allow the connection of external sensors.

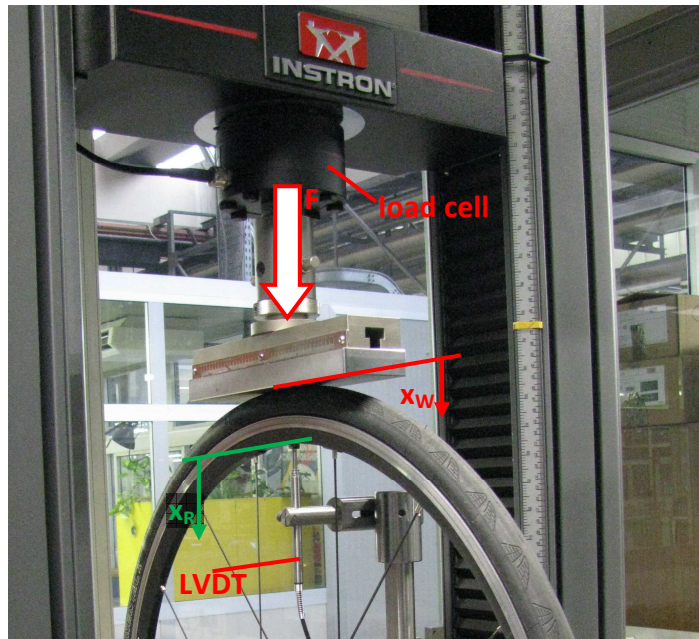


Fig. 4.29 Measuring system.



Fig. 4.30 NI USB-6008 data acquisition system.

#### 4.4.3 Testing protocol

The testing protocol was defined in order to synchronize the signals acquired by means of the Instron 5966 and the LVDT signal acquired through the NI USB-6008. The tests are performed in force control mode, and the force command is represented by 40 consecutive steps, each one of an amplitude of 50 N and a duration of 8 s (fig. 4.31). The test starts from a 10 N preload, which

ensures the tire/plate contact; a maximum load of 2000 N is reached during the test, and the test has a total of 347 s. A sampling frequency of 100 Hz is set for both the Instron and NI USB-6008 acquisition systems.

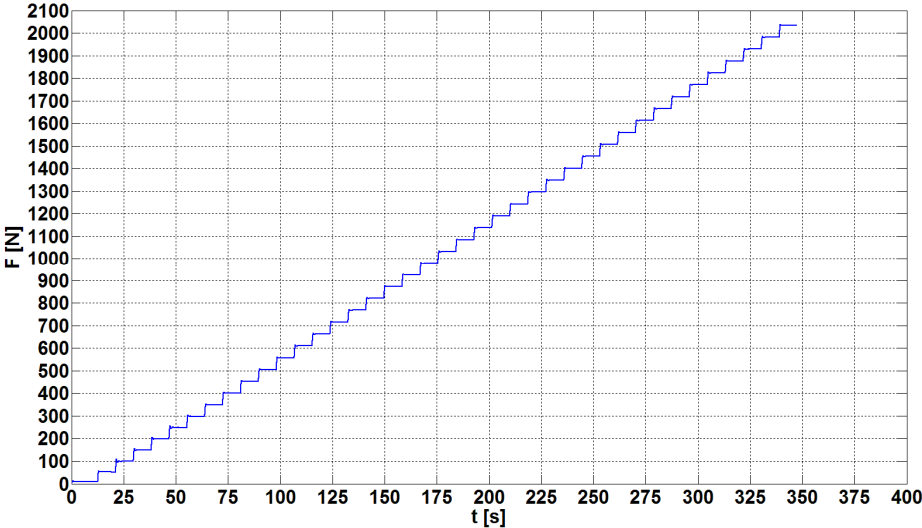


Fig. 4.31 Example of force signal acquired during a test.

#### 4.4.4 Data analysis

The data analysis is divided in the following 3 stages:

##### 1) Filtering of the LVDT signal

The LVDT signal presents a noise component; and the signal is therefore filtered through a 4 poles Butterworth lowpass filter with a cutoff frequency of 0.5 Hz (fig. 4.32).

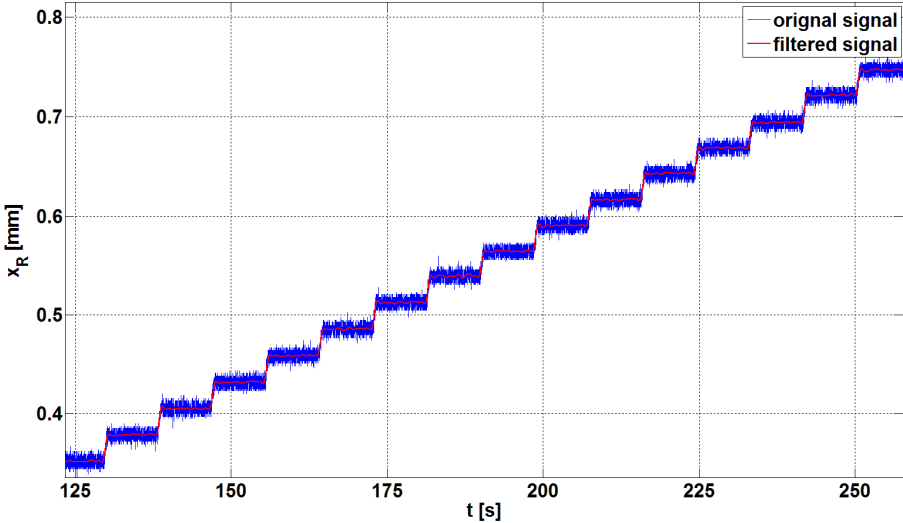
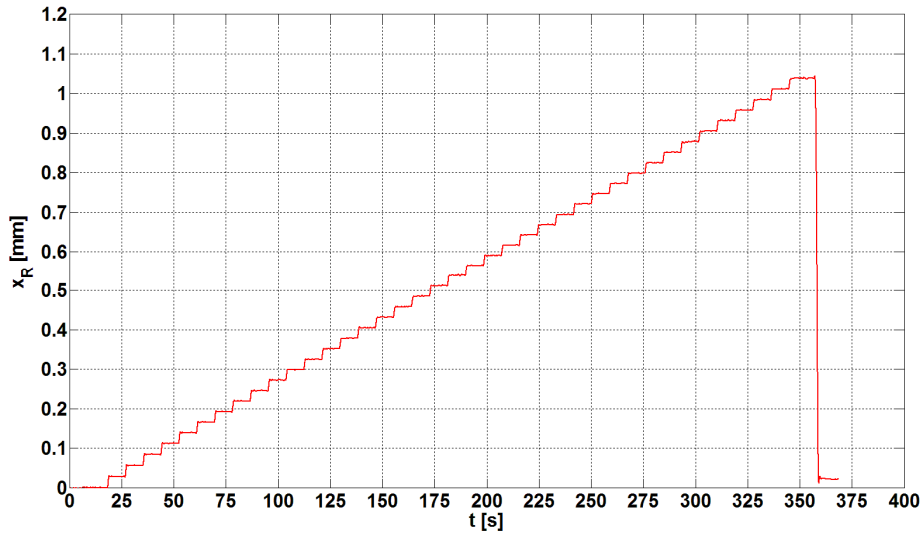


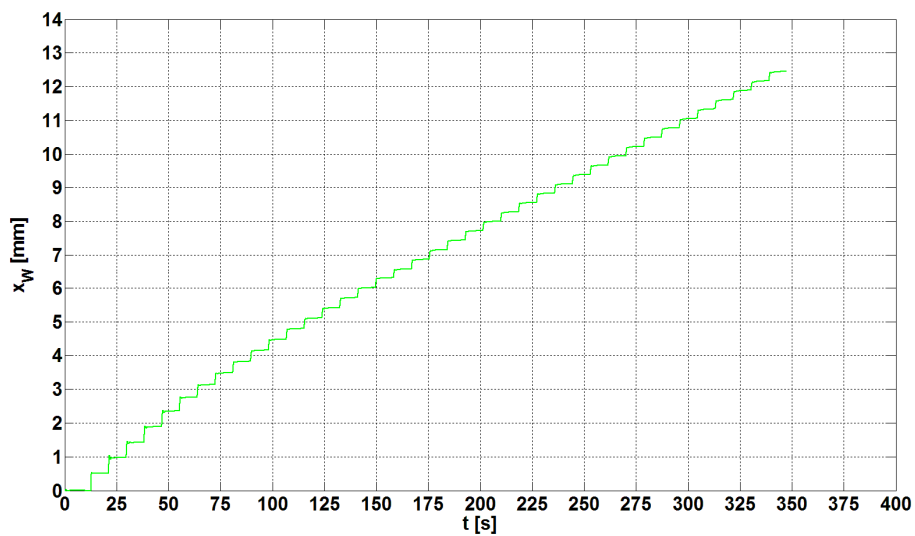
Fig. 4.32 Particular of the LVDT original and filtered signal.

2) Computation of the signals mean value at each step

The figure 4.33 shows an example of the Wheel and Rim displacement signals ( $x_W$  and  $x_R$ ). The mean value of the force  $F$ , of the Wheel displacement  $x_W$  and of the Rim displacement  $x_R$  signals is calculated for each step obtaining a total of 40 mean values for each signal.



(a)



(b)

Fig. 4.33 Example of the displacement signals of Wheel (a) and Rim (b) system.

### 3) Wheel and Rim stiffness computation

If we consider the  $i$ -th step, the Wheel, the Rim, and the Tire stiffness are calculated as it follows:

$$K_{Wi} = \frac{F_i}{x_{Wi}} \quad (1)$$

$$K_{Ri} = \frac{F_i}{x_{Ri}} \quad (2)$$

$$K_{Ti} = \left( \frac{1}{K_{Wi}} - \frac{1}{K_{Ri}} \right)^{-1} \quad (3)$$

For each step, a value of Wheel, Rim, and Tire stiffness is therefore calculated obtaining stiffness curves with 40 points (fig. 4.34-36).

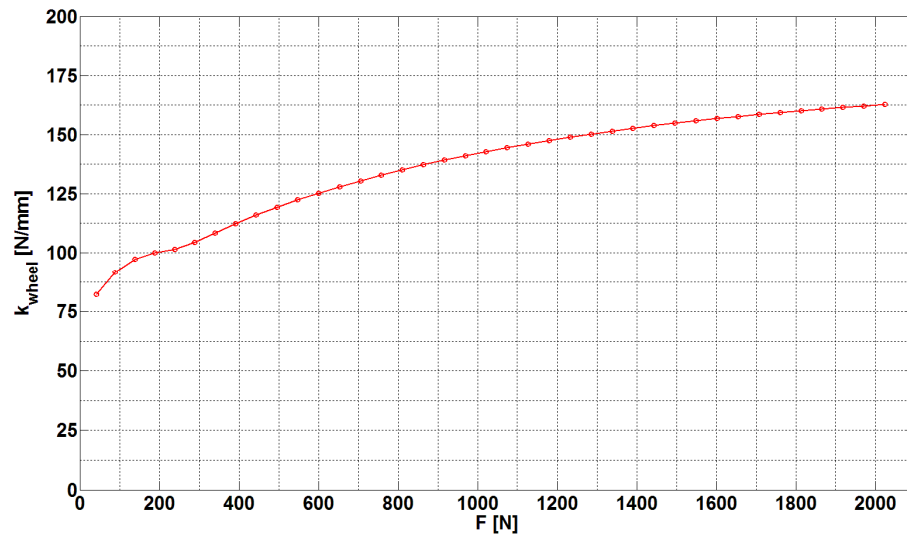


Fig 4.34 Example of a Wheel stiffness curve obtained for a racing wheel.

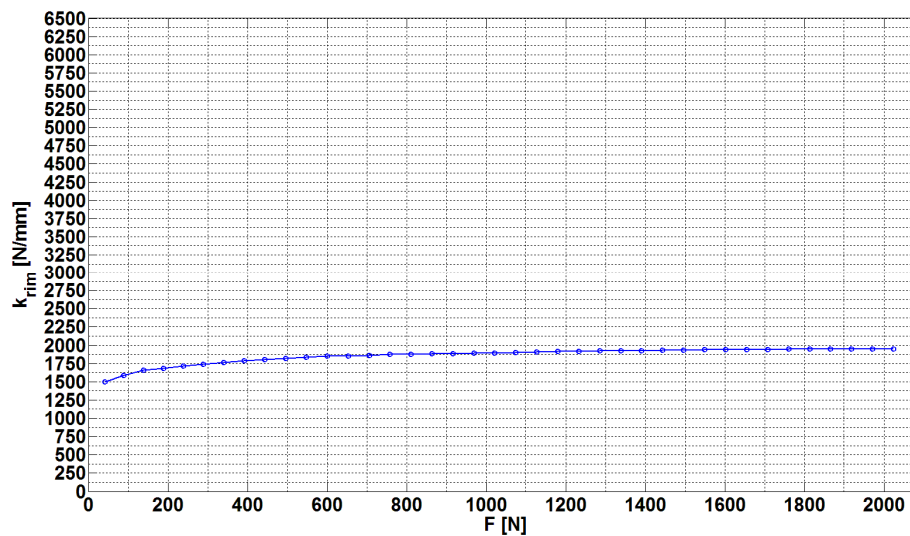


Fig 4.34 Example of a Rim stiffness curve obtained for a racing wheel.

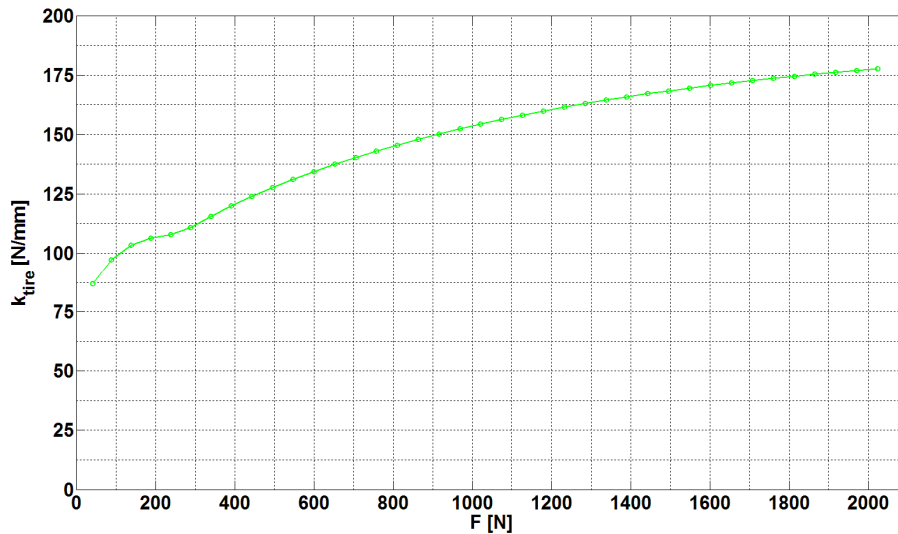


Fig 4.34 Example of a Tire stiffness curve obtained for a racing wheel.

#### 4.5 Conclusions and possible further developments

A new methodology for evaluating the radial structural properties of racing bicycle wheels was proposed: the constant behaviour of the Tire, obtained from different wheels during the static, cyclic and bump tests, was assumed as a validation of the test methods and of the overall approach. This fact suggests also the possibility of studying the tire stiffness and damping properties using the present approach.

Great differences in Rim stiffness were obtained among the tested wheels. These differences were not confirmed in terms of radial stiffness of the Wheel assembly at the typical cycling pressure of 8 bar. The tire stiffness was therefore able to mask the rim differences.

The method was suitable to highlight an unstable behaviour of wheels under radial loads and to give a measure of the corresponding radial critical load.

The constant trend of the Rim stiffness curves reveals that the Rim stiffness is not influenced by spokes pre-tension levels for load lower than the critical value.

The Rim dissipated the 3÷10% of the total energy dissipated by the Wheel. The energy absorbed by the Rim system resulted inversely proportional to the Rim stiffness.

The Tire pressure strongly influences the Wheel stiffness, which is linearly dependent on an estimated factor of 14.4.

The radial tests were performed with the tested wheel resting on a static position in a realistic constraint. The execution of the same tests with a rolling wheel can improve the replication of the real load conditions. The measurement of the spokes tension and of the lateral deformation of the rear wheels could give information useful to better understand the wheel deformed configuration and to analyse the phenomenon, which causes the irregular trend of the rear Rim stiffness, obtained after the cyclic and the bump tests.

The correlation between the wheels radial structural behaviour and the perceived comfort are discussed in the Chapter 10.

# Chapter 5

## Wheels vibration transmissibility

### 5.1 Introduction

The wheels vibration transmissibility is a characteristic inversely correlated to the vibrational comfort properties of bicycle wheels. In order to compare the vibrational comfort properties of racing wheels using a quantitative approach, two methods for measuring the wheels vibration transmissibility were developed, simulating road conditions.

A new full bicycle laboratory test method (fig. 5.1.a) was developed in the Laboratory of Machine design of University of Padova, to evaluate the vibration transmissibility of different bicycle wheels assembled on the same bicycle, in terms of magnitude of wheels transfer function: lower values of transfer function magnitude should correlate with better vibrational comfort.

The wheel transfer function was also measured through a second test method (fig. 5.1.b) developed in Campagnolo testing laboratories, in which the wheel, constrained to a swinging arm, was excited by means of a shaker.

The adopted model, the materials, the testing protocols and the results obtained for the two test methods are presented in this chapter.



(a)



(b)

Fig. 5.1. (a) Full bicycle test bench developed in the University of Padova Laboratories; (b) test bench with a swinging arm developed in Campagnolo laboratories.

## 5.2 Full bicycle laboratory test method (University lab.)

### 5.2.1 Adopted model

The schematic of the test bench and the adopted model, represented by means of a blocks diagram, are visible in figure 5.2.

The rear wheel system **WR**, composed by tire, rim, spokes and hub, is analysed through the test method. This system was excited by the actuator shaft vertical displacement, reproducing a sine function of 0.6 mm constant amplitude, and sweeping in frequency. The system input and output are:

- Input:  $a_{in}$ . Vertical acceleration imposed by means of the actuator shaft motion.
- Output:  $a_{out}$ . Vertical acceleration measured at the rear wheel axis.

The WR system is characterised by its transfer function, which relates the input of the system  $a_{in}$  with its output  $a_{out}$ . With the developed method, the transfer function magnitude was evaluated for different frequencies from 1 to 100 Hz.

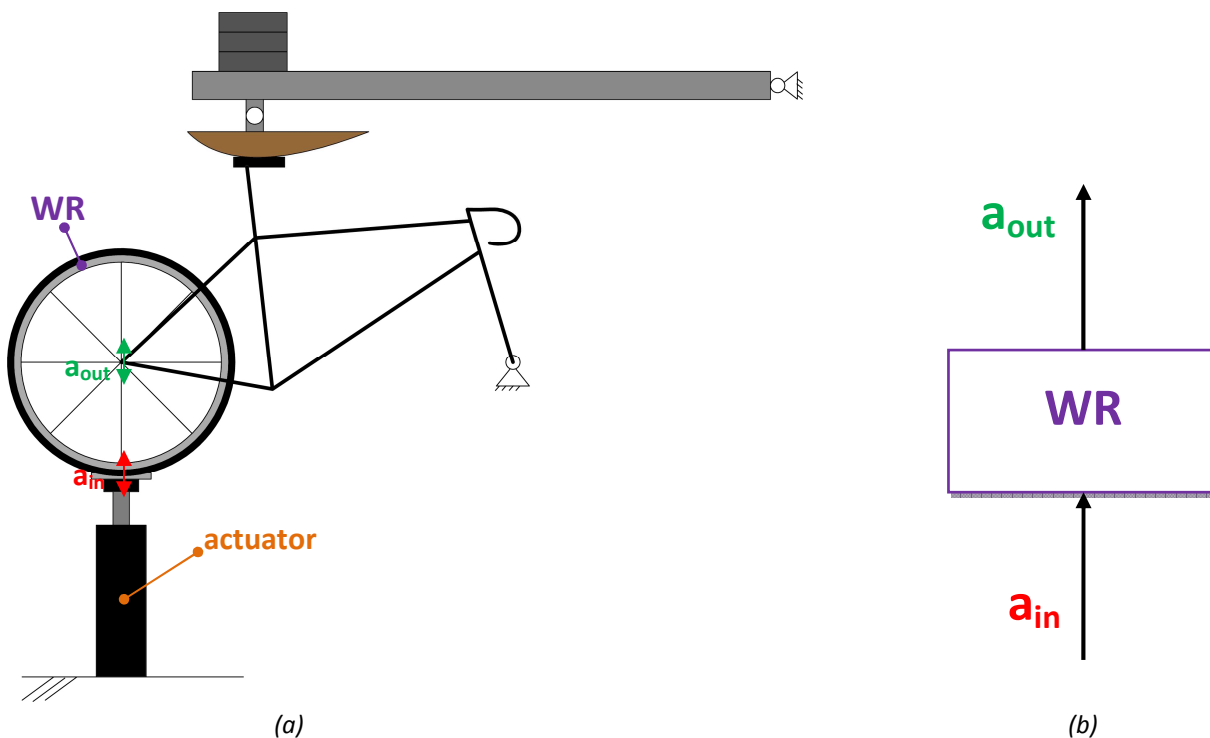


Fig. 5.2. (a) Schematic of the tests bench; (b) adopted model.

### 5.2.2 Test bench setup

The test bench (fig. 5.3) was equipped with the full bicycle in order to better reproduce the real wheel constraint and load conditions. The front fork was constrained to the test bench by a hinge at the front wheel axis (A). The rear wheel was resting on an aluminium plate fixed to the load cell

of a vertical servohydraulic MTS 242 cylinder (B) with a 15 kN load cell and a  $\pm 100$  mm stroke LVDT.

The static vertical load acting to the rear wheel was applied by a wooden dummy bottom (C), shaped in accordance to UNI 10814, resting on the saddle and connected to the extremity of a swinging beam by a ball joint (D). The other beam extremity was hinged to the test bench at a distance of 1.3 m from the dummy bottom hinge.

Dead weights (34.6 kg) (E) were positioned right above the dummy bottom hinge in order to reach a static vertical load of 535 N at the rear wheel support plate. This value represents the static ground reaction force acting at rear wheel, measured with a 74 kg - 177 cm cyclist positioned on the same bicycles.



Fig.5.3 Test bench. A: front fork axle hinge; B: servohydraulic cylinder; C: wooden dummy bottom; D: swinging beam; E: dead weights.



### 5.2.3 Measuring system

Accelerations at the support plate (fig. 5.4.a) and at the rear wheel axis (fig. 5.4.b) were measured by two uni-axial piezoelectric accelerometers, model SoMat HLS 1100 (+/- 50 g full scale, 0.3 - 15000 Hz bandpass).

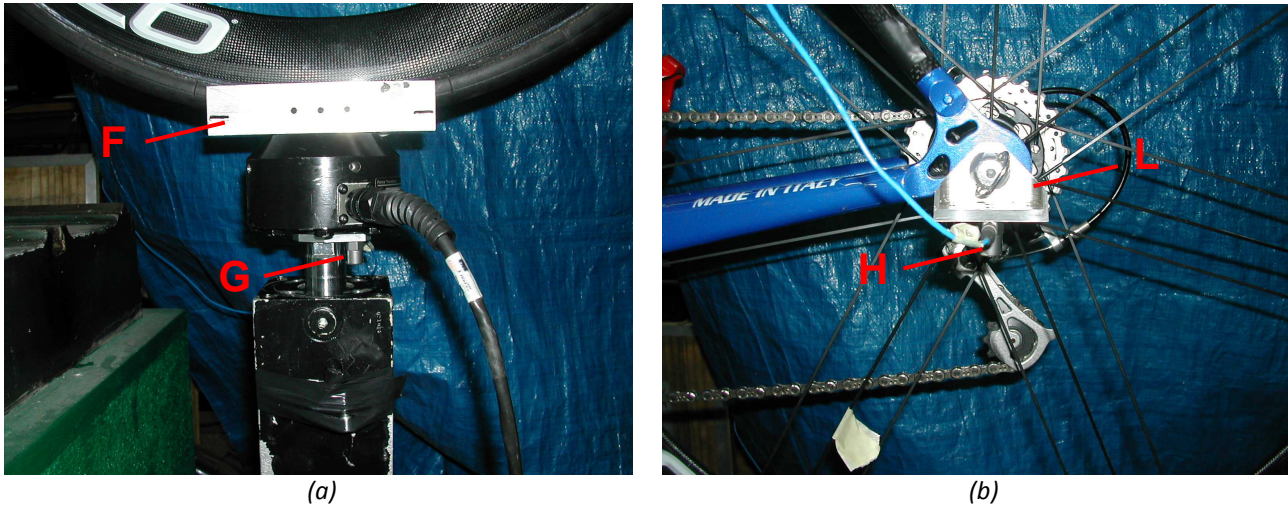


Fig. 5.4. (a) F: wheel support plate; G: accelerometer; (b) H: rear wheel axis accelerometer; L: accelerometer support device.

Acceleration signals were recorded by means of SoMat eDAQ Lite acquisition system, at 5 kHz sampling rate, +/- 50 g full scale.

The cylinder shaft displacement was measured through its internal LVDT ( $\pm 100$  mm stroke), and recorded by means of the MTS test bench control system.

### 5.2.4 Wheels considered for the tests

The same four different rear wheels (named AR, BR, CR, DR, see § 4.3.2) considered for the radial stiffness tests were also considered for the vibrational tests. The wheels, all equipped with the same tubular tire (Continental "Sprinter" 700x23) inflated at 8 bar, were different for material, rim profile, spokes number and disposition. The table 5.1 summarizes again the rear wheels characteristics.

| Wheel | Rim depth         | Rim material | Hub material | Spokes Nr. | Spokes Pattern                        | Spokes material | Mass*  |
|-------|-------------------|--------------|--------------|------------|---------------------------------------|-----------------|--------|
| AR    | Low<br>H 20 mm    | Composite    | Composite    | 24         | Radial left side<br>2x sprockets side | Steel           | 1320 g |
| BR    | High<br>H 50 mm   | Composite    | Aluminium    | 21         | Triplets                              | Steel           | 1340 g |
| CR    | Medium<br>H 30 mm | Composite    | Composite    | 24         | 2x                                    | Composite       | 1190 g |
| DR    | Medium<br>H 30 mm | Aluminium    | Aluminium    | 21         | Triplets                              | Steel           | 1420 g |

Tab. 5.1 Tested rear wheels characteristics (\* mass including tire and sprockets).

### 5.2.5 Testing protocol

This **WR** system was excited by the actuator shaft vertical displacement reproducing a sine function of 0.6 mm constant amplitude and sweeping in frequency. The actuator drive signal (fig. 5.5) was divided into blocks, each block being characterized by a different frequency level starting from 1 Hz and ending at 100 Hz, with discrete frequency increments of 2.5 Hz from 2.5 to 100 Hz.

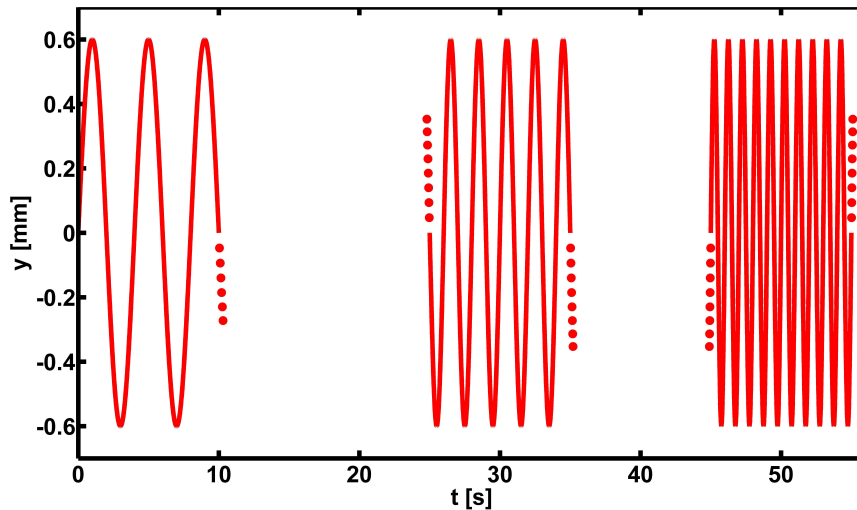


Fig. 5.5 Actuator drive signal.

| Block nr. | f [Hz] | Block nr. | f [Hz] | Block nr. | f [Hz] | Block nr. | f [Hz] |
|-----------|--------|-----------|--------|-----------|--------|-----------|--------|
| 1         | 1.0    | 11        | 25.0   | 21        | 50.0   | 31        | 75.0   |
| 2         | 2.5    | 12        | 27.5   | 22        | 52.5   | 32        | 77.5   |
| 3         | 5.0    | 13        | 30.0   | 23        | 55.0   | 33        | 80.0   |
| 4         | 7.5    | 14        | 32.5   | 24        | 57.5   | 34        | 82.5   |
| 5         | 10.0   | 15        | 35.0   | 25        | 60.0   | 35        | 85.0   |
| 6         | 12.5   | 16        | 37.5   | 26        | 62.5   | 36        | 87.5   |
| 7         | 15.0   | 17        | 40.0   | 27        | 65.0   | 37        | 90.0   |
| 8         | 17.5   | 18        | 42.5   | 28        | 67.5   | 38        | 92.5   |
| 9         | 20.0   | 19        | 45.0   | 29        | 70.0   | 39        | 95.0   |
| 10        | 22.5   | 20        | 47.5   | 30        | 72.5   | 40        | 97.5   |
|           |        |           |        |           |        | 41        | 100.0  |

Tab. 5.2 Frequency level corresponding to each drive signal block.

All tests were performed with the same tubular tires inflated at 8 bar and controlled by a precision pressure gauge (0.05 bar accuracy, fig. 4.7).

## 5.2.6 Data analysis

### Frequency analysis of the acceleration signals

A frequency analysis of both actuator shaft (**input**) and rear wheel axle (**output**) acceleration signals was performed for each command block (fig. 5.6). Discrete Fourier transform DFT of signals was computed by FFT algorithm. In order to obtain leakage-free spectrums with 0.1 Hz resolution, a total of 50000 samples was considered on each FFT execution, corresponding to an integer number of input sine function periods.

The analysis of each input acceleration spectrum  $A_{in}(f)$  was performed to verify the correct execution of the related command block.

The characteristics of the frequency analysis are summarized below:

- FFT algorithm for the DFT computation;
- Sampling frequency  $f_s = 5$  kHz;
- Rectangular window for each block;
- Block window length: 50000 points, 10 s period -> integer number of input sine function periods for a leakage-free spectra;
- Spectra frequency resolution = 0.1 Hz.

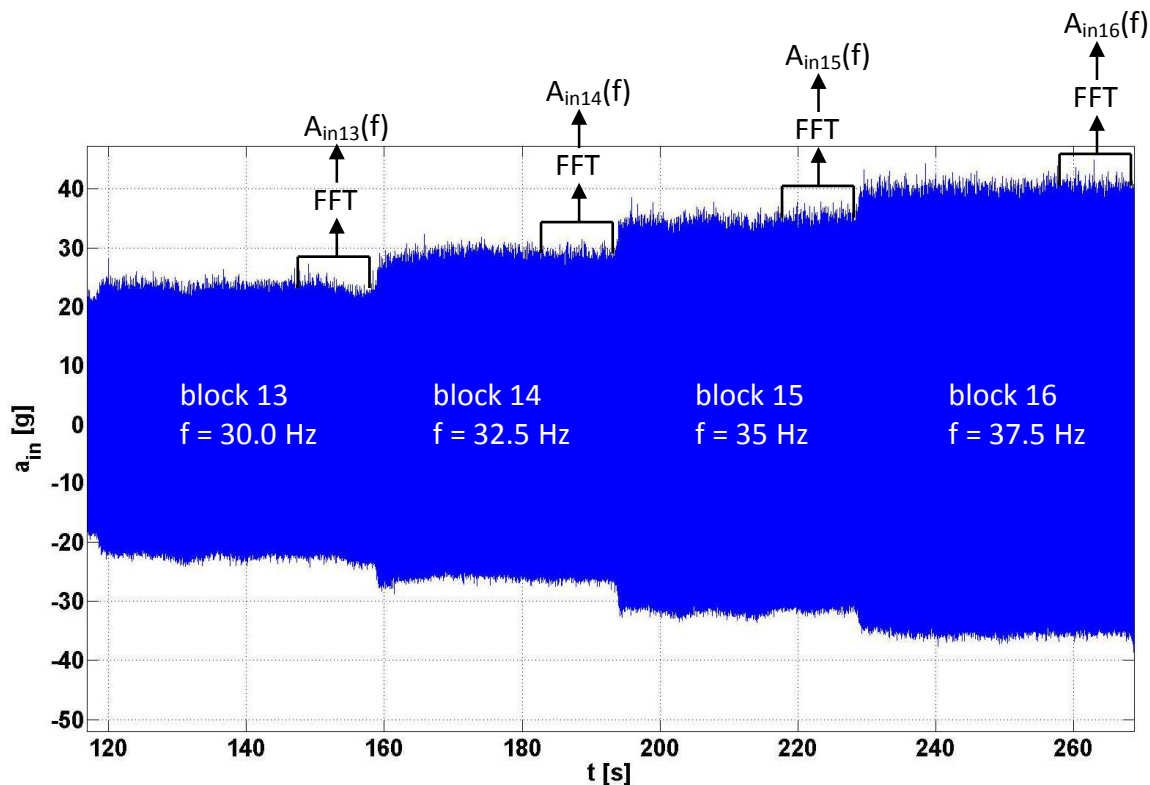
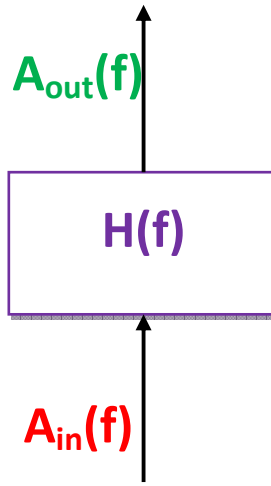


Fig. 5.6 Example of the blocks selection for the FFT computation of the  $a_{in}(t)$  signal.

### Transfer function computation

Transfer function magnitude  $|H_k(\mathbf{f})|$  (fig. 5.7) was calculated for each k-th tested wheel, point by point at each excitation frequency  $f_i$ . Each transfer function value  $|H_k(f_i)|$  was calculated as the ratio between the output spectrum magnitude peak value  $|A_{out,k}(f_i)|$ , calculated at the excitation frequency, and the corresponding input spectrum magnitude  $|A_{in,k}(f_i)|$ , as expressed in (1).

$$|H_k(f_i)| = \frac{|A_{ar,k}(f_i)|}{|A_{in,k}(f_i)|} \quad (1)$$



*Fig. 5.7 Schematic of the wheel input/output relationship.*

The percentage relative difference  $\varepsilon_r(f_i)$  between maximum and minimum value of  $|H_k(f_i)|$  computed for tested wheels was calculated (2) at each frequency in order to evaluate how differences between vibrational transmissibility of different wheels varied within the considered frequency range.

$$\varepsilon_r(f_i) = \frac{\max(|H_k(f_i)|) - \min(|H_k(f_i)|)}{\max(|H_k(f_i)|)} \cdot 100 \quad (2)$$

### **5.2.7 Results**

The curves of vibrational transmissibility  $|H(f)|$  calculated for the four tested wheels are reported in decibel scale versus the test frequency in figure 5.8. The overall shape of all curves within the 1-100 Hz interval resulted to be very similar and to be characterized by a peak around 7.5 Hz, a major valley around 12.5 Hz, an increasing portion from 15 to 20 Hz, a relative peak around 22.5 Hz, again an increasing portion of the curve between 25 and 47.5 Hz, an absolute peak around 50 Hz, a decreasing portion from 55 to 67.5 Hz and an irregular tail portion from 70 to 100 Hz.

In the frequency intervals between 5 and 10 Hz and between 42.5 and 67.5 Hz, input vibrations were amplified by all tested wheels, as expressed by transmissibility magnitudes greater than zero

dB. On the opposite, input vibrations coming from the cylinder were damped by all tested wheels in the frequency intervals between 10 Hz and 42.5 Hz and for frequency greater than 67.5 Hz. At frequency levels lower than 7.5 Hz, results were conditioned by low signal to noise ratio, possibly due to the dynamic characteristics of the piezoelectric accelerometers used: the input spectrum magnitude obtained at 1, 2.5 and 5 Hz shows, in addition to the component corresponding to the excitation frequency, a constant component and other components with frequency greater than the excitation frequency (fig. 5.9).

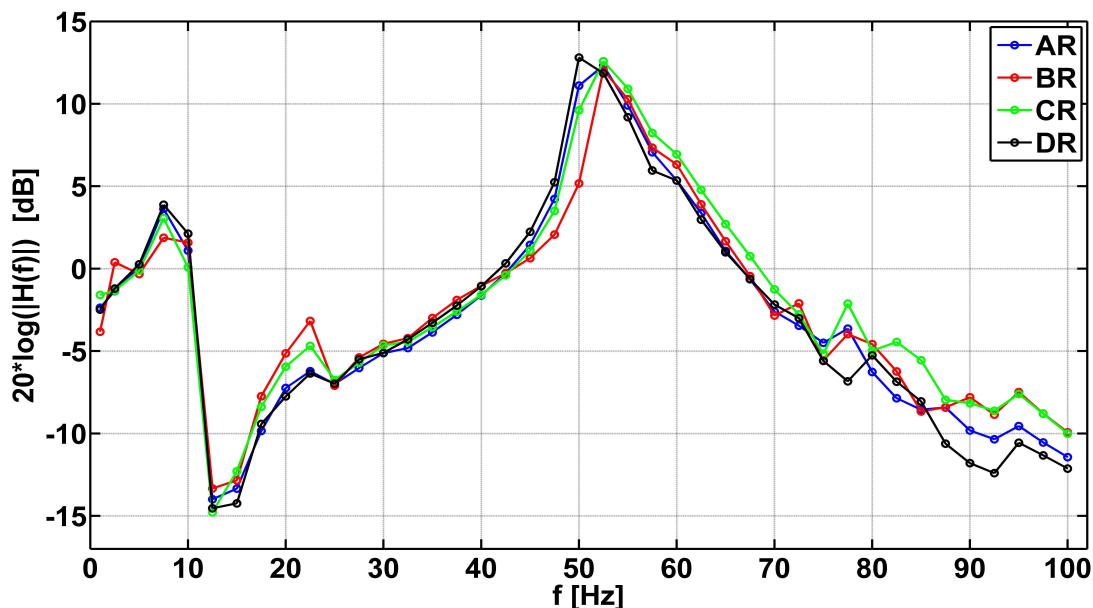


Figure 5.8 Transfer function magnitude calculated for the four tested rear wheels.

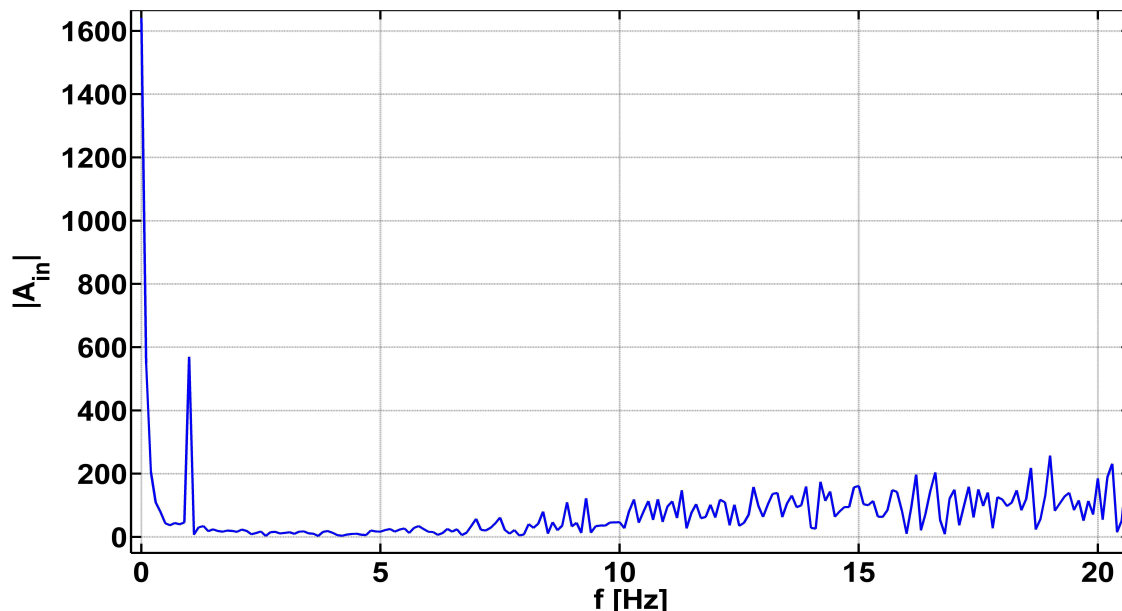


Figure 5.9 Input signal spectrum corresponding to 1 Hz excitation frequency, which shows the constant component, and components with frequency greater than excitation frequency.

The curves irregularities that were noticed as a trend at high frequency (range 70 - 100 Hz) could be attributed to a complex tire damping behaviour or to resonances coming from other components of the assembly. A more detailed analysis of this phenomenon is therefore suggested. The output signal spectra obtained for 10 - 30 Hz excitation frequency range showed the presence of components with frequency multiple of the excitation frequency (Fig. 5.10). This suggests the presence of a nonlinear behaviour of wheel system probably due to tire damping characteristics.

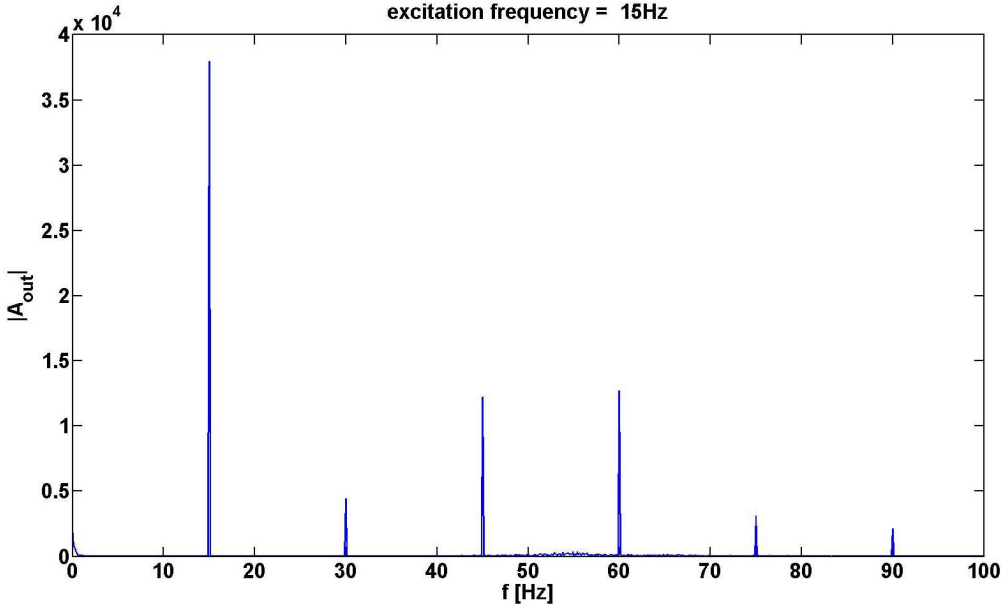


Fig. 5.10 Output signal spectrum corresponding to 15 Hz excitation frequency, which shows components with frequency multiple of the excitation frequency.

The plot of the relative differences  $\epsilon_r(f_i)$  between maximum and minimum values of  $|H_k(f_i)|$ , expressed in percent, is reported in figure 5.11. The scatter resulted to be between 15% and 30 % for frequencies ranging from 7.5 to 22.5 Hz, lower than 10 % for frequencies between 25 and 42.5 Hz, reaching the maximum value of 58 % at 50 Hz, and between 15 and 25 % for frequencies ranging from 55 to 67.5 Hz. At high frequencies range (70 - 100 Hz) the irregularity of  $\epsilon_r$  curve reflects the irregular shape of  $|H(f)|$  curves.

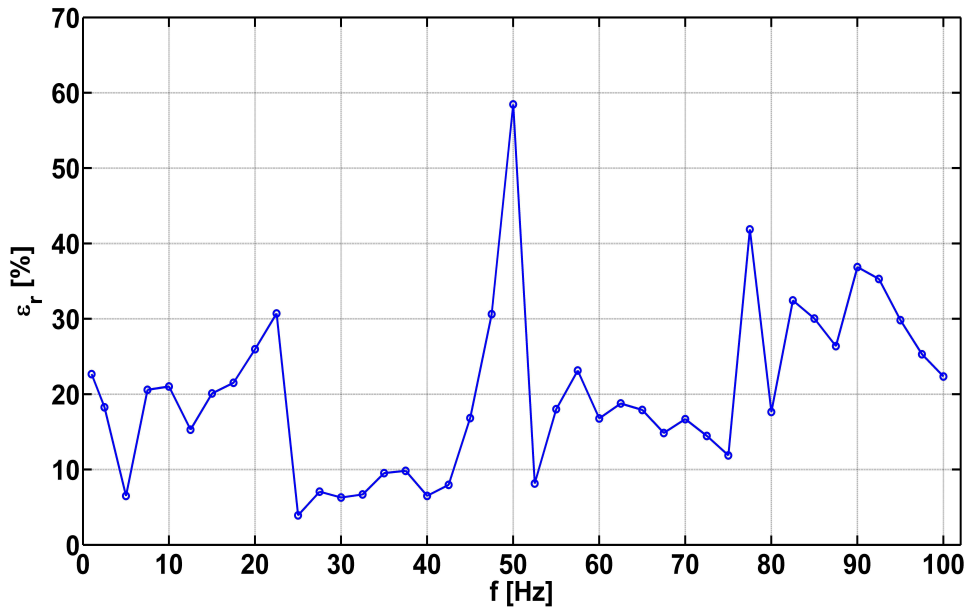


Figure 5.11 Relative difference  $\epsilon_r$  [%] between maximum and minimum value of  $|Hk(f_i)|$ , calculated for the four tested wheels.

This plot can indicate the frequency intervals where greater differences among the tested wheels were found, and it suggested a further analysis among them in order to quantify the comfort properties of wheels within the frequency domain.

Ranking of wheels, from a comfort point of view, was therefore based on the inverse values of the vibration transmissibility, and varied within the frequency range considered. Table 5.3 shows the wheels comfort properties ranking, based on the inverse of the transfer function magnitude, obtained for frequency level or range with  $\epsilon_r$  reater than 10% and not affected by any irregularity.

| Ranking  | f = 7.5 Hz | f = 12.5 Hz | f = [15-20 Hz] | f = 22.5 Hz | f = 50 Hz   | f = [55-67.5 Hz] |
|----------|------------|-------------|----------------|-------------|-------------|------------------|
| 1(best)  | B          | C           | D              | D           | B           | D                |
| 2        | C: + 14.5% | D: + 2.8%   | A: + 4.1%      | A: + 1.6%   | C: + 66.7%  | A: + 4.6%        |
| 3        | A: + 22.3% | A: + 9.5%   | C: + 20.4%     | C: + 21.3%  | A: + 97.9%  | B: + 10.7%       |
| 4(worst) | D: + 25.9% | B: + 18.1%  | B: + 24.6%     | B: + 44.3%  | D: + 140.8% | C: + 22.4%       |

Table 5.3 Wheels comfort ranking, based on the inverse of transfer function magnitude.

Great differences among the four curves were found around 22.5 Hz, where the highest value of  $|H(f)|$  was calculated for BR wheel (high profile carbon fibre rim) followed by CR (medium profile carbon fibre rim). Lowest values of  $|H(f)|$  were calculated for AR (low profile carbon fibre rim) and DR (medium profile aluminium rim), whose curves resulted to be very close. Highest differences between maximum and minimum values of  $|H(f)|$  were calculated at 50 Hz (Fig. 7) where the ranking resulted to be exactly reversed with respect to the ranking previously mentioned around 22.5 Hz: the highest value of vibration transmissibility was found for DR wheel followed by AR, CR and BR.

Some limitations of the present study can be found in some aspects of the experimental setup and in the small number of tested wheels. About the experimental setup, the use of a wooden dummy can be seen as a significant difference with respect to the real presence of soft tissues in a real

cyclist body: nevertheless, silicon dummies were intentionally avoided to exclude any change in the mechanical properties of the silicon at the saddle interface during the testing of the four wheels. Furthermore, the saddle was kept consistent throughout the tests, again to reduce the number of variables that could influence the phenomenon. On the other hand, previous pilot studies [6] had shown that fixing the deadweight rigidly to the seatpost excites the frame/seatpost modes of vibrations, introducing an additional input to the bicycle system and masking the wheel behaviour. This resulted in a transfer function curve, which presents a complete different shape, if compared with the curves showed above (fig. 5.12), and reveals that the bicycle constraint and load systems can heavily affect the results obtained in the wheels analysis. The comparison between the transfer function curves of figure 5.12 with the acceleration spectra (fig. 5.13), measured at the rear wheel axis during field tests performed on different road surfaces (Giubilato & Petrone, [7]), shows that more realistic results are obtained with the test bench equipped with the wooden dummy bottom.

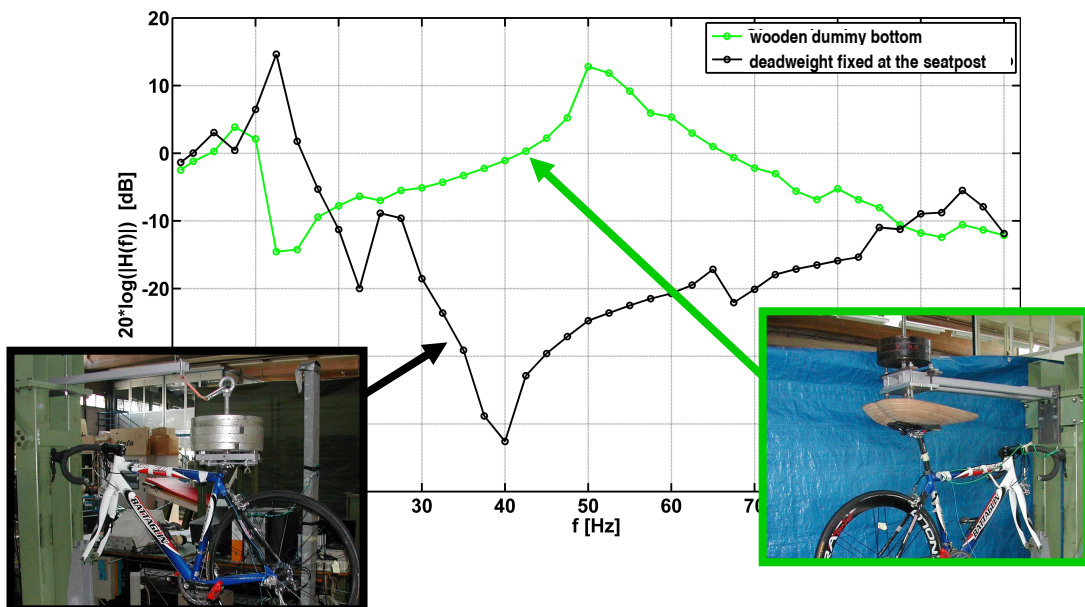


Fig. 5.12 Effect of the dead weights positioning system on the shape of the transfer function curves.

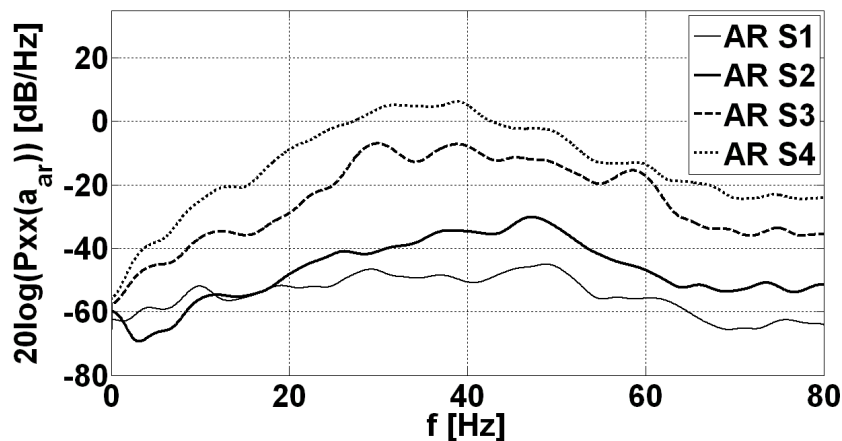


Fig. 5.13 PSD spectra of the acceleration signal measured at the rear wheel axes during field tests performed with the same wheelset, at a constant speed of 25 km/h, on road surfaces with different macrotexture (S1: smooth asphalt; S2: drainina asphalt; S3: city pavè; S4: cobblestones surface).



## 5.3 Swinging arm laboratory test method (Campagnolo lab.)

### 5.3.1 Adopted model

The test bench schematic is visible on figure 5.14.a. This schematic was developed in order to isolate the Wheel system from the other bicycle variables. The Wheel system is divided into the Rim and Tire subsystems (fig. 5.14.b), according to the approach adopted for the radial stiffness tests (see § 4.2). The input and the output of each system are represented by accelerations.

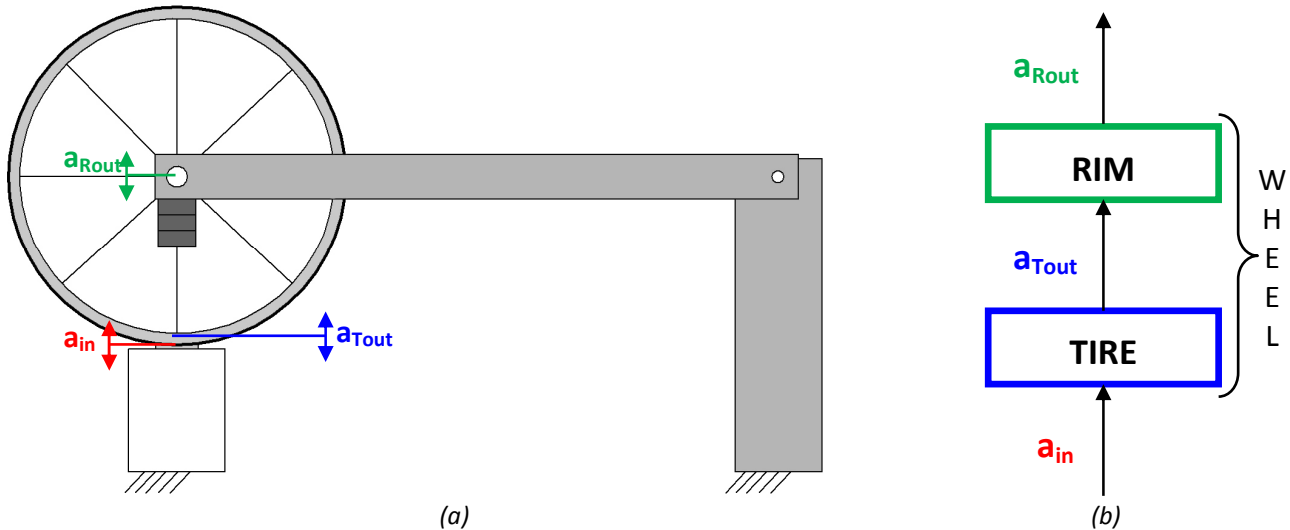


Fig. 5.14. (a) Schematic of the tests bench; (b) adopted model.

### 5.3.2 Test bench setup

The tested wheel axis was fixed at the free extremities of a 1 m long swinging arm (fig. 5.15, A) composed by two longitudinal beams and a transverse beam. The other extremities of the arm were hinged to two columns (B) constrained at the ground. An aluminium profile with a square section 90x90 mm was used for the columns and for the beams that compose the swinging arm. The tested wheel was resting on an aluminium plate (C) fixed on the shaker shaft. A static vertical load of 330 N was applied to the wheel fastening four cylindrical dead weights (26 kg total weight) at the free extremities of the swinging arm (D).

The LDS shaker (E) was leaning on the floor in vertical position, and its main characteristics are listed below:

- Maximum force: 489 N sine mode, 294 N random mode.
- Testing frequency range: 5 – 2400 Hz.
- Maximum displacement: 19 mm peak to peak.

The characteristics of the shaker were not suitable for testing the wheels with a static vertical load of 330 N. Two additional springs (fig. 5.16, F) were therefore positioned between the wheel support plate and a steel plate (G), integral to the frame of the shaker. These springs furnished an auxiliary force to the shaker during the static and dynamic wheel support. Since the tests were

performed in acceleration control mode, and since the accelerometer used by the controller of the shaker (H) was fixed on the upper face of the wheel support plate, the characteristics of the springs did not affect the tests execution.

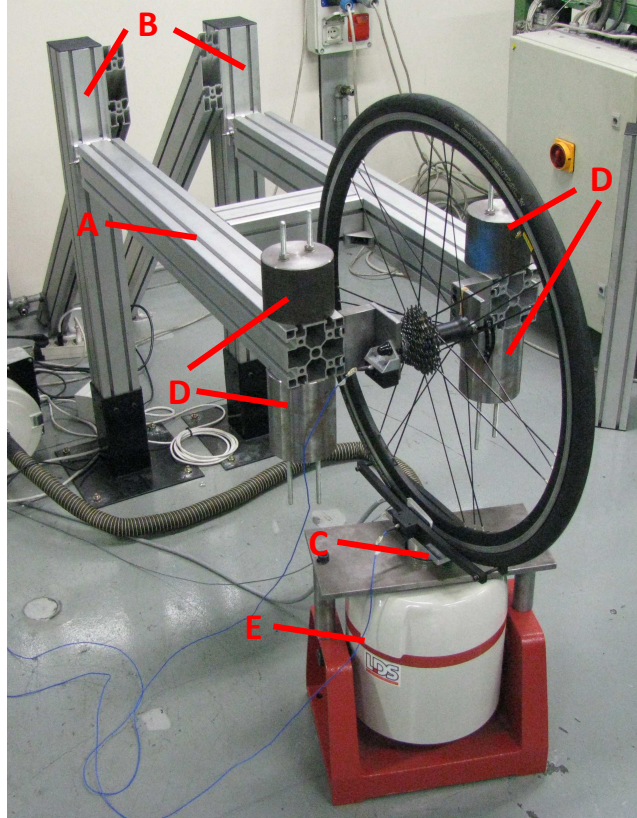


Fig. 5.15 Test bench. A: swinging arm; B: columns; C: wheel support plate; D: dead weights; E: LDS shaker.

### 5.3.3 Measuring system

Three uniaxial accelerometers were used for measuring the vertical acceleration at the wheel support plate  $a_{in}$  (fig. 5.16, H), at the rim braking surface  $a_{T_{out}}$  (I), and at the wheel axis  $a_{R_{out}}$  (L). The acceleration signal of the wheel support plate was sampled by the LDS control system of the shaker, and it was used for the testing control and for the measurement of the input quantity of the Wheel system (fig. 5.14). Since the LDS control system cannot sample more than two channels, the other two accelerometer signals were recorded at 1 kHz sampling frequency by means of an IMC PL2 data acquisition system. The accelerometer for the measurement of  $a_{T_{out}}$ , the output acceleration of the Tire system (fig. 5.14), was fixed to the rim braking surface through two horizontal rods (fig. 5.16), made in charged polymeric material, fastened together at the extremities by means of two screws. A thin rubber film with high friction coefficient was placed at the interface between the rods and the rim braking surface for deleting any relative motions between them. The accelerometer at the wheel axis was fixed to a stiff aluminium support fastened at the wheel lock. The accelerometers characteristics are summarized in table 5.4.

| CHANNEL NAME | ACCELEROMETER MODEL | MEASURING RANGE | FREQUENCY RANGE |
|--------------|---------------------|-----------------|-----------------|
| $a_{in}$     | DeltaTron 4513      | $\pm 500$ g     | 1 Hz – 10 kHz   |
| $a_{Tout}$   | SoMat HLS 1100      | $\pm 50$ g      | 0.3 Hz – 15 kHz |
| $a_{Rout}$   | SoMat HLS 1100      | $\pm 50$ g      | 0.3 Hz – 15 kHz |

Tab. 5.4 Characteristics of the accelerometers.

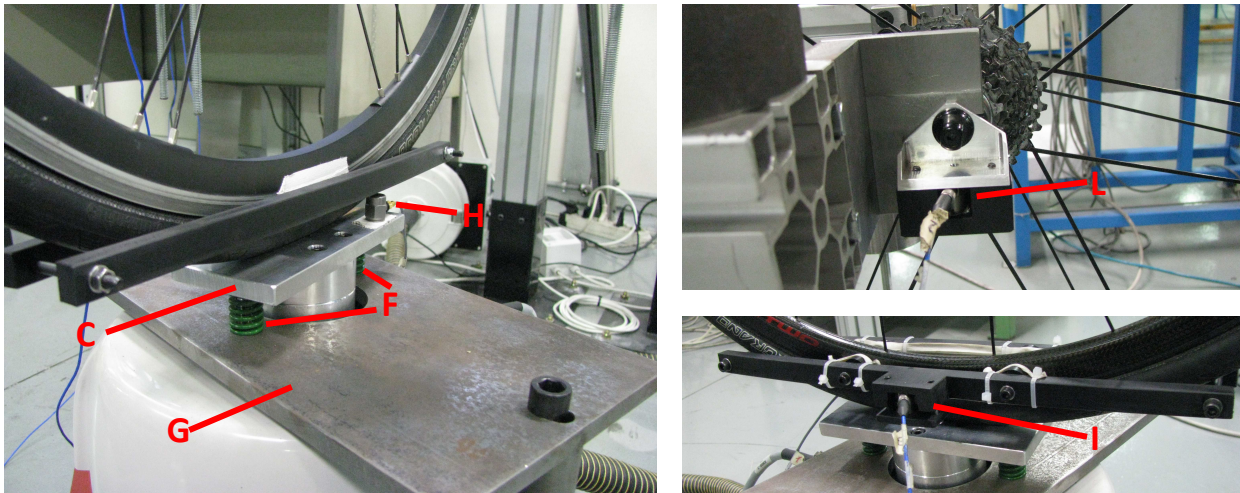


Fig. 5.16 Details of the test bench and of the measurement system. C: wheel support plate; F: auxiliary springs; G: steel plate fixed to the shaker frame; H: uniaxial accelerometer positioned on the wheel support plate; I: accelerometer positioned at the wheel braking surface; L: accelerometer positioned at the wheel axis.

### 5.3.4 Testing protocol

A sine continuous sweep, with  $\pm 0.3$  mm amplitude, from 16 to 50 Hz with a rate of 1 oct/min, and a total duration of 102 s was the shaker driving signal. The shaker was driven in acceleration control mode, and the drive signal was defined in the frequency domain.

On one hand, the sweep could not start from frequencies lower than 16 Hz for the following reasons:

- the shaker lowest testing frequency is equal to 5 Hz;
- in the  $10 \div 14$  Hz frequency range, the tire showed a resonance, causing a high amplitude of the wheel bouncing motion, which produced the overcoming of the shaker displacement limits.

On the other hand, the sweep maximum frequency was limited by shaker maximum force.

The figure 5.17 shows the spectra of the shaker shaft acceleration measured during a test. From 42 to 45 Hz the spectra showed an irregularity. A FEM modal analysis of a 1 m long beam in the free-free configuration, defined with the same section and material properties of the aluminium profile used for the test bench, showed that the beams used for the test bench structure have a first bending mode at a frequency of 54 Hz (fig. 5.18), and a second twisting mode corresponding

to 74 Hz (fig. 5.19). Since the first vibrational modes of the aluminium profiles correspond to frequencies close to the frequency range at which the irregular trend of the shaker shaft spectra is visible, this irregularity is probably caused by the resonance of the test bench structure, which affects the command executed by the shaker. This observation is confirmed by the noise emitted by the swinging arm while the shaker is crossing the 42 – 45 Hz range.

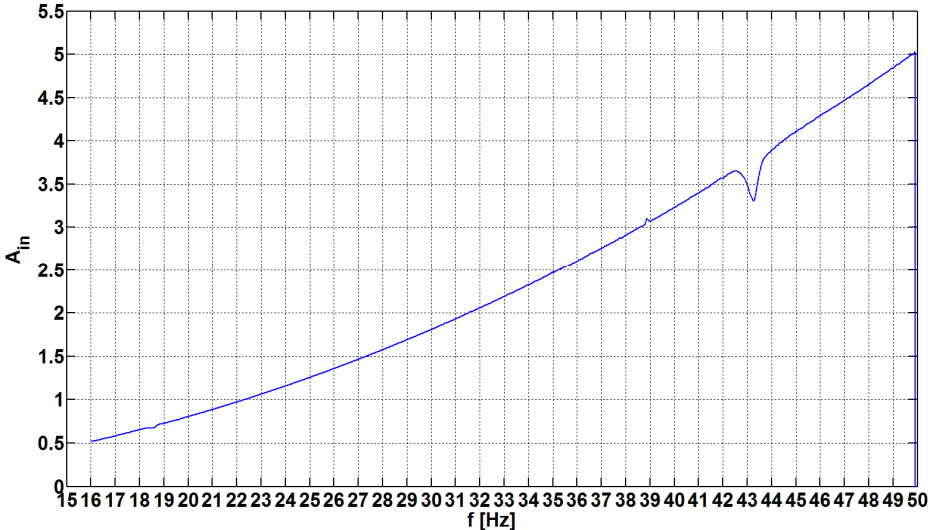


Fig. 5.17 Shaker shaft acceleration spectra measured during a test.



Fig. 5.18 First bending mode at 54 Hz of a 90x90 aluminium profile, 1 m long.

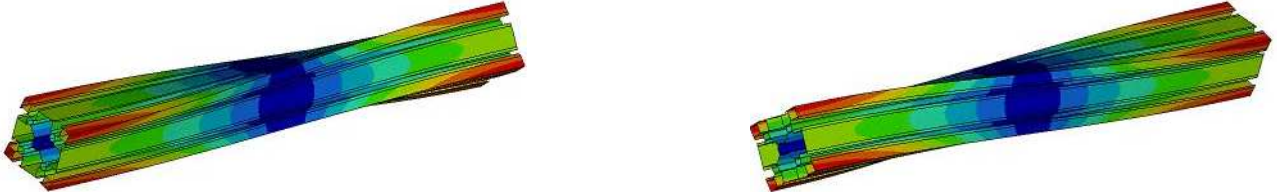


Fig. 5.19 Second twisting mode at 74 Hz of a 90x90 aluminium profile, 1 m long.

### 5.3.5 Data analysis

#### Frequency analysis of $a_{Rout}$ and $a_{Tout}$

The power spectral density (PSD) of the acceleration measured at the rim braking surface and at the wheel axle was performed applying the Welch method. Each signal acquisition was segmented into 100 sections with a duration of 10 s, each one with 90% overlap (1 s spacing) and windowed with a Hamming window.

The method adopted for the frequency analysis was chosen in order to smooth the spectra and the transfer function curves.

#### Rim transfer function computation

The transfer function of the Rim system was calculated as the ratio between the power spectral density of  $a_{Rout}$  and  $a_{Tout}$ .

$$H_R(f) = \frac{PSD(a_{Rout})}{PSD(a_{Tout})} \quad (2)$$

#### Tire transfer function computation

The measuring system configuration had been changed for the pilot tests carried out to analyse the tire behaviour. During these tests, the acceleration signals at the wheel support plate and at the rim braking surface ( $a_{in}$  and  $a_{Tout}$ ) were both recorded through the LDS shaker control system. This configuration was adopted because during these pilot tests only two accelerometers were available, therefore the acceleration at the wheel axis was not measure.

The Tire transfer function was directly calculated by the LDS controller as the ratio between the spectra obtained through the FFT of the input and output signals:

$$H_T(f) = \frac{A_{Tout}(f)}{A_{in}(f)} \quad (3)$$

### 5.3.6 Results

#### Rim transfer function

The Rim transfer function was calculated for three different front wheels (named EF, FF, GF) after a pilot test session. The wheels characteristics are summarized in table 5.5.

The Rim transfer function curves showed in figure 5.20 present a common shape characterized by a constant trend from 16 to 19 Hz, a discontinuity at 19 Hz, an increasing portion in the 19-29/30 Hz range, a peak between 29 and 30 Hz, a valley in the 33-37 Hz interval, a following asymptotic increasing trend with a discontinuity at 38 Hz.

The second discontinuity appeared at a double frequency of the first, probably caused by a resonance phenomenon of the test bench structure. A further more detailed analysis is therefore

needed to better understand this aspect.

The peak and the valley of three curves are characterized by different frequency and amplitude. The peak amplitude seems to be inversely correlated with the wheels radial stiffness, which is higher for the EF wheel (blue curve) and lower for the FF wheel (red curve). The radial stiffness is directly correlated with the rim depth, and thus inversely correlated with the spokes length. The wheels transmissibility of the small amplitude vibrations seems therefore to be directly correlated with the spokes length: wheels with longer spokes transmit fewer vibrations. A deeper rim absorbs more vibrations than an equivalent tensioned spoke portion with a length equal to the rim depth. This observation is based on the preliminary results, while more results related to different wheel models are needed to confirm it.

| Wheel | Rim depth         | Rim material | Rim radial stiffness | Hub material | Spokes Nr. | Spokes Pattern | Spokes material | Mass  |
|-------|-------------------|--------------|----------------------|--------------|------------|----------------|-----------------|-------|
| EF    | High<br>H 105 mm  | Composite    | 4780 N/mm            | Aluminium    | 16         | Radial         | Steel           | 873 g |
| FF    | Low<br>H 20 mm    | Composite    | 2000 N/mm            | Composite    | 22         | Radial         | Steel           | 590 g |
| GF    | Medium<br>H 35 mm | Aluminium    | 2370 N/mm            | Aluminium    | 16         | Radial         | Steel           | 653 g |

Tab. 5.5 Tested front wheels characteristics.

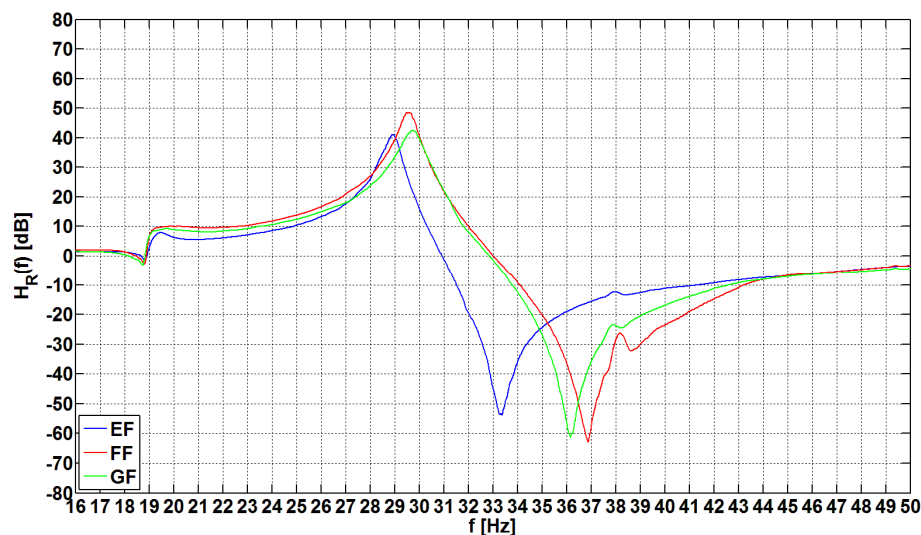


Fig. 5.20 Transfer function curves calculated for the Rim system of three different front wheels.

### Tire transfer function

The figure 5.21 shows the transfer function calculated for the same tire assembled on a wheel with or without the inner tube in the tubeless configuration. The tests were performed keeping the pressure at a constant value of 6 bar.

The curves present the same discontinuity observed for the Rim transfer function at 19 Hz. They present a decreasing trend until 38 Hz where there is a valley, while after the valley the curves

amplitude increasing with the frequency reaching a peak at 45-46 Hz. The curves valley corresponds to the second discontinuity observed in the Rim curves, a further analysis is needed in order to verify if there are any correlations between them. The differences in terms of amplitude and frequency observed between the two curves at the valley and peak does not find any correspondences in a theoretical analysis of the tires damping behaviour.

During the tests performed for defining the definitive testing protocol, a wheel bouncing motion was observed in the frequency range of 10-14 Hz, which caused the stop of the tests due to the overcoming of the shaker displacement limits. In this range is therefore supposed to be a tire resonance.

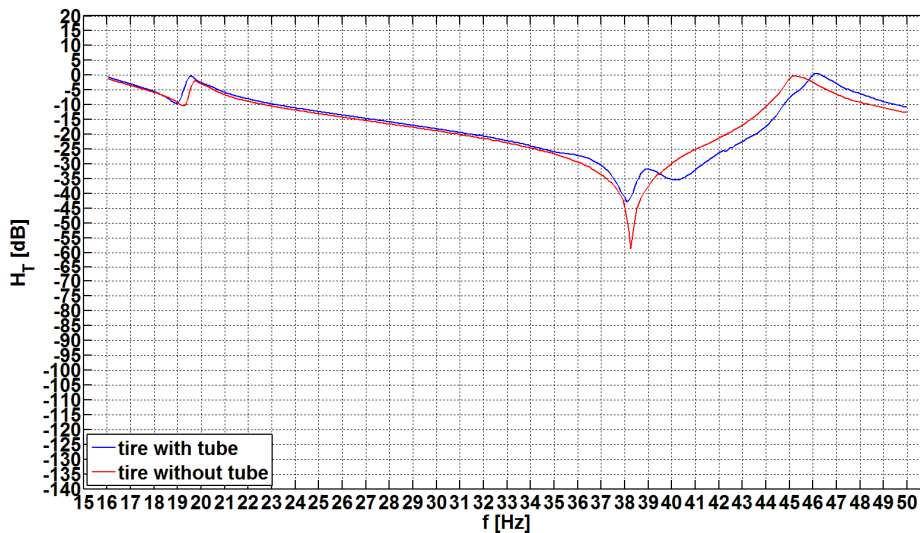


Fig. 5.21 Tire transfer function calculated for a tire with the tube and in the tubeless configuration.

## 5.4 Conclusions and possible further developments

The methods developed allow the evaluation of the wheels vibrational transmissibility.

The transfer function obtained for different wheel models, after the full bicycle laboratory tests, showed a similar shape, which agreed with the acceleration spectra measured at the rear wheel axis during the field tests performed on different road surfaces. This aspect testified that the real load and constraint systems were well reproduced in the test bench developed. A limitation of the present study is, however, the use of a wooden dummy, which stiffness and damping behaviours have significant differences with respect to the real presence of soft tissues in a real cyclist body. Further developments of the present work will therefore include the presence of a real rider sitting on the saddle, gripping the handlebar and having the shoes connected to clipless pedals: synchronously to the frequency sweep, the rider will be asked to express his subjective evaluation of the degree of discomfort felt at different body parts, to obtain also a perceived comfort ranking to compare with the vibration ranking presented in table 5.3. The ranking between different wheels in terms of vibrational comfort properties varies with the frequency range considered. This aspect highlights the effect of the tire, which can mask the Rim system behaviour. A further study of the tire characteristics using this method represents a useful further research activity. The

method proposed in the present study can be applied for measuring the vibration transmissibility of other bicycles components (such as frame, seatpost, saddle, fork, stem, handlebar..), whose structural behaviour can affect the entity of vibrations perceived by the cyclist during cycling on irregular roads. The contribution of each component to the vibration damping or amplification can be therefore quantified and compared at different frequency ranges reproducing the real load and constraint conditions.

The real load and constraint conditions were not well reproduced in the swinging arm laboratory test method developed in Campagnolo laboratories, which represented a conventional test method. This test method was limited by the materials available for the test bench setup. The low stiffness of the test bench structure produced resonance phenomena of the structure, which affected the tests results. The maximum force and the frequency range of the shaker resulted to be not suitable for the tests even if the force limitations were overcome with an engineering solution, which did not affect the test execution. The results showed an inverse correlation between the wheels vibration transmissibility and the radial stiffness that has to be confirmed by additional tests. The test bench can be improved following the same schematic but adopting a more stiff structure, a shaker with a higher maximum force and a frequency range that starts from a lower level.





# Chapter 6

## Saddles vibration transmissibility

### 6.1 Introduction

The modern construction of bicycle saddles expresses the research of manufacturers towards saddle concepts, construction, and production technologies, in order to satisfy the user requirements of optimal pressure distribution, vibration damping, friction properties, and thermal/perspiration qualities, all combined with the minimum cost and mass.

Aim of this work was to develop an experimental method to measure and compare the saddle vibration transmissibility as an engineering product characteristics. On the basis of the former methods developed for evaluating the wheels vibrational transmissibility (chapter 5), and of the former experiences of the research group applied to the study of bicycle shorts [4], a new laboratory test method was developed to evaluate the vibration transmissibility of different bicycle saddles models in terms of trend and magnitude of their transfer functions.

### 6.2 Adopted model

The test bench schematic is visible on figure 6.1.a. The test bench was developed for measuring the vibration transmissibility of the **Saddle** system **S** (fig. 6.1.b). The input and output considered for the system are:

- Input:  $\mathbf{a}_{in}$ . Vertical acceleration imposed by means of the actuator shaft motion.
- Output:  $\mathbf{a}_{out}$ . Vertical acceleration of the upper surface of the wooden dummy bottom measured at the rear wheel axis.

The saddle fixation device and the wooden dummy bottom were supposed to have negligible damping characteristics if compared with the saddles characteristics.

The Saddle system is commonly composed by an upper shell, covered by a soft padding and a top cover, giving the external shape to the saddle, constrained at the tail and the nose to the rails, which are clamped to the seatpost within their straight portion. Since the rails stiffness is higher if compared with the other components, the Saddle damping behaviour is theoretically mainly affected by the shell and the padding characteristics.

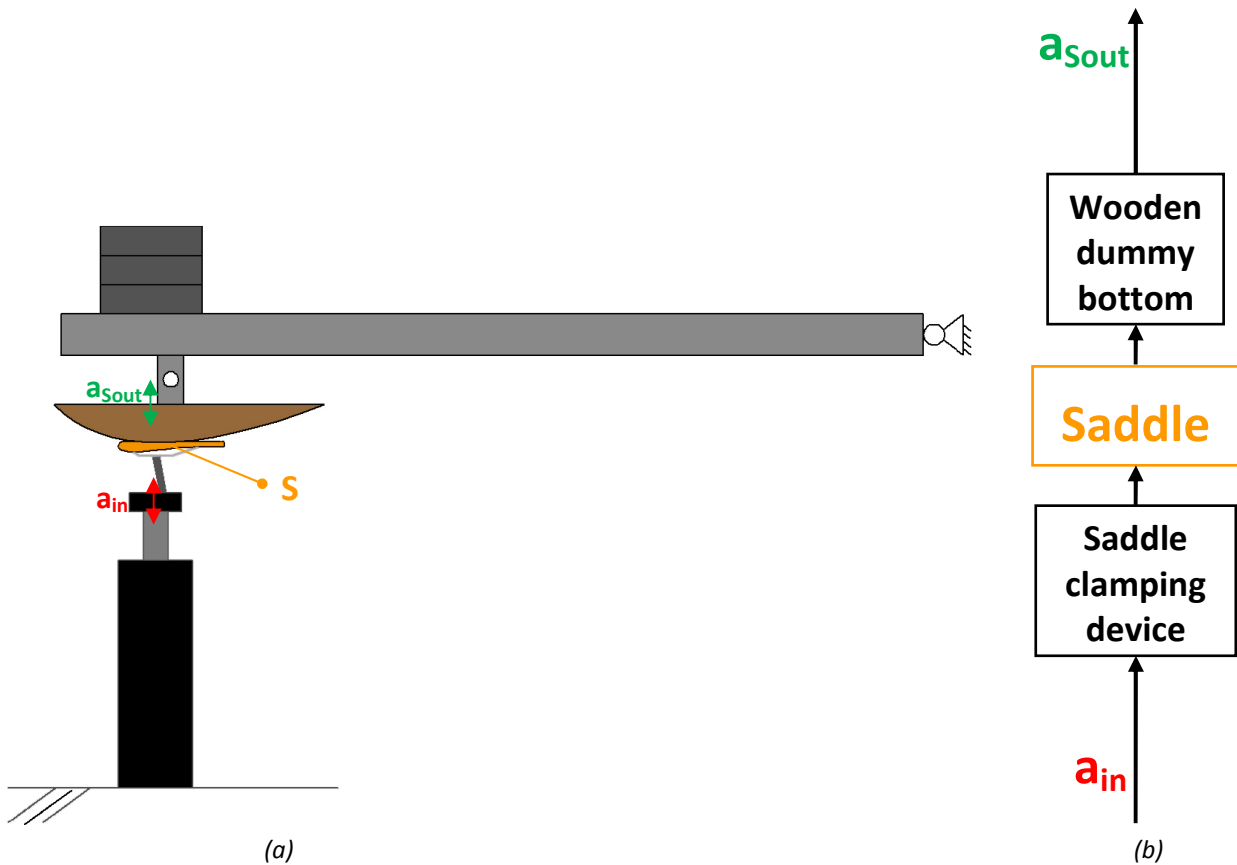


Fig. 6.1. (a) Schematic of the tests bench; (b) adopted model.

### 6.3 Test bench setup

A commercial aluminium seatpost was cut at about 50 mm from the saddle clamp and welded to an adaptor aluminium plate (fig. 6.3) to fix it to the 15 kN load cell of a 200 mm stroke vertical MTS 242 servohydraulic cylinder. The vertical axis of the cylinder was therefore intentionally in line with the centre of the saddle clamp (fig. 6.2).

The static vertical load acting on the saddle was applied by a wooden dummy bottom (fig. 6.2, C) shaped according to UNI 10814, usually employed for the durability tests of chairs. The dummy was free of swivel about three axis by means of a ball-socket joint connected to a steel swinging arm (B) hinged horizontally to a fixed structure 1.3 m apart. The dummy was resting on the saddle (D), and it was loaded by a set of dead weights (A) in order to have a total static load of 50 kg on the saddle, as measured by the cylinder load cell (G).

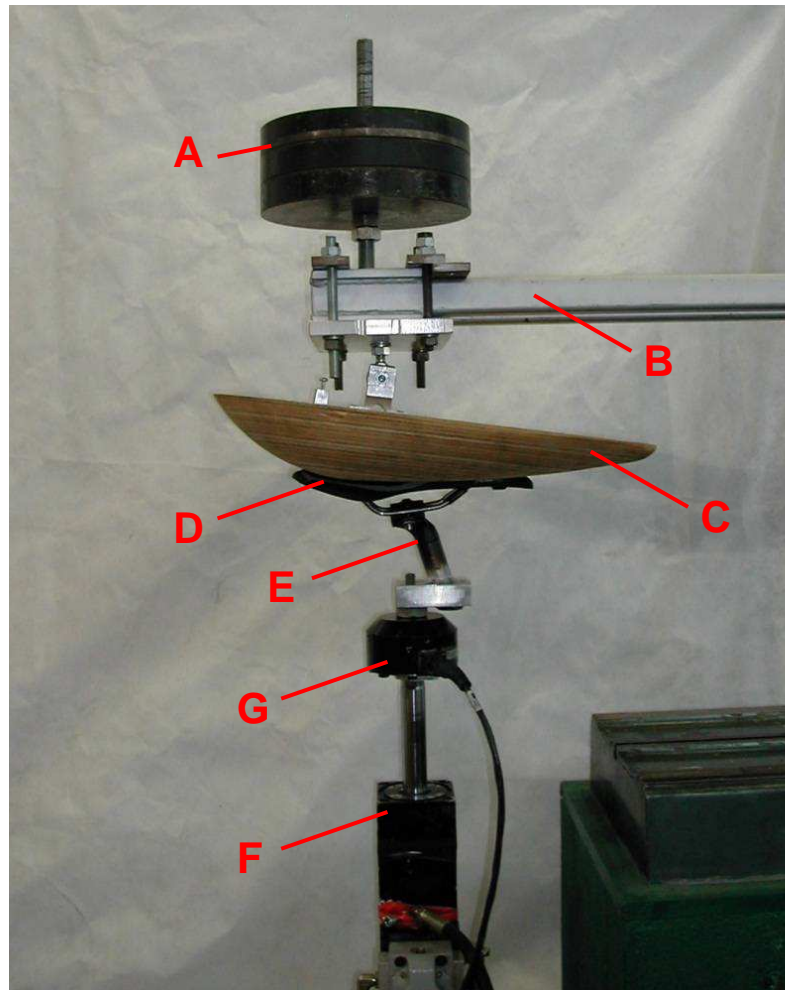
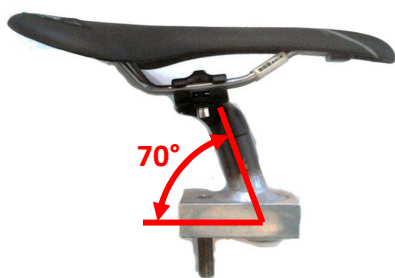
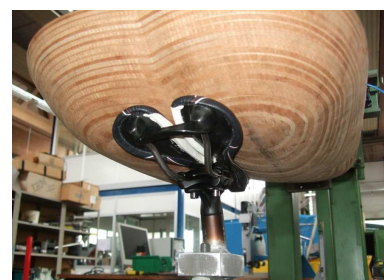


Fig. 6.2 Test bench: (A) Dead weights of 34.5 kg; (B) Swinging arm and ball joint fixation system; (C) Wooden dummy bottom (D) Saddle under test; (E) Seatpost; (F) Servohydraulic cylinder.



(a)



(b)

Fig. 6.3. (a) Particular of the saddle clamping device; (b) view from the bottom of the Dummy-Saddle interface.

### 6.3.1 Saddle and wooden dummy bottom positioning

The longitudinal mean axis  $x$  on the saddle upper surface was considered as the saddle reference system (fig. 6.4). Its origin corresponds to the shell section 75 mm wide. This section is considered by the saddles manufacturing for conventionally identifying the contact point between the saddle and the perineum region.

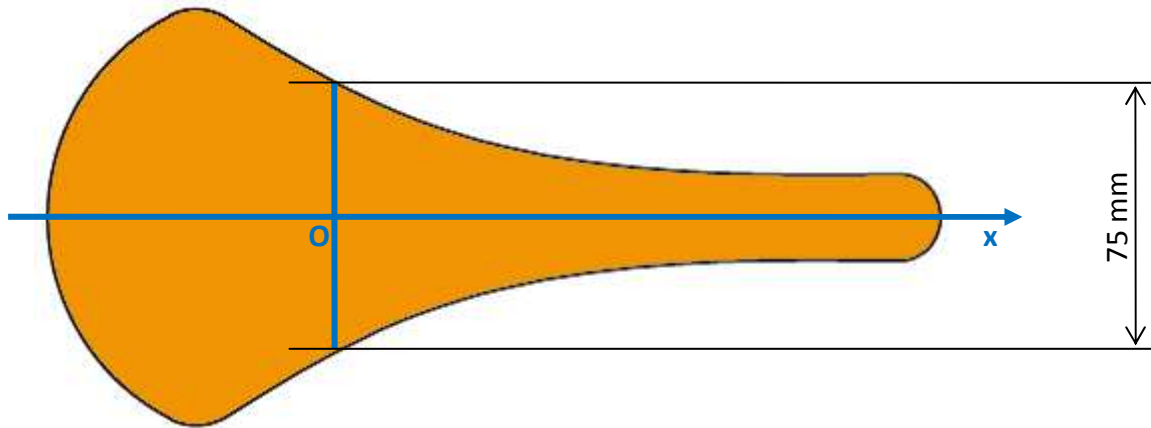


Fig. 6.4 Reference system defined for the saddle upper surface.

The saddles were consistently clamped in the middle of the rails straight portion, with null roll and pitch angles with respect to the horizontal plane tangential to the upper surface at the origin of the x-axis, measured by means of a digital inclinometer (fig. 6.5).

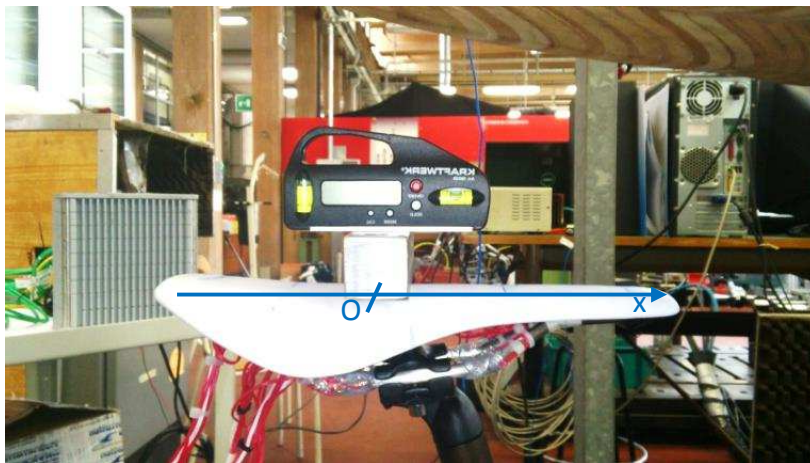


Fig. 6.5 Positioning of the saddle.

The wooden dummy bottom was fixed through a ball joint to one of the two steel plates used for fixing the dead weights to the swinging beam (fig. 6.6). The relative position between the saddle and the dummy bottom was identified by the longitudinal distance  $x_{DW}$  (the subscript "D" stays for Dead Weights) of the dead weights vertical axis from the origin of saddle reference system (fig. 6.6).

A saddle instrumented with strain gauges placed on different positions of the rails and of the shell lower surface [35] was used for defining the standard position of the wooden dummy bottom. The static saddle deformation was measured with a cyclist (1.80 m height, 70 kg weight) on a medium size racing bicycle in a static position grabbing the handlebar at upper surface of the shift derailleurs commands. The shell deformed configuration obtained during this test was compared to the shell deformation resulted from a static test carried out positioning the dummy bottom in

four different longitudinal positions:

- $x_{DW} = -4 \text{ mm}, +10 \text{ mm}, +16 \text{ mm}, +36 \text{ mm}$

The deformation of the shell obtained with the cyclist resting on the bicycle and with the dummy bottom in the four positions is respectively showed in figure 6.7.a and 6.7.b-e. The diagrams report the deformation normalized respect to the highest epsilon value obtained from the test. The stacked lines reports the normalized epsilon measured for the longitudinal strain channels along the shell s-axis. The longitudinal shell s-axis is on the middle of the shell lower surface, its coordinates increasing from points close to the tail ( $s=0$ ) to points close to the tip ( $s=182$ ). The bar at  $s=92$  reports the normalized transverse strain measured on the s-axis at  $s=92 \text{ mm}$ . The bars at  $\epsilon_x(y40)$  and  $\epsilon_y(y40)$  are relative to the normalized epsilon, respectively for the x and y strain measured by the strain gauge placed laterally at  $y=40 \text{ mm}$ .

The best results were obtained for  $x_{DW} = +16 \text{ mm}$  (fig. 6.7.d). This was therefore chosen as the standard testing configuration.

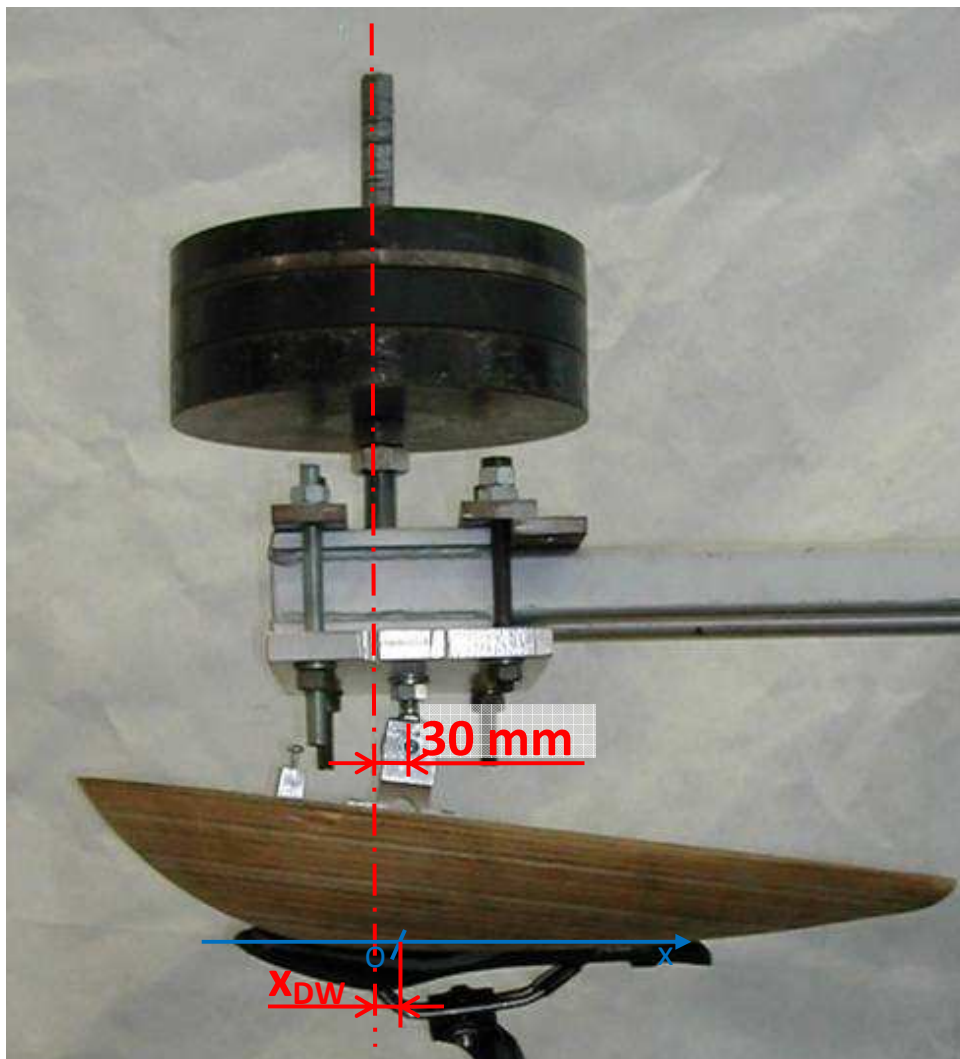


Fig. 6.6 Identification of the position of the wooden dummy bottom.

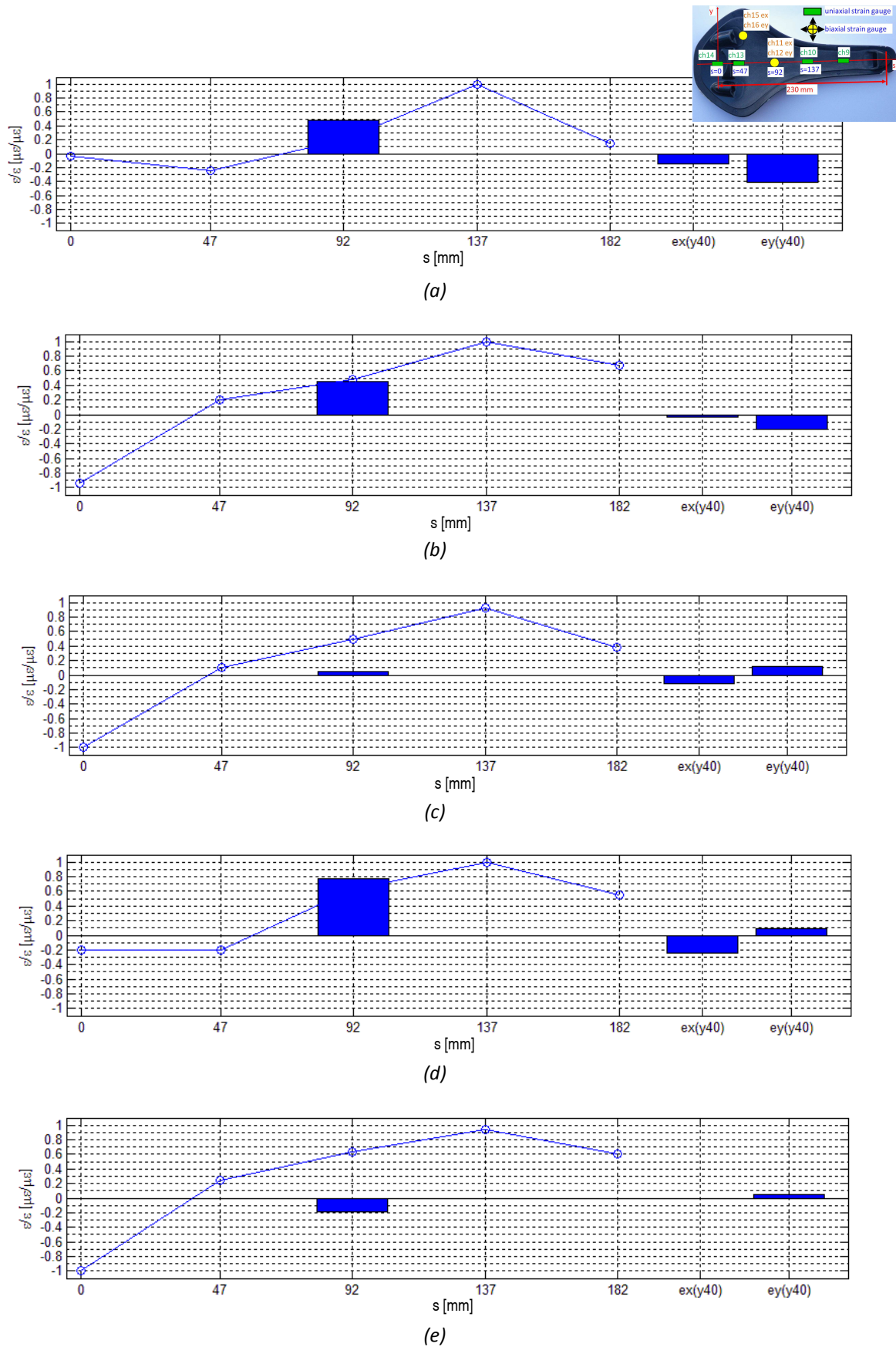


Fig. 6.7 Shell deformed configuration: (a) cyclist in static position; (b)  $x_{DW}=-4$ ; (c)  $x_{DW}=+10$ ; (d)  $x_{DW}=+16$ ; (e)  $x_{DW}=-36$ .

## 6.4 Measuring system

The vertical acceleration of the cylinder shaft ( $a_{in}$ , fig. 6.8.a, H) and at the dummy bottom upper surface ( $a_{out}$ , fig. 6.8.b, I) were measured by two uni-axial piezoelectric accelerometers, model SoMat HLS 1100 (+/- 50 g full scale, 0.3 - 15000 Hz bandpass).

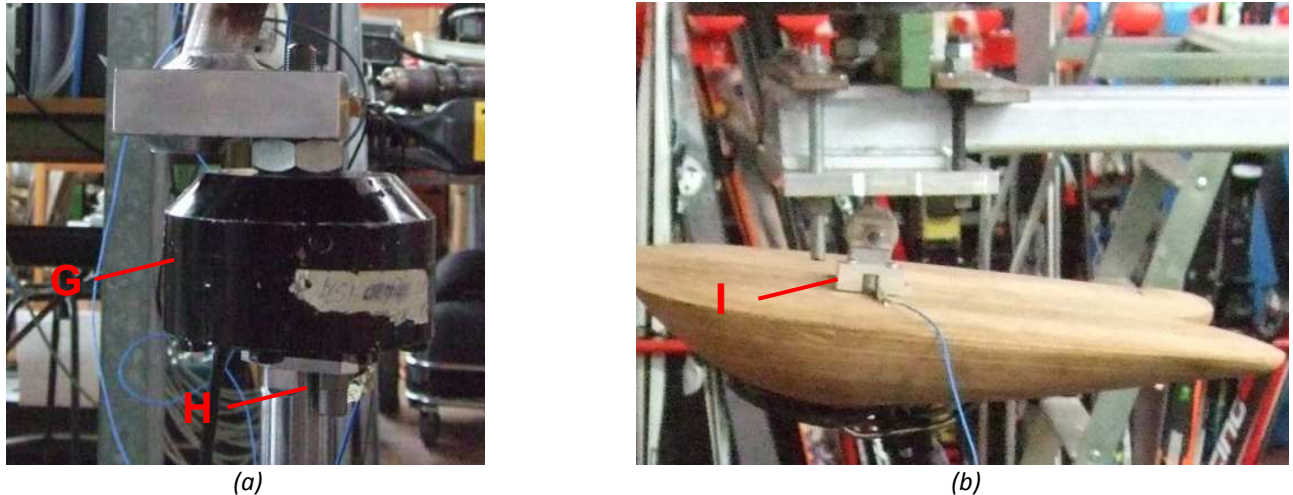


Fig. 6.8. (a) G: cylinder load cell; H: accelerometer fixed to the cylinder shaft; (b) I: uni-axial accelerometer fixed to the upper surface of the dummy bottom.

Acceleration signals were recorded by means of SoMat eDAQ Lite acquisition system, at 5 kHz sampling rate.

The cylinder shaft displacement was measured through its internal LVDT ( $\pm 100$  mm stroke), and recorded by means of the MTS test bench control system.

## 6.5 Saddles considered for the tests

Six saddles were selected for the study. The saddles were produced by different manufacturers, and were different for geometric dimensions, shell construction, and padding thickness; the saddles A-E were for MTB or racing bicycle, whereas the saddle F, which presented the biggest dimensions and the highest padding thickness, was for a comfort city bike use. The table 6.1 shows the geometrical properties of the tested saddles, no data concerning their stiffness or the properties of their materials were available.

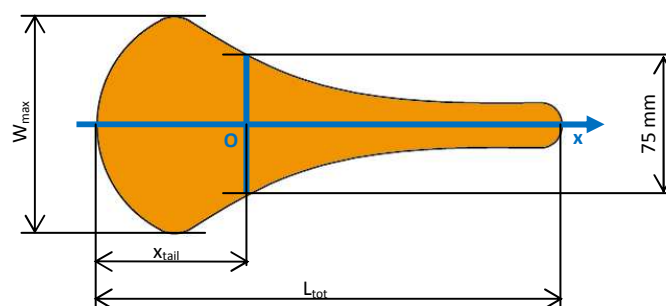








Fig. 6.9 Main geometrical characteristics of the saddles.



| Saddle  | $L_{tot}$ : total length [mm] | $W_{max}$ : maximum width [mm] | $t_p$ : padding thickness at 75mm width [mm] | $X_{tail}$ : longitudinal distance of the tail from the 75 mm width point [mm] |
|---|-------------------------------|--------------------------------|--|--|
| <b>Saddle A: Fizik Antares</b><br>             | 27.1                          | 14.5                           | 4.2  | 11.2   |
| <b>Saddle B: Fizik Gobi</b><br>                | 27.5                          | 12.5                           | 5.0  | 12.2   |
| <b>Saddle C: Selle Bassano Mission</b><br>    | 27.0                          | 13.2                           | 5.0  | 11.0   |
| <b>Saddle D: Selle Italia Flite</b><br>      | 27.7                          | 14.3                           | 5.1  | 13.0   |
| <b>Saddle E: Selle San Marco Aspide</b><br>  | 27.6                          | 13.2                           | 4.0  | 11.1   |
| <b>Saddle F: Selle Italia Air Active</b><br> | 26.2                          | 17.4                           | 7.5  | 14.3   |

Tab. 6.1 Geometrical characteristics of the tested saddles.

## 6.6 Testing protocol

The actuator drive signal was the same used for the characterization of the wheels vibration transmissibility by means of the full bicycle laboratory test (see § 5.2.5). During the test, each saddle was excited by the actuator shaft vertical displacement, reproducing a sine function of 0.6 mm constant amplitude, and sweeping in frequency. The actuator drive signal (fig. 6.10) was divided into blocks, each block characterized by a different frequency level starting from 1 Hz, and ending at 100 Hz, with discrete frequency increments of 2.5 Hz from 2.5 to 100 Hz.

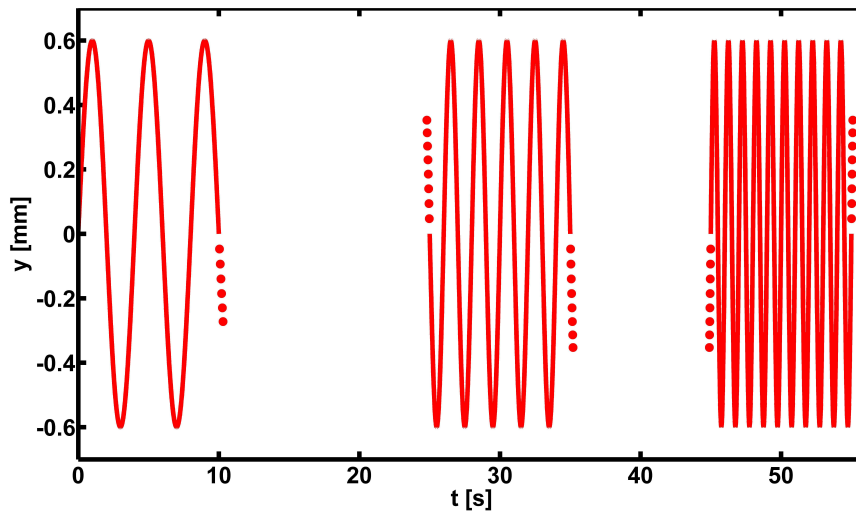


Fig. 6.10 Actuator drive signal.

| Block nr. | f [Hz] | Block nr. | f [Hz] | Block nr. | f [Hz] | Block nr. | f [Hz] |
|-----------|--------|-----------|--------|-----------|--------|-----------|--------|
| 1         | 1.0    | 11        | 25.0   | 21        | 50.0   | 31        | 75.0   |
| 2         | 2.5    | 12        | 27.5   | 22        | 52.5   | 32        | 77.5   |
| 3         | 5.0    | 13        | 30.0   | 23        | 55.0   | 33        | 80.0   |
| 4         | 7.5    | 14        | 32.5   | 24        | 57.5   | 34        | 82.5   |
| 5         | 10.0   | 15        | 35.0   | 25        | 60.0   | 35        | 85.0   |
| 6         | 12.5   | 16        | 37.5   | 26        | 62.5   | 36        | 87.5   |
| 7         | 15.0   | 17        | 40.0   | 27        | 65.0   | 37        | 90.0   |
| 8         | 17.5   | 18        | 42.5   | 28        | 67.5   | 38        | 92.5   |
| 9         | 20.0   | 19        | 45.0   | 29        | 70.0   | 39        | 95.0   |
| 10        | 22.5   | 20        | 47.5   | 30        | 72.5   | 40        | 97.5   |
|           |        |           |        |           |        | 41        | 100.0  |

Tab. 6.2 Frequency level corresponding to each drive signal block.

## 6.7 Data analysis

The methods employed for the frequency analysis of the acceleration signals and for the transfer function computation are the same adopted during the data analysis of the wheels vibration transmissibility tests (see § 5.2.6). The methods are here presented again for giving a complete treatise of the overall method. In addition to them, the saddle comfort index computation is

presented in the following paragraphs.

Frequency analysis of the acceleration signals

A frequency analysis of both actuator shaft (**input**) and Dummy (**output**) acceleration signals was performed for each command block (fig. 5.6). Discrete Fourier transform DFT of signals was computed by FFT algorithm. In order to obtain leakage-free spectrums with 0.1 Hz resolution, a total of 50000 samples was considered on each FFT execution, corresponding to an integer number of input sine function periods.

The analysis of each input acceleration spectrum  $A_{in}(f)$  was performed to verify the correct execution of the related command block.

The characteristics of the frequency analysis are summarized below:

- FFT algorithm for the DFT computation.
- Sampling frequency  $f_s = 5$  kHz.
- Rectangular window for each block.
- Block window length: 50000 points, 10 s period -> integer number of input sine function periods for a leakage-free spectra.
- Spectra frequency resolution = 0.1 Hz.

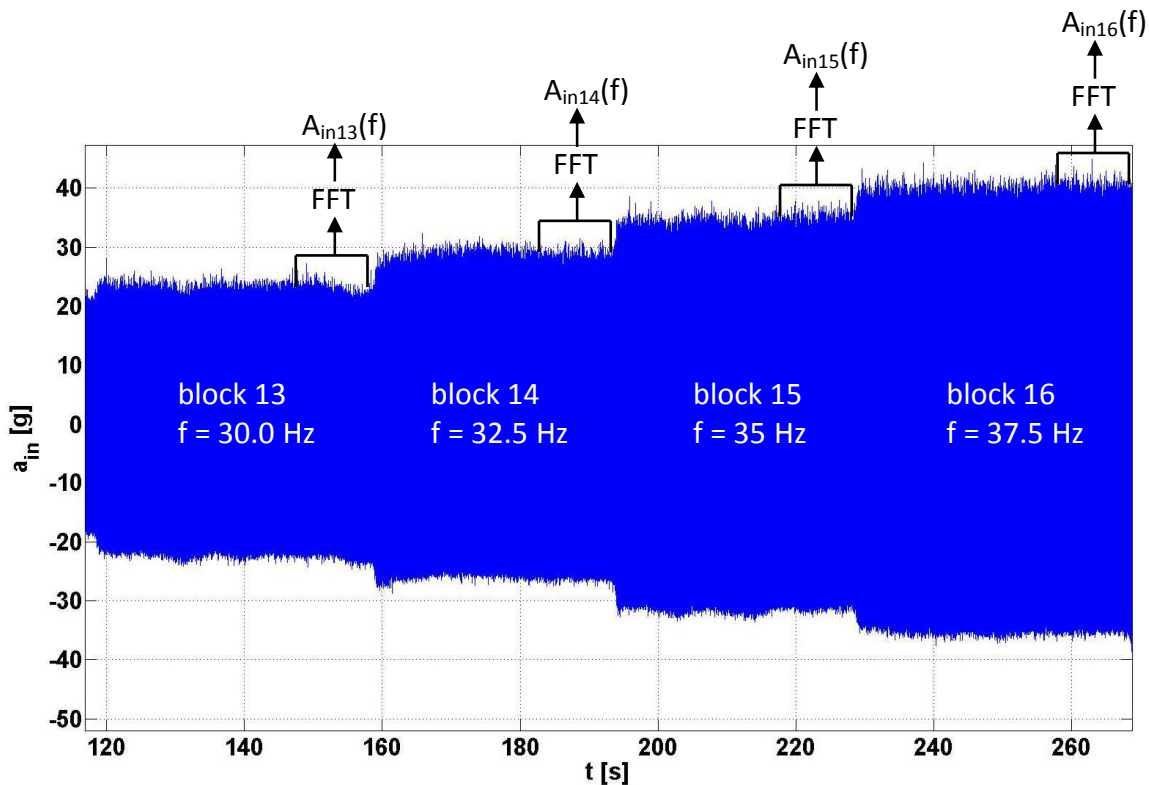


Fig. 6.11 Example of the blocks selection for the FFT computation of the  $a_{in}(t)$  signal.

### Transfer function computation

Transfer function magnitude  $|H_{s,k}(f)|$  (fig. 5.7) was calculated for each k-th tested saddle, point by point at each excitation frequency  $f_i$ . Each transfer function value  $|H_{s,k}(f_i)|$  was calculated as the ratio between the output spectrum magnitude peak value  $|A_{sout,k}(f_i)|$ , calculated at the excitation frequency, and the corresponding input spectrum magnitude  $|A_{in,k}(f_i)|$  as expressed in (1).

$$|H_{s,k}(f_i)| = \frac{|A_{sout,k}(f_i)|}{|A_{in,k}(f_i)|} \quad (1)$$

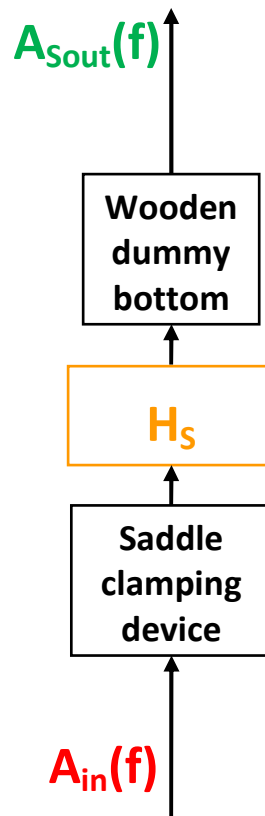


Fig. 6.12 Schematic of the saddle input/output relationship.

Transfer functions obtained from equation (1) were weighted by the frequency weighting curve  $W_k$  proposed by ISO 2631-1 [12], which expresses the human body sensibility in seated position along the vertical Z axis (fig. 6.13).

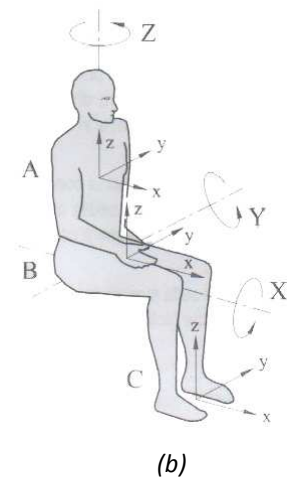
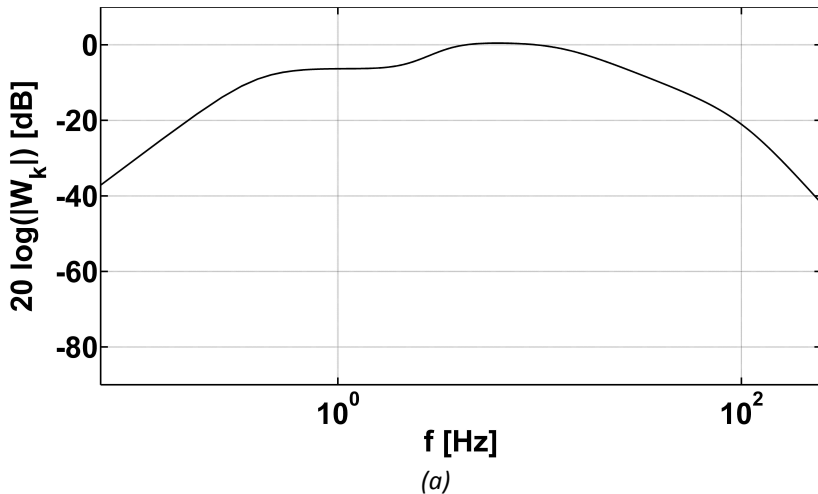


Fig. 6.13. (a) Frequency weighting curve  $W_k$ ; (b) orthogonal axis of human body in seated position.

Comfort index computation

A Vibrational Comfort Index, based on the inverse value of the area below the transfer function curve in the 1- F Hz interval (fig. 6.14), was introduced as a possible engineering characterization of saddles (2). Both the original transfer functions and the ISO weighted transfer functions were used for the index calculation.

$$VCI_F = \frac{1}{\int_1^F H(f)df} \quad F = 100\text{Hz} , 40\text{Kz} \tag{2}$$

From the observation that only in the interval between 1 Hz and 40 Hz the weight function showed values higher than -10 db (fig. 6.13.a), the VCI values were calculated over the full range (F = 100 Hz) and the smaller range of higher human sensibility (F = 40 Hz).

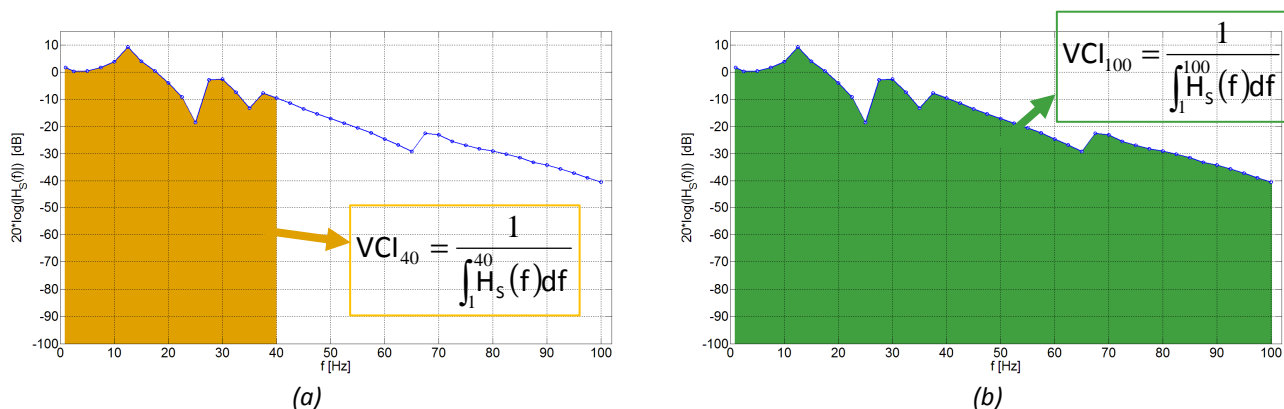


Fig. 6.14 Vibrational comfort index computation: (a)  $VCI_{40}$ ; (b)  $VCI_{100}$ .

## 6.8 Results

The shape of the curves originally obtained for the six saddles resulted to be similar (fig 6.15): it was characterized by a main resonance peak around 10 Hz, with a transmissibility magnitude around 10-15 dB, and minor peaks between 25 and 30 Hz, where transmissibility magnitude resulted around -5 dB. From 25-30 Hz onwards, all saddles tended to attenuate vibrations, and the transmissibility magnitude were all lower than - 40 dB at 100 Hz. The weighted curves (fig 6.16) present the same shape of the originals, and progressive lower amplitude from frequencies greater than 15 Hz.

High differences between the curves can be seen for all the testing frequencies. The ranking of saddles vibration based on the transmissibility curves resulted to vary with the frequency range. The saddle F, which was for city bike/comfort use and presented the highest padding thickness and the biggest dimensions, showed the lowest amplitude for the main peak, a sharp valley at 87.5 Hz, and constant low amplitude in the curve portions with a monotonic decreasing trend. These results are confirmed by the vibrational comfort indexes calculated considering both the original ( $VCI_{100}$ ,  $VCI_{40}$ , fig. 6.17), and the weighted curves ( $VCI_{W100}$ ,  $VCI_{W40}$ , fig. 6.18): all the highest indexes values had been calculated for the saddle F. The saddle F resulted therefore the most comfortable from a vibrational point of view.

The same ranking between the vibrational transmissibility of the tested wheels was obtained considering the  $VCI_{100}$  and the  $VCI_{40}$ . The two indexes  $VCI_{W100}$  and  $VCI_{W40}$  (fig. 6.18) calculated for the weighted curves resulted respectively +20% and +26% greater than the corresponding indexes (fig. 6.17) calculated for the original curves. The ranking among the tested wheels is different if we consider the indexes calculated for the original curves or for the weighted curves: the saddles B and C resulted more comfortable than the saddle A, considering the  $VCI_{100}$  (fig. 6.17.a) and, contrarily, less comfortable if we consider the  $VCI_{W100}$  (fig. 6.18.a). These results suggest the need of performing a subjective evaluation test session in order to definitely correlate the cyclists saddle comfort evaluation results with the engineering results, and to identify which  $VCI_F$  formulation expresses in the most proper way the cyclist's feelings. If we consider the sports saddles (saddles A-E), the highest VCI values were calculated for the saddle D, which had the oldest construction characteristics, and presented the highest padding thickness. The indexes calculated for the other four saddles (saddle A, B, C, E), which were all modern saddles with the same destination of use and with comparable main dimensions, do not show high differences.

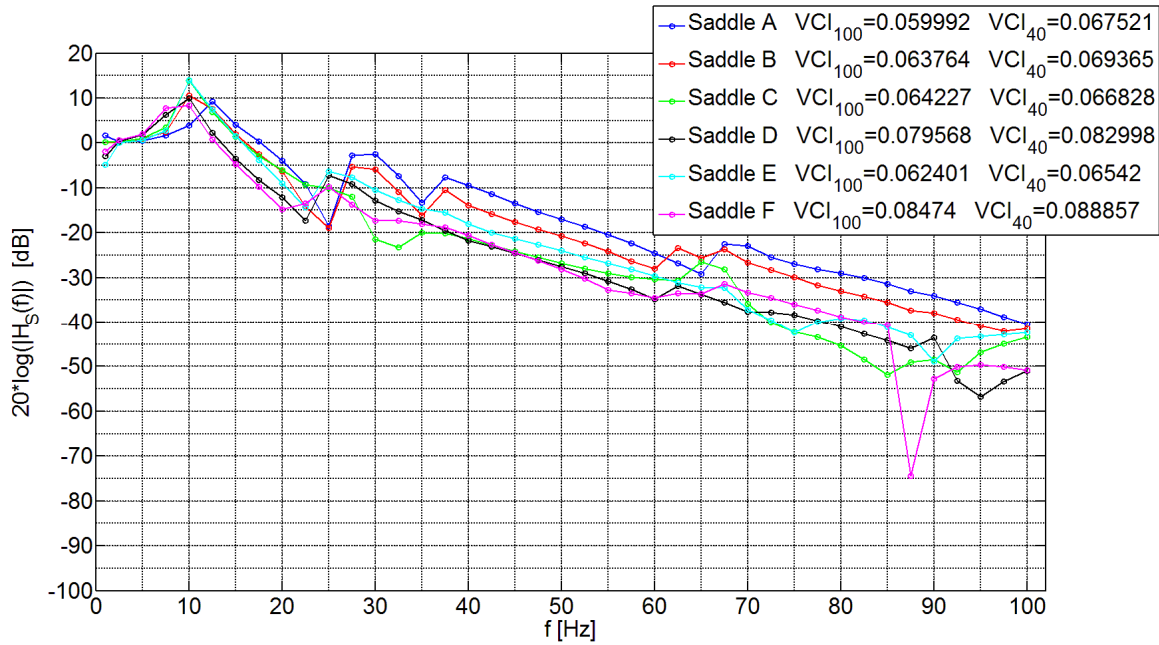


Fig. 6.15 Transfer function curves resulted for the six tested saddles with the wooden dummy bottom in the standard position ( $x_{DW} = +16$  mm).

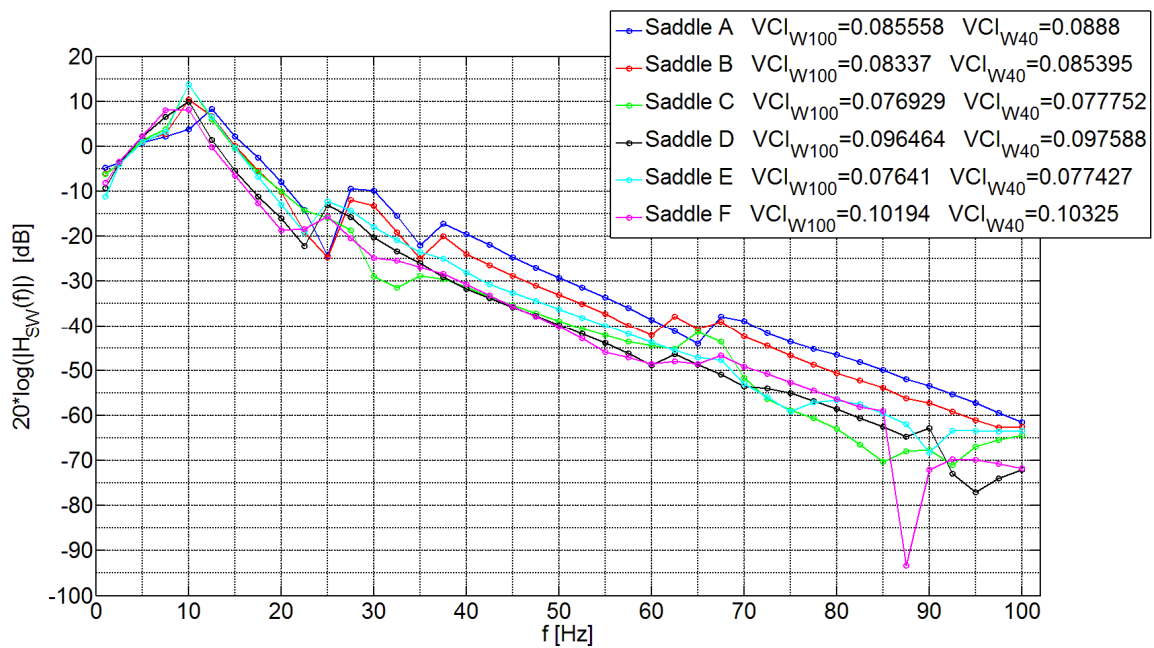


Fig. 6.16 Transfer function curves weighted through the  $W_k$  weighting curve (ISO 2631 [12]) with the wooden dummy bottom in the standard position ( $x_{DW} = +16$  mm).

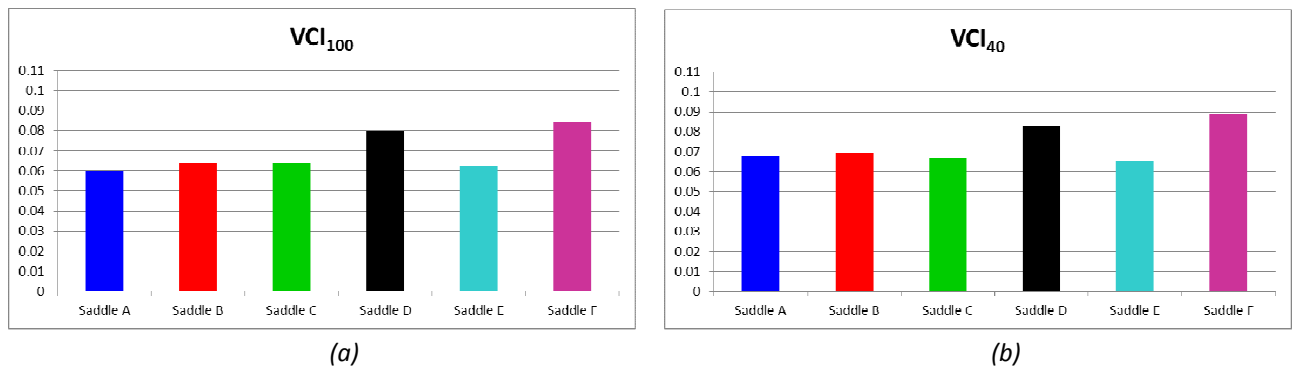


Fig. 6.17 Vibrational comfort indexes calculated considering the original curves from 1 to 100 Hz (a) and from 1 to 40 Hz (b).

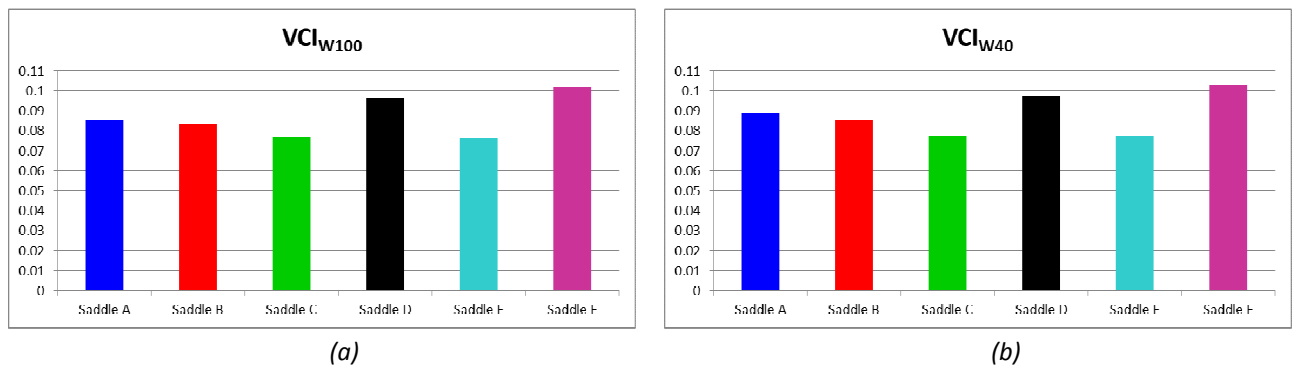


Fig. 6.17 Vibrational comfort indexes calculated considering the weighted curves from 1 to 100 Hz (a) and from 1 to 40 Hz (b).

The effect of the wooden dummy bottom position on the saddle vibration transmissibility was investigated. The saddle A was tested adopting three different longitudinal positions for the wooden dummy bottom (fig. 6.18):

- Pos. 1:  $x_{DW} = -4$  mm (backward position);
- Pos. 2:  $x_{DW} = +16$  mm (central position);
- Pos. 3:  $x_{DW} = +36$  mm (forward position).

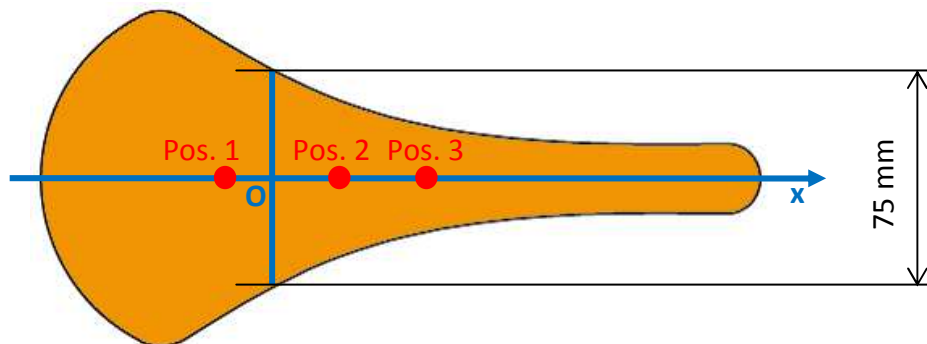


Fig. 6.18 Qualitative representation of the three wooden dummy bottom positions.



The respective three curves of figure 6.19, and the corresponding indexes (fig 6.20) show that the wooden dummy bottom position influences the measured vibrational transmissibility. This is due to a change of the pressure distribution at the dummy/saddle interface. The definition of a standard position to be kept constant during the test of different saddles is therefore very important for reliable comparison between their vibration transmissibility.

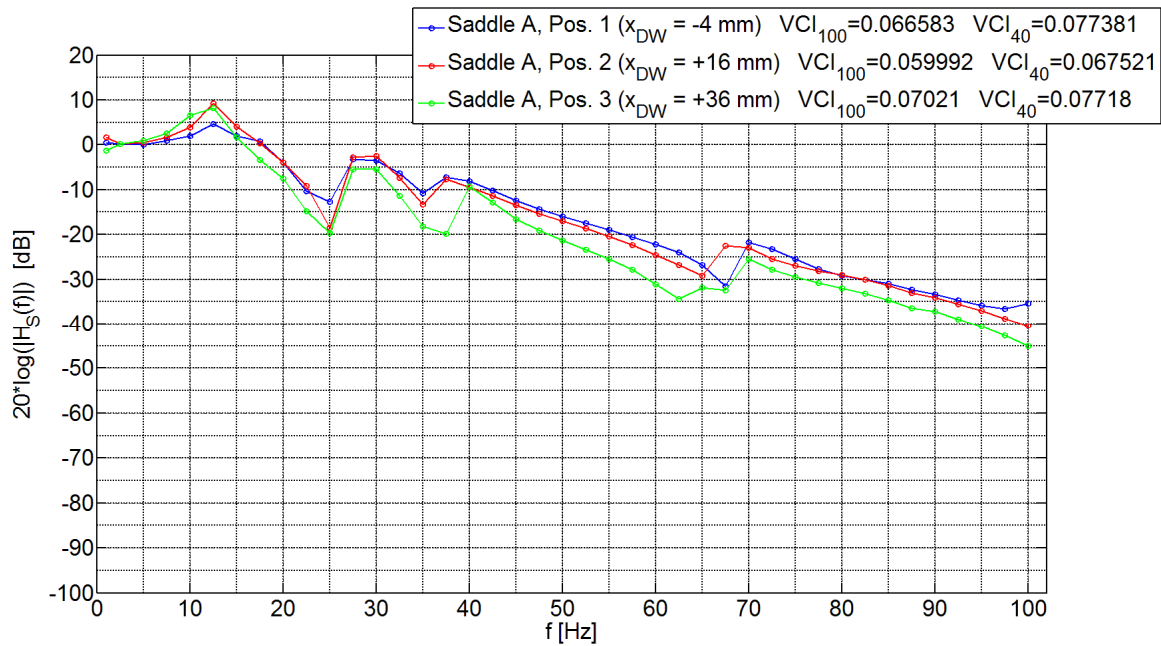


Fig. 6.19 Transfer function curves obtained for the tested saddle A with the wooden dummy bottom in three different positions.

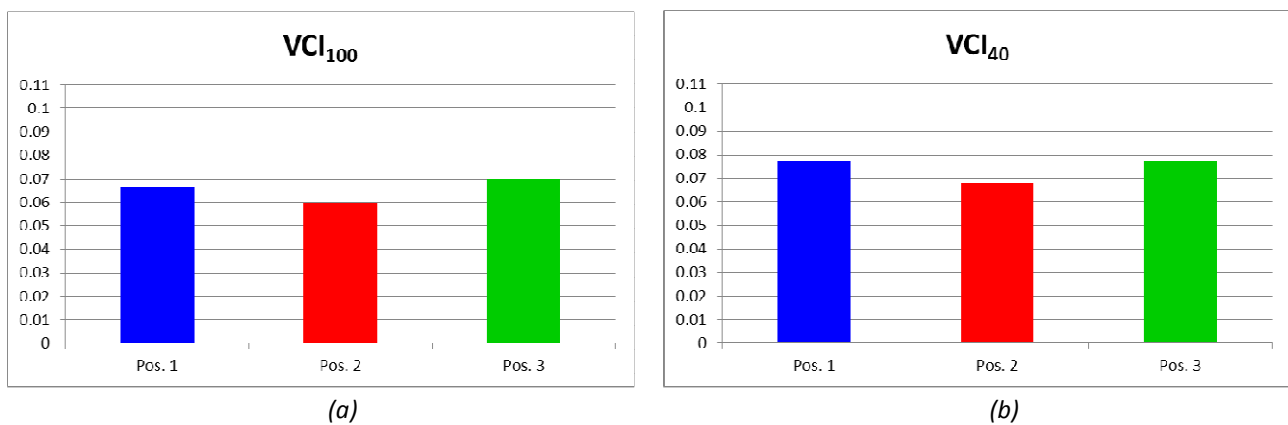


Fig. 6.20 Vibrational comfort indexes  $VCI_{100}$  (a) and  $VCI_{40}$  (b) calculated for the tested saddle A with the wooden dummy bottom in three different positions.

## 6.9 Conclusions

The works report the experimental method developed for the engineering characterization of bicycle saddles in terms of vibrational transmissibility. The use of a vertical servohydraulic cylinder holding the saddle, the application of a standard bottom shaped dummy loaded on the saddle, and the use of two accelerometers allowed to acquire the transmissibility curves of six saddles, and to introduce an integral Vibrational Comfort Index (VCI) to rank the saddles.

The results testify the ability of the developed test method to quantify the differences among different saddles from the vibrational point of view; it is also worthy to highlight the limitations of the study.

The main limitation of the work can be found in the absence, for the moment, of information regarding the perceived comfort behaviour of the saddles, based on customers questionnaires: this will be the first further development of the work, in order to check if the VCI introduced in the work is clearly correlated with a vibrational perceived comfort score of the saddle.

A second limitation can be recognized in the fact that the test setup is conventional, and involves the use of a wooden dummy that, despite shaped in accordance with an international standard, it has not the elastic, damping, and friction properties of a human bottom. This can be seen as a disadvantage with respect to the aim of characterizing the saddles with an engineering characteristics that should intentionally correlate with the perceived vibrational comfort: however, technically speaking, it was intentionally decided to tests the saddle involving the lowest number of external factors that can influence the tests results and with the most repeatable and reproducible set of test tools. For this reason, the adoption of a more anthropomorphic dummy, with a replica of the pelvis bone geometry and of the human soft tissues by a cast of silicon or other materials was not considered at this stage: previous experiences in this direction regarding the mechanical characterization of seat cushions showed that it can be very difficult to reproduce the dummy consistency throughout the world, and that the durability of the dummy surface and bulk properties can be hardly achieved.

The standard wooden dummy bottom position was defined through a comparison of the shell deformation measured for a real cyclist, and for the dummy in four different positions. The additional measurement and comparison of the pressure distribution at the cyclist/saddle and at the dummy/saddle interface can improve the standard positioning of the dummy, and can give more information regarding the possibility to develop a standard dummy bottom with a different shape that better reproduce the pressure distribution of the cyclist.

Another interesting development of this study consists in the correlation of the vibration transmissibility curves with constructive and structural saddle characteristics in order to support the manufacturers process towards more comfortable products, fulfilling the customers' requirements.



## ***Part 3***

**Correlation between the user quality requirements and the engineering parameters of racing bicycle wheels**



# Chapter 7

## Introduction to the analysis of the user requirements

### 7.1 Background

The adoption of a user-centred approach for the design and the engineering characterization of sports equipment improves, for the product developed, the possibilities of accomplishing the user needs. A user-centred approach involves interdisciplinary activities in the product development, linking the analysis of the product characteristics to the user quality requirements. The analysis of the product characteristics, which can be represented by the architectural characteristics, the technological characteristics, and the engineering parameters measurable by means of laboratory tests, have to be therefore connected to a detailed analysis of the user requirements and of the relationships between these two fields (see chapter 2).

Most of the modern methods proposed for the product development, highlight the importance of the voice of costumers (VOC) analysis, and propose specific methods to identify and organize the user requirements. QFD [16] (Quality Function Deployment) is an important method for the product development, dedicated to translate client requirements into activities for developing products and services. It involves some methods for the identification and organization of the user quality requirements, and for computing the correlation between them and the product characteristics. Despite the difficulties in its application (Carnevalli & Miguel [24]) regarding the interpretation of the customer voice, the definition of the correlation coefficients, the ambiguity in the distinction between the quality demanded, and quality characteristics, the work in group has been widely used in multiple fields for numerous years, and a huge quantity of works can be found in the literature.

### 7.2 Literature review

The user-centred analysis of sports equipment has been mainly carried out following the standard QFD approach.

Usma-Alvarez *et al.* [26] applied the QFD on rugby wheelchair design for the identification of the relevant performance parameters to be used as reference in the wheelchair customization. They performed meetings and interviews with groups of athletes, coaches, and manufactures, obtaining seventeen user requirements based on anecdotal evidence. The adoption of the standard QFD method resulted in house of quality matrix, in which the correlation coefficients between the user requirements and the product characteristics were represented by qualitative symbols.

In the work of Clifton *et al.* [21], the research was focused on the identification of design attributes of a new generation running shoe by relating key performance parameters to the requirements of a specific user group. They started with the identification of the first set of most important parameters through the review of the available literature. In the second stage, they modified this set of parameters after the analysis of the results of web surveys to athletes of different level and from different Countries. The final result of the research was represented by relative importance of different user needs across each of the ability-based groups of users.

Darques *et al.* [19] described the use of QFD for the design of skis. Key geometric and structural characteristics were correlated to eight subjective performance parameters for giant slalom skis using a QFD matrix of statistical correlations and user requirements. The overall impact of the key product characteristics on the various facets of ski performance requirements was then able to be determined by the authors.

The benefits, which arise from a systematic user-centred design procedure, were highlighted by Subic *et al.* [23] in the work regarding the identification of potential design innovation opportunities through a benchmarking analysis of modern snowboards. In the first stage of this work, which summarize the PhD research of Clifton [20], the authors collected through online surveys and interviews the qualitative data relating to customer requirements. At a later stage, the technical characteristics of the snowboard have been presented for having been correlated, in the last stage, with the user requirements adopting the QFD techniques. In the end the research determined the key design characteristics influencing the feel and performance of snowboards for both freestyle and freeride riding styles.

In their work published in 2008, and focused on the review, analysis (of 157 articles published between 2002 and 2006), and classification of the literature on QFD, Carnevalli & Miguel [24] have highlighted that, in most of the cases, the work goals were about adapting QFD for a specific application; there are several studies regarding the improvement of the method introducing other tools and techniques, but in most of the cases, applications are confined to the house of quality matrix, that may reduce the method's potential benefits.

I did not find any work in literature regarding the analysis of the user requirements of the bicycle or of the bicycle components.

In addition to the difficulties in the QFD application highlighted by Carnevalli & Miguel [24], affecting the results of the analysis, the works here analysed present the following common limitations.

- Identification of the user requirements: the methods adopted for the identification of the user requirements often do not follow a structured approach [21, 23, 26], resulting in outcomes affected by the subjective influence of the analyst.
- Description of the user requirements: in most of the cases [21] the user requirements are described as technical characteristics. There is a lack of a sharp distinction between the definitions of the quality requirements and of the technical characteristics of the product. It is

usual to ask the user to directly evaluate the technical features, adopting a technical language. In this way the risk of non-comprehension or of misunderstanding could highly affect the reliability of the research.

- Correlation between the user requirements and the product characteristics: the correlation coefficients obtained following the standard QFD method come from the logical reasoning of a selected workgroup based on shared experiences [19, 202, 23, 26]. They are therefore conditioned by their arbitrary behaviour and do not allow a quantitative analysis of the correlations.

### **7.3 Approach adopted in this thesis**

In my work I tried to overcome the common limitations through the methods presented in the following chapters of this part.

- Identification and organization of user quality requirements: the theory and the corresponding structured method proposed in ODI (Outcome Driven Innovation) [17], for discovering the customers' needs with respect to a considered product, was conveniently adapted obtaining a rigorous method for discovering and organizing the wheels quality requirements evaluated by the cyclists during road riding. The objectivity and the repeatability of this rigorous approach represent its main characteristics.
- Description of the user requirements: the user requirements were identified through the metrics, which were identified to be typical of cyclists in the evaluation of the execution of the actions performed during road riding. The cyclists were therefore asked to give an evaluation in terms of what were identified to be their proper metrics of judgement.
- Correlation between the user requirements and the product characteristics: the relationship between the user requirements and the wheels technical characteristics was evaluated by means of a method based on the computation of Pearson correlation coefficients. In this way a quantitative analysis, free from any subjective influence, has been obtained.

The methods developed considering the racing bicycle wheels have a generic behaviour, and are suitable to be used for the study of others sports equipment.





# Chapter 8

## Identification and organization of wheels quality requirements

### 8.1 Introduction

The method developed for the identification and organization of the **quality requirements** used by the cyclists for evaluating the wheels behaviours during road cycling, is presented in this chapter. The user quality requirements can be divided into the following five macro-categories (see § 2.1): usability, comfort, performance, safety, and aesthetic/emotional requirements. This work was focused on the **comfort and performance requirements** of the wheels, perceived by the cyclists during road riding. Objectivity and repeatability are the characteristics pursued during the development of the method here presented.

The structured approach of ODI (Outcome Driven Innovation) [17], regarding the research and analysis of the customers' needs, was adopted and conveniently adapted for the specific purpose of this work, as presented in the first part of this chapter. The results of this stage of the work are showed and discussed in the second part.

### 8.2 Introduction of ODI

ODI (Outcome Driven Innovation) [17] is a method proposed by Ulwick (CEO of Strategyn inc.) for the management of the innovation processes of companies. It is based on the need-first approach for the innovation process management, and proposes structured methods with the aim to support a systematic innovation process. Innovation is defined as “the process of devising a product or service concept that satisfies the customer’s needs”. ODI starts from a detailed VOC (Voice Of Costumers) analysis for establishing the guidelines for the idea generation, and for the definition of the final business model. In the following paragraphs the basic concepts defined by ODI regarding the VOC analysis are presented, analysis that represents its key stage.

#### Jobs-to-be-done theory

According to the Jobs-to-be-done theory, customers buy products and services for a specific purpose: to get jobs done. A **job** is defined as it follows:

*“The fundamental goals customers are trying to accomplish or problems they are trying to solve in a given situation”.*

The **metrics** used by the customers for measuring the goodness of the execution of a job are what ODI calls “**desired outcomes** or customer **need**”. ODI gives this way a definition of **need**, and places the real goal of innovation in helping customers to better execute a job or to do new jobs. During the VOC analysis, the analyst has to ask to the customers “What are you trying to get done?”. The direct question “What do you need?” is conceptually wrong, and might generate misleading answers.

Job and desired outcome statements

Jobs and Desired Outcomes are expressed following a standardized structure of statements (fig. 8.1). A standard format for the expression of the needs let to overcome the ambiguities involved in the interpretation of the customer’s words, proposed by QFD [16] and others VOC methods.

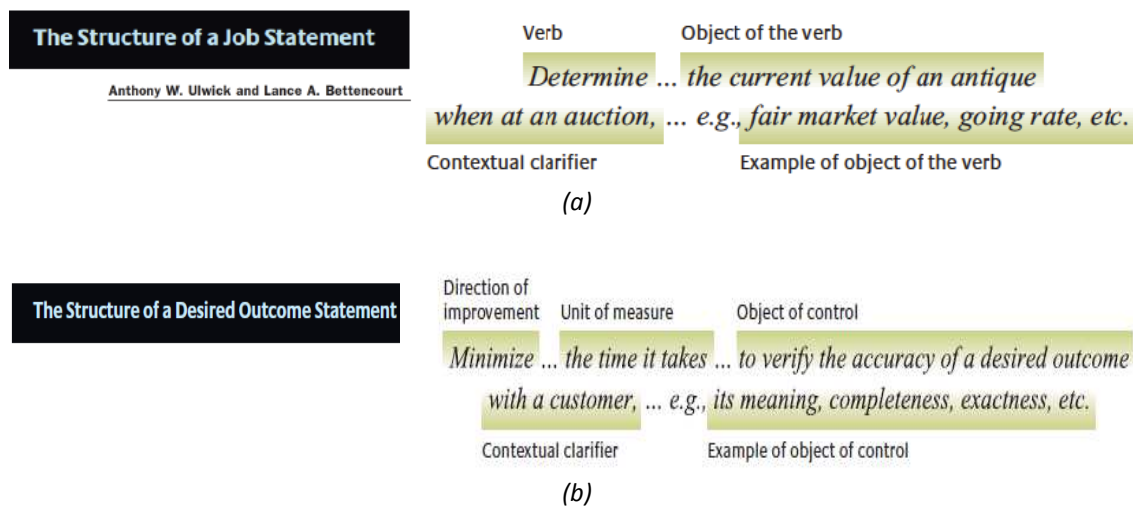


Fig. 8.1 Structure proposed for the Job (a) and Desired Outcome (b) statement. Figure extracted from [17].

Job map

Jobs can be grouped into two main categories: the functional and the emotional jobs. The **functional jobs** are processes: they can be analysed as such, and divided into **process steps**; each step can be analysed for recognising the **metrics** used by the customers for evaluating its successful execution (fig. 8.2). A functional job is typically divided into 8÷12 process steps, each step evaluated by the user through 6÷12 metrics (needs or desired outcomes), obtaining a total of 50÷150 needs for any given job.

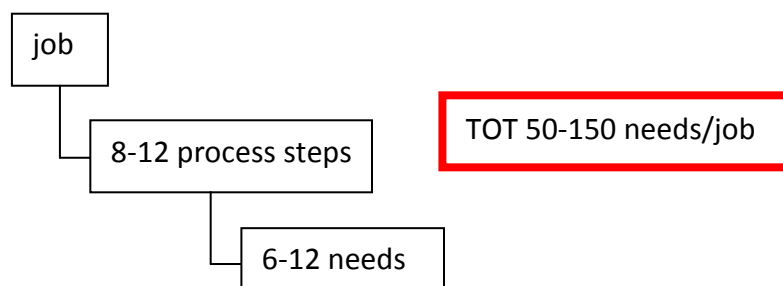


Fig. 8.2 Schematic of the relationship between job, process steps and needs.

A functional job is described by means of a **job map** (fig. 8.3), in which it has been broken down into its discrete process steps. The job map describes what the user is trying to get done, rather than what he is trying to do.

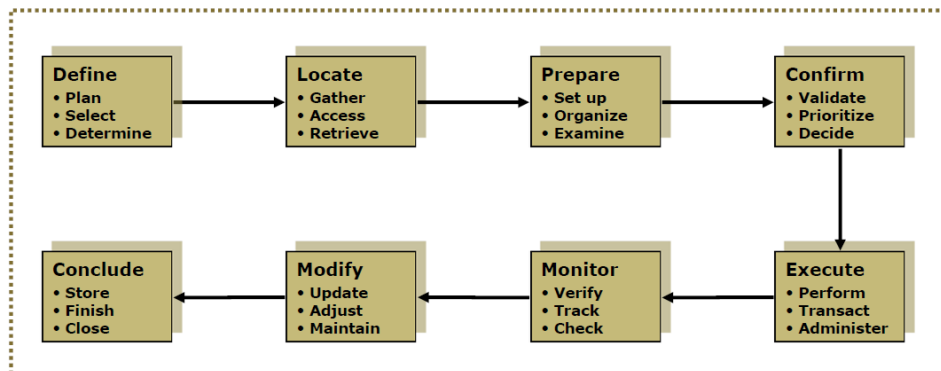


Fig. 8.3 Generic structure of a job map that shows the categories of the typical process steps. Figure extracted from [17].

The figures 8.4 and 8.5 show two examples of job maps that agree with the generic structure.

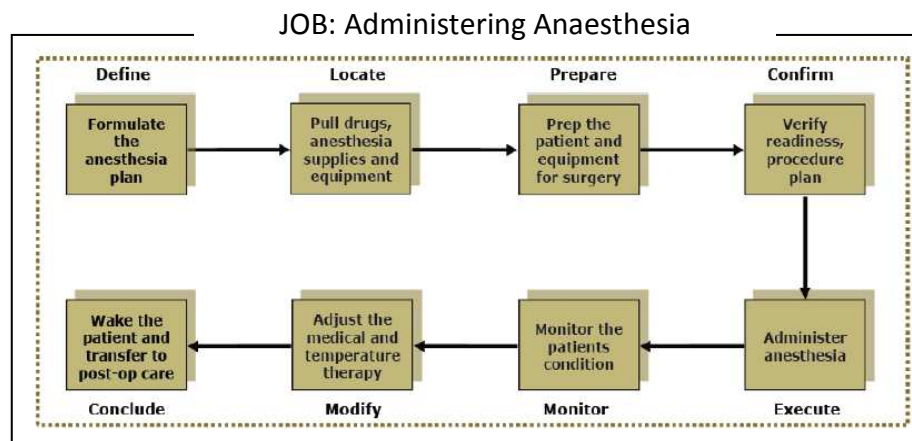


Fig. 8.4 Example of a job map regarding the administration of anaesthesia. Figure extracted from [17].

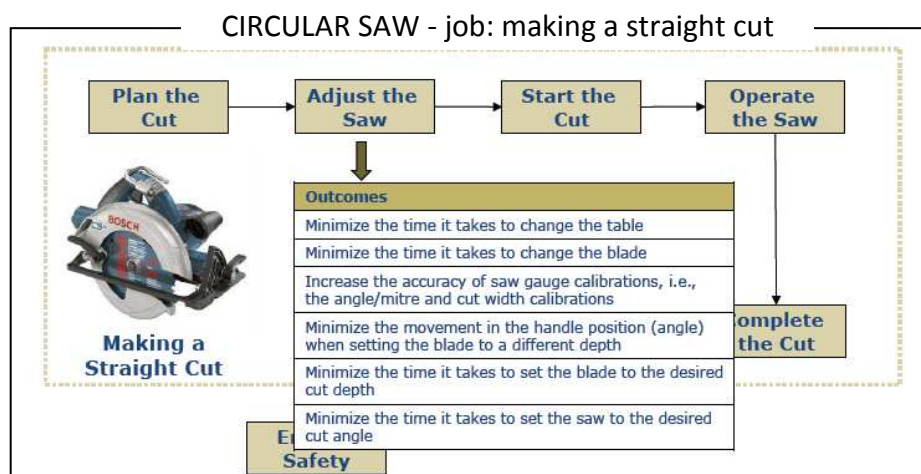


Fig. 8.5 Example of a job map regarding the execution of a straight cut with a circular saw. For a process step the desired outcomes are also listed. Figure extracted from [17].

## Hierarchy of customer needs

In the hierarchy of customer needs chart (fig. 8.6) the jobs relating to a considered product are divided according to their typology or their hierarchical relationship.

# Hierarchy of Customer Inputs

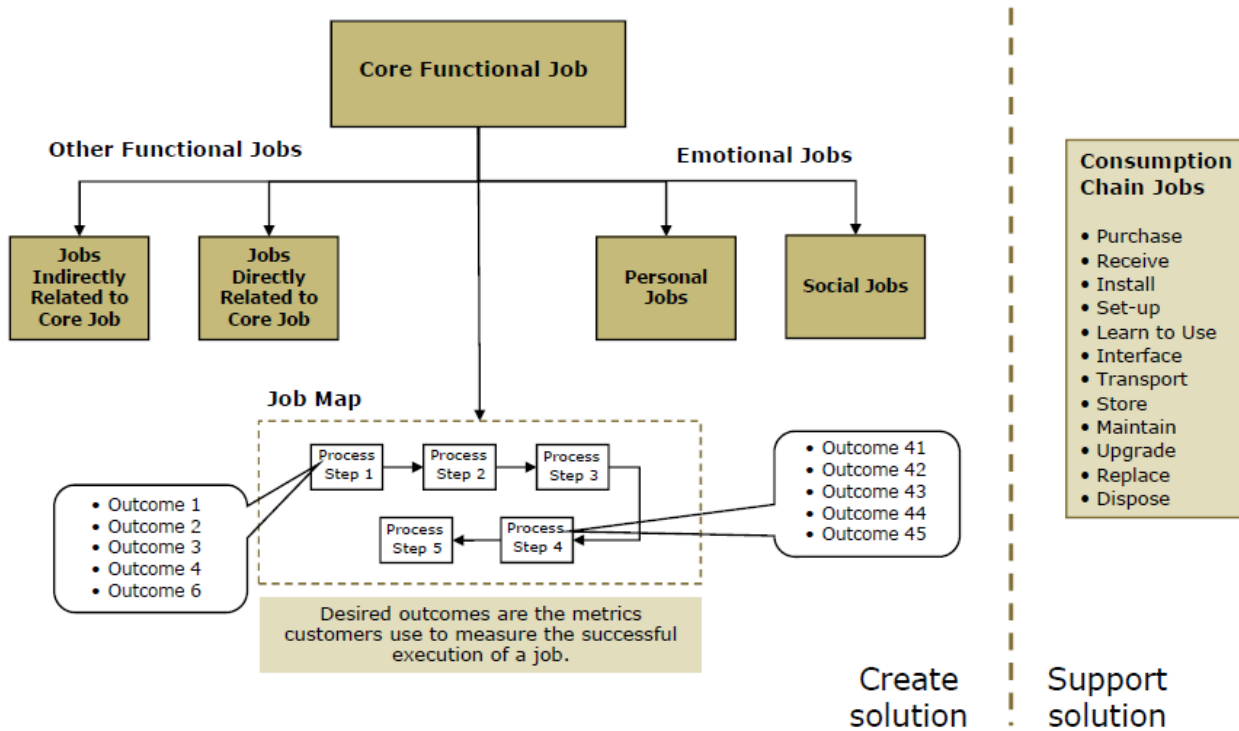


Fig. 8.6 Structure of the Hierarchy of Customer Inputs. Figure extracted from [17].

## Methods for recognising jobs and needs

ODI does not recommend a univocal method for discovering and analysing jobs and needs. In this activity the method is not the main factor, but establishing an interaction with the customer, knowing what inputs you are looking for is the key. It presents a set of activities to choose from depending on the case [18]:

- brainstorming sessions;
- interviews with single people or small groups;
- semi-structured interviews with selected customers;
- focused group;
- direct observation;
- analysis of the existing market researches.

ODI, however, suggests the following four-steps approach for capturing the desired outcomes.

- 1) Personal interviews: at this stage the jobs are identified and the relative job map is defined.
- 2) Ethnographic or observational interviews: the context, in which the jobs are getting done, is

examined in order to obtain useful elements for preparing the next two stages.

3) Personal, small group or large group interviews: identification of the user metrics.

4) Additional interviews: detailed definition of jobs and metrics.

### 8.3 Method developed in this work

The “jobs-to-be-done” theory proposed in ODI was adapted for collecting and organizing the perceived quality requirements of racing wheels evaluated by the cyclists. This theory and the relative structured method proposed in ODI for discovering the customers’ needs with respect to a considered product was conveniently adapted for the purpose of this work. If we refer to the job classification in the Hierarchy of Customer Inputs chart (fig. 8.5), in this work the emotional jobs were ignored.

- The **actions** performed by the cyclist during the use of the racing bicycle, such as the sprint, the braking, the execution of a curve, etc., were the functional jobs considered. The approach started considering that the cyclist aims to accomplish the different actions involved in the use of the bicycle.
- Each action was divided into subsequent **phases**, which represent the process steps of the job. Some actions were divisible into different phases, such as the turning action that could be divided into the entry into the curve, the steady turning phase in the middle of the curve, and the exit from the curve. Other actions, such as the sprint action, could not be divided into following phases. The phases of each action were represented through a sequential schematic, following the structure proposed by the job map.
- The influence of the wheels on the goodness of the execution of each action or phase is evaluated by the cyclist using a set of **metrics**. During the execution of each action or phase the cyclist expects to reach specific **desired outcomes** regarding each metric.
- The evaluations expressed by the testers through the identified metrics were combined to obtain the evaluation of a lower number of wheels **quality requirements**. They summarize the testers’ evaluation on wheels perceived performance and comfort, and they result to be easier to manage during the reporting activity than the 35 metrics. The connection between each metrics and each performance parameter was established following the logical relationship between their respective definitions.

Jobs, process steps, and needs of standard ODI has been therefore adapted into cyclist actions, phases, and cyclist metrics (fig. 8.7). The metrics evaluation has been then summarised through the quality requirements linked to them. The cyclist evaluation of the wheels was then obtained through the metrics, which were identified to be typical of cyclists. The adoption of structured

frameworks, and a clear definition of what a metrics is, let to identify, organize, and analyse the user requirements in an objective and repeatable way.

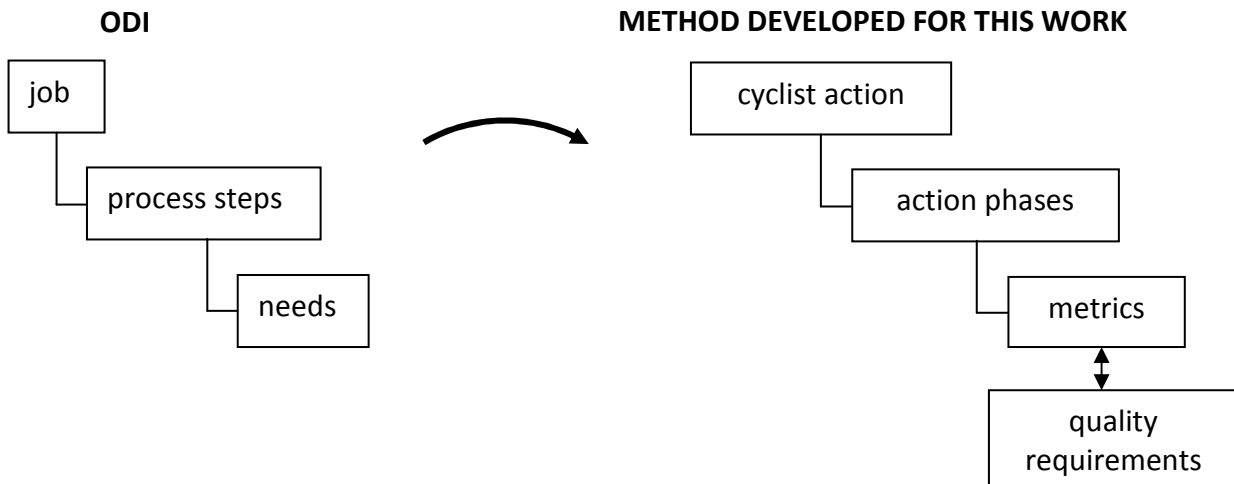


Fig. 8.7 Schematic of the ODI adaptation for the method developed in the capture of the wheels quality requirements.

The developed method follows the four stages listed below:

- 1) identification of the **actions** performed by the cyclist during racing bicycle riding;
- 2) identification of the consecutive **phases**, in which each action can be divided;
- 3) identification of the **metrics**, or evaluation parameters, used by the cyclists for evaluating the goodness of the outcome of each action's phase;
- 4) combination of the metrics in order to obtain a recapitulatory set of quality requirements, following the logical relationship between their respective definitions.

The adopted approach can be represented in the conceptual schematic of figure 8.8. A net of links between the metrics and the quality requirements is here highlighted. Each metrics can contribute to the evaluation of one or more quality requirements; each quality requirement can be evaluated through the contribution of one or more metrics.

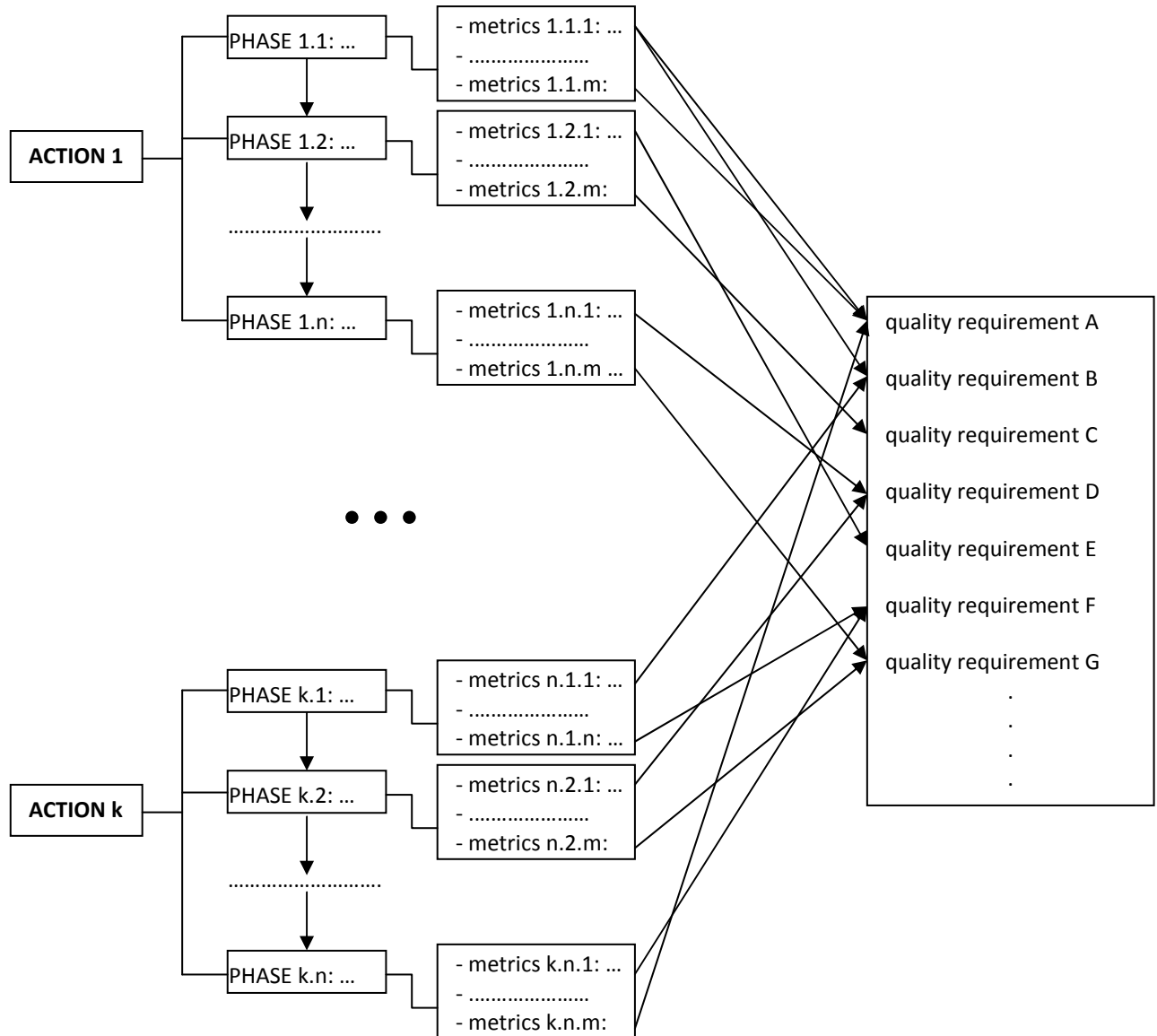


Fig. 8.8 Representation of the conceptual approach adopted for the identification and organization of the wheels quality requirements.

1-3) Methods for recognising actions, phases and metrics

The first three stages regarding the identification of actions, phases and metrics were carried out performing the following three activities:

- a) Elaboration of a first set of actions, phases, and respective metrics, based on an observational analysis and on the personal cycling experience.
- b) Execution of personal and group interviews with 13 cyclists, selected from different categories (racers, high level amateurs, low level amateurs), for reviewing and integrating the first set of actions, phases, and metrics. The interviews systematically followed these phases:



- introduction to the research activity and to the approach adopted;
- presentation and review of the actions performed with a racing bicycle that were recognized during the previous interviews;
- definition of possible actions to be added;
- examination, for each action, of the phases and metrics used by the interviewed cyclist;

At the end of each interview, the list of actions, phases, and metrics was uploaded.

- c) Final analysis of the list of actions, phases, and metrics to organize them and to delete redundant elements.

#### 4) Definition of the wheels quality requirements

The definition obtained for each metrics was analysed for defining the quality requirements, which can summarize it. Different metrics could refer to the same quality requirement, and each metrics could be linked to different quality requirements. The set of quality requirements represent therefore a summary of the metrics definitions.

## **8.4 Results**

12 typical actions performed by the cyclists during racing bicycle riding were identified: 8 actions cannot be divided into subsequent phases; 2 of the remaining 4 actions are divided into 2 phases, and the other 2 are divided into 3 phases for a total of 10 phases. The actions and the corresponding phases are evaluated through a total of 35 metrics.

The actions, the phases and the corresponding metrics individuated for racing bicycle wheels are listed below.

A.1 Sprint action, standing on the pedals, during uphill riding, starting from low speed ( $V < 17$  km/h)

M.1.1 Quickness in transforming cyclist actions into bicycle acceleration

M.1.2 Ratio between the bicycle acceleration and the force involved in the strokes on pedals

A.2 Uphill riding at constant speed

P.2.1 Uphill riding at low speed ( $V < 17$  km/h)

M.2.1.1 Body effort needed for keeping the constant speed

P.2.2 Uphill riding at high speed ( $V > 17$  km/h)

M.2.2.1 Body effort needed for keeping the constant speed

P.2.3 Passage from uphill to downhill

M.2.3.1 Acceleration of the bicycle due to the decrease of the road slope

A.3 Cycling on a straight flat road without the drafting effect of other cyclists

P.3.1 Cycling on a flat road at constant speed

M.3.1.1 Body effort needed for keeping the constant speed

M.3.1.2 Deceleration of the bicycle perceived when the cyclist stops to pedal

- P.3.2 Presence of lateral wind or turbulences due to the effect of a car or a truck
  - M.3.2.1 Decrease of bicycle stability due to lateral wind
  
- A.4 Cycling on a straight flat road with the drafting effect of other cyclists
  - M.4.1.1 Body effort needed for keeping the constant speed
  - M.4.1.2 Deceleration of the bicycle perceived when the cyclist stops to pedal
  
- A.5 Sprint action, standing on the pedals, during flat road riding, starting from high speed ( $V > 30$  km/h)
  - M.5.1 Quickness in transforming cyclist actions into bicycle acceleration
  - M.5.2 Speed level reached by the bicycle at the end of the sprint action
  
- A.6 Cycling on a downhill road
  - M.6.1 Acceleration of the bicycle during the downhill road riding
  - M.6.2 Variation of the bicycle stability with the speed increase
  - M.6.3 Decrease of bicycle stability due to lateral wind
  
- A.7 Braking action
  - P7.1 Initial braking phase
    - M.7.1.1 Entity of how the first braking phase resulted gradual or sudden
    - M.7.1.2 Time elapsed between the beginning of the brake lever movement and the beginning of the bicycle deceleration, during rainy conditions
  - P7.2 Central and final braking phase
    - M.7.2.1 Ratio between the deceleration for the bicycle and the command force applied to the brake levers
    - M.7.2.2 Decrease of the braking performance during the braking action
    - M.7.2.3 Entity of the vibrations perceived during the braking action
  
- A.8 Performing a curve
  - P.8.1 Entry into the curve
    - M.8.1.1 Quickness of curve entering
    - M.8.1.2 Body effort needed for entering in a curve
    - M.8.1.3 Easiness of curve entering
  - P.8.2 Steady turning (middle of the curve)
    - M.8.2.1 Precision in following the turning path
    - M.8.2.2 Body effort needed for the steady turning phase
    - M.8.2.3 Number of actions needed to correct the turning path
    - M.8.2.4 Decrease of bicycle stability due to lateral wind
  - P.8.3 Exit from the curve
    - M.8.3.1 Speed of the bicycle at the exit from the curve
    - M.8.3.2 Body effort needed for accelerating the bicycle at the curve exit
  
- A.9 Performing two consecutives curves
  - M.9.1 Quickness in the direction change
  - M.9.2 Body effort needed for the direction change
  
- A.10 Cycling on roads with an asphalt characterized by a big grain (e.g. draining asphalt)
  - M.10.1 Entity of the vibrations perceived at the hands, the feet, and the lumbar area

A.11 Cycling on uneven roads with consecutive obstacles such as holes and/or asphalt patches

M.11.1 Entity of the body stress due to the overcoming of the consecutive obstacles

M.11.2 Entity of the muscular fatigue spotted at the end of the cycling session

A.12 Cycling on uneven roads with isolated obstacles such as potholes, asphalt holes, bumps, and asphalt patches

M.12.1 Entity of the body stress due to the overcoming of the obstacles

The 35 metrics are summarized through the following 13 wheels quality requirements:

- QR.1: Reactivity during a sprint, starting from low speed ( $V < 17$  km/h)
- QR.2: Reactivity during a sprint, starting from high speed ( $V > 30$  km/h)
- QR.3: Reactivity during uphill road cycling, at constant low speed ( $V < 17$  km/h)
- QR.4: Reactivity during uphill road cycling, at constant high speed ( $V > 17$  km/h)
- QR.5: Handling
- QR.6: Rad Holding
- QR.7: Vibrational Comfort
- QR.8: Impulsive Comfort
- QR.9: Forward Rolling Efficiency
- QR.10: Braking Power
- QR.11: Braking Regularity
- QR.12: Stability in Absence of Wind
- QR.13: Stability to Crosswind

Table 8.1 shows the metrics, which contribute to the evaluation of each quality requirement. As expected, a quality requirement can be linked to one or more metrics, and a metrics can contribute to the evaluation of one or more quality requirements. As can be seen in the results of the subjective evaluation test, showed in the next chapter, the wheels reactivity is felt by the cyclist in different ways, depending on the action. For this reason, four quality requirements are represented by the wheels reactivity evaluated during different actions.

|         | QR.1 | QR.2 | QR.3 | QR.4 | QR.5 | QR.6 | QR.7 | QR.8 | QR.9 | QR.10 | QR.11 | QR.12 | QR.13 |
|---------|------|------|------|------|------|------|------|------|------|-------|-------|-------|-------|
| M.1.1   | x    |      |      |      |      |      |      |      |      |       |       |       |       |
| M.1.1   | x    |      |      |      |      |      |      |      |      |       |       |       |       |
| M.2.1   | x    |      | x    |      |      |      |      |      |      |       |       |       |       |
| M.2.2.1 |      |      |      | x    |      |      |      |      |      |       |       |       |       |
| M.2.3.1 |      |      |      |      |      |      |      |      | x    |       |       |       |       |
| M.3.1.1 |      |      |      |      |      |      |      |      | x    |       |       |       |       |
| M.3.1.2 |      |      |      |      |      |      |      |      | x    |       |       |       |       |
| M.3.2.1 |      |      |      |      |      |      |      |      |      |       |       |       | x     |
| M.4.1   |      |      |      |      |      |      |      |      | x    |       |       |       |       |
| M.4.2   |      |      |      |      |      |      |      |      | x    |       |       |       |       |
| M.5.1   |      | x    |      |      |      |      |      |      |      |       |       |       |       |
| M.5.2   |      | x    |      |      |      |      |      |      |      |       |       |       |       |
| M.6.1   |      |      |      |      |      |      |      |      | x    |       |       |       |       |
| M.6.2   |      |      |      |      |      |      |      |      |      |       |       | x     |       |
| M.6.3   |      |      |      |      |      |      |      |      |      |       |       |       | x     |
| M.7.1.1 |      |      |      |      |      |      |      |      |      |       | x     |       |       |
| M.7.1.2 |      |      |      |      |      |      |      |      |      |       | x     |       |       |
| M.7.2.1 |      |      |      |      |      |      |      |      |      | x     |       |       |       |
| M.7.2.2 |      |      |      |      |      |      |      |      |      | x     |       |       |       |
| M.7.2.3 |      |      |      |      |      |      |      |      |      |       | x     |       |       |
| M.8.1.1 |      |      |      |      | x    |      |      |      |      |       |       |       |       |
| M.8.1.2 |      |      |      |      | x    |      |      |      |      |       |       |       |       |
| M.8.1.3 |      |      |      |      | x    |      |      |      |      |       |       |       |       |
| M.8.2.1 |      |      |      |      |      | x    |      |      |      |       |       |       |       |
| M.8.2.2 |      |      |      |      |      | x    |      |      |      |       |       |       |       |
| M.8.2.3 |      |      |      |      |      | x    |      |      |      |       |       | x     |       |
| M.8.2.4 |      |      |      |      |      |      |      |      |      |       |       |       | x     |
| M.8.3.1 |      |      |      |      | x    |      |      |      |      |       |       |       |       |
| M.8.3.2 | x    | x    |      |      | x    |      |      |      |      |       |       |       |       |
| M.9.1   |      |      |      |      | x    |      |      |      |      |       |       |       |       |
| M.9.2   |      |      |      |      | x    |      |      |      |      |       |       |       |       |
| M.10.1  |      |      |      |      |      |      | x    |      |      |       |       |       |       |
| M.11.1  |      |      |      |      |      |      |      | x    |      |       |       |       |       |
| M.11.2  |      |      |      |      |      |      |      | x    |      |       |       |       |       |
| M.12.1  |      |      |      |      |      |      |      | x    |      |       |       |       |       |

Tab. 8.1 List of the metrics, which contribute to the evaluation of each quality requirement.



# Chapter 9

## Subjective evaluation tests

### 9.1 Introduction

A subjective evaluation test session was organized and carried out in order to collect the cyclist evaluations on the perceived quality requirements of three different wheelsets. The three wheels models selected represent, among the models available for the research team, the models with the highest differences with respect to the greatest number of engineering characteristics measured in laboratory tests. Thirty-three cyclists took part in the tests; they were selected from different categories. The testing path was conveniently chosen in order to present, in few kilometres, most of the typical situations encountered during road cycling. During the tests, each tester was asked to express an assessment about the performance of the tested wheels through the metrics, which were identified to be typical of cyclists (see Chapter 8). A questionnaire, opportunely formulated, was used for this purpose.

All the activities regarding the preparation and execution of the subjective evaluation tests, the data analysis, and the results obtained are presented in details in this chapter.

### 9.2 Selection of the wheelsets

Three different wheelsets were selected for the subjective evaluation tests. The selected wheels models represent, among the models available for the research team, the models with the highest differences with respect to the engineering characteristics measured in laboratory tests that were identified, through a preliminary analysis, to mainly influence the perceived quality requirements. As explained in Chapter 2, the engineering parameters are represented by the **basic engineering characteristics**, such as mass, inertial, stiffness, and damping properties, and by the **engineering complex indexes**, which give a technical measurement of the quality requirements perceived by the cyclist. At the beginning of this activity, the wheels were characterized considering only the following five basic engineering characteristics:

- $m$ [kg]: mass;
- $I$ [ $\text{kg}\cdot\text{m}^2$ ]: polar inertia;
- $K_{\text{side}}$  [N/m]: lateral stiffness;
- $K_{\text{torx}}$  [Nm/rad]: torsional stiffness;
- $K_{\text{rad}}$  [N/m]: radial stiffness.

A preliminary application of the standard QFD [16] was performed in order to identify the ranking between the influence that each basic engineering characteristic has on the perceived quality

requirements. The table 9.1 shows the House of Quality matrix obtained matching each quality requirement, identified in the previous work phase (see Chapter 8), with each basic engineering characteristic. At this stage, the correlation coefficients were chosen by a selected technical workgroup following the standard QFD method. They are therefore affected by all QFD limitations (see § 7.2). The four quality requirements

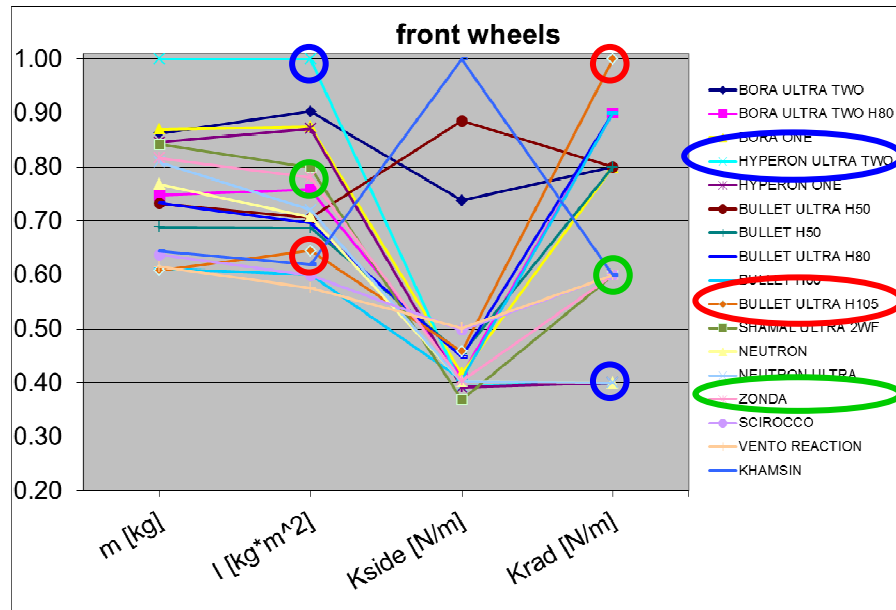
|                                | Customer importance [%] | m [kg] | I [kg·m <sup>2</sup> ] | K <sub>torx</sub> [Nm/rad] | K <sub>side</sub> [N/m] | K <sub>rad</sub> [N/m] | TOTAL  |
|--------------------------------|-------------------------|--------|------------------------|----------------------------|-------------------------|------------------------|--------|
| Reactivity                     | 30                      | 9      | 9                      | 3                          | 1                       | 1                      |        |
| Handling                       | 6.3                     | 9      | 9                      | 0                          | 3                       | 0                      |        |
| Road holding                   | 6.3                     | 1      | 3                      | 0                          | 3                       | 0                      |        |
| Vibrational comfort            | 6.3                     | 1      | 1                      | 0                          | 0                       | 9                      |        |
| Impulsive comfort              | 20                      | 3      | 3                      | 0                          | 1                       | 9                      |        |
| Rolling efficiency             | 20                      | 0      | 3                      | 0                          | 0                       | 0                      |        |
| Braking characteristics        | 1                       | 1      | 3                      | 0                          | 0                       | 1                      |        |
| Stability in Absence of Wind   | 5                       | 3      | 9                      | 0                          | 3                       | 1                      |        |
| Stability to Crosswind         | 5                       | 3      | 3                      | 0                          | 1                       | 0                      |        |
| <b>Weighted importance</b>     |                         | 430.3  | 534.9                  | 90                         | 107.8                   | 272.7                  | 1435.7 |
| <b>Relative importance [%]</b> |                         | 29.97  | 37.26                  | 6.27                       | 7.51                    | 18.99                  | 100.00 |

Tab. 9.1 House of Quality matrix obtained through a preliminary application of the standard QFD for the wheels selection.

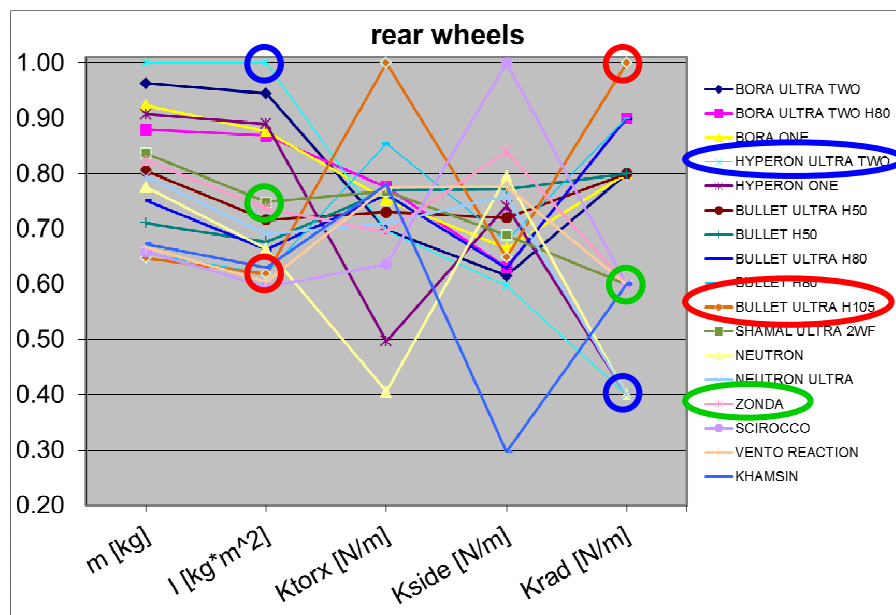
| Basic engineering characteristics | Relative Importance [%] |
|-----------------------------------|-------------------------|
| I [kg·m <sup>2</sup> ]            | 37.26                   |
| m [kg]                            | 29.97                   |
| K <sub>rad</sub> [N/m]            | 18.99                   |
| K <sub>side</sub> [N/m]           | 7.51                    |
| K <sub>torx</sub> [Nm/rad]        | 6.27                    |

Tab. 9.2 Ranking between the relative importance of the basic engineering characteristics obtained after the application of QFD.

From this preliminary QFD analysis, the wheels polar inertia I resulted the basic engineering characteristics, which mainly influence the wheels quality requirements perceived by the cyclist. It is followed by the mass m and by the radial stiffness K<sub>rad</sub>. Since the mass and the polar inertia are mutually correlated, the wheels choice was done considering the inertia and the radial stiffness. The three wheelsets were selected among the wheel models produced by Campagnolo in 2012. The charts of figure 9.1 and the normalized values of the basic engineering characteristics measured for all available wheels are plotted. The three wheels were selected in order to have the best, the worst, and the wheel with intermediate characteristics, regarding the polar inertia and the radial stiffness of both the front and rear wheels (fig. 9.1).



(a)



(b)

Fig. 9.1 Normalized values of the basic engineering characteristics of the Campagnolo front (a) and rear (b) wheels produced in 2012. The values are normalized in respect to the best values: lowest values for mass and inertia, highest values for stiffness.

Table 9.3 shows the constructive and the basic engineering characteristics of the selected wheels, their basic engineering characteristics normalized with respect to the best value are showed in figure 9.4. The wheels were all suitable for clincher, and were assembled with the same model of tire: Continental Grand Prix 4000 S.





Wheelset A: Campagnolo Bullet 105      Wheelset B: Campagnolo Zonda      Wheelset C: Campagnolo Hyperon

Fig. 9.2 Wheelsets selected for the subjective evaluation tests.

| Wheelset | Constructive characteristics |  |   |              | Basic engineering characteristics measured by means of laboratory tests |   |  |                                      |   |
|----------|------------------------------|--|---|--------------|---|---|--|--------------------------------------|---|
|          | Rim depth                    | 1-Rim material<br>2-Braking surface material | Spokes Nr. and Pattern<br>Front<br>Rear | Hub bearings | Mass<br>Front<br>Rear [g]   | Inertia<br>Front<br>Rear [kg·m <sup>2</sup> ] | Lateral stiffness<br>Front<br>Rear [N/m] | Torsional stiffness<br>Rear [Nm/rad] | Radial stiffness<br>Front<br>Rear [N/m] |
| A        | High<br>H 105 mm             | 1 - Composite<br>2 - Aluminium               | 16 radial<br>18 triplets                | Ceramic      | 873<br>1025   | $5.96 \cdot 10^{-2}$<br>$6.19 \cdot 10^{-2}$  | $48 \cdot 10^3$<br>$41 \cdot 10^3$       | $4.98 \cdot 10^3$                    | $4.81 \cdot 10^3$<br>$3.94 \cdot 10^3$  |
| B        | Medium<br>H 35 mm            | 1 - Aluminium<br>2 - Aluminium               | 16 radial<br>21 triplets                | Standard     | 653<br>868  | $4.74 \cdot 10^{-2}$<br>$5.43 \cdot 10^{-2}$  | $50 \cdot 10^3$<br>$54 \cdot 10^3$       | $5.44 \cdot 10^3$                    | $2.36 \cdot 10^3$<br>$2.55 \cdot 10^3$  |
| C        | Low<br>H 20 mm               | 1 - Composite<br>2 - Composite               | 22 radial<br>24 2x                      | Ceramic      | 589<br>771  | $3.91 \cdot 10^{-2}$<br>$4.27 \cdot 10^{-2}$  | $44 \cdot 10^3$<br>$42 \cdot 10^3$       | $5.26 \cdot 10^3$                    | $1.95 \cdot 10^3$<br>$1.96 \cdot 10^3$  |

Table 9.3 Constructive and engineering characteristics of the three wheelset selected for the subjective evaluation tests.

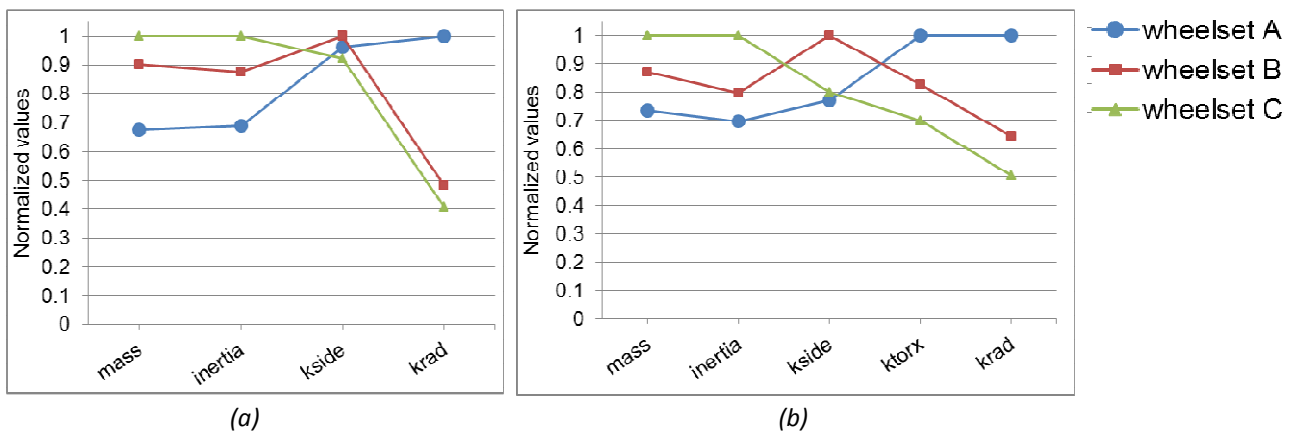


Fig. 9.4 Normalized basic engineering characteristics measured for the selected front (a) and rear (b) wheels.

The decals placed on the rim that indicate the wheel model, were removed in order to avoid that the opinions of the testers were influenced by previous bias due to conditioning popular rumors or past testing experiences.

### 9.3 Selection of the testers

Thirty-three cyclists took part in the tests. They were selected from different categories, ranging from professional and amateur racers to low level amateur, in order to get a representative and unbiased sample [22]. A classification of the cyclist categories was proposed in order to characterize each cyclist depending on its level and experience (tab. 9.4).

| Category name   | Number of testers |
|---|-------------------|
| PR: professional racer  | 0                 |
| AR: pre-professional racer. Cyclist that takes part in competitions in the categories which precede the professional activity.                        | 6                 |
| PRE: ex-professional racer  | 1                 |
| AM1: high level amateur. Amateur cyclist that takes part in amateur competitions, and/or uses the bicycle during all the year, more than once a week. | 13                |
| AM2: medium level amateur. Amateur cyclist that uses the bicycle only during the hot seasons one or more times a week.                                | 7                 |
| AM3: low level amateur. Amateur cyclist that uses the bicycle occasionally.   | 6                 |
|   | Total: 33         |

Tab. 9.4 Classification of the cyclist category

The testers were chosen using a data base, previously created in VBA (Visual Basic for Application, Excel), in which for each tester the data regarding his category, the contacts, the availability for the tests, the current, the past cycling activity, and the characteristics of the used bicycle were specified in details.

### 9.4 Construction of the questionnaire

A questionnaire, with multiple choice answers, was developed for collecting the evaluation of the testers regarding the tested wheelsets. In the questionnaire, the assessment of the cyclist, regarding the outcomes of the 12 actions performed with the tested wheelsets, was obtained through the metrics that were identified to be typical for the cyclists (see 8.3-4). Each of the 35 queries involved the evaluation of a metric; the Likert scale from 1 to 5 was adopted for the multiple choice answers. The structure of the queries (fig. 9.5) allowed the tester to express his opinion on the three wheelset adopting a relative scale. Since the evaluation using an absolute scale could highlight the differences among the experience and the sensibility of different cyclists, asking the relative evaluation of the three wheelsets was expected to decrease the dispersion of

the grades given by different testers, to the same wheelset, regarding the same question. With the aim of increasing the reliability of the answers, each question gave also the optional answer “I could not feel what is requested”, and also for some queries “I have not done this action during the test”. The tester was so dissuaded from giving not justified answers.

## 1 PERFORMING A CURVE



1.1.1 The quickness of curve entering resulted to be:

| Wheelset | 1<br>very low            | 2<br>low                 | 3<br>sufficient          | 4<br>high                | 5<br>very high           | I was not able<br>to feel it |
|----------|--------------------------|--------------------------|--------------------------|--------------------------|--------------------------|------------------------------|
| A        | <input type="checkbox"/> | <input type="checkbox"/> | <input type="checkbox"/> | <input type="checkbox"/> | <input type="checkbox"/> | <input type="checkbox"/>     |
| B        | <input type="checkbox"/> | <input type="checkbox"/> | <input type="checkbox"/> | <input type="checkbox"/> | <input type="checkbox"/> | <input type="checkbox"/>     |
| C        | <input type="checkbox"/> | <input type="checkbox"/> | <input type="checkbox"/> | <input type="checkbox"/> | <input type="checkbox"/> | <input type="checkbox"/>     |

Fig. 9.5 Example of a multiple answer question inserted into the questionnaire.

If the cyclist heard particular sounds during the test, he could specify its behaviour and the corresponding action through a dedicated format inserted at the end of the questionnaire (fig 9.6).

## SOUNDS OR NOISE EVALUATION

If, during the test, the cyclist heard particular sounds, he could specify below its behaviour and the corresponding action

| ACTIONS   | Wheelset A               |                          | Wheelset B               |                          | Wheelset C               |                          | eventual notes |
|---|--------------------------|--------------------------|--------------------------|--------------------------|--------------------------|--------------------------|----------------|
|   | loud sound               | likable sound            | loud sound               | likable sound            | loud sound               | likable sound            |                |
| 1. Sprint action, standing on the pedals, during uphill riding, starting from low speed ( $V < 17$ km/h)        | <input type="checkbox"/> | <input type="checkbox"/> | <input type="checkbox"/> | <input type="checkbox"/> | <input type="checkbox"/> | <input type="checkbox"/> | _____          |
| 2. Uphill riding at constant speed  | <input type="checkbox"/> | <input type="checkbox"/> | <input type="checkbox"/> | <input type="checkbox"/> | <input type="checkbox"/> | <input type="checkbox"/> | _____          |
| 3. Cycling on a straight flat road without the drafting effect of other cyclists                                | <input type="checkbox"/> | <input type="checkbox"/> | <input type="checkbox"/> | <input type="checkbox"/> | <input type="checkbox"/> | <input type="checkbox"/> | _____          |
| 4. Cycling on a straight flat road with the drafting effect of other cyclists                                   | <input type="checkbox"/> | <input type="checkbox"/> | <input type="checkbox"/> | <input type="checkbox"/> | <input type="checkbox"/> | <input type="checkbox"/> | _____          |
| 5. Sprint action, standing on the pedals, during flat road riding, starting from high speed ( $V > 30$ km/h)    | <input type="checkbox"/> | <input type="checkbox"/> | <input type="checkbox"/> | <input type="checkbox"/> | <input type="checkbox"/> | <input type="checkbox"/> | _____          |
| 6. Cycling on a downhill road   | <input type="checkbox"/> | <input type="checkbox"/> | <input type="checkbox"/> | <input type="checkbox"/> | <input type="checkbox"/> | <input type="checkbox"/> | _____          |
| 7. Braking action   | <input type="checkbox"/> | <input type="checkbox"/> | <input type="checkbox"/> | <input type="checkbox"/> | <input type="checkbox"/> | <input type="checkbox"/> | _____          |
| 8. Performing a curve   | <input type="checkbox"/> | <input type="checkbox"/> | <input type="checkbox"/> | <input type="checkbox"/> | <input type="checkbox"/> | <input type="checkbox"/> | _____          |
| 9. Performing two consecutives curves   | <input type="checkbox"/> | <input type="checkbox"/> | <input type="checkbox"/> | <input type="checkbox"/> | <input type="checkbox"/> | <input type="checkbox"/> | _____          |
| 10. Cycling on roads with an asphalt characterized by a big grain (e.g. draining asphalt)                       | <input type="checkbox"/> | <input type="checkbox"/> | <input type="checkbox"/> | <input type="checkbox"/> | <input type="checkbox"/> | <input type="checkbox"/> | _____          |
| 11. Cycling on uneven roads with consecutive obstacles such as holes and/or asphalt patches                     | <input type="checkbox"/> | <input type="checkbox"/> | <input type="checkbox"/> | <input type="checkbox"/> | <input type="checkbox"/> | <input type="checkbox"/> | _____          |
| 12. Cycling on uneven roads with isolated obstacles such as potholes, asphalt holes, bumps, and asphalt patches | <input type="checkbox"/> | <input type="checkbox"/> | <input type="checkbox"/> | <input type="checkbox"/> | <input type="checkbox"/> | <input type="checkbox"/> | _____          |

Fig. 9.6 Section of the questionnaire, in which the testers could give information regarding the particular sounds heard during the tests.

The final version of the questionnaire, visible in the appendix A, was defined after a pilot test session carried out with 6 different testers for verifying the contents of the questions and the ease of the used language.

### 9.5 Selection of the testing road path

The testing path was selected in order to obtain the following characteristics:

- it has to present most of the typical situations encountered during road cycling;
- its length and altitude gap gradient have to let the tester to ride through it for three times without spending too much energy;
- an area close to road path for logistic operations and for the change of the wheels is necessary;

The road path was selected in a hill zone of Bassano del Grappa (V) – Italy. It therefore presented all the characteristics listed above:

- length: 12 km;
- vertical drop: 260 m.

The characteristics of the different path sections are reported in table 9.5, and in the chart of figure 9.7.

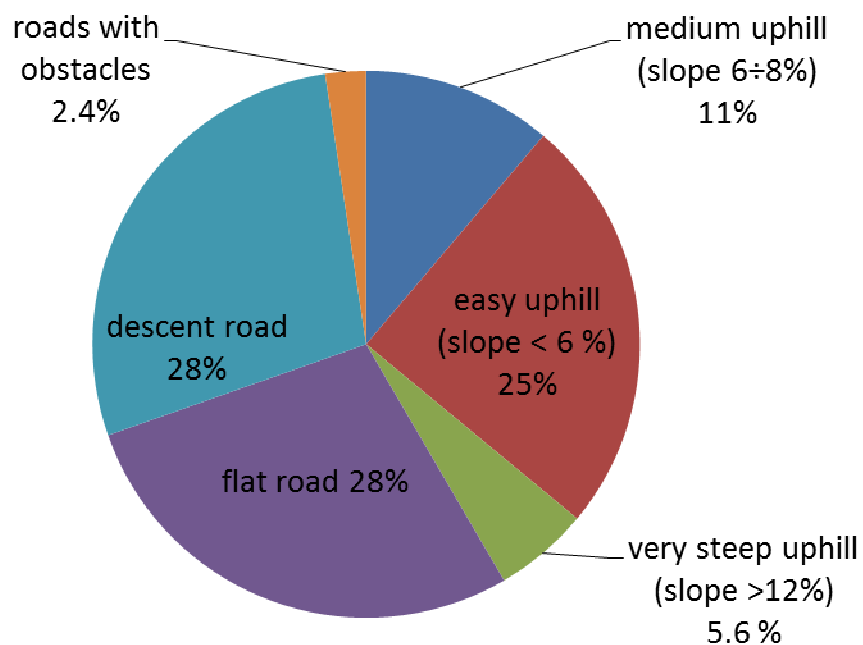


Fig. 9.7 Characteristics of the selected road path.

| Description of the path section | Length [km] | Relative length [%] |
|---------------------------------|-------------|---------------------|
| medium uphill (slope = 6÷8%)    | 1.4         | 11.2                |
| easy uphill (slope < 6 %)       | 3.1         | 24.8                |
| very steep uphill (slope > 12%) | 0.7         | 5.6                 |
| flat road                       | 3.5         | 28                  |
| descent road                    | 3.5         | 28                  |
| roads with obstacles            | 0.3         | 2.4                 |

*Tab. 9.5 Characteristics of the selected road path.*

## 9.6 Execution of the test session

The 33 testers were divided into 4 groups. The test session was performed during two days, and each half-day was reserved for the tests of a group. Before the first testing run, the cyclist performed a reconnaissance of the testing path with a van for nine people driven by myself. During the reconnaissance, I presented the testing activities and the testing path.

During the tests, each cyclist had to ride on the testing road path once for each wheelset. The testers performed the tests using their own bicycle, of which only the wheels were changed. The wheels were equipped with the same clincher model inflated at the same pressure (8 bar). The only variable of the tests was therefore represented by the wheelset. Three wheelsets for each model were available for the tests, in order to give the possibility to test the same model by three cyclists at the same time.

At the end of each run, every tester had to answer to the questionnaire with multiple choice answers for evaluating the outcome of the 12 actions performed with the tested wheelset. While the testers were answering to the questionnaire, two professional operators were employed in the change of the wheelsets of the bicycles (fig. 9.8).

The test session was performed during the sunny days of May, with a temperature of 22 °C, and with perfectly dry road asphalt all along the length of the testing path.



*Fig. 9.8 Operation of wheels change while the testers were answering to the questionnaire.*

## 9.7 Data analysis

A VBA (Visual Basic for Applications) for Excel program was developed for inserting, and automatically archiving in a dedicated database, the answers given by the 33 testers during the questionnaire compilation. A Matlab® program, which interfaced directly with the Excel database, was developed for the statistical analysis [22] of the questionnaires results.

The questionnaire was composed by 35 queries, each query corresponding to a metrics of evaluation. The indexes listed below were adopted for identifying the variables involved in the data analysis:

- i: index of query or metrics;
  - j: index of wheelset;
  - k: index of tester;
  - m: index of quality requirement.
- In the first step of the data analysis, the **mean grades** attributed by the testers to each wheelset was calculated for every query (or metrics) through two methods:
    - 1) *Mean relative grades*  $G_{rel,avg,i,j}$ : the average difference between the grades, given by the testers to the j-th tested wheelset, and the grade, given to the tested wheelset evaluated as the worst (2). In this way, an evaluation of the tested wheels was obtained using a relative scale.

**1 Sprint action, standing on the pedals, during uphill riding, starting from low speed (V<17 km/h)**

**1.1** The quickness whereby the sprint action was converted into the bicycle acceleration resulted to be:

| Wheelset | 1<br><i>very low</i>     | 2<br><i>low</i>                     | 3<br><i>normal</i>       | 4<br><i>high</i>                    | 5<br><i>very high</i>               | <i>I was not able to feel it</i> |
|----------|--------------------------|-------------------------------------|--------------------------|-------------------------------------|-------------------------------------|----------------------------------|
| A        | <input type="checkbox"/> | <input checked="" type="checkbox"/> | <input type="checkbox"/> | <input type="checkbox"/>            | <input type="checkbox"/>            | <input type="checkbox"/>         |
| B        | <input type="checkbox"/> | <input type="checkbox"/>            | <input type="checkbox"/> | <input checked="" type="checkbox"/> | <input type="checkbox"/>            | <input type="checkbox"/>         |
| C        | <input type="checkbox"/> | <input type="checkbox"/>            | <input type="checkbox"/> | <input type="checkbox"/>            | <input checked="" type="checkbox"/> | <input type="checkbox"/>         |

Fig. 9.9 Example of the answers to the query 1.1 given by the tester number 4.

| Wheelset | <i>Relative grades <math>G_{rel,1,4}</math></i> |
|----------|---|
| A        | 0   |
| B        | +2  |
| C        | +3  |

Tab. 9.6 Example of the relative grades calculated for the query nr. 1 (i=1) and the tester nr. 4 (k=4).

Computation of the relative grade regarding the i-th query, obtained by the j-th wheelset, and given by the k-th tester:

$$G_{rel,i,j,k} = G_{abs,i,j,k} - \min(G_{abs,i,A,k}, G_{abs,i,B,k}, G_{abs,i,C,k}) \quad (1)$$

$G_{abs,i,j,k}$ : absolute grade the i-th query, obtained by the j-th wheelset, and given by the k-th tester.

Computation of the average relative grade regarding the i-th query, for the j-th wheelset:

$$G_{rel,avg,i,j} = \frac{\sum_{k=1}^{33} G_{rel,i,j,k}}{33} \quad (2)$$

2) *Mean absolute grades*  $G_{abs,avg,i,j}$ : average absolute grade given by the testers to the j-th tested wheelset and regarding the i-th query (3):

$$G_{abs,avg,i,j} = \frac{\sum_{k=1}^{33} G_{abs,i,j,k}}{33} \quad (3)$$

- The **mean standard deviation** between the grades given by the 33 testers, regarding each query and each wheelset was calculated for both the relative (8) and absolute (9) grades. This allowed the comparison between the dispersions of the relative and absolute scales.

Standard deviation between the relative (4) and absolute (5) grades given by the 33 testers to the j-th wheelset, regarding the i-th query:

$$SD_{rel,i,j} = \frac{1}{33-1} \cdot \sum_{k=1}^{33} (G_{rel,i,j,k} - G_{rel,avg,i,j}) \quad (4)$$

$$SD_{abs,i,j} = \frac{1}{33-1} \cdot \sum_{k=1}^{33} (G_{abs,i,j,k} - G_{abs,avg,i,j}) \quad (5)$$

Average standard deviation between the relative (6) and absolute (7) grades given by the 33 testers to the 3 wheelset, regarding the i-th query:

$$SD_{rel,avg,i} = \frac{\sum_{j=1}^3 (SD_{rel,i,j})}{3} \quad (6)$$

$$SD_{abs,avg,i} = \frac{\sum_{j=1}^3 (SD_{abs,i,j})}{3} \quad (7)$$

Average standard deviation between the relative (8) and absolute (9) grades given by the 33 testers to the 3 wheelset, regarding the 35 queries:

$$SD_{rel,avg} = \frac{\sum_{i=1}^{35} (SD_{rel,avg,i})}{35} \quad (8)$$

$$SD_{abs,avg} = \frac{\sum_{i=1}^{35} (SD_{abs,avg,i})}{35} \quad (9)$$

- The mean **evaluation** of the testers, regarding each **quality requirement** of each tested wheelset, was calculated as the average of its mean relative grades computed for the metrics, which were connected to the considered quality requirement (see § 8.3, tab. 8.1). The relative grades were considered instead of the absolute grades because, as can be seen in the next paragraph, they are characterized by lower dispersion. If we consider, for example, the quality requirement 6 (QR.6) of the wheelset A, which is connected to the three metrics M.8.2.1, M.8.2.2, M.8.2.3 (see tab. 8.1), its evaluation grade is calculated as it follows:

$$QR.6_{grade,avg,A} = \frac{G_{rel,avg,M.8.2.1,A} + G_{rel,avg,M.8.2.2,A} + G_{rel,avg,M.8.2.3,A}}{3} \quad (9)$$

## 9.8 Results

The average standard deviation between the relative (8) and absolute (9) grades given by the 33 testers to the 3 wheelset, regarding the 35 queries ( $SD_{rel,avg}$ ,  $SD_{abs,avg}$ ) is respectively equal to 0.77 and 0.84 grades. The lower dispersion of the relative grades confirms that, asking the testers for an evaluation expressed adopting a relative scale, results in less variable and, therefore, more reliable outcomes.

The highest values of the standard deviation  $SD_{rel,avg,i}$  between the relative grades given by the 33 testers to the 3 wheelset, regarding each single query, was obtained for the metrics M.6.2, M.8.1.3, M.8.2.3. For these metrics, which are respectively the variation of the bicycle stability with the speed increase during downhill riding, the easiness of curve entering, and the number of actions needed to correct the turning path, the  $SD_{rel,avg,i}$  is between 0.9 and 1 grade. This could testify that these queries resulted difficult to be understood, or that the corresponding metrics were difficult to be perceived and assessed.

The highest percentage, equal to 10%, of answers corresponding to “I could not feel what is requested”, was obtained for the query regarding the metrics M.11.2: the entity of the muscular fatigue, due to the overcoming of consecutive obstacles, spotted at the end of the cycling session. For the other queries, less than 5% of answers gave the same results.



Figure 9.10 shows the mean evaluation grades calculated for the 3 tested wheelsets, regarding the 13 quality requirements.

The wheels Reactivity, evaluated by the cyclists during the four actions, in which it is perceived, shows variations of the wheelsets ranking, and differences between the wheels evaluation. If we compare the results obtained for QR.1 and QR.2, which correspond to the wheels Reactivity evaluated during a sprint, starting respectively from low and high speed, the wheelset C obtained the best evaluation regarding both. This wheelset is the wheel with the lowest mass and polar inertia (tab. 9.3). The ranking between the wheelset A and B changes from QR.1 to QR.2; the differences between the wheelset C and the others two wheelsets is maximum for QR.1 and decreases for QR.2. These variations are due to a change of the contribution of each resistance force to the resultant force, which is opposed to the bicycle motion. During a sprint starting from low speed (QR.1), the characteristics of lightness and low inertia of the wheelset C enhance its performances. Whereas as the speed increases, the aerodynamic resistance increases itself, enhancing the performances of the wheelset A, that presented the highest rim depth (tab. 9.3) and therefore the lowest drag coefficient [46-53]. These argumentations can explain also the variation of the differences between the grades of the tested wheelsets, variation that can be seen for the reactivity evaluated during the uphill riding at low and high speed (QR.3, QR.4).

The Handling (QR.5) and the Road Holding (QR.6) shows the same ranking among the wheels, with the wheelset C evaluated as the best, followed by the wheelset B and A. The high mass and inertia of the wheelset A penalize its evaluations regarding these two QR. Higher differences between the wheelsets were perceived for the metrics linked to the Handling quality requirement, which summarizes the perceived wheels behaviour during the entry into the curve, the exit from the curve, and the direction change. The wheels behaviours resulted therefore easily to be perceived by the testers during the transient action phases.

The same ranking, with the wheelset C evaluated as the best, followed by the wheelset B and A, was obtained for the Vibrational and the Impulsive Comfort (QR.7, QR.8), highlighting the inverse relationship between the wheels comfort properties and the radial stiffness (tab. 9.3): the stiffest wheelset A resulted the less comfortable.

The wheelset A, assembled with ceramic bearings and characterized by the highest rim depth, which corresponds to the lowest drag coefficient [46-53], resulted in the best Forward Rolling Efficiency (QR.9). The ceramic bearings used for the assemblage of the wheelset C, gave it a perceived Forward Rolling Efficiency greater than the wheelset B, which had a higher rim depth but was assembled with standard bearings. This observation puts in evidence the positive effect of the low rolling resistance of the ceramic bearings.

The Braking Power (QR.10) resulted clearly higher for the wheelset C, which had the rim braking surface made in composite material. On the contrary, the same wheelset showed the worst Braking Regularity (QR.11). The wheelsets A and B, which braking surface was made in aluminium, presented negligible differences regarding both the braking power and the braking regularity.

Considering the wheels Stability in Absence of Wind (QR.12) and Stability to Crosswind (QR.13), the worst evaluation was always attributed to the wheelset A. The highest lateral area heavily

affects its Stability to Crosswind; its high inertia contributes to decrease also the perceived Stability in Absence of Wind. The low differences between the rim depth of the wheelsets B and C resulted in the same evaluation of these two wheelsets regarding the Stability to Crosswind.

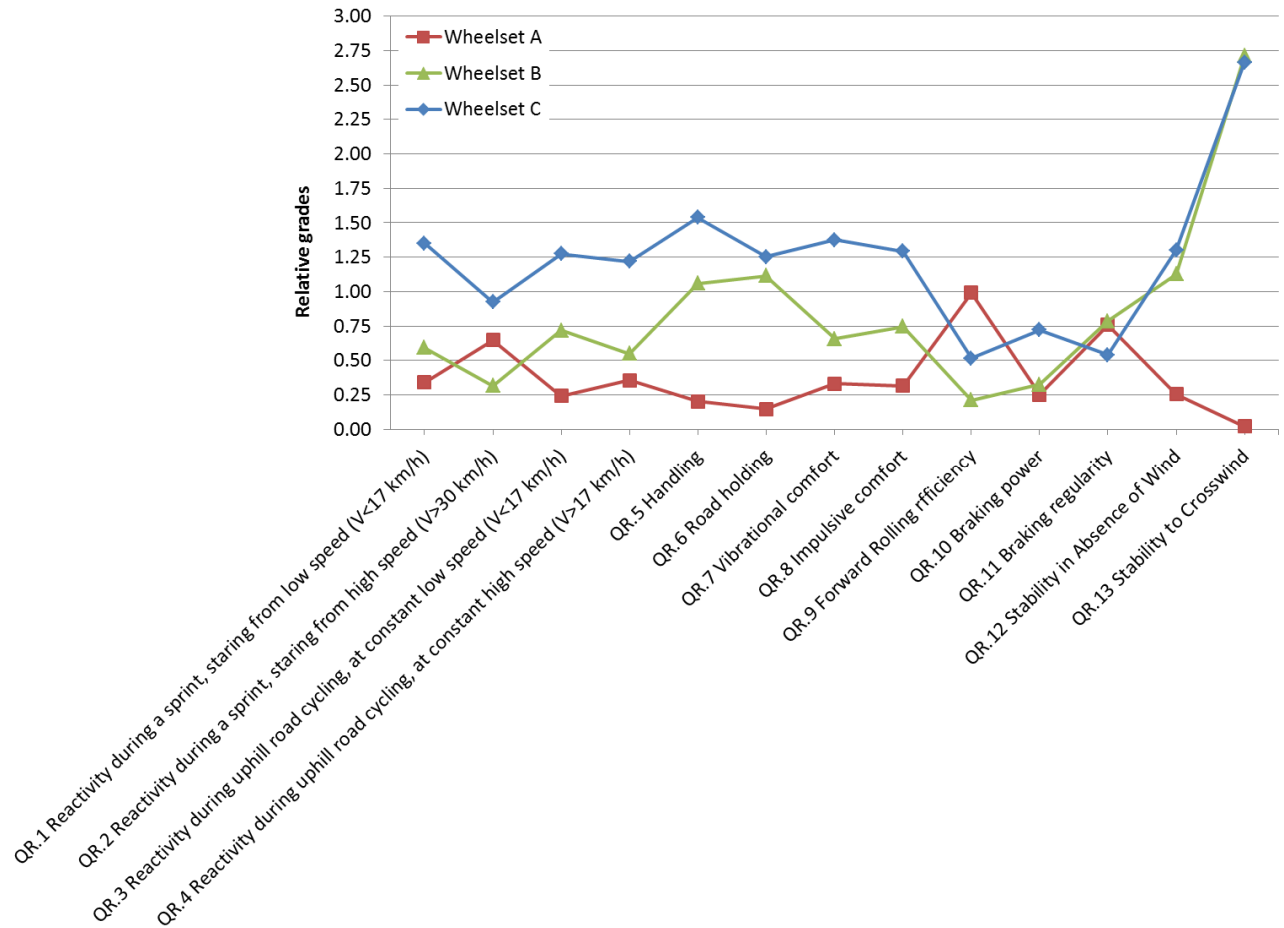


Fig. 9.10 Resulting mean evaluation grades calculated for the 3 tested wheelsets, regarding the 13 quality requirements.

### 9.9 Conclusions

The structured features of the user-centred method developed for collecting and organizing the wheels quality requirements minimize the influence of the analyst, and enhance the characteristics of repeatability. This method, developed considering the racing bicycle wheels, is applicable to other sports equipment. The subjective evaluation test method, the choice of the road path, and the querying method resulted to be suitable for the purpose of this work, and appreciated by the testers.

High differences between the tested wheelsets were perceived by the testers among all the wheels quality requirements. This suggested the development of the engineering complex indexes presented in the Part 4.

The identification and organization of the user quality requirements, united to a subjective evaluation test session, can represent the starting stages in the definition of a methodology for the systematic collection of the subjective evaluation during the product development.



# ***Appendix A***

**Questionnaire used during the  
subjective evaluation tests**





## EVALUATION OF THE QUALITY REQUIREMENTS OF RACING BICYCLE WHEELS

Name: \_\_\_\_\_

Surname: \_\_\_\_\_

Date: \_\_\_\_\_

Place: \_\_\_\_\_

Weather conditions: \_\_\_\_\_

### Introduction to the questionnaire

The purpose of this questionnaire is to collect the assessment of the cyclist on the perceived quality requirements of the tested racing bicycle wheels.

The tester is asked to give its evaluation about the actions executed during the tests through the metrics that, by means of a previous specific analysis, were identified to be typical of the cyclists.

Since this is an experimental activity, every suggestion or critique is well accepted.

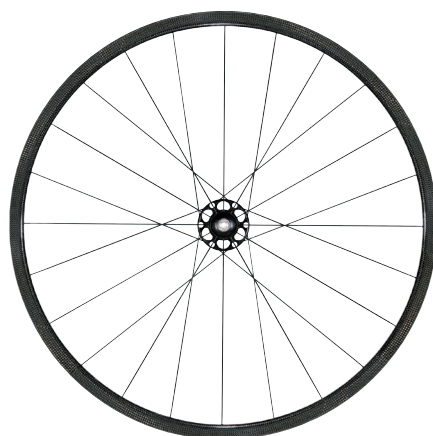
We encourage you to give the answers with sincerity, you are free to answer that you cannot evaluate what requested.

### TESTED WHEELSETS:

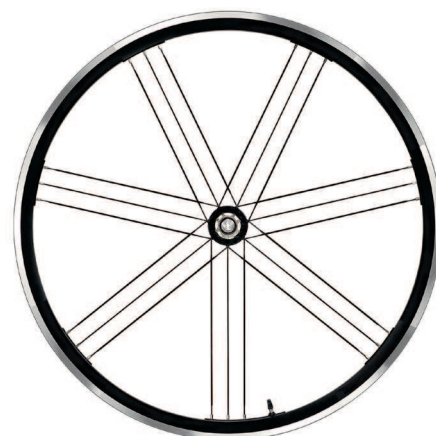
A



B



C



## 1 SPRINT ACTION, STANDING ON THE PEDALS, DURING UPHILL RIDING, STARTING FROM LOW SPEED ( $V < 17$ KM/H)

1.1 The quickness whereby the sprint action was converted into the bicycle acceleration resulted:

| Wheelset | 1<br>very low            | 2<br>low                 | 3<br>adequate            | 4<br>high                | 5<br>very high           | I was not able to<br>feel it |
|----------|--------------------------|--------------------------|--------------------------|--------------------------|--------------------------|------------------------------|
| A        | <input type="checkbox"/> | <input type="checkbox"/> | <input type="checkbox"/> | <input type="checkbox"/> | <input type="checkbox"/> | <input type="checkbox"/>     |
| B        | <input type="checkbox"/> | <input type="checkbox"/> | <input type="checkbox"/> | <input type="checkbox"/> | <input type="checkbox"/> | <input type="checkbox"/>     |
| C        | <input type="checkbox"/> | <input type="checkbox"/> | <input type="checkbox"/> | <input type="checkbox"/> | <input type="checkbox"/> | <input type="checkbox"/>     |

1.2 The acceleration of the bicycle, if compared to the force involved in the stroke on pedals, resulted:

| Wheelset | 1<br>very low            | 2<br>low                 | 3<br>adequate            | 4<br>high                | 5<br>very high           | I was not able to<br>feel it |
|----------|--------------------------|--------------------------|--------------------------|--------------------------|--------------------------|------------------------------|
| A        | <input type="checkbox"/> | <input type="checkbox"/> | <input type="checkbox"/> | <input type="checkbox"/> | <input type="checkbox"/> | <input type="checkbox"/>     |
| B        | <input type="checkbox"/> | <input type="checkbox"/> | <input type="checkbox"/> | <input type="checkbox"/> | <input type="checkbox"/> | <input type="checkbox"/>     |
| C        | <input type="checkbox"/> | <input type="checkbox"/> | <input type="checkbox"/> | <input type="checkbox"/> | <input type="checkbox"/> | <input type="checkbox"/>     |

## 2 UPHILL RIDING AT CONSTANT SPEED

### 2.1 Uphill riding at low speed ( $V < 17$ km/h)

2.1.1 The body effort needed for keeping the constant uphill speed resulted:

| WHEELSET | 1<br>very high           | 2<br>high                | 3<br>acceptable          | 4<br>low                 | 5<br>very low            | I was not able to<br>feel it |
|----------|--------------------------|--------------------------|--------------------------|--------------------------|--------------------------|------------------------------|
| A        | <input type="checkbox"/> | <input type="checkbox"/> | <input type="checkbox"/> | <input type="checkbox"/> | <input type="checkbox"/> | <input type="checkbox"/>     |
| B        | <input type="checkbox"/> | <input type="checkbox"/> | <input type="checkbox"/> | <input type="checkbox"/> | <input type="checkbox"/> | <input type="checkbox"/>     |
| C        | <input type="checkbox"/> | <input type="checkbox"/> | <input type="checkbox"/> | <input type="checkbox"/> | <input type="checkbox"/> | <input type="checkbox"/>     |

### 2.2 Uphill riding at high speed ( $V > 17$ km/h)

2.2.1 The body effort needed for keeping the constant uphill speed resulted:

| WHEELSET | 1<br>very high           | 2<br>high                | 3<br>acceptable          | 4<br>low                 | 5<br>very low            | I was not able to<br>feel it |
|----------|--------------------------|--------------------------|--------------------------|--------------------------|--------------------------|------------------------------|
| A        | <input type="checkbox"/> | <input type="checkbox"/> | <input type="checkbox"/> | <input type="checkbox"/> | <input type="checkbox"/> | <input type="checkbox"/>     |
| B        | <input type="checkbox"/> | <input type="checkbox"/> | <input type="checkbox"/> | <input type="checkbox"/> | <input type="checkbox"/> | <input type="checkbox"/>     |
| C        | <input type="checkbox"/> | <input type="checkbox"/> | <input type="checkbox"/> | <input type="checkbox"/> | <input type="checkbox"/> | <input type="checkbox"/>     |

### 2.3 Passage from uphill to downhill

2.3.1 The acceleration of the bicycle due to the decrease of the road slope resulted:

| Wheelset | 1<br>very low            | 2<br>low                 | 3<br>adequate            | 4<br>high                | 5<br>very high           | I was not able to<br>feel it |
|----------|--------------------------|--------------------------|--------------------------|--------------------------|--------------------------|------------------------------|
| A        | <input type="checkbox"/> | <input type="checkbox"/> | <input type="checkbox"/> | <input type="checkbox"/> | <input type="checkbox"/> | <input type="checkbox"/>     |
| B        | <input type="checkbox"/> | <input type="checkbox"/> | <input type="checkbox"/> | <input type="checkbox"/> | <input type="checkbox"/> | <input type="checkbox"/>     |
| C        | <input type="checkbox"/> | <input type="checkbox"/> | <input type="checkbox"/> | <input type="checkbox"/> | <input type="checkbox"/> | <input type="checkbox"/>     |

### 3 CYCLING ON A STRAIGHT FLAT ROAD WITHOUT THE DRAFTING EFFECT OF OTHER CYCLISTS

#### 3.1 Cycling on a flat road at constant speed

3.1.1 The body effort needed for keeping the constant speed resulted:

| WHEELSET | 1<br>very high           | 2<br>high                | 3<br>acceptable          | 4<br>low                 | 5<br>very low            | I was not able to<br>feel it |
|----------|--------------------------|--------------------------|--------------------------|--------------------------|--------------------------|------------------------------|
| A        | <input type="checkbox"/> | <input type="checkbox"/> | <input type="checkbox"/> | <input type="checkbox"/> | <input type="checkbox"/> | <input type="checkbox"/>     |
| B        | <input type="checkbox"/> | <input type="checkbox"/> | <input type="checkbox"/> | <input type="checkbox"/> | <input type="checkbox"/> | <input type="checkbox"/>     |
| C        | <input type="checkbox"/> | <input type="checkbox"/> | <input type="checkbox"/> | <input type="checkbox"/> | <input type="checkbox"/> | <input type="checkbox"/>     |

3.1.2 The deceleration of the bicycle perceived when the cyclist stops to pedal resulted:

| WHEELSET | 1<br>very high           | 2<br>high                | 3<br>acceptable          | 4<br>low                 | 5<br>very low            | I was not able to<br>feel it |
|----------|--------------------------|--------------------------|--------------------------|--------------------------|--------------------------|------------------------------|
| A        | <input type="checkbox"/> | <input type="checkbox"/> | <input type="checkbox"/> | <input type="checkbox"/> | <input type="checkbox"/> | <input type="checkbox"/>     |
| B        | <input type="checkbox"/> | <input type="checkbox"/> | <input type="checkbox"/> | <input type="checkbox"/> | <input type="checkbox"/> | <input type="checkbox"/>     |
| C        | <input type="checkbox"/> | <input type="checkbox"/> | <input type="checkbox"/> | <input type="checkbox"/> | <input type="checkbox"/> | <input type="checkbox"/>     |

#### 3.2 Presence of lateral wind or turbulences due to the effect of a car or a truck

3.2.1 The decrease of the bicycle stability due to lateral wind resulted:

| WHEELSET | 1<br>very high           | 2<br>high                | 3<br>acceptable          | 4<br>low                 | 5<br>very low            | I was not able to<br>feel it | There was not<br>side wind during<br>the test |
|----------|--------------------------|--------------------------|--------------------------|--------------------------|--------------------------|------------------------------|---|
| A        | <input type="checkbox"/> | <input type="checkbox"/> | <input type="checkbox"/> | <input type="checkbox"/> | <input type="checkbox"/> | <input type="checkbox"/>     | <input type="checkbox"/>                      |
| B        | <input type="checkbox"/> | <input type="checkbox"/> | <input type="checkbox"/> | <input type="checkbox"/> | <input type="checkbox"/> | <input type="checkbox"/>     | <input type="checkbox"/>                      |
| C        | <input type="checkbox"/> | <input type="checkbox"/> | <input type="checkbox"/> | <input type="checkbox"/> | <input type="checkbox"/> | <input type="checkbox"/>     | <input type="checkbox"/>                      |

### 4 CYCLING ON A STRAIGHT FLAT ROAD WITH THE DRAFTING EFFECT OF OTHER CYCLISTS

4.1 The body effort needed for keeping the constant speed resulted:

| WHEELSET | 1<br>very high           | 2<br>high                | 3<br>acceptable          | 4<br>low                 | 5<br>very low            | I was not able to<br>feel it |
|----------|--------------------------|--------------------------|--------------------------|--------------------------|--------------------------|------------------------------|
| A        | <input type="checkbox"/> | <input type="checkbox"/> | <input type="checkbox"/> | <input type="checkbox"/> | <input type="checkbox"/> | <input type="checkbox"/>     |
| B        | <input type="checkbox"/> | <input type="checkbox"/> | <input type="checkbox"/> | <input type="checkbox"/> | <input type="checkbox"/> | <input type="checkbox"/>     |
| C        | <input type="checkbox"/> | <input type="checkbox"/> | <input type="checkbox"/> | <input type="checkbox"/> | <input type="checkbox"/> | <input type="checkbox"/>     |

4.2 The deceleration of the bicycle perceived when the cyclist stops to pedal resulted:

| WHEELSET | 1<br>very high           | 2<br>high                | 3<br>acceptable          | 4<br>low                 | 5<br>very low            | I was not able to<br>feel it |
|----------|--------------------------|--------------------------|--------------------------|--------------------------|--------------------------|------------------------------|
| A        | <input type="checkbox"/> | <input type="checkbox"/> | <input type="checkbox"/> | <input type="checkbox"/> | <input type="checkbox"/> | <input type="checkbox"/>     |
| B        | <input type="checkbox"/> | <input type="checkbox"/> | <input type="checkbox"/> | <input type="checkbox"/> | <input type="checkbox"/> | <input type="checkbox"/>     |
| C        | <input type="checkbox"/> | <input type="checkbox"/> | <input type="checkbox"/> | <input type="checkbox"/> | <input type="checkbox"/> | <input type="checkbox"/>     |



## 5 SPRINT ACTION, STANDING ON THE PEDALS, DURING FLAT ROAD RIDING, STARTING FROM HIGH SPEED (V>30 KM/H)

5.1 The quickness whereby the sprint action was converted into the bicycle acceleration resulted:

| Wheelset | 1<br>very low            | 2<br>low                 | 3<br>normal              | 4<br>high                | 5<br>very high           | I was not able to<br>feel it | I did not perform<br>this action during<br>the test |
|----------|--------------------------|--------------------------|--------------------------|--------------------------|--------------------------|------------------------------|---|
| A        | <input type="checkbox"/> | <input type="checkbox"/> | <input type="checkbox"/> | <input type="checkbox"/> | <input type="checkbox"/> | <input type="checkbox"/>     | <input type="checkbox"/>                            |
| B        | <input type="checkbox"/> | <input type="checkbox"/> | <input type="checkbox"/> | <input type="checkbox"/> | <input type="checkbox"/> | <input type="checkbox"/>     | <input type="checkbox"/>                            |
| C        | <input type="checkbox"/> | <input type="checkbox"/> | <input type="checkbox"/> | <input type="checkbox"/> | <input type="checkbox"/> | <input type="checkbox"/>     | <input type="checkbox"/>                            |

5.2 The speed level reached by the bicycle at the end of the sprint action resulted:

| Wheelset | 1<br>very low            | 2<br>low                 | 3<br>adequate            | 4<br>high                | 5<br>very high           | I was not able to<br>feel it | I did not perform<br>this action during<br>the test |
|----------|--------------------------|--------------------------|--------------------------|--------------------------|--------------------------|------------------------------|---|
| A        | <input type="checkbox"/> | <input type="checkbox"/> | <input type="checkbox"/> | <input type="checkbox"/> | <input type="checkbox"/> | <input type="checkbox"/>     | <input type="checkbox"/>                            |
| B        | <input type="checkbox"/> | <input type="checkbox"/> | <input type="checkbox"/> | <input type="checkbox"/> | <input type="checkbox"/> | <input type="checkbox"/>     | <input type="checkbox"/>                            |
| C        | <input type="checkbox"/> | <input type="checkbox"/> | <input type="checkbox"/> | <input type="checkbox"/> | <input type="checkbox"/> | <input type="checkbox"/>     | <input type="checkbox"/>                            |

## 6 CYCLING ON A DOWNHILL ROAD

6.1 The acceleration of the bicycle during the downhill road riding resulted:

| WHEELSET | 1<br>very low            | 2<br>low                 | 3<br>adequate            | 4<br>high                | 5<br>very high           | I was not able to<br>feel it |
|----------|--------------------------|--------------------------|--------------------------|--------------------------|--------------------------|------------------------------|
| A        | <input type="checkbox"/> | <input type="checkbox"/> | <input type="checkbox"/> | <input type="checkbox"/> | <input type="checkbox"/> | <input type="checkbox"/>     |
| B        | <input type="checkbox"/> | <input type="checkbox"/> | <input type="checkbox"/> | <input type="checkbox"/> | <input type="checkbox"/> | <input type="checkbox"/>     |
| C        | <input type="checkbox"/> | <input type="checkbox"/> | <input type="checkbox"/> | <input type="checkbox"/> | <input type="checkbox"/> | <input type="checkbox"/>     |

6.2 The variation of the bicycle stability with the speed increase resulted:

| WHEELSET | 1<br>very low            | 2<br>low                 | 3<br>acceptable          | 4<br>high                | 5<br>very high           | I was not able to<br>feel it |
|----------|--------------------------|--------------------------|--------------------------|--------------------------|--------------------------|------------------------------|
| A        | <input type="checkbox"/> | <input type="checkbox"/> | <input type="checkbox"/> | <input type="checkbox"/> | <input type="checkbox"/> | <input type="checkbox"/>     |
| B        | <input type="checkbox"/> | <input type="checkbox"/> | <input type="checkbox"/> | <input type="checkbox"/> | <input type="checkbox"/> | <input type="checkbox"/>     |
| C        | <input type="checkbox"/> | <input type="checkbox"/> | <input type="checkbox"/> | <input type="checkbox"/> | <input type="checkbox"/> | <input type="checkbox"/>     |

6.3 The decrease of the bicycle stability due to lateral wind resulted:

| WHEELSET | 1<br>very high           | 2<br>high                | 3<br>acceptable          | 4<br>low                 | 5<br>very low            | I was not able to<br>feel it | There was not<br>side wind during<br>the test |
|----------|--------------------------|--------------------------|--------------------------|--------------------------|--------------------------|------------------------------|---|
| A        | <input type="checkbox"/> | <input type="checkbox"/> | <input type="checkbox"/> | <input type="checkbox"/> | <input type="checkbox"/> | <input type="checkbox"/>     | <input type="checkbox"/>                      |
| B        | <input type="checkbox"/> | <input type="checkbox"/> | <input type="checkbox"/> | <input type="checkbox"/> | <input type="checkbox"/> | <input type="checkbox"/>     | <input type="checkbox"/>                      |
| C        | <input type="checkbox"/> | <input type="checkbox"/> | <input type="checkbox"/> | <input type="checkbox"/> | <input type="checkbox"/> | <input type="checkbox"/>     | <input type="checkbox"/>                      |

## 7 BRAKING ACTION

### 7.1 Initial braking phase

7.1.1 The beginning of the braking action resulted:

| RUOTE | 1<br><i>very sudden</i>  | 2<br><i>sudden</i>       | 3<br><i>normal</i>       | 4<br><i>gradual</i>      | 5<br><i>very gradual</i> | <i>I was not able to feel it</i> |
|-------|--------------------------|--------------------------|--------------------------|--------------------------|--------------------------|----------------------------------|
| A     | <input type="checkbox"/> | <input type="checkbox"/> | <input type="checkbox"/> | <input type="checkbox"/> | <input type="checkbox"/> | <input type="checkbox"/>         |
| B     | <input type="checkbox"/> | <input type="checkbox"/> | <input type="checkbox"/> | <input type="checkbox"/> | <input type="checkbox"/> | <input type="checkbox"/>         |
| C     | <input type="checkbox"/> | <input type="checkbox"/> | <input type="checkbox"/> | <input type="checkbox"/> | <input type="checkbox"/> | <input type="checkbox"/>         |

7.1.2 The time elapsed between the beginning of the brake lever movement and the beginning of the bicycle deceleration, during rainy conditions, resulted:

| WHEELSET | 1<br><i>very high</i>    | 2<br><i>high</i>         | 3<br><i>normal</i>       | 4<br><i>low</i>          | 5<br><i>very low</i>     | <i>I was not able to feel it</i> | <i>The test was performed with dry conitions</i> |
|----------|--------------------------|--------------------------|--------------------------|--------------------------|--------------------------|----------------------------------|--|
| A        | <input type="checkbox"/> | <input type="checkbox"/> | <input type="checkbox"/> | <input type="checkbox"/> | <input type="checkbox"/> | <input type="checkbox"/>         | <input type="checkbox"/>                         |
| B        | <input type="checkbox"/> | <input type="checkbox"/> | <input type="checkbox"/> | <input type="checkbox"/> | <input type="checkbox"/> | <input type="checkbox"/>         | <input type="checkbox"/>                         |
| C        | <input type="checkbox"/> | <input type="checkbox"/> | <input type="checkbox"/> | <input type="checkbox"/> | <input type="checkbox"/> | <input type="checkbox"/>         | <input type="checkbox"/>                         |

### 7.2 Central and final braking phase

7.2.1 The deceleration of the bicycle, if compared with the force applied to the brake levers, resulted:

| WHEELSET | 1<br><i>very low</i>     | 2<br><i>low</i>          | 3<br><i>adequate</i>     | 4<br><i>high</i>         | 5<br><i>very high</i>    | <i>I was not able to feel it</i> |
|----------|--------------------------|--------------------------|--------------------------|--------------------------|--------------------------|----------------------------------|
| A        | <input type="checkbox"/> | <input type="checkbox"/> | <input type="checkbox"/> | <input type="checkbox"/> | <input type="checkbox"/> | <input type="checkbox"/>         |
| B        | <input type="checkbox"/> | <input type="checkbox"/> | <input type="checkbox"/> | <input type="checkbox"/> | <input type="checkbox"/> | <input type="checkbox"/>         |
| C        | <input type="checkbox"/> | <input type="checkbox"/> | <input type="checkbox"/> | <input type="checkbox"/> | <input type="checkbox"/> | <input type="checkbox"/>         |

7.2.2 The decrease of the braking performance during the braking action resulted:

| WHEELSET | 1<br><i>very high</i>    | 2<br><i>high</i>         | 3<br><i>acceptable</i>   | 4<br><i>low</i>          | 5<br><i>very low</i>     | <i>I was not able to feel it</i> |
|----------|--------------------------|--------------------------|--------------------------|--------------------------|--------------------------|----------------------------------|
| A        | <input type="checkbox"/> | <input type="checkbox"/> | <input type="checkbox"/> | <input type="checkbox"/> | <input type="checkbox"/> | <input type="checkbox"/>         |
| B        | <input type="checkbox"/> | <input type="checkbox"/> | <input type="checkbox"/> | <input type="checkbox"/> | <input type="checkbox"/> | <input type="checkbox"/>         |
| C        | <input type="checkbox"/> | <input type="checkbox"/> | <input type="checkbox"/> | <input type="checkbox"/> | <input type="checkbox"/> | <input type="checkbox"/>         |

7.2.3 The entity of the vibrations perceived during the braking action resulted:

| WHEELSET | 1<br><i>very high</i>    | 2<br><i>high</i>         | 3<br><i>acceptable</i>   | 4<br><i>low</i>          | 5<br><i>very low</i>     | <i>I was not able to feel it</i> |
|----------|--------------------------|--------------------------|--------------------------|--------------------------|--------------------------|----------------------------------|
| A        | <input type="checkbox"/> | <input type="checkbox"/> | <input type="checkbox"/> | <input type="checkbox"/> | <input type="checkbox"/> | <input type="checkbox"/>         |
| B        | <input type="checkbox"/> | <input type="checkbox"/> | <input type="checkbox"/> | <input type="checkbox"/> | <input type="checkbox"/> | <input type="checkbox"/>         |
| C        | <input type="checkbox"/> | <input type="checkbox"/> | <input type="checkbox"/> | <input type="checkbox"/> | <input type="checkbox"/> | <input type="checkbox"/>         |

## 8 PERFORMING A CURVE



8.1.1 The quickness of curve entering resulted:

| WHEELSET | 1<br>very low            | 2<br>low                 | 3<br>adequate            | 4<br>high                | 5<br>very high           | I was not able to feel it |
|----------|--------------------------|--------------------------|--------------------------|--------------------------|--------------------------|---------------------------|
| A        | <input type="checkbox"/> | <input type="checkbox"/> | <input type="checkbox"/> | <input type="checkbox"/> | <input type="checkbox"/> | <input type="checkbox"/>  |
| B        | <input type="checkbox"/> | <input type="checkbox"/> | <input type="checkbox"/> | <input type="checkbox"/> | <input type="checkbox"/> | <input type="checkbox"/>  |
| C        | <input type="checkbox"/> | <input type="checkbox"/> | <input type="checkbox"/> | <input type="checkbox"/> | <input type="checkbox"/> | <input type="checkbox"/>  |

8.1.2 The body effort needed for entering in a curve resulted:

| WHEELSET | 1<br>very high           | 2<br>high                | 3<br>acceptable          | 4<br>low                 | 5<br>very low            | I was not able to feel it |
|----------|--------------------------|--------------------------|--------------------------|--------------------------|--------------------------|---------------------------|
| A        | <input type="checkbox"/> | <input type="checkbox"/> | <input type="checkbox"/> | <input type="checkbox"/> | <input type="checkbox"/> | <input type="checkbox"/>  |
| B        | <input type="checkbox"/> | <input type="checkbox"/> | <input type="checkbox"/> | <input type="checkbox"/> | <input type="checkbox"/> | <input type="checkbox"/>  |
| C        | <input type="checkbox"/> | <input type="checkbox"/> | <input type="checkbox"/> | <input type="checkbox"/> | <input type="checkbox"/> | <input type="checkbox"/>  |

8.1.3 The entry into the curve phase, generally resulted:

| WHEELSET | 1<br>very difficult      | 2<br>difficult           | 3<br>normal              | 4<br>easy                | 5<br>very easy           | I cannot give an assessment about that |
|----------|--------------------------|--------------------------|--------------------------|--------------------------|--------------------------|--|
| A        | <input type="checkbox"/> | <input type="checkbox"/> | <input type="checkbox"/> | <input type="checkbox"/> | <input type="checkbox"/> | <input type="checkbox"/>               |
| B        | <input type="checkbox"/> | <input type="checkbox"/> | <input type="checkbox"/> | <input type="checkbox"/> | <input type="checkbox"/> | <input type="checkbox"/>               |
| C        | <input type="checkbox"/> | <input type="checkbox"/> | <input type="checkbox"/> | <input type="checkbox"/> | <input type="checkbox"/> | <input type="checkbox"/>               |



8.2.1 The precision in following the turning path resulted:

| WHEELSET | 1<br>very low            | 2<br>low                 | 3<br>adequate            | 4<br>high                | 5<br>very high           | I was not able to feel it |
|----------|--------------------------|--------------------------|--------------------------|--------------------------|--------------------------|---------------------------|
| A        | <input type="checkbox"/> | <input type="checkbox"/> | <input type="checkbox"/> | <input type="checkbox"/> | <input type="checkbox"/> | <input type="checkbox"/>  |
| B        | <input type="checkbox"/> | <input type="checkbox"/> | <input type="checkbox"/> | <input type="checkbox"/> | <input type="checkbox"/> | <input type="checkbox"/>  |
| C        | <input type="checkbox"/> | <input type="checkbox"/> | <input type="checkbox"/> | <input type="checkbox"/> | <input type="checkbox"/> | <input type="checkbox"/>  |

8.2.2 The body effort needed for the steady turning phase resulted:

| WHEELSET | 1<br>very high           | 2<br>high                | 3<br>acceptable          | 4<br>low                 | 5<br>very low            | I was not able to feel it |
|----------|--------------------------|--------------------------|--------------------------|--------------------------|--------------------------|---------------------------|
| A        | <input type="checkbox"/> | <input type="checkbox"/> | <input type="checkbox"/> | <input type="checkbox"/> | <input type="checkbox"/> | <input type="checkbox"/>  |
| B        | <input type="checkbox"/> | <input type="checkbox"/> | <input type="checkbox"/> | <input type="checkbox"/> | <input type="checkbox"/> | <input type="checkbox"/>  |
| C        | <input type="checkbox"/> | <input type="checkbox"/> | <input type="checkbox"/> | <input type="checkbox"/> | <input type="checkbox"/> | <input type="checkbox"/>  |

**8.2.3** The number of actions performed to correct the turning path resulted:

| WHEELSET | 1<br>very high           | 2<br>high                | 3<br>acceptable          | 4<br>low                 | 5<br>absent              | <i>I cannot give<br/>an assessment<br/>about that</i> |
|----------|--------------------------|--------------------------|--------------------------|--------------------------|--------------------------|---|
| A        | <input type="checkbox"/> | <input type="checkbox"/> | <input type="checkbox"/> | <input type="checkbox"/> | <input type="checkbox"/> | <input type="checkbox"/>                              |
| B        | <input type="checkbox"/> | <input type="checkbox"/> | <input type="checkbox"/> | <input type="checkbox"/> | <input type="checkbox"/> | <input type="checkbox"/>                              |
| C        | <input type="checkbox"/> | <input type="checkbox"/> | <input type="checkbox"/> | <input type="checkbox"/> | <input type="checkbox"/> | <input type="checkbox"/>                              |

**8.2.4** The decrease of the bicycle stability due to lateral wind resulted:

| WHEELSET | 1<br>very high           | 2<br>high                | 3<br>acceptable          | 4<br>low                 | 5<br>very low            | <i>I was not able to<br/>feel it</i> | <i>There was not<br/>side wind during<br/>the test</i> |
|----------|--------------------------|--------------------------|--------------------------|--------------------------|--------------------------|--------------------------------------|--|
| A        | <input type="checkbox"/> | <input type="checkbox"/> | <input type="checkbox"/> | <input type="checkbox"/> | <input type="checkbox"/> | <input type="checkbox"/>             | <input type="checkbox"/>                               |
| B        | <input type="checkbox"/> | <input type="checkbox"/> | <input type="checkbox"/> | <input type="checkbox"/> | <input type="checkbox"/> | <input type="checkbox"/>             | <input type="checkbox"/>                               |
| C        | <input type="checkbox"/> | <input type="checkbox"/> | <input type="checkbox"/> | <input type="checkbox"/> | <input type="checkbox"/> | <input type="checkbox"/>             | <input type="checkbox"/>                               |


**8.3.1** The speed of the bicycle at the exit from the curve resulted:

| WHEELSET | 1<br>very low            | 2<br>low                 | 3<br>adequate            | 4<br>high                | 5<br>very high           | <i>I was not able to<br/>feel it</i> |
|----------|--------------------------|--------------------------|--------------------------|--------------------------|--------------------------|--------------------------------------|
| A        | <input type="checkbox"/> | <input type="checkbox"/> | <input type="checkbox"/> | <input type="checkbox"/> | <input type="checkbox"/> | <input type="checkbox"/>             |
| B        | <input type="checkbox"/> | <input type="checkbox"/> | <input type="checkbox"/> | <input type="checkbox"/> | <input type="checkbox"/> | <input type="checkbox"/>             |
| C        | <input type="checkbox"/> | <input type="checkbox"/> | <input type="checkbox"/> | <input type="checkbox"/> | <input type="checkbox"/> | <input type="checkbox"/>             |

**8.3.2** The body effort needed for accelerating the bicycle at the curve exit resulted:

| WHEELSET | 1<br>very high           | 2<br>high                | 3<br>acceptable          | 4<br>low                 | 5<br>very low            | <i>I was not able to<br/>feel it</i> |
|----------|--------------------------|--------------------------|--------------------------|--------------------------|--------------------------|--------------------------------------|
| A        | <input type="checkbox"/> | <input type="checkbox"/> | <input type="checkbox"/> | <input type="checkbox"/> | <input type="checkbox"/> | <input type="checkbox"/>             |
| B        | <input type="checkbox"/> | <input type="checkbox"/> | <input type="checkbox"/> | <input type="checkbox"/> | <input type="checkbox"/> | <input type="checkbox"/>             |
| C        | <input type="checkbox"/> | <input type="checkbox"/> | <input type="checkbox"/> | <input type="checkbox"/> | <input type="checkbox"/> | <input type="checkbox"/>             |

## 9 PERFORMING TWO OR MORE CONSECUTIVES CURVES

9.1 The quickness of the direction changes resulted:

| WHEELSET | 1<br>very low            | 2<br>low                 | 3<br>adequate            | 4<br>high                | 5<br>very high           | I was not able to<br>feel it |
|----------|--------------------------|--------------------------|--------------------------|--------------------------|--------------------------|------------------------------|
| A        | <input type="checkbox"/> | <input type="checkbox"/> | <input type="checkbox"/> | <input type="checkbox"/> | <input type="checkbox"/> | <input type="checkbox"/>     |
| B        | <input type="checkbox"/> | <input type="checkbox"/> | <input type="checkbox"/> | <input type="checkbox"/> | <input type="checkbox"/> | <input type="checkbox"/>     |
| C        | <input type="checkbox"/> | <input type="checkbox"/> | <input type="checkbox"/> | <input type="checkbox"/> | <input type="checkbox"/> | <input type="checkbox"/>     |

9.2 The body effort needed for the direction change resulted:

| WHEELSET | 1<br>very high           | 2<br>high                | 3<br>acceptable          | 4<br>low                 | 5<br>very low            | I was not able to<br>feel it |
|----------|--------------------------|--------------------------|--------------------------|--------------------------|--------------------------|------------------------------|
| A        | <input type="checkbox"/> | <input type="checkbox"/> | <input type="checkbox"/> | <input type="checkbox"/> | <input type="checkbox"/> | <input type="checkbox"/>     |
| B        | <input type="checkbox"/> | <input type="checkbox"/> | <input type="checkbox"/> | <input type="checkbox"/> | <input type="checkbox"/> | <input type="checkbox"/>     |
| C        | <input type="checkbox"/> | <input type="checkbox"/> | <input type="checkbox"/> | <input type="checkbox"/> | <input type="checkbox"/> | <input type="checkbox"/>     |

## 10 CYCLING ON ROADS WITH AN ASPHALT CHARACTERIZED BY A BIG GRAIN (E.G. DRAINING ASPHALT)

10.1 The entity of the vibrations perceived at the hands, the feet, and the lumbar area, resulted:

| WHEELSET | 1<br>very high           | 2<br>high                | 3<br>acceptable          | 4<br>low                 | 5<br>very low            | I was not able to<br>feel it |
|----------|--------------------------|--------------------------|--------------------------|--------------------------|--------------------------|------------------------------|
| A        | <input type="checkbox"/> | <input type="checkbox"/> | <input type="checkbox"/> | <input type="checkbox"/> | <input type="checkbox"/> | <input type="checkbox"/>     |
| B        | <input type="checkbox"/> | <input type="checkbox"/> | <input type="checkbox"/> | <input type="checkbox"/> | <input type="checkbox"/> | <input type="checkbox"/>     |
| C        | <input type="checkbox"/> | <input type="checkbox"/> | <input type="checkbox"/> | <input type="checkbox"/> | <input type="checkbox"/> | <input type="checkbox"/>     |

## 11 CYCLING ON UNEVEN ROADS WITH CONSECUTIVE OBSTACLES SUCH AS HOLES AND/OR ASPHALT PATCHES

11.1 The entity of the body stress due to the overcoming of the consecutives obstacles resulted:

| WHEELSET | 1<br>very high           | 2<br>high                | 3<br>acceptable          | 4<br>low                 | 5<br>very low            | I was not able to<br>feel it | I did not encounter<br>any obstacle during<br>the test |
|----------|--------------------------|--------------------------|--------------------------|--------------------------|--------------------------|------------------------------|--|
| A        | <input type="checkbox"/> | <input type="checkbox"/> | <input type="checkbox"/> | <input type="checkbox"/> | <input type="checkbox"/> | <input type="checkbox"/>     | <input type="checkbox"/>                               |
| B        | <input type="checkbox"/> | <input type="checkbox"/> | <input type="checkbox"/> | <input type="checkbox"/> | <input type="checkbox"/> | <input type="checkbox"/>     | <input type="checkbox"/>                               |
| C        | <input type="checkbox"/> | <input type="checkbox"/> | <input type="checkbox"/> | <input type="checkbox"/> | <input type="checkbox"/> | <input type="checkbox"/>     | <input type="checkbox"/>                               |

11.2 The entity of the muscular fatigue spotted at the end of the cycling session resulted:

| WHEELSET | 1<br>very high           | 2<br>high                | 3<br>acceptable          | 4<br>low                 | 5<br>very low            | The test was<br>too short for<br>perceiving it | I did not encounter<br>any obstacle during<br>the test |
|----------|--------------------------|--------------------------|--------------------------|--------------------------|--------------------------|--|--|
| A        | <input type="checkbox"/> | <input type="checkbox"/> | <input type="checkbox"/> | <input type="checkbox"/> | <input type="checkbox"/> | <input type="checkbox"/>                       | <input type="checkbox"/>                               |
| B        | <input type="checkbox"/> | <input type="checkbox"/> | <input type="checkbox"/> | <input type="checkbox"/> | <input type="checkbox"/> | <input type="checkbox"/>                       | <input type="checkbox"/>                               |
| C        | <input type="checkbox"/> | <input type="checkbox"/> | <input type="checkbox"/> | <input type="checkbox"/> | <input type="checkbox"/> | <input type="checkbox"/>                       | <input type="checkbox"/>                               |

## 12 CYCLING ON UNEVEN ROADS WITH ISOLATED OBSTACLES SUCH AS POTHOLES, ASPHALT HOLES, BUMPS, AND ASPHALT PATCHES

12.1 The entity of the body stress due to the overcoming of the obstacles resulted:

| WHEELSET | 1<br>very high           | 2<br>high                | 3<br>acceptable          | 4<br>low                 | 5<br>very low            | I was not able to<br>feel it | I did not encounter<br>any obstacle during<br>the test |
|----------|--------------------------|--------------------------|--------------------------|--------------------------|--------------------------|------------------------------|--|
| A        | <input type="checkbox"/> | <input type="checkbox"/> | <input type="checkbox"/> | <input type="checkbox"/> | <input type="checkbox"/> | <input type="checkbox"/>     | <input type="checkbox"/>                               |
| B        | <input type="checkbox"/> | <input type="checkbox"/> | <input type="checkbox"/> | <input type="checkbox"/> | <input type="checkbox"/> | <input type="checkbox"/>     | <input type="checkbox"/>                               |
| C        | <input type="checkbox"/> | <input type="checkbox"/> | <input type="checkbox"/> | <input type="checkbox"/> | <input type="checkbox"/> | <input type="checkbox"/>     | <input type="checkbox"/>                               |

## SOUNDS OR NOISE EVALUATION

If, during the test, the cyclist heard particular sounds, he could specify below its behaviour and the corresponding action

| ACTIONS   | Wheelset A               |                          | Wheelset B               |                          | Wheelset C               |                          | eventual notes |
|---|--------------------------|--------------------------|--------------------------|--------------------------|--------------------------|--------------------------|----------------|
|   | loud<br>sound            | likable<br>sound         | loud<br>sound            | likable<br>sound         | loud<br>sound            | likable<br>sound         |                |
| 1. Sprint action, standing on the pedals, during uphill riding, starting from low speed ( $V < 17$ km/h)        | <input type="checkbox"/> | <input type="checkbox"/> | <input type="checkbox"/> | <input type="checkbox"/> | <input type="checkbox"/> | <input type="checkbox"/> | _____          |
| 2. Uphill riding at constant speed  | <input type="checkbox"/> | <input type="checkbox"/> | <input type="checkbox"/> | <input type="checkbox"/> | <input type="checkbox"/> | <input type="checkbox"/> | _____          |
| 3. Cycling on a straight flat road without the drafting effect of other cyclists                                | <input type="checkbox"/> | <input type="checkbox"/> | <input type="checkbox"/> | <input type="checkbox"/> | <input type="checkbox"/> | <input type="checkbox"/> | _____          |
| 4. Cycling on a straight flat road with the drafting effect of other cyclists                                   | <input type="checkbox"/> | <input type="checkbox"/> | <input type="checkbox"/> | <input type="checkbox"/> | <input type="checkbox"/> | <input type="checkbox"/> | _____          |
| 5. Sprint action, standing on the pedals, during flat road riding, starting from high speed ( $V > 30$ km/h)    | <input type="checkbox"/> | <input type="checkbox"/> | <input type="checkbox"/> | <input type="checkbox"/> | <input type="checkbox"/> | <input type="checkbox"/> | _____          |
| 6. Cycling on a downhill road   | <input type="checkbox"/> | <input type="checkbox"/> | <input type="checkbox"/> | <input type="checkbox"/> | <input type="checkbox"/> | <input type="checkbox"/> | _____          |
| 7. Braking action   | <input type="checkbox"/> | <input type="checkbox"/> | <input type="checkbox"/> | <input type="checkbox"/> | <input type="checkbox"/> | <input type="checkbox"/> | _____          |
| 8. Performing a curve   | <input type="checkbox"/> | <input type="checkbox"/> | <input type="checkbox"/> | <input type="checkbox"/> | <input type="checkbox"/> | <input type="checkbox"/> | _____          |
| 9. Performing two consecutives curves   | <input type="checkbox"/> | <input type="checkbox"/> | <input type="checkbox"/> | <input type="checkbox"/> | <input type="checkbox"/> | <input type="checkbox"/> | _____          |
| 10. Cycling on roads with an asphalt characterized by a big grain (e.g. draining asphalt)                       | <input type="checkbox"/> | <input type="checkbox"/> | <input type="checkbox"/> | <input type="checkbox"/> | <input type="checkbox"/> | <input type="checkbox"/> | _____          |
| 11. Cycling on uneven roads with consecutive obstacles such as holes and/or asphalt patches                     | <input type="checkbox"/> | <input type="checkbox"/> | <input type="checkbox"/> | <input type="checkbox"/> | <input type="checkbox"/> | <input type="checkbox"/> | _____          |
| 12. Cycling on uneven roads with isolated obstacles such as potholes, asphalt holes, bumps, and asphalt patches | <input type="checkbox"/> | <input type="checkbox"/> | <input type="checkbox"/> | <input type="checkbox"/> | <input type="checkbox"/> | <input type="checkbox"/> | _____          |

## GENERAL NOTES

MOD. A: \_\_\_\_\_  
 \_\_\_\_\_  
 \_\_\_\_\_

MOD. B: \_\_\_\_\_  
 \_\_\_\_\_  
 \_\_\_\_\_

MOD. C: \_\_\_\_\_  
 \_\_\_\_\_  
 \_\_\_\_\_



# Chapter 10

## Correlation between the user quality requirements and the engineering parameters of wheels

### 10.1 Introduction

In the previous two chapters, the methods adopted for the identification and organization of the user quality requirements, and the activities concerning the subjective evaluation tests were presented. The 13 discovered quality requirements were evaluated by 33 cyclists during the tests of 3 different wheelset conveniently selected in order to present high differences with respect to the most important engineering characteristics. The evaluation of the quality requirements of the three selected wheelsets (fig. 9.10) was considered for the development of a method for computing the correlation coefficients between each quality requirement and each basic engineering characteristic. The correlation method presented in this chapter allows a **quantitative** analysis of the relationship between the quality requirements and the engineering characteristics, overcoming the arbitrary feature of QFD (see chapter 7).

### 10.2 Correlation method according to standard QFD

QFD [16] proposes a method for computing the correlation between the user quality requirements and the product characteristics. The  $j$ -th product characteristics  $PC_j$  and the  $i$ -th quality requirements  $QR_i$  represent respectively the columns and rows headers of the House of Quality Matrix (fig. 10.1). The quality requirements, discovered in a previous stage, are arranged in order of user importance  $UI_i$ . The list of the product characteristic is defined by an opportunely selected workgroup composed by members from the technical, sales, and marketing department. The correlation coefficients  $c_{ij}$  between the quality requirements and the product characteristics are assigned by the workgroup, which refers to the following typical scale:

- $c_{ij} = 0$  -> no correlation;
- $c_{ij} = 1$  -> low correlation;
- $c_{ij} = 3$  -> medium correlation;
- $c_{ij} = 9$  -> high correlation.

The numbers can often be replaced by a corresponding set of symbols.

The relative weight of each product characteristic  $PC_j$  on the influence of the user quality requirements is the final outcome of the House of Quality Matrix, and it is calculated following the



so called “Independent Scoring Method”:

$$W_{abs,j} = \sum_{i=1}^{n_{QR}} c_{i,j} \cdot U_i \text{ weight of PC}_j \text{ in absolute scale} \quad (1)$$

$$W_{rel,j} = \frac{W_{abs,j}}{\sum_{j=1}^{n_{PC}} W_{abs,j}} \cdot 100 \text{ relative percentage weight of PC}_j \quad (2)$$

$n_{QR}$ : number of quality requirements

$n_{PC}$ : number of product characteristics

|                      |                                   | PRODUCT CHARACTERISTICS |                 |                 |                 |            |
|----------------------|-----------------------------------|-------------------------|-----------------|-----------------|-----------------|------------|
|                      |                                   | PC <sub>1</sub>         | PC <sub>2</sub> | PC <sub>3</sub> | PC <sub>4</sub> |            |
| QUALITY REQUIREMENTS | User Importance<br>U <sub>i</sub> |                         |                 |                 |                 |            |
|                      | QR <sub>3</sub>                   | 3                       | 1               | 1               | 9               |            |
|                      | QR <sub>2</sub>                   | 1                       | 3               | 9               | 0               |            |
|                      | QR <sub>1</sub>                   | 0                       | 1               | 3               | 9               |            |
|                      | QR <sub>4</sub>                   | 9                       | 0               | 1               | 9               |            |
|                      | QR <sub>6</sub>                   | 3                       | 0               | 0               | 3               |            |
|                      | QR <sub>5</sub>                   | 1                       | 1               | 0               | 1               | <b>TOT</b> |
|                      | <b>W<sub>abs,j</sub></b>          | 2.67                    | 1.30            | 3.17            | 5.87            | 13.01      |
|                      | <b>W<sub>rel,j</sub></b>          | 20.52 %                 | 9.99 %          | 24.37 %         | 45.12 %         |            |

Fig. 10.1 Example of QFD House of Quality Matrix

In the example reported on figure 10.1, PC<sub>4</sub> resulted in the product characteristic that has the highest impact on the user quality requirements.

The so obtained correlation coefficients are based on the logical reasoning and shared experiences of the workgroup, and they have therefore an arbitrary behaviour that does not allow a quantitative analysis of the correlations. These limitations were overcome through the method presented below.

### 10.3 Correlation method adopted in this work

The correlation coefficients between the quality requirements (QR) and the engineering characteristics (EC) were calculated applying the Pearson’s coefficients computation method [22]. A diagram was prepared for each (QR<sub>i</sub>, EC<sub>j</sub>) couple, in which the average grades given by the testers to QR<sub>i</sub> and the values measured for EC<sub>j</sub> were respectively reported in the x and y axis (fig. 10.2). Each tested wheelset was therefore represented on the diagram by a point, and the QR<sub>i</sub>/EC<sub>j</sub>

correlation coefficient was calculated as the R parameter of the linear least square fitting curve. The correlation coefficients were reported on the “House of Quality” correlation matrix of the QFD method [16]. The sign of the correlation coefficients indicates if the  $QR_i/EC_i$  correlation is direct (+) or inverse (-): the correlation is high if  $|R|>0.9$ , medium if  $0.7<|R|<0.9$ , low if  $|R|<0.7$ , and there is no correlation if  $|R|<0.5$  (fig. 10.3).

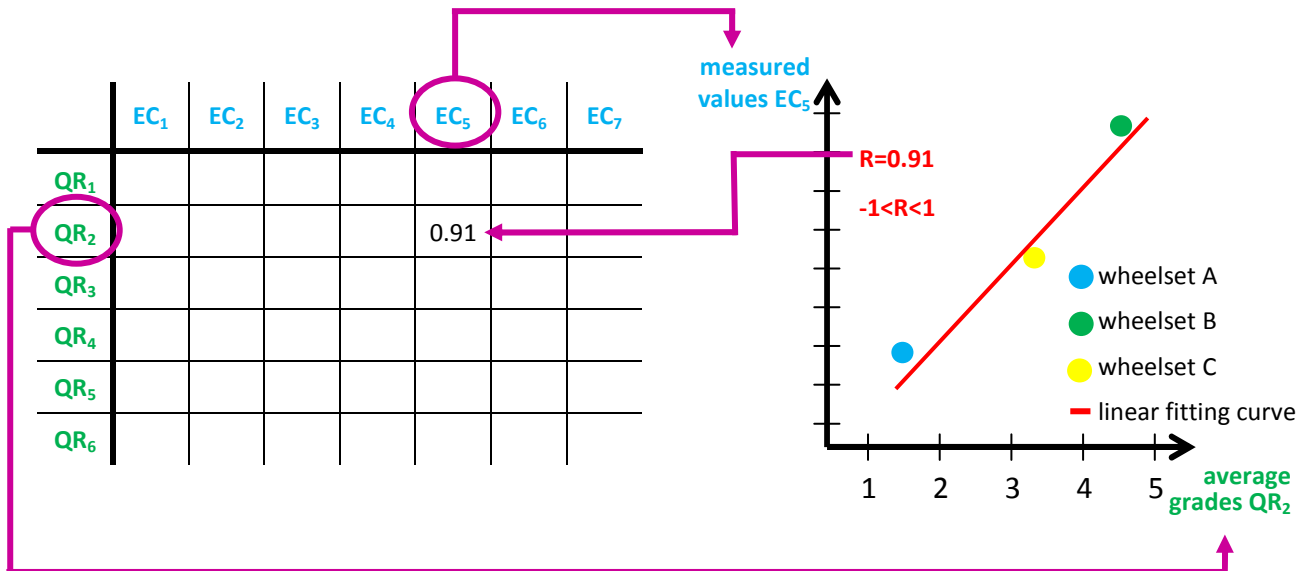


Fig. 10.2 Example of the correlation coefficient computation, between the quality requirement  $QR_2$  and the engineering characteristic  $EC_5$ .

The data regarding the engineering characteristics and the quality requirements evaluation of at least three wheelset are needed for the application of this method. The ideal correlation coefficients can be obtained if each engineering characteristic can independently be varied. Since, for practical reasons, the independent variation of each engineering characteristic was difficult to be carried out, the best solution was represented by the selection of three wheelsets, which presented high differences with respect to the engineering characteristics that, through a preliminary study (see § 9.2), resulted to heavily influence the quality requirements. The results so obtained were therefore conditioned by the mutual correlation between the engineering characteristics, as better explained in the § 10.4.

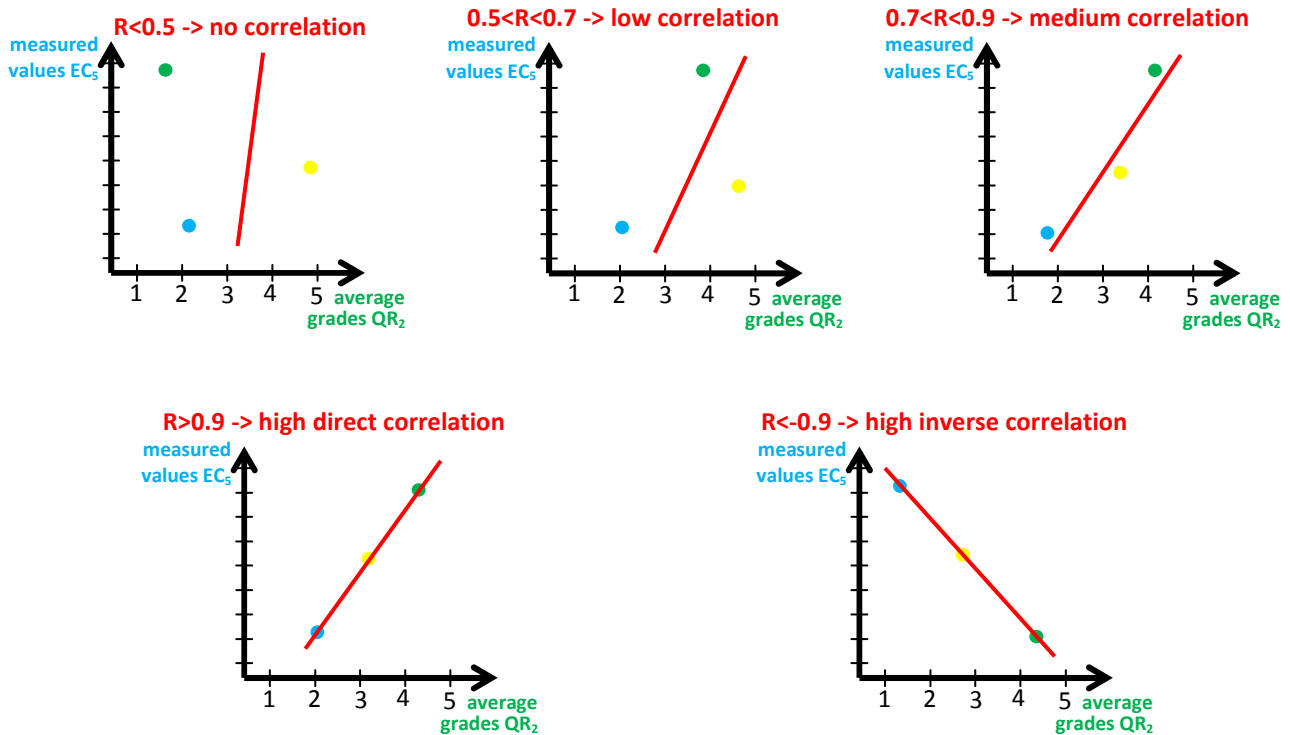


Fig. 10.3 Qualitative representation of the different ranges of the correlation coefficients.

## 10.4 Results

The calculated correlation coefficients between the user quality requirements and the basic engineering characteristics are showed in the table 10.1. Some high or low correlation coefficients have to be considered significant, because they agree with the dynamical analysis of the actions, in which the related quality requirement is evaluated. These coefficients are marked with green circles in the table 10.1. In other cases, the mutual relationship between the different engineering characteristics, causes high correlation coefficients, which have to be considered not significant. For example, the high correlation coefficients obtained between the radial stiffness and QR.1, QR.3, QR.5, and QR.6 (marked with yellow circles in the tab. 10.1), are caused by its high correlation with the wheel mass and the inertia, as reported in table 10.2. For some perceived quality requirements, such as the Forward Rolling Efficiency (QR.9) and the Breaking Regularity (QR.11), no high correlation coefficients were calculated with all engineering characteristics: this suggested the need to develop additional measurement methods for engineering characteristics that were not yet evaluated. The high correlations (red circle mark) resulted for the Braking Power (QR.10), the Stability in Absence of Wind (QR.12), and the Stability to Crosswind (QR.13), with the Mass, Inertia, and Radial Stiffness, are due to the relationship of these basic engineering characteristics with other characteristics, directly correlated with these quality requirements, but not currently evaluated.

Wheels Mass and Inertia (BEC.1, BEC.2) resulted well correlated with three of the four quality

requirements concerning the wheels Reactivity: QR.1, QR.3, and QR.4. The wheels Reactivity evaluated during a sprint, starting from high speed (QR.2), shows low correlation coefficients with wheels mass and inertia. This is due to a change of the contribution of each resistance force with the increase of the bicycle speed, which enhances the effect of the wheels aerodynamic behaviour.

The Radial Stiffness has a high inverse correlation with the Impulsive Comfort: wheels with high radial stiffness less absorb the loads induced by the obstacle overcoming. The Vibrational Comfort is not well expressed by the Radial Stiffness, as demonstrated by their medium correlation.

The low correlation coefficients obtained for the Torsional and Side Stiffness with all quality requirements are caused by the low differences presented by the three tested wheelsets among these two basic engineering characteristics (fig. 9.4).

|  | BASIC ENGINEERING CHARACTERISTICS |                                |                                     |                                  |                                 |
|--|-----------------------------------|--------------------------------|-------------------------------------|----------------------------------|---------------------------------|
|  | BEC.1<br>m [kg]                   | BEC.2<br>I [kgm <sup>2</sup> ] | BEC.3<br>K <sub>torx</sub> [Nm/rad] | BEC.4<br>K <sub>side</sub> [N/m] | BEC.5<br>K <sub>rad</sub> [N/m] |
| QR.1 Reactivity during a sprint, starting from low speed (V<17 km/h)           | -0.883                            | -0.942                         | -0.307                              | -0.647                           | -0.808                          |
| QR.2 Reactivity during a sprint, starting from high speed (V>30 km/h)          | -0.260                            | -0.401                         | -0.899                              | -0.262                           | -0.123                          |
| QR.3 Reactivity during uphill road cycling, at constant low speed (V<17 km/h)  | -0.969                            | -0.994                         | -0.076                              | -0.687                           | -0.924                          |
| QR.4 Reactivity during uphill road cycling, at constant high speed (V>17 km/h) | -0.870                            | -0.933                         | -0.333                              | -0.640                           | -0.792                          |
| QR.5 Handling  | -0.999                            | -0.994                         | 0.127                               | -0.690                           | -0.982                          |
| QR.6 Rad holding   | -0.980                            | -0.938                         | 0.365                               | -0.655                           | -0.997                          |
| QR.7 Vibrational comfort   | -0.912                            | -0.962                         | -0.245                              | -0.662                           | -0.845                          |
| QR.8 Impulsive comfort   | -0.962                            | -0.991                         | -0.100                              | -0.684                           | -0.915                          |
| QR.9 Forward Rolling efficiency  | 0.756                             | 0.649                          | -0.770                              | 0.462                            | 0.839                           |
| QR.10 Braking power  | 0.836                             | 0.908                          | -0.393                              | -0.622                           | -0.751                          |
| QR.11 Braking regularity   | 0.667                             | 0.770                          | 0.613                               | 0.523                            | 0.556                           |
| QR.12 Stability in Absence of Wind   | 0.987                             | 0.952                          | 0.324                               | -0.665                           | -0.999                          |
| QR.13 Stability to Crosswind   | 0.946                             | 0.886                          | 0.480                               | -0.621                           | -0.981                          |

Tab. 10.1 Correlation coefficients calculated between each quality requirement and each basic engineering characteristic (BEC).

|                                  | BEC.1<br>m [kg] | BEC.2<br>I [kgm <sup>2</sup> ] | BEC.3<br>K <sub>torx</sub> [Nm/rad] | BEC.4<br>K <sub>side</sub> [N/m] | BEC.5<br>K <sub>rad</sub> [N/m] |
|----------------------------------|-----------------|--------------------------------|-------------------------------------|----------------------------------|---------------------------------|
| BEC.1 m [kg]                     | 1.00            | 0.98                           | 0.70                                | -0.21                            | 0.99                            |
| BEC.2 I [kgm <sup>2</sup> ]      |                 | 1.00                           | 0.70                                | -0.02                            | 0.94                            |
| BEC.3 K <sub>torx</sub> [Nm/rad] |                 |                                | 1                                   | -0.10                            | 0.67                            |
| BEC.4 K <sub>side</sub> [N/m]    |                 |                                |                                     | 1.00                             | -0.35                           |
| BEC.5 K <sub>rad</sub> [N/m]     |                 |                                |                                     |                                  | 1                               |

Tab. 10.1 Mutual correlation between the basic engineering characteristics (BEC).

## **10.5 Conclusions**

The method developed for the computation of the correlation coefficients allows to obtain a quantitative correlation, based on statistics and experimental evidence, between the quality requirements and the engineering characteristics of racing bicycle wheels. This aspect represents a significant improvement of the method proposed by QFD [16].

The results did not show any inconsistency and the high and low correlation coefficients agreed with the expected analysis of the bicycle riding dynamics. The results also highlighted the interdependence between the different basic engineering characteristics, and suggested to measure additional engineering characteristics for a complete characterization of the wheels. In particular, the low correlation coefficients calculated between the Forward Rolling Efficiency and all basic engineering characteristics, suggested the need to characterize the aerodynamic behavior of the wheels and the rolling resistance of the hubs.

The overall approach resulted to be suitable for the scope: methods developed are applicable to other sports equipment.

## ***Part 4***

**Development of engineering complex indexes of  
racing bicycle wheels**



# Chapter 11

## Engineering complex indexes

### 11.1 Introduction

In the previous part it was found that the user evaluates the wheels behaviour using a set of 13 quality requirements. During the subjective evaluation tests, the testers have expressed their assessment about the 13 quality requirements of three different wheelsets. The results of this test session showed that high differences between the tested wheelsets were perceived by the testers among all the quality requirements. This put in evidence the need to develop the **engineering complex indexes**, which represent a technical measurement of the quality requirements perceived by the cyclist. A set of six engineering complex indexes was therefore obtained through a scientific approach, which combined the analysis of the subjective evaluation of the cyclists with the technical analysis of the bicycle dynamics. The engineering complex indexes are the final result of the integrated method developed for the engineering characterization of the wheels. They represent an innovative tool for the user-centred product design.

### 11.2 General approach for the development and validation of a complex index

The development of the six indexes followed the same general approach summarized in the following points. The approach, developed for the bicycle wheels, is applicable to other sports equipment.

- **Purpose** of the index development: obtaining an index that expresses the user evaluation about the quality requirement, which the index refers to.
- **Phase 1**: analysis of the **user evaluation** regarding the quality requirement considered, and the correlation coefficients with the basic engineering characteristics.
- **Phase 2**: analysis of the **bicycle dynamics** during the actions performed by the cyclist, in which the considered quality requirement is evaluated.
- **Phase 3**: on the bases of the results of the two previous analysis, the expression of the index is then formulated. The index can derive from a physical interpretation of the phenomenon, in order to reduce at minimum the introduction of empirical weighting factors.



- **Phase 4:** research of the **data** needed for the index computation through the execution of field tests with a dedicated instrumented bicycle, or by means of the literature analysis.
- **Phase 5:** the **index is validated** through the computation of the correlation coefficient with the quality requirement that it has to express. If the correlation coefficient is greater than 0.9, which corresponds to a high correlation, the index is validated.

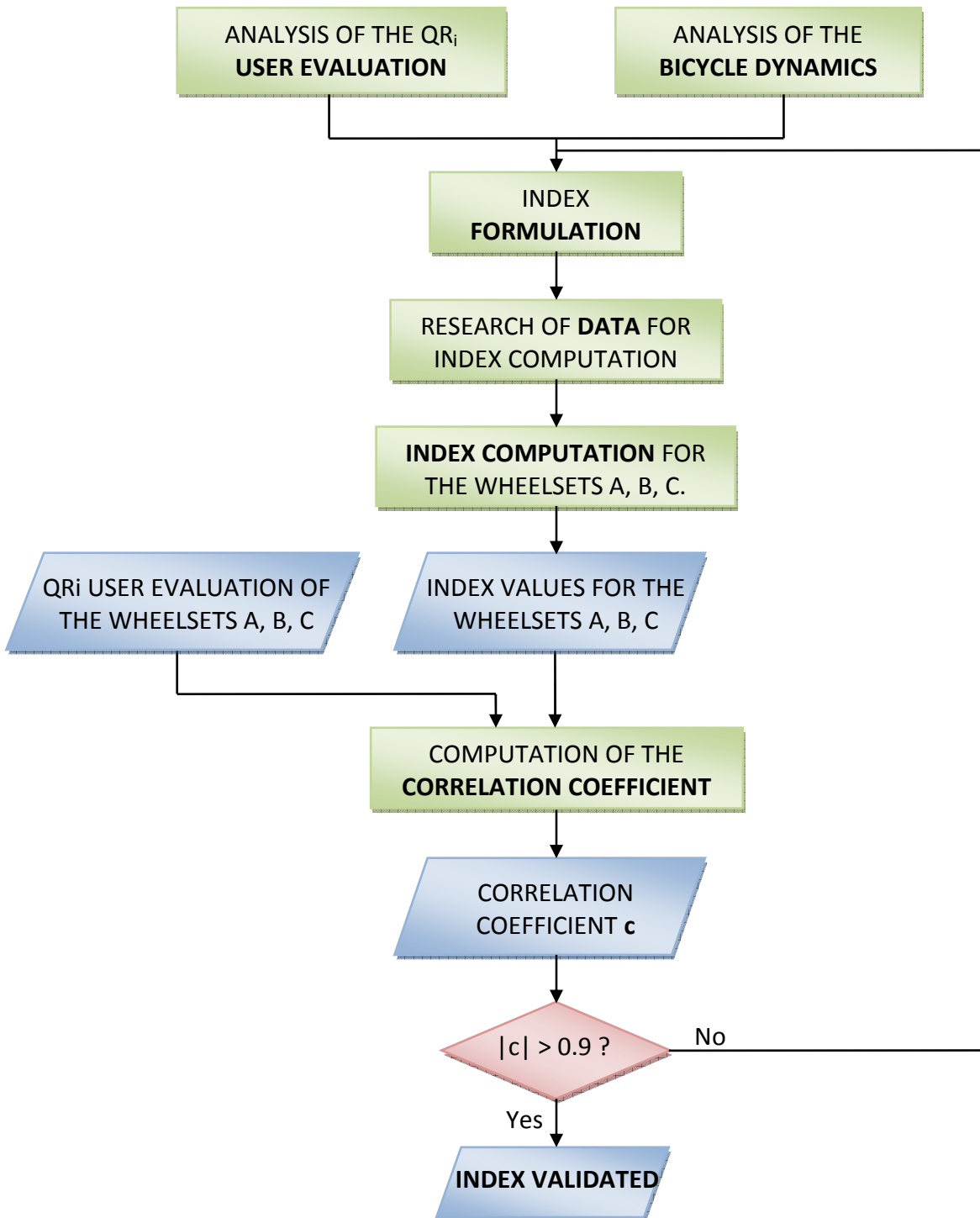


Fig. 11.1 Schematic of the development process of the engineering complex indexes regarding the quality requirement  $QR_i$ .

### 11.3 Developed Indexes and their definition

The six developed indexes are listed and defined below. The development of the indexes was mainly conditioned by the set of data available from the laboratory tests or from the literature. Due to the lack of data needed for the indexes computation, it was not possible to develop some of those indexes that are not included in the list, such as the indexes of braking power and braking regularity.

- **Reactivity Index:** *wheel quickness in transforming cyclist actions into bicycle acceleration.*
- **Handling Index:** *influence of the wheel on the easiness of bicycle manoeuvring.*
- **Road Holding Index:** *influence of the wheel on the precision of the bicycle in following the turning path.*
- **Impulsive Comfort Index:** *comfort properties of the wheels when subjected to impulsive loads.*
- **Index of Forward Rolling Efficiency:** *entity of the forces acting against the wheel forward rolling.*
- **Index of stability to crosswind:** *influence of the wheel on the bicycle response to the presence of lateral wind.*

The formulation of each index is presented in details in the following chapters, together with the activities relating the acquisition or research of data useful for the indexes computation.

### 11.4 Literature review

A set of performance indexes is proposed in the analysis of the motorcycle handling properties (V. Cossalter, [28]). These indexes express the relationship between the rider input and the motorcycle output, both measured by means of an instrumented motorcycle. Different indexes are evaluated for five different typical manoeuvres as showed on table 11.1.

| Manoeuvre               | Calculated Indexes   | Notes   |
|-------------------------|--|---|
| Steady turning test     | roll index = $\tau / \varphi$<br>acceleration index = $\frac{\tau}{V^2 / R_c}$     | $\tau$ : steering torque<br>$\varphi$ : roll angle<br>V: motorcycle speed<br>$R_c$ : curve radius |
| U-turn test             | Koch index = $\frac{\tau_{peak}}{V \cdot \dot{\varphi}_{peak}}$                    |   |
| Slalom test             | roll transfer function = $\frac{\tau}{\varphi}(v)$                                 | v: frequency  |
| Lane change test        | roll index of lane change = $\frac{\tau_{p-p}}{V_{avg} \cdot \dot{\varphi}_{p-p}}$ | p-p subscript: peak-peak  |
| Obstacle avoidance test | Obstacle avoidance index: temporal delay between $\tau$ and $\varphi$              |   |

Tab. 11.1 Indexes calculated during the different tests performed for the evaluation of the handling properties of a motorcycle [28].

These indexes are directly measured during defined field tests, requiring therefore the instrumentation of each analysed motorcycle. The approach adopted in this thesis is different. The engineering complex indexes were theoretically founded and experimentally validated. They can be calculated for every considered wheel using the data regarding the basic engineering characteristics of the wheel, measured during the standard laboratory characterization of the wheels.

There are no studies regarding the development of engineering complex indexes, which express the user's evaluation about the sports equipment under test. This represents the most innovative perspective of the user-centred approach developed in this thesis for the characterization of sports equipment.

# Chapter 12

## Reactivity Index

### 12.1 Introduction

Aim of this phase of the work was the development of a method for the engineering computation of wheels “reactivity” as perceived by the cyclists. Wheels Reactivity is one of the main performance requirements evaluated by the cyclists during road cycling, and it is defined as it follows:

*quickness whereby the wheel transforms the cyclist’s into bicycle accelerations*

The Reactivity of a bicycle wheel depends on its basic engineering characteristics (mass, inertia, and stiffness), and their influence is counted with a scientific approach based essentially on the computation of the energy absorbed by the wheel during a chosen action.

The theoretical approach and the development stages concerning the index formulation are presented in the first part of this chapter. Later, the data needed for the index computation, acquired by means of dedicated field tests, and the results regarding the index validation are showed in details.

### 12.2 Approach

The Reactivity is correlated with the energy absorbed by the wheels during a sprint. In fact, during a sprint with rider standing on the pedals, the motion of each wheel is the sum of four contributions:

- $x$ : translation in the direction of the bicycle motion;
- $\theta$ : rotation around the wheel axis;
- $\varphi$ : lateral roll motion around the axis, which links the points of contacts of the two wheels with the road surface;
- $\delta$ : rotation around the steering axis (only for front wheels).

The speed variation of each wheel motion component involves a contribution to the increment of the **kinetic energy absorbed** by the wheel. The rotation  $\delta$  of the front wheel around the steering axis was neglected because of the low value reached by the steering angle during a sprint. In addition to these, the elastic energy due to the wheel deformation has to be considered. The total energy  $E^-$  absorbed by a wheel during a sprint is the sum of the kinetic and deformation energies. Less total energy absorbed by a wheelset corresponds to a faster response of the wheelset to the

cyclist action, or higher reactivity. The different contribution to the total energy absorbed by a wheel during a sprint is showed in details in the next paragraph.

### 12.3 Energy absorbed by a wheel during a sprint

The contribution of each kinetic or deformation energy to the total energy absorbed by a wheel during a print is presented below. The energy necessary for overcoming the aerodynamic resistance, the rolling resistance of tires and hubs, and the gyroscopic effects of the wheels were not considered in this dissertation.

- **Translational kinetic energy increment**

The wheel can be modeled as a body of mass  $m$  (fig. 12.1) subjected to a translational motion with speed  $v$ . The bicycle acceleration involves an increase of the wheel translational speed  $\Delta v$ , and  $\Delta E_{K,transl}$  is the relative kinetic energy increment:

$$\Delta E_{K,transl} = \frac{1}{2} \cdot m \cdot \Delta v^2 \tag{1}$$

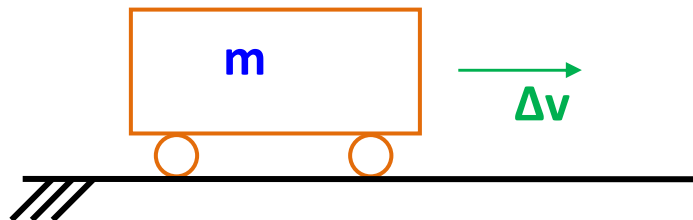


Fig. 12.1 Wheel model for the computation of the translational kinetic energy increment.

- **Potential energy increment due to road slope**

During the uphill riding, the road slope causes a proportional resistant force, which contrasts the translational motion of the wheel (fig. 12.2). Since the longitudinal force  $F_L$  is needed to balance this resistant force, a forward translation of the wheel for a distance  $d$  requires an increment of the potential energy of the wheel:

$$\Delta E_{pot,slope} = m \cdot g \cdot \sin(\alpha) \cdot d \tag{2}$$

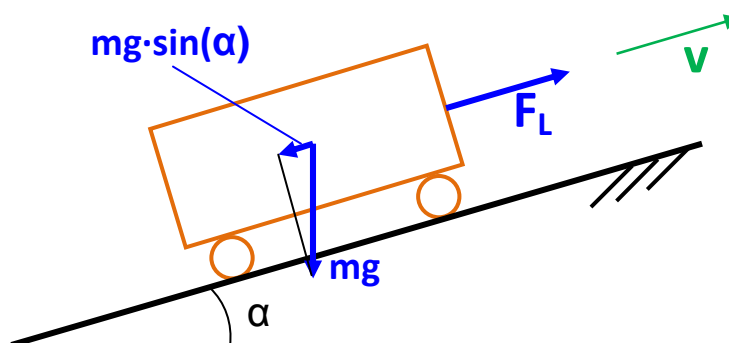


Fig. 12.2 Schematic of the forces due to the road slope.

- **Rotational kinetic energy increment**

The bicycle acceleration involves an increase of the rotational velocity  $\Delta\omega$  of the wheel (fig. 12.3), and  $\Delta E_{K,rot}$  is the relative kinetic energy increment:

$$\Delta E_{K,rot} = \frac{1}{2} \cdot I_p \cdot \Delta\omega \quad (3)$$

$I_p$ : polar moment of inertia of the wheel [ $\text{kg} \cdot \text{m}^2$ ].



Fig. 12.3 Schematic of the wheel motion component, which causes the rotational kinetic energy increment.

- **Lateral roll kinetic energy**

$\Delta E_{K,roll,i}$  is the energy required to sustain the lateral roll motion of the wheel during the  $i$ -th stroke on pedal of the considered sprint phase (fig. 12.4).

$$\Delta E_{K,roll,i} = \frac{1}{2} \cdot \left( \frac{I_p}{2} + m \cdot r_w^2 \right) \cdot \Delta\dot{\phi}^2 \quad (4)$$

$\dot{\phi}$ : lateral roll speed of the wheel [rad/s].

$r_w$ : wheel radius [m].

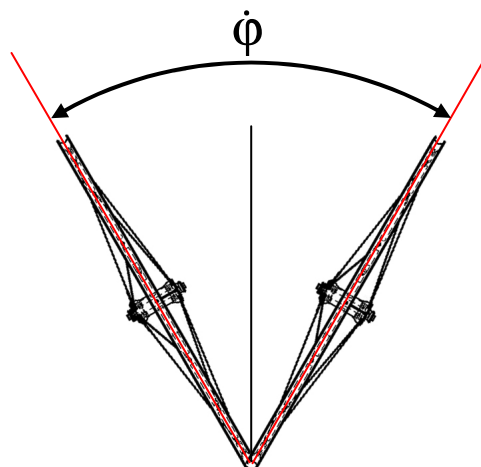


Fig. 12.4 Schematic of the lateral roll motion of the wheel.

- **Torsional deformation work**

$\Delta W_{D,torx,i}$  is the work needed during the  $i$ -th stroke on pedals to obtain the torsional elastic deformation of the rear wheel (only rear wheels have a torsional deformation):

$$\Delta W_{D,tor,i} = \frac{1}{2} \frac{\Delta M_{D,i}^2}{K_{torx}} \tag{5}$$

$M_D$ : drive torque acting at rear hub axis [Nm].

$K_{torx}$ : torsional stiffness of the rear wheel [Nm/rad].

To better understand this phenomenon, we can consider a model with the rear wheel constrained at its external circumference (fig. 12.4): the application of the driving torque  $M_D$  at the rear wheel hub causes the torsional deformation  $\theta$  of the wheel.

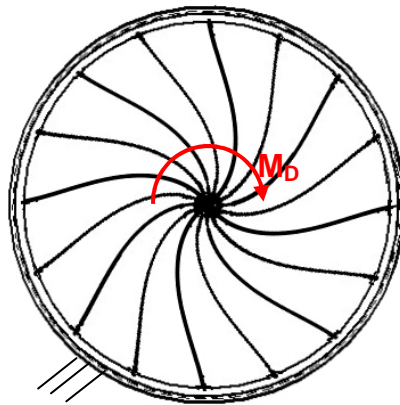


Fig. 12.5 Schematic of torsional deformation of the rear wheel due to the driving torque.

During the  $i$ -th stroke on pedal,  $\Delta M_{D,i}$  is defined as the difference between the torque peak and valley, as showed in figure 12.5.

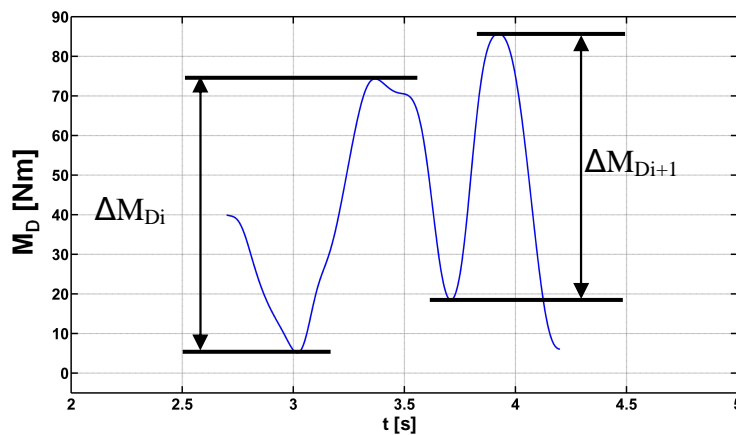


Fig. 12.6 Example of the driving torque concerning two strokes on pedal measured during the field test.

A complete torque-deformation cycle related to one stroke on pedals can be qualitatively represented as in figure 12.6. It is divided into two consecutive phases: the first phase is characterized by a torque increase, and the second one by a torque decrease. The deformation work  $\Delta W_{D,torx,i}$  involved during the first phase, and caused by the elastic deformation of the wheel, is partially returned to the bicycle/cyclist system during the decreasing torque phase due to the wheel elastic rebound. The returned energy  $E_{ret}$  is the difference between the deformation work  $\Delta W_{D,torx,i}$  and the energy  $E_{diss}$  dissipated by the wheel during the torque cycle.

$$E_{ret} = \Delta W_{D,torx} - E_{diss} \quad (6)$$

The return of energy is not an instantaneous phenomenon; therefore, an experimental study would be necessary for verifying if its contribution is entirely, partially or not at all useful for the bicycle motion. The estimation of the energy dissipated  $E_{diss}$  requires the data concerning the damping behaviour of the wheel. Since these data were not available for the research team during the work, the returned energy  $E_{ret}$  was assumed to be equal to zero.

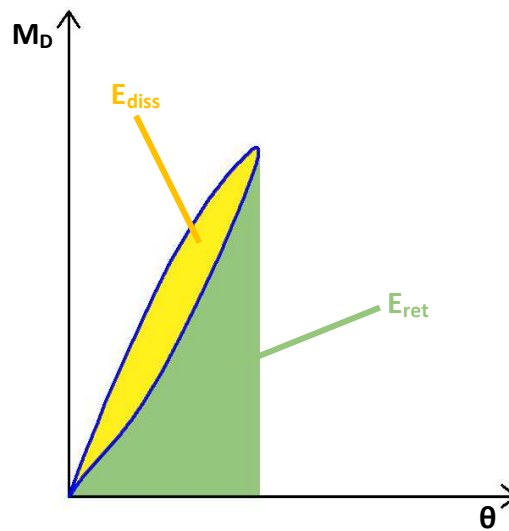


Fig. 12.7 Qualitative representation of a complete torque-deformation cycle, and the different energy contributions involved.

- **Side deformation work**

$\Delta W_{D,side,i}$  is the work needed during the  $i$ -th stroke on pedal to obtain the side elastic deformation of the wheel (fig. 12.8.b).

$$\Delta W_{D,side,i} = \frac{1}{2} \frac{(F_v \cdot \sin(\varphi_0))^2}{k_{side}} \quad (7)$$



$M_D$  = drive torque acting at rear hub axis [Nm].

$k_{side}$  = wheel lateral bending stiffness [N/m].

$F_{Wf/rz}$  : front/rear wheel static vertical reaction force acting at the point of contact between the wheel and the road surface [N].

The side elastic deformation is caused by the side component  $F_{Y_w, Wf/r}$  (front/rear) of the vertical force  $F_V$  acting to the considered wheel. The direction of  $F_{Y_w, Wf/r}$  is normal to the wheel symmetry plane, considered in the wheel not deformed configuration (fig. 12.8.b). During a sprint, the vertical load  $F_V$  is a dynamic load that depends on the mass of the bicycle components and of the cyclist, on the bicycle geometry, and on the cyclist's pedalling style. Since no data about the vertical force  $F_V$ , obtained from field tests, were available during the work,  $F_V$  was assumed to be the static vertical load acting at the front or at the rear wheel.  $F_{Y_w, Wf/r}$  is equal to zero if the wheel is in vertical position, and it reaches its maximum value at the maximum wheel's roll angle  $\varphi_0$  which was assumed to be equal to the bicycle roll angle. The energy returned during the  $F_{Y_w, Wf/r}$  decreasing phase (fig. 12.9) was assumed to be equal to zero for the same considerations concerning the torsional deformation work.

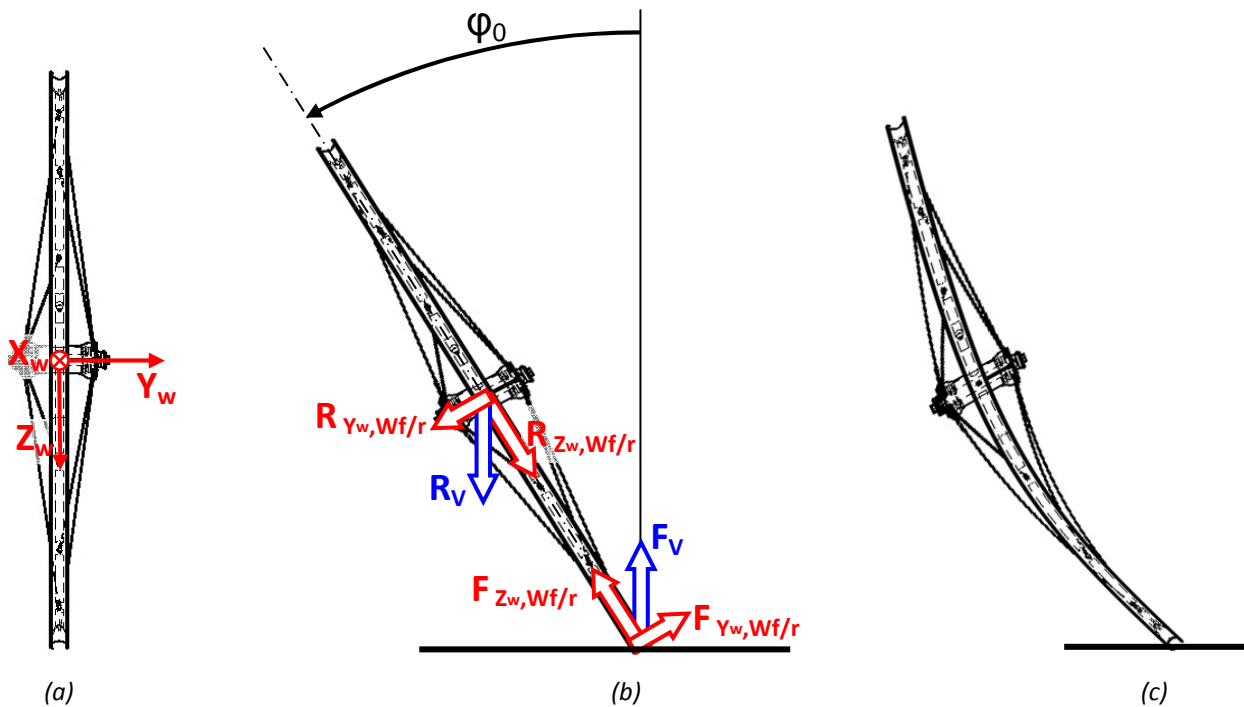


Fig. 12.8. (a) Reference system of the wheel; (b) forces acting to a front/rear wheel at a roll angle equal to  $\varphi_0$ ; (c) side deformed configuration of a wheel.

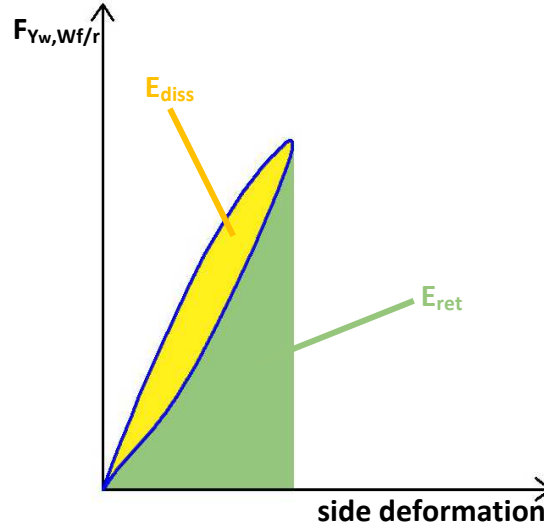


Fig. 12.9 Qualitative representation of a complete side force-deformation cycle and the different energy contributions involved.

## 12.4 Reactivity index computation

During a sprint, the total energy  $E_{W,f/r}^-$  absorbed by the front (8) and the rear (9) wheels is respectively obtained by the sum of five and six components:

$$E_{Wf}^- = \Delta E_{K,transl} + E_{transl,slope} + \Delta E_{K,rot} + \Delta E_{K,roll,i} + \sum_{i=1}^{n_{ped}} \Delta W_{D,side,i} \quad [J] \quad (8)$$

$$E_{Wr}^- = \Delta E_{K,transl} + E_{transl,slope} + \Delta E_{K,rot} + \Delta E_{K,roll,i} + \sum_{i=1}^{n_{ped}} \Delta W_{D,torx,i} + \sum_{i=1}^{n_{ped}} \Delta W_{D,side,i} \quad [J] \quad (9)$$

$n_{ped}$  = number of strokes on pedals applied during the sprint phase considered.

The Reactivity Index  $R_{W,f/r}$  was defined as the inverse of the total energy absorbed by the wheel.

$$R_{W,f/r} = \frac{1}{E_{Wf/r}^-} \quad \left[ \frac{1}{J} \right] \quad (10)$$

The subscript “f” or “r” indicates if the index is calculated for a front or a rear wheel. Higher values of  $R_{W,f/r}$  correspond to less energy absorbed by the wheel considered, which means faster response of the wheel to cyclist sprint action or higher wheel reactivity.

If we consider a wheelset, the index is calculated as the inverse of the sum of the energy absorbed by the front and rear wheels that compose the wheelset:

$$R_w = \frac{1}{E_{wf}^- + E_{wr}^-} \begin{bmatrix} 1 \\ J \end{bmatrix} \quad (11)$$

## 12.5 Data considered for the index computation

The parameters involved in the Reactivity Index computation were obtained through the analysis of the data acquired during dedicated field tests on an instrumented racing bicycle. As presented in details in Part 5 of this thesis, some of the sensors that equipped the instrumented bicycle were opportunely chosen for measuring the parameters needed for the computation of the Reactivity Index. The analysed sprint action is represented by a sprint, performed standing on pedals, while the tester was riding on an uphill with medium road slope (10 %), starting from a constant speed of 15 km/h, and with 39/21 gear ratio. The characteristics of the considered sprint action are listed below:

- tester: professional track cyclist, sprinter, 21 years old, 180 cm height, 75 kg weight;
- road slope: 10 %;
- speed at the sprint start: 15 km/h;
- gear ratio: 39/21;
- sprint duration: 10 s.

Every sprint is characterised by three phases. During the initial phase, the acceleration of the bicycle increases, reaching its maximum value in the second phase, and gradually decreasing during the final third phase. The sprint phase represented by the two strokes on pedals corresponding to the maximum acceleration of the bicycle, was considered as the **reference action** for the computation of the Reactivity Index.

The translational and rotational speed ( $v$ ,  $\omega$ ), the drive torque applied at the rear wheel  $M_D$ , the lateral roll angle  $\phi$ , and the lateral roll speed  $\dot{\phi}$ , where obtained by the field tests analysis.

The vertical load  $F_{wf/rz}$  acting at front and rear wheel was assumed constant during the sprint. The total vertical load was assumed equal to 900 N, and its distribution 30 % to front wheel and 70 % to rear wheel.

The mass  $m$ , the polar inertia  $I_p$ , the torsional stiffness  $K_{torx}$ , and the lateral stiffness  $K_{side}$  are the basic engineering characteristics of the wheel, measured by means of the standard laboratory tests.

### 12.5.1 Analysis of the data acquired during the field tests

The parameters directly measured during the field test, which were useful for the estimation of the data needed for the Reactivity Index computation, are described together with the sensor used for their measurement in the table 12.1.

| Parameter            | Description                  | Sensor  |
|----------------------|------------------------------|---|
| V [km/h]             | Bicycle speed                | Magnetic sensor and GPS.  |
| M <sub>BB</sub> [Nm] | Torque at the bottom bracket | Spider arms of the crankset instrumented with strain gauges.            |
| $\dot{\Phi}$ [rad/s] | Lateral roll speed           | Gyroscope inside of the Inertial Measurement Unit (IMU)                 |
| $\Phi$ [rad]         | Lateral roll angle           | Computed by the Inertial Measurement Unit through a dedicated algorithm |

Tab. 12.1 List of the parameters measured during the field test, which were useful for the computation of the Reactivity Index.

A Matlab® program was compiled to analyse the rough data following the stages listed below.

- **Computation of bicycle acceleration a [m/s<sup>2</sup>]**

The acceleration of the bicycle was calculated performing a numerical differentiation of the speed signal.

- **Computation of the drive torque M<sub>D</sub> [Nm]**

The drive torque M<sub>D</sub> was obtained by the ratio of the torque measured at the bottom bracket, by means of the instrumented crankset, with the gear ratio  $\tau_{CS}$  between the chainring and the sprocket:

$$\tau_{CS} = \frac{39}{21} \quad (12)$$

$$M_D = \frac{M_{BB}}{\tau_{CS}} \quad [\text{Nm}] \quad (13)$$

- **Selection of the sprint and of its section with maximum acceleration**

A figure with three charts was created for the selection of the test section corresponding to the sprint to be analysed (fig. 12.10). The bicycle speed and acceleration are reported in the upper chart, the middle one shows the drive torque, whereas the lateral roll angle and speed are plotted in the lower one.

At the beginning of the test (fig. 12.10), the tester was in a stationary condition. At the 5<sup>th</sup> second, he started to pedal reaching in 5 s a speed of 15 km/h. He kept the speed constant until the beginning of the sprint at 41 s. The beginning of the sprint was characterised by a sudden increase of the drive torque, of the speed, of the acceleration, and of the lateral roll angle and speed. During the sprint, the acceleration reached a relative maximum followed by a gradual decrease, the speed increased with an asymptotical trend, the driving torque progressively decreased while the lateral roll angle and roll speed did not show high variations. After the

sprint, the bicycle progressively decelerated until the stop at the end of the test. The test part regarding the sprint (fig. 12.11), and the section of the sprint corresponding to the maximum acceleration of the bicycle (fig. 12.12) were consecutively selected.

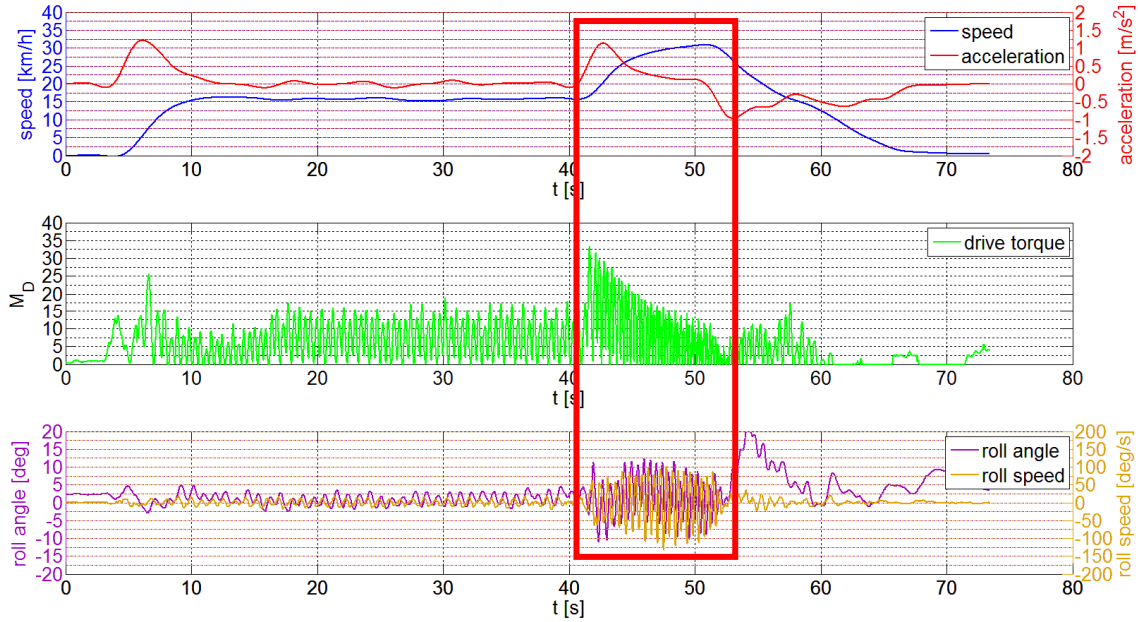


Fig. 12.10 Signals acquired or calculated for the entire test duration and selection of the sprint.

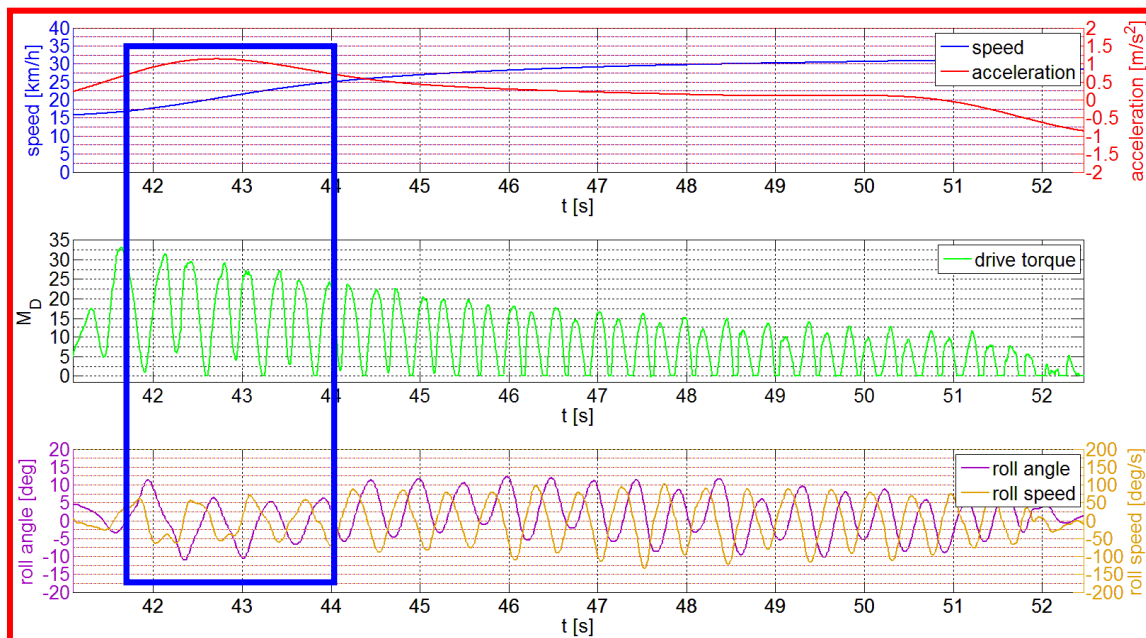


Fig. 12.11 Selection of the sprint section characterized by the maximum acceleration of the bicycle.

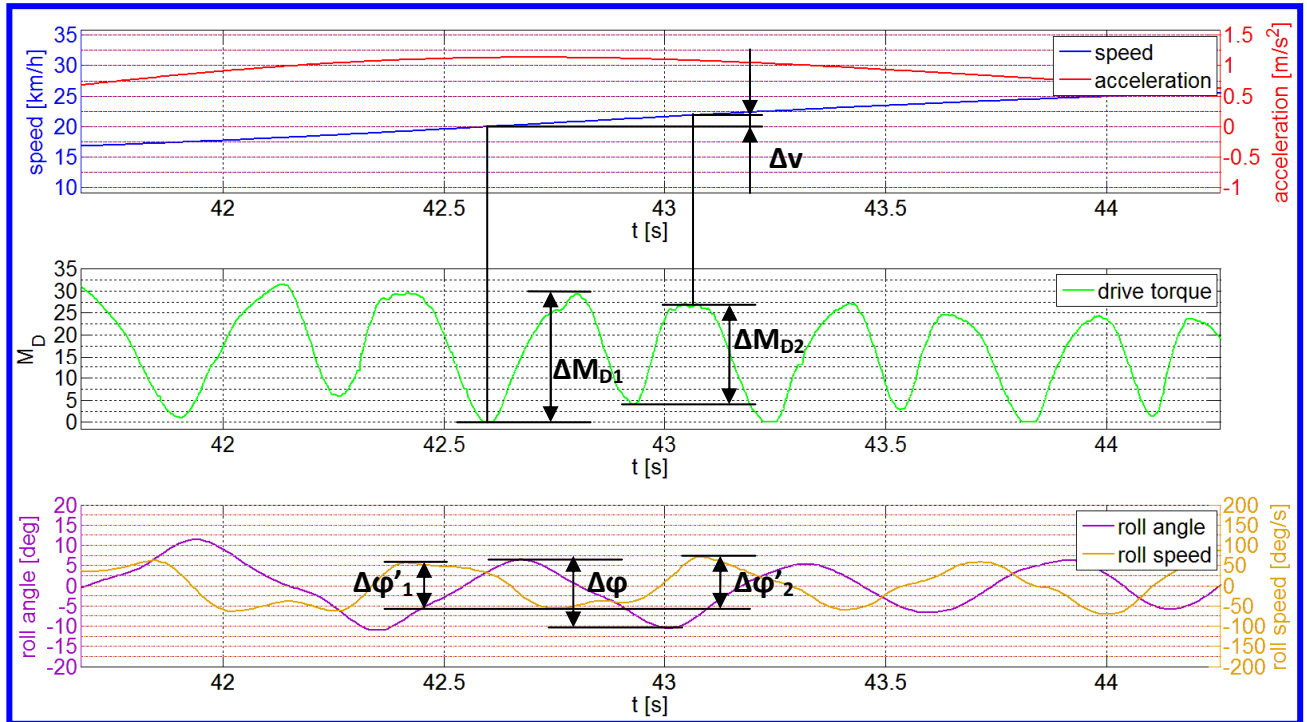


Fig. 12.12 Sprint section characterized by the maximum acceleration of the bicycle. Selection of the two strokes on pedals corresponding to the maximum acceleration. Calculation of  $\Delta v$ ,  $\Delta M_D$ ,  $\Delta \phi$ , and  $\Delta \phi'$ .

- **Calculation of  $\Delta v$ ,  $\Delta M_D$ ,  $\phi_0$ , and  $\Delta \phi'$ .**

Referring to the figure 12.12, the two strokes on pedals corresponding to the acceleration peak were identified considering the drive torque signal.

- The total drive torque increment  $\Delta M_D$  was calculated as the sum of the differences between two consecutive couples of peak – valley:

$$\Delta M_D = \Delta M_{D1} + \Delta M_{D2} = 51.13 \text{ Nm} \quad (14)$$

- The speed increment  $\Delta v$  was obtained subtracting the speed corresponding to the first torque valley from the speed corresponding to the second torque peak.

$$\Delta v = 1.97 \text{ km/h}$$

- The roll angle  $\phi_0$  was calculated as the absolute mean value of the two consecutive peak and valley which correspond respectively to the stroke on pedal with the right ( $\phi > 0$ ) and left leg:

$$\phi_0 = \frac{|\Delta \phi|}{2} = 0.14 \text{ rad} \quad (15)$$

- The total roll speed difference  $\Delta \dot{\phi}$  was calculated as the sum of the differences between

three consecutive points of relative maximum or minimum:

$$\Delta\dot{\phi} = \Delta\dot{\phi}_1 + \Delta\dot{\phi}_2 = 3.8 \frac{\text{rad}}{\text{s}} \quad (16)$$

- **Calculation of  $\Delta\omega$  and  $d$**

- The rotational speed increment  $\Delta v$  was calculated as it follows:

$$\Delta\omega = \frac{\Delta v}{r_w} = 1.7 \frac{\text{rad}}{\text{s}} \quad (17)$$

- The parameter  $d$  represents the distance between the first torque valley and the second torque peak considered.

$$d = 2.73 \text{ m}$$

### 12.5.2 Summary of the data considered for the computation of the Reactivity Index

The parameters considered for the computation of the Reactivity Index, and the respective values and source are summarized in the table 12.2.

| Parameter                                    | Description  | Source                                     |
|--|--|--|
| $\Delta v = 1.97 \text{ km/h}$               | Translational speed increment  | Data analysis of field test                |
| $\Delta\omega = 1.7 \text{ rad/s}$           | Rotational speed increment   | Data analysis of field test                |
| $\Delta\phi' = 3.8 \text{ rad/s}$            | Total lateral roll speed variation                                     | Data analysis of field test                |
| $\Delta M_D = 51.13 \text{ Nm}$              | Total drive torque variation   | Data analysis of field test                |
| $\phi_0 = 3.8 \text{ rad}$                   | Lateral roll angle   | Data analysis of field test                |
| $d = 2.37 \text{ m}$                         | Distance   | Data analysis of field test                |
| Road slope = 10%                             | Road slope   | Characteristic of the testing road         |
| $\alpha = 5.71 \text{ deg}$                  | Road slope angle   | Characteristic of the testing road         |
| $g \cdot \sin(\alpha) = 0.976 \text{ m/s}^2$ | Component of the gravitational acceleration opposed to the bike motion | Characteristic of the testing road         |
| $F_{wFz} = 270 \text{ N}$                    | Static vertical load acting at front wheel                             | Assumed value                              |
| $F_{wRz} = 630 \text{ N}$                    | Static vertical load acting at rear wheel                              | Assumed value                              |
| $\tau_{CS} = 39/21$                          | Gear ratio   | Characteristic of the field test execution |
| $r_w = 0.321 \text{ m}$                      | Radius of a racing bicycle wheel                                       | Constructive characteristic of the wheel   |

Tab. 12.2 Summary of the data considered for the computation of the Reactivity Index.

## 12.6 Index validation and discussion

The figure 12.13 shows the correlation coefficients calculated between the Reactivity Index and each of the four quality requirements, regarding the Reactivity evaluated during the execution of four different action phases (see § 8.4). Correlation coefficients greater than 0.9, which means high correlation (see § 10.3), were obtained between the Reactivity Index and QR.1, QR.2, QR.3. These three quality requirements correspond to the wheels Reactivity evaluated respectively during a sprint starting from low speed, during uphill road cycling at constant low speed, and during uphill road cycling at high speed. The Reactivity Index can therefore well represent these three quality requirements, for which it is **validated**.

The low correlation coefficient obtained with the wheels Reactivity perceived during a sprint, starting from high speed (QR.2), highlights that the developed Reactivity Index does not express the perception of this quality requirement. In order to obtain an index that results highly correlated with this quality requirement, an additional Reactivity Index should be developed, adopting the same approach, but considering a different set of parameters and introducing two additional contributions to the total energy absorbed by the wheel. The set of parameters has to be obtained from field tests, in which the reference sprint is performed on a flat road, starting from a speed greater than 30 km/h. The energy required for overcoming the aerodynamic resistance of the wheel, and the rolling resistance of the hub, is needed for the computation of the Reactivity Index that expresses the wheels Reactivity during a sprint starting from high speed. The study of the aerodynamic behaviour of the wheels, and of the rolling resistance of the hub, represents two further activities necessary to obtain a complete analysis of the wheels reactivity.

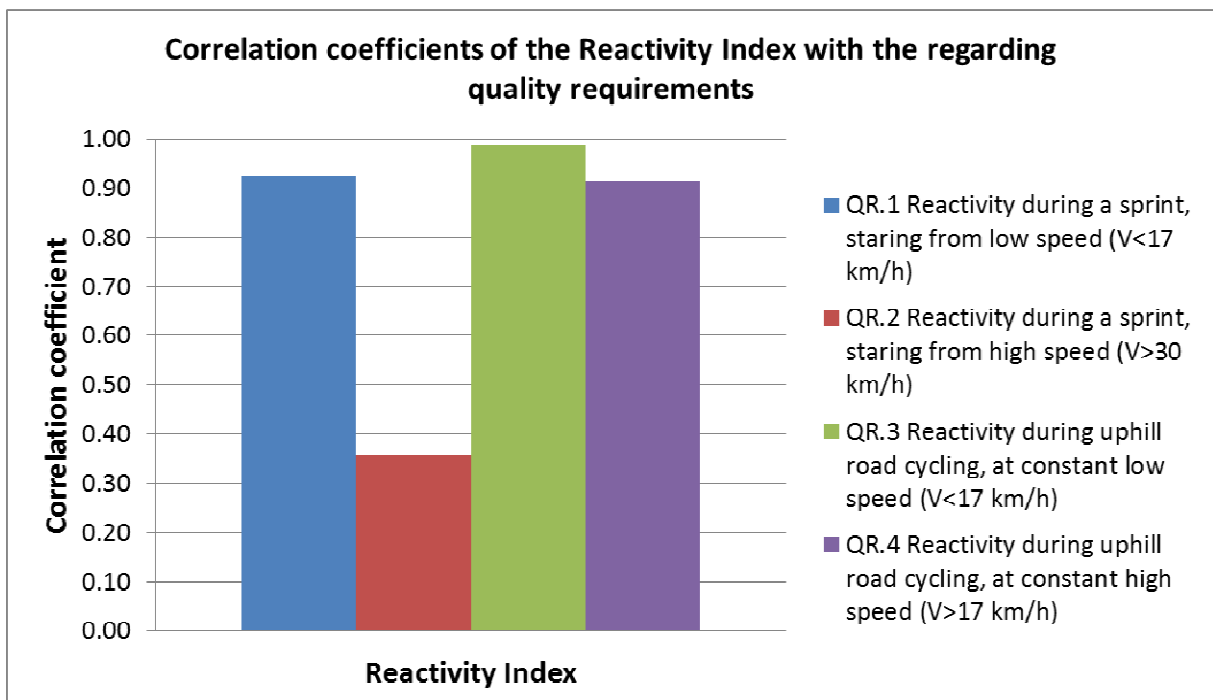


Fig. 12.13 Correlation coefficients calculated between the Reactivity Index and the four different quality requirements concerning the evaluation of the reactivity.





# Chapter 13

## Handling and Road Holding Index

### 13.1 Introduction

**Handling** and **Road Holding** are two quality requirements evaluated by the cyclist during the typical manoeuvres performed with the racing bicycle, such as the execution of a single curve with high or low radius, or of two consecutive curves. The Handling expresses the influence of the wheels on the feelings of the cyclist during the transient phases involved in the accomplishment of the manoeuvres listed above. The Road Holding expresses the influence of the wheels on the directional stability of the bicycle, or on the precision of the bicycle in following the turning path. The formulation of two indexes that express respectively the Handling and the Road Holding quality requirements of the wheels, is presented in this chapter.

In their book, Wilson & Papadopoulos [27] presented an analysis of the bicycle handling, mainly focused on the steering action, and on the bicycle balancing; they also briefly explored the human factors, which affect the cyclist feelings in bicycle manoeuvring.

A set of indexes is proposed for the analysis of the Handling properties of the motorcycle (V. Cossalter, [28]; see § 11.4). The indexes (tab. 11.1), evaluated for five different typical manoeuvres, are directly measured through an instrumented motorcycle, and represent the relationship between the input of the rider (e.g. steering torque), and the output of the motorcycle (e.g. roll angle). The indexes developed in this work started from theoretical considerations about the bicycle dynamics, similar to those regarding the analysis of the motorcycle handling. The parameters needed for their computation were obtained from the data analysis of dedicated field tests, and, as the formulations of the indexes were established, only the data regarding the basic engineering characteristics of the wheels were needed for the indexes computation.

### 13.2 Handling Index

#### 13.2.1 Approach

The Handling quality requirement summarizes the evaluation of the cyclist among the wheels influence on the bicycle dynamics during the transient actions, such as the entry into the curve, the exit from the curve, or the change of direction. The Handling Index of a wheel is correlated to the energy absorbed by the wheel itself, during the accomplishment of a transient action. The results regarding the analysis of the motorcycle Handling [28] show that the motion component

that presents the highest variation of its speed during the passage from two steady states is the lateral roll motion of the motorcycle. The highest variation of the lateral roll motion was reached during the change of direction involved in the execution of two consecutive curves, and it is proportional with the cruising speed. Since these results can be extended to all two wheeled vehicles, the change of direction involved during the execution of two consecutive curves at high speed was considered as the reference transient action for the computation of the wheel Handling Index.

During a change of direction, the motion of a bicycle wheel is the sum of five components:

- $x$ : translation in the direction of the bicycle motion;
- $\theta$ : rotation around the wheel axis;
- $\varphi$ : lateral roll motion around the axis, which links the points of contacts of the two wheels with the road surface;
- $\psi$ : yaw motion around the vertical axis, which is moving from the centre of curvature of the first curve to the centre of curvature of the second one;
- $\delta$ : rotation around the steering axis (only for front wheels).

The speed variation of each wheel motion component involves a contribution to the increment of the **kinetic energy absorbed** by the wheel. In addition to these, the elastic energy due to the wheel deformation has to be considered. The total energy  $E^-$  absorbed by a wheel during a sprint is the sum of the kinetic and deformation energies. Less energy absorbed by the wheel can be perceived by the cyclist as an increase of the quickness, or a decrease of the body effort needed for the change of direction, which means higher Handling Index.

### **13.2.2 Energy absorbed by a wheel during a change of direction**

The change of direction is the phase of passage from a right to a left curve or vice versa.

The total kinetic energy absorbed by a wheel during a direction changing is given by the speed variation of each component of the wheel motion. The translational speed  $v$ , the rotational speed  $\omega$ , and the yaw speed  $\psi'$  were neglected in this dissertation, due to their lower variation in comparison with the other two components.

The cyclist was assumed not to perform any braking action or stroke on pedal during the change of direction. Among the three forces acting at the wheel, represented by the vertical, the longitudinal, and the side force, the last one is the only force that therefore presents a variation. The wheel deformation work is consequently caused only by the variation of the side force  $F_S$ .

The aerodynamic force and the gyroscopic effects were not considered in this treatise.

Each energy contribution to the total energy absorbed by a wheel is presented in details in the following points.

- **Lateral roll kinetic energy**

$\Delta E_{K,roll}$  is the energy required to sustain the lateral roll motion of the wheel during the change of direction (fig. 13.1).

$$\Delta E_{K,roll} = \frac{1}{2} \cdot \left( \frac{I_p}{2} + m \cdot r_w^2 \right) \cdot \Delta \dot{\phi}^2 \quad (1)$$

$I_p$ : polar moment of inertia of the wheel [ $\text{kg} \cdot \text{m}^2$ ].

$m$ : wheel mass [kg].

$\dot{\phi}$ : lateral roll speed of the wheel [rad/s].

$r_w$ : wheel radius [m].

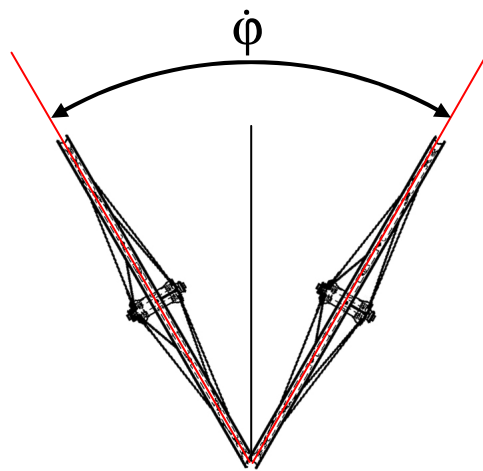


Fig. 13.1 Schematic of the lateral roll motion of the wheel.

- **Steering kinetic energy**

The direction changing involves a steering action, in which the front wheel rotates around the steering axis (fig. 13.2).  $\Delta E_{K,steering}$  is the energy required to sustain the wheel rotation around the steering axis during the change of direction (fig. 13.2). This energy component regards only the front wheels.

$$\Delta E_{K,steering} = \frac{1}{2} \cdot \left( \frac{I_p}{2} + m \cdot f^2 \right) \cdot \Delta \dot{\delta}^2 \quad (2)$$

$\dot{\delta}$ : steering speed of the front wheel [rad/s].

$f$ : forward offset of the fork [m].

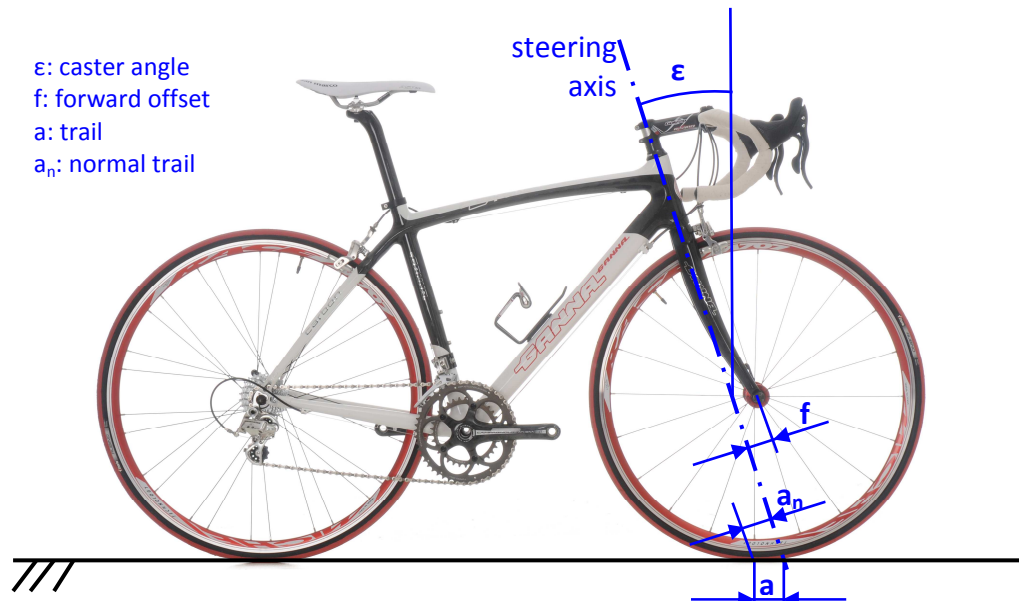


Fig. 13.2 Schematics of the geometrical parameters of the bicycle front assembly

- **Side deformation work**

During the execution of a curve, each wheel (fig. 13.3.b) is subjected to a vertical force  $F_{V,Wf/r}$  (subscript  $Wf/r$  = front/rear Wheel), which is supposed to be constant, and to a side force  $F_{S,Wf/r}$  which, during the change of the bicycle direction, varies its versus and modulus. The resultant of  $F_{V,Wf/r}$  and  $F_{S,Wf/r}$  can be decomposed into two orthogonal components,  $F_{Y_w,Wf/r}$  and  $F_{Z_w,Wf/r}$ , which are parallel respectively to the  $Y_w$  and  $Z_w$  axis of the wheel reference system. The variation of  $F_{Y_w,Wf/r}$ , due to the variation of  $F_S$ , causes the side deformation work  $\Delta W_{D,side}$  of the wheel:

$$\Delta W_{D,side,i} = \frac{1}{2} \frac{(\Delta F_{Y_w,Wf/r})^2}{k_{side}} \quad (3)$$

$M_D$  = drive torque acting at rear hub axis [Nm].

$k_{side}$  = wheel lateral bending stiffness [N/m].

$F_{Wf/rZ}$  : front/rear wheel static vertical reaction force acting at the point of contact between the wheel and the road surface [N].

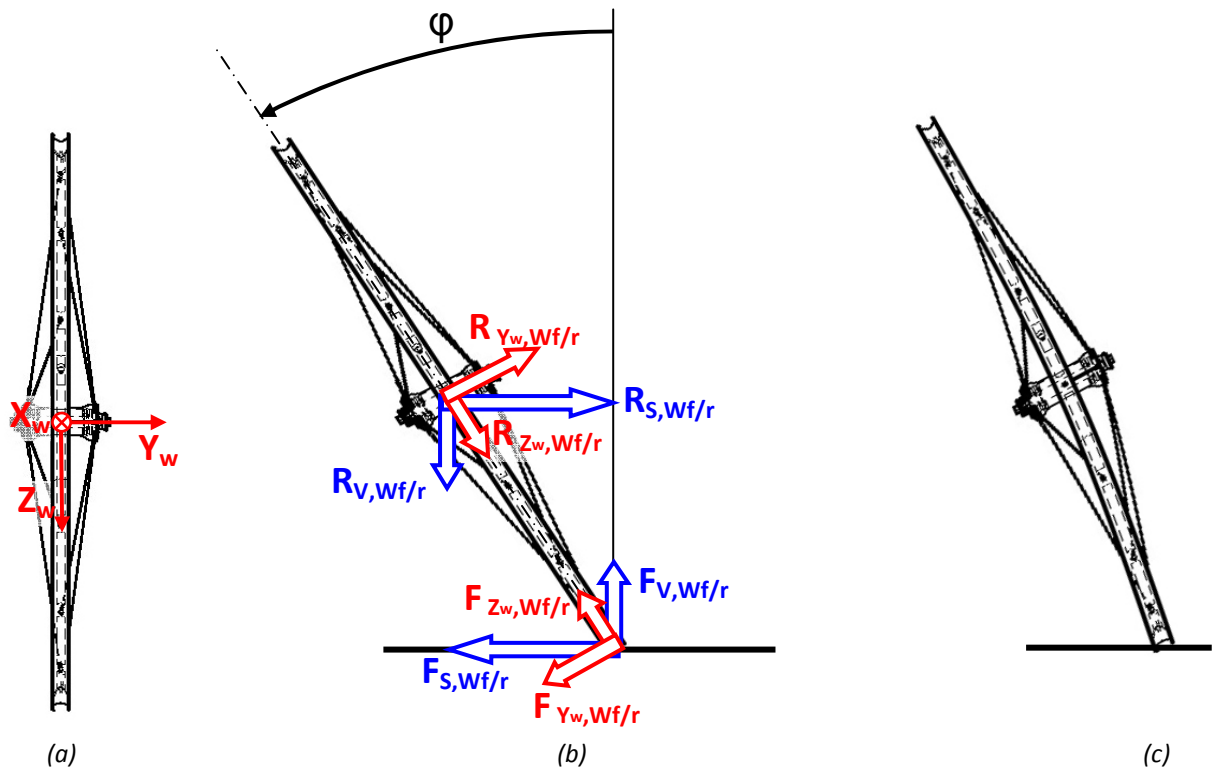


Fig. 13.3. (a) Reference system of the wheel; (b) forces acting on a front/rear wheel at a roll angle equal to  $\varphi$ , during the execution of a left curve; (c) side deformed configuration of the wheel.

A complete force-deformation cycle can be qualitatively represented as in figure 13.4. It is divided into two consecutive phases: the first phase is characterized by a force increase, and the second one by a force decrease. The deformation work  $\Delta W_{D,side}$  involved during the first phase, and caused by the elastic deformation of the wheel, is partially returned to the bicycle/cyclist system during the decreasing force phase due to the wheel elastic rebound. The returned energy  $E_{ret}$  is the difference between the deformation work  $\Delta W_{D,side}$ , and the energy  $E_{diss}$  dissipated by the wheel during the torque cycle.

$$E_{ret} = \Delta W_{D,side} - E_{diss} \quad (4)$$

The return of energy is not an instantaneous phenomenon; therefore, an experimental study would be necessary for verifying if its contribution is entirely, partially or not at all useful for the bicycle motion. The estimation of the energy dissipated  $E_{diss}$  requires the data concerning the damping behaviour of the wheel. Since these data were not available for the research team during the work, the returned energy  $E_{ret}$  was assumed to be equal to zero.

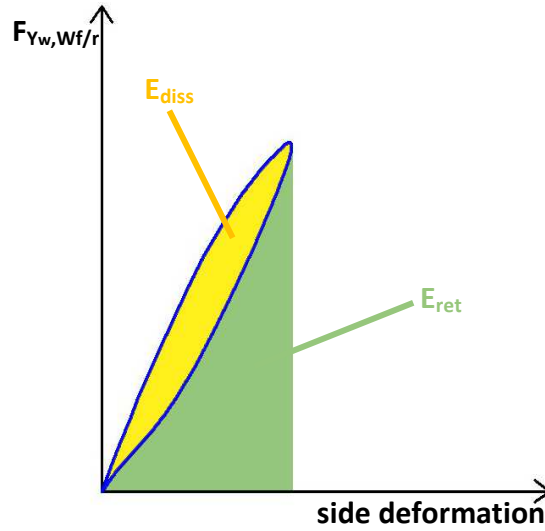


Fig. 13.4 Qualitative representation of a complete side force-deformation cycle, and the different energy contributions involved.

### 13.2.3 Handling Index formulation

During a change of direction, the total energy  $E_{W,f/r}^-$  absorbed by the front (5) and the rear (6) wheels is respectively obtained by the sum of three and two components:

$$E_{Wf}^- = \Delta E_{K,roll} + \Delta E_{K,steering} + \Delta W_{D,side} \quad [J] \quad (5)$$

$$E_{Wr}^- = \Delta E_{K,roll} + \Delta W_{D,side} \quad [J] \quad (6)$$

The Handling Index  $H_{W,f/r}$  was defined as the inverse of the total energy absorbed by the wheel.

$$H_{W,f/r} = \frac{1}{E_{Wf/r}^-} \quad \left[ \frac{1}{J} \right] \quad (7)$$

The subscript “f” or “r” indicates if the index is calculated for a front or a rear wheel. Higher values of  $R_{f/r}$  correspond to less energy absorbed by the wheel during the change of direction, which means a faster or easier manoeuvre, or less body effort spent by the cyclist to accomplish it.

If we consider a wheelset, the index is calculated as the inverse of the sum of the energy absorbed by the front and rear wheels that compose the wheelset:

$$H_w = \frac{1}{E_{Wf}^- + E_{Wr}^-} \quad \left[ \frac{1}{J} \right] \quad (8)$$

#### 13.2.4 Data considered for Handling Index computation

Some of the parameters needed for the Handling Index computation were obtained through the analysis of the data acquired during dedicated field tests on the same instrumented racing bicycle used for the Reactivity Index Computation. As presented in details in Part 5 of this thesis, some of the sensors that equipped the instrumented bicycle were opportunely chosen for measuring also the parameters needed for the computation of the Handling Index. The analysed field test corresponded to a road downhill, performed by a professional cyclist on the instrumented racing bicycle. The field tests characteristics are listed below:

- tester: professional track cyclist, sprinter, 21 years old, 180 cm height, 75 kg weight;
- length: 9.6 km;
- vertical drop: 580 m;
- average speed: 48.74 km/h;
- maximum speed: 65 km/h;
- test duration: 11' 49'';
- number of curves: 51, including 10 hairpin turns;
- total weight of tester + bicycle + data acquisition system: 95 kg.

The change of direction between the two consecutive curves presenting the highest values of the lateral roll angle of the bicycle, was considered as the **reference action** for the computation of the Handling Index. The lateral roll speed  $\dot{\phi}$ , and the side force  $F_{Yw,Wf/r}$  acting on the wheel, were estimated through the field tests analysis. The total side force  $F_{S,B}$  was supposed to be equally distributed between the front and the rear wheel.

Since no data about the steering angle or steering speed were collected from the field test, the steering speed  $\dot{\delta}$  was estimated from the data acquired by V. Cossalter [28] during a slalom test performed with a motorcycle, at a speed of 54.7 km/h, on a path defined by a set of traffic cones, positioned along a straight line at a relative distance of 14 m. No other data regarding the steering angle or steering speed of two wheeled vehicles were found in literature.

The mass  $m$ , the polar inertia  $I_p$ , and the lateral stiffness  $K_{side}$  are the basic engineering characteristics of the wheel, measured by means of the standard laboratory tests.

#### ***Analysis of the data acquired during the field tests***

The parameters directly measured during the field test, which were useful for the estimation of the data needed for the Handling Index computation, are described together with the sensor used for their measurement in the table 13.1.



| Parameter                     | Description  | Sensor  |
|-------------------------------|--|---|
| V [km/h]                      | Bicycle speed  | Magnetic sensor and GPS.  |
| $\dot{\varphi}$ [rad/s]       | Lateral rolling speed  | Gyroscope inside of the Inertial Measurement Unit (IMU)                 |
| $\varphi$ [rad]               | Lateral roll angle   | Computed by the Inertial Measurement Unit through a dedicated algorithm |
| $a_{y_b}$ [m/s <sup>2</sup> ] | Lateral acceleration along the Y <sub>B</sub> axis of the Bicycle reference system | Tri-axial accelerometer inside of the Inertial Measurement Unit (IMU)   |

Tab. 13.1 List of the parameters measured during the field test, which were useful for the computation of the Handling Index.

A Matlab® program was compiled to analyse the rough data following the stages listed below.

- **Computation of the side force  $F_s$  acting on a front or rear wheel**

The tri-axial accelerometer internal to the Inertial Measurement Unit, furnished a measurement of the acceleration along the Y<sub>B</sub> axis (fig. 13.5.b) relating to the reference system of the bicycle (fig. 13.5.a).



Fig. 13.5. (a) Reference system adopted for the bike; (b) acceleration along the Y<sub>B</sub> axis measured during the execution of a left curve.

Since the accelerometer is capacitive, it could measure also the static acceleration. During the execution of a curve, with the bicycle laterally inclined of the  $\varphi$  roll angle, the acceleration  $a_{y_b}$  along the Y<sub>B</sub> axis of the bicycle reference system is the sum of the components, regarding the same axis, of the gravitational  $g$  and centrifugal  $a_{s,B}$  acceleration acting on the bicycle (fig. 13.6):

$$a_{y_b} = a_{s,B} \cdot \cos(\varphi) - g \cdot \sin(\varphi) \quad (9)$$

The centrifugal acceleration  $a_{S,B}$ , which is an apparent acceleration for the Bicycle system, is therefore obtained through the (10).

$$a_{S,B} = \frac{a_{y_B}}{\cos(\varphi)} + g \cdot \text{tg}(\varphi) \quad (10)$$

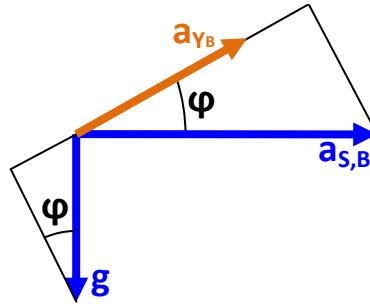


Fig. 13.6 Schematic of the components of the  $a_{y_B}$  acceleration measured during the field test.

The total side force  $F_{S,B}$  acting on the bicycle/cyclist system, and allowing the bicycle to accomplish the curve, is the product of the centrifugal acceleration with the total bicycle/cyclist mass (11).

$$F_{S,B} = a_{S,B} \cdot m_{\text{Bike,tot}} \quad (11)$$

Since the total side force  $F_{S,B}$  was supposed to be equally distributed between the front and the rear wheel, the side forces acting at the front and rear wheel ( $F_{S,Wf/r}$ , fig. 13.3) was obtained as it follows:

$$F_{S,Wf} = F_{S,Wr} = \frac{F_{S,B}}{2} \quad (12)$$

$F_{Y_w,Wf/r}$  is the component of  $F_{S,Wf/r}$  along the  $Y_w$  axis of the wheel (13).

$$F_{Y_w,Wf/r} = F_{S,Wf} \cdot \cos(\varphi) \quad (13)$$

- **Signals filtering**

The signals acquired during the field test presented an irregular component due to the vibration of the bicycle caused by the road irregularities. Since the analysis of the vibrations did not represent the aim of the data analysis, they represented a signal disturbance, and their effect was therefore eliminated through a filtering operation. A four poles Butterworth lowpass filter was used for filtering all the signals, considering a cutoff frequency of 0.5 Hz. The figure 13.7 shows an example of the effect of the filtering operations on the roll speed signal.

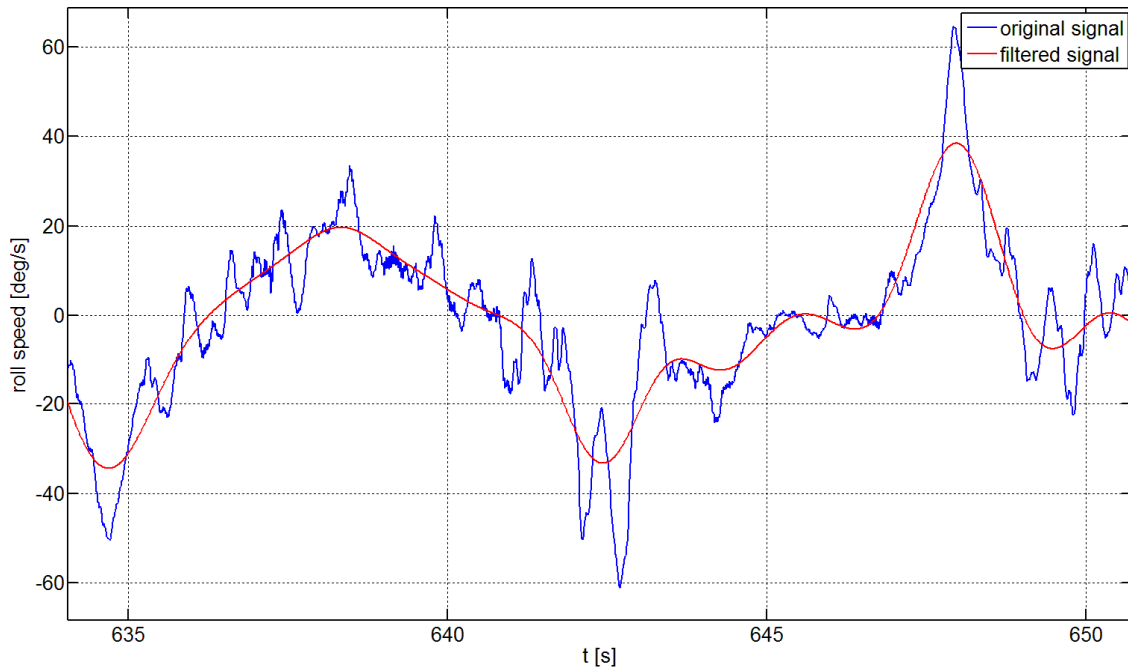


Fig. 13.7 Effect of the filtering operation on the lateral roll speed signal.

- **Selection of the reference change of direction**

A figure with three charts was created for the selection of the test section corresponding to the change of direction to be analysed (fig. 13.8). The bicycle speed  $v$  is reported in the upper chart: the middle one shows the lateral roll angle  $\varphi$  and roll speed  $\varphi'$ , whereas the side force acting on the wheel  $F_{Yw}$  is plotted in the lower one.

For the conventions of the Inertial Measurement Unit, a positive roll angle indicates a side inclination of the bicycle on the right, corresponding therefore to a right curve. Two consecutive peak/valley corresponds to the execution of two consecutive right and left curves. The two test sections are characterised by a sequence of several consecutive curves and high absolute values of peaks and valleys. The first one is visible between 240 s and 300 s, and the second one from 600 s to 700 s. The 10 deep valleys showed by the bicycle speed, with values around 25 km/h, correspond to the execution of 10 hairpin turns.

The test section regarding two consecutive curves, which present high peak/valley of the roll angle, and the reference change of direction corresponding to the maximum variation of the roll speed, were consecutively selected considering respectively the charts of figure 13.8 and 13.9.

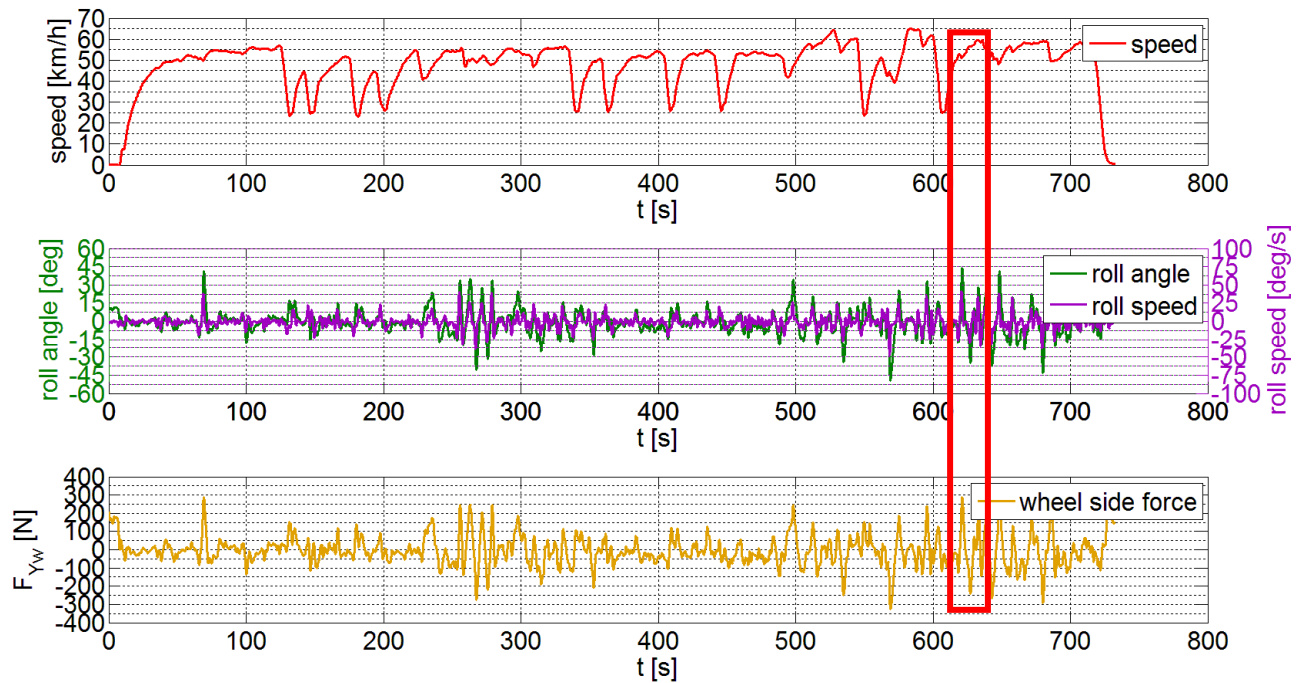


Fig. 13.8 Signals acquired or calculated for the entire test duration, and selection of two consecutive curves.

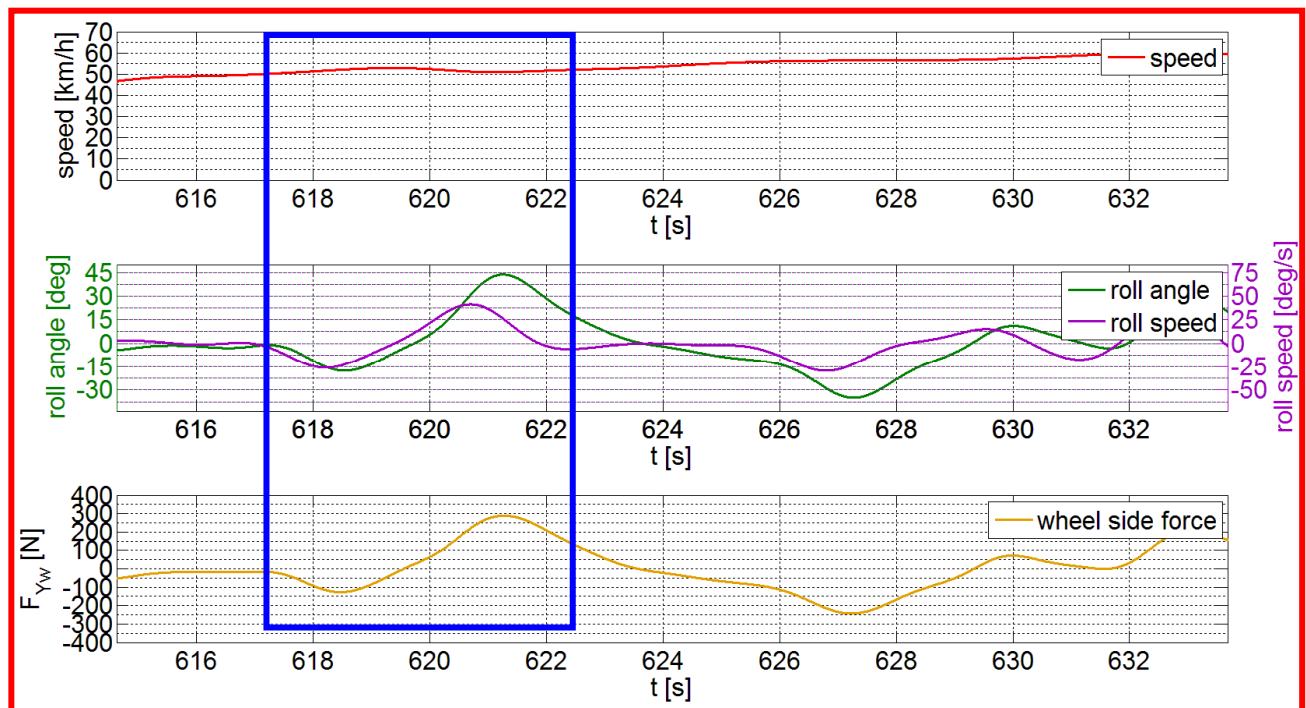


Fig. 13.9 Selection of the test section for computing the parameters regarding the reference change of direction, which presented the highest variation of roll speed.

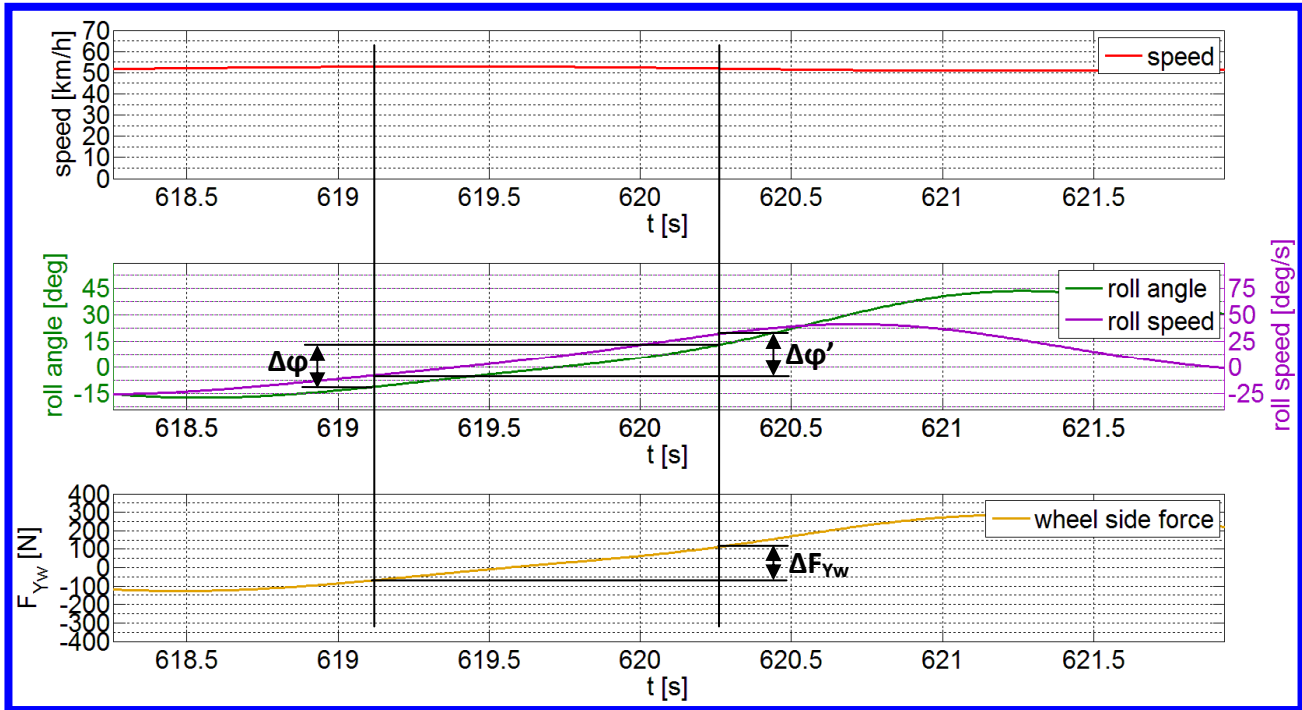


Fig. 13.10 Reference direction change characterized by the maximum variation of roll speed. Calculation of  $\Delta F_{Yw}$ ,  $\Delta\phi$ , and  $\Delta\phi'$ .

• **Calculation of  $\Delta F_{Yw}$ ,  $\Delta\phi_0$ , and  $\Delta\phi'$**

Referring to the figure 13.10, the section of the direction changing corresponding to a variation of the roll angle from  $-10^\circ$  to  $+10^\circ$  was considered as the reference change of direction phase. All parameters were therefore calculated as the difference between their initial and final values concerning the reference change of direction phase. The duration of the reference change of direction phase is equal to 0.97 s.

**Summary of the data considered for the computation of the Handling Index**

The parameters considered for the computation of the Handling Index, and the respective values and source are summarized in the table 13.2.

| Parameter                               | Description   | Source                                     |
|---|---|--|
| $\Delta\phi' = 0.65 \text{ rad/s}$      | Lateral roll speed variation                        | Data analysis of field test                |
| $\Delta\delta' = 0.32 \text{ rad/s}$    | Steering speed variation                            | Literature: V. Cossalter [28]              |
| $v_{avg} = 56.48 \text{ km/h}$          | Translational speed increment                       | Data analysis of field test                |
| $\Delta F_{Yw,Wf/r} = 149.1 \text{ Nm}$ | Total drive torque difference                       | Data analysis of field test                |
| $\Delta\phi = 0.34 \text{ rad}$         | Lateral roll angle                                  | Data analysis of field test                |
| $f = 0.05 \text{ m}$                    | Forward offset of the front assembly of the bicycle | Constructive characteristic of the bicycle |
| $r_w = 0.321 \text{ m}$                 | Radius of a racing bicycle wheel                    | Constructive characteristic of the wheel   |

Tab. 13.2 Summary of the data considered for the computation of the Handling Index.

### 13.2.5 Handling Index validation

The figure 13.11 shows the correlation coefficient calculated between the Handling Index and the Handling quality requirement (QR.5). The correlation coefficient is close to unity. The Handling Index therefore expresses very well the wheels behaviour perceived by the cyclist during the transient phases of the typical manoeuvres performed with the racing bicycle. The high correlation allows to validate the index and the approach adopted for its formulation.

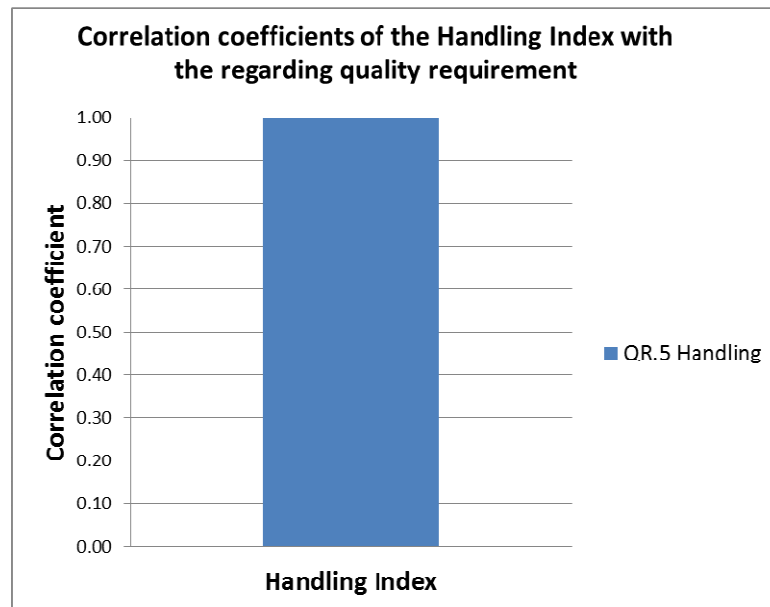


Fig. 13.11 Correlation coefficient calculated between the Handling Index and the Handling quality requirement (QR.5).

## 13.3 Road Holding Index

### 13.3.1 Approach and formulation

The Road Holding Index aims to represent a technical measurement of the cyclist evaluation about the wheel influence on the precision of the bicycle in following the turning path.

During the central phase of the curve, the bicycle motion is approximately in a steady condition. In this phase, the wheel motion is given by the sum of three components:

- $x$ : translation in the direction of the bicycle motion;
- $\theta$ : rotation around the wheel axis;
- $\psi$ : yaw motion, around the vertical axis coinciding with the centre of curvature of the turning path (yaw axis).

A gyroscopic effect is generated by a rigid body rotating around an axis, which is rotating itself around a second axis not parallel to the first. In the steady turning condition (fig. 13.12), the wheel rotates around the hub axis with a speed  $\omega$ , and the hub axis rotates in turn with a speed  $\psi'$  around the vertical axis coinciding with the centre of curvature of the turning path. A gyroscopic

effect is therefore presented by the wheel in these conditions of motion. The value of the gyroscopic moment is equal to the vector product between the angular momentum  $I_p \cdot \omega$  of the wheel around the hub axis, and the angular speed  $\psi'$  of the hub axis around the yaw axis (14).

$$M_{\text{gyro}, \psi, Wf/r} = I_p \cdot \omega \cdot \psi' \cdot \cos(\varphi) \quad (14)$$

$I_p$ : polar moment of inertia of the wheel [ $\text{kg} \cdot \text{m}^2$ ].

$\omega$ : wheel rolling speed around the hub axis [ $\text{rad/s}$ ].

$\psi'$ : rotational speed of the wheel around the yaw axis [ $\text{rad/s}$ ].

$\varphi$ : lateral roll angle of the wheel [ $\text{rad}$ ].

Since the hub and the yaw axis are orthogonal, the axis of the gyroscopic moment is perpendicular to both. It corresponds to the  $X_w$  axis of the reference system of the wheel. Since the verso of the moment agrees with the right-hand rule, the effect of the gyroscopic moment is to right the bicycle, inducing a roll motion in the direction of the external side of the curve. The gyroscopic moment needed a cyclist action for balancing it, so an increase of the moment involves an increase of the body effort needed to balance it, and therefore to maintain the curving path.

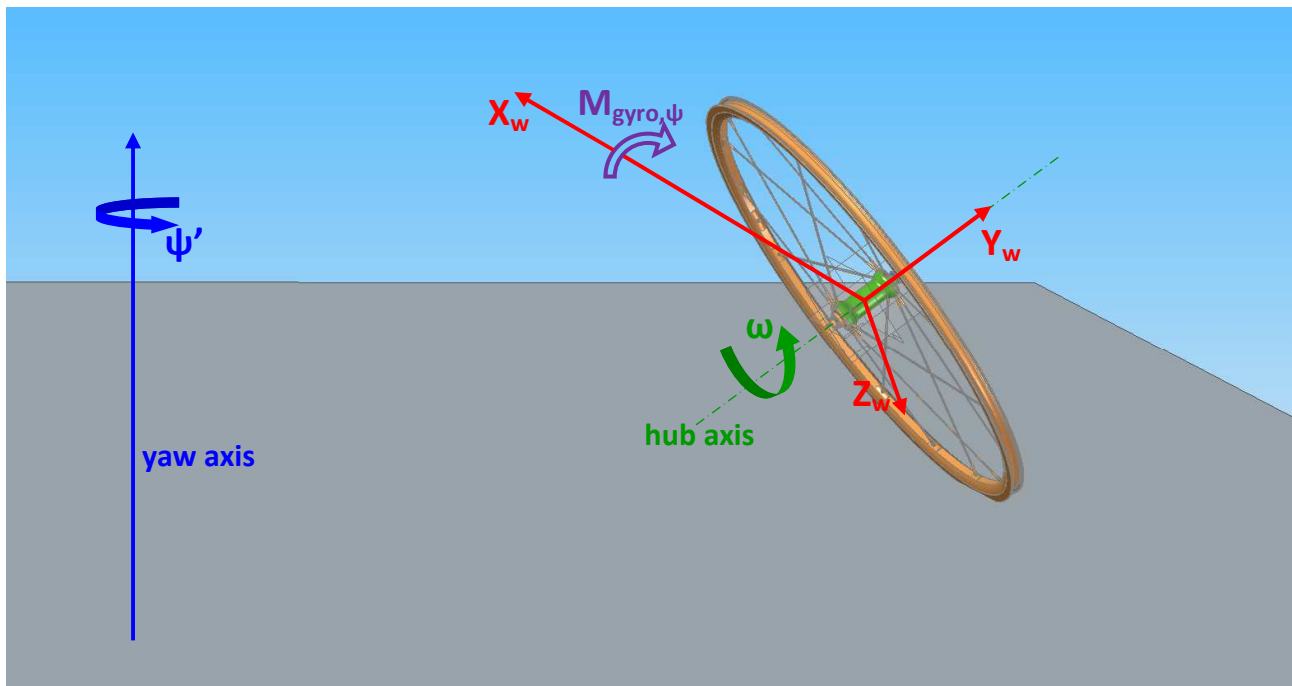


Fig. 13.12 Gyroscopic effect generated by a front or rear wheel during the steady turning.

The Road Holding Index  $RHI_{Wf/r}$  was defined as the inverse of the gyroscopic moment that the cyclist has to balance during the execution of a curve:

$$RHI_{Wf/r} = \frac{1}{M_{gyro,\psi,Wf/r}} \left[ \frac{1}{Nm} \right] \quad (15)$$

If the wheelset is considered, the index is calculated as the inverse of the sum of gyroscopic effects of the front and the rear wheel:

$$RHI_w = \frac{1}{M_{gyro,\psi,Wf} + M_{gyro,\psi,Wr}} \left[ \frac{1}{Nm} \right] \quad (16)$$

### 13.3.2 Data considered for Road Holding Index computation

As for Handling and Reactivity Index, the parameters needed for the Road Holding Index computation were obtained through the analysis of the data acquired during dedicated field tests on the instrumented racing bicycle. Some of the sensors that equipped the instrumented bicycle were opportunely chosen for measuring also the parameters needed for the computation of the Road Holding Index (see Part 5). The analysed field test corresponded to the same road downhill considered for the Handling Index, performed by a professional cyclist on the instrumented racing bicycle. The field tests characteristics are again listed below:

- tester: professional track cyclist, sprinter, 21 years old, 180 cm height, 75 kg weight;
- length: 9.6 km;
- vertical drop: 580 m;
- average speed: 48.74 km/h;
- maximum speed: 65 km/h;
- test duration: 11' 49'';
- number of curves: 51, including 10 hairpin turns;
- total weight of tester + bicycle + data acquisition system: 95 kg.

The central phase of a curve performed at high speed, that presented high value of the lateral roll angle of the bicycle, was considered as the **reference action** for the computation of the Road Holding Index. The forward rolling motion  $\omega$  of the wheel around the hub axis, the lateral roll angle  $\varphi$ , and the yaw speed  $\dot{\psi}$ , were estimated through the field tests analysis.

The mass of the polar inertia  $I_p$  is a basic engineering characteristics of the wheel measured by means of the standard laboratory tests.



### Analysis of the data acquired during the field tests

The parameters directly measured during the field test, which were useful for the estimation of the data needed for the Road Holding Index computation, are described together with the sensor used for their measurement in the table 13.3.

| Parameter                     | Description   | Sensor  |
|-------------------------------|---|---|
| V [km/h]                      | Bicycle speed   | Magnetic sensor and GPS.  |
| $\varphi$ [rad]               | Lateral roll angle  | Computed by the Inertial Measurement Unit through a dedicated algorithm |
| $a_{Y_B}$ [m/s <sup>2</sup> ] | Lateral acceleration along the $Y_B$ axis of the Bicycle reference system | Tri-axial accelerometer inside of the Inertial Measurement Unit (IMU)   |

Tab. 13.3 List of the parameters measured during the field test, which were useful for the computation of the Road Holding Index.

A Matlab® program was compiled to analyse the rough data following the stages listed below.

- **Computation of the yaw speed  $\psi'$**

The yaw speed  $\psi'$  can be calculated as the ration between the bicycle forward speed  $v$  and the curvature radius  $R_c$  of the turning path (17).

$$\psi' = \frac{v}{R_c} \left[ \frac{\text{rad}}{\text{s}} \right] \quad (17)$$

The bicycle speed  $v$  was directly measured during the field test, and its relationship with the curvature radius  $R_c$  is represented by the equation of the centrifugal acceleration (see § 13.2.4, fig. 13.6):

$$a_{s,B} = \frac{v^2}{R_c} \quad (18)$$

$$R_c = \frac{v^2}{a_{s,B}} \quad (19)$$

The centrifugal acceleration was calculated following the (10).

- **Signals filtering**

The signal irregularities due to the vibrational phenomena of the bicycle were eliminated through the signal filtering with a four poles Butterworth lowpass filter, considering a cutoff frequency of 0.5 Hz (see § 13.2.4, fig. 13.7).

- **Selection of the reference curve**

A figure with three charts was created for the selection of the test section corresponding to the curve to be analysed (fig. 13.8). The bicycle speed  $v$  is reported in the upper chart, the middle one shows the lateral roll angle  $\varphi$  and roll speed  $\varphi'$ , whereas the yaw speed  $\psi'$  is plotted in the lower one.

For the general description of the test we can refer to the § 13.2.4.

The test section regarding two consecutive curves, which present high absolute values of the roll angle, was selected considering the figure 13.13. Among the two curves, the curve that was performed at the highest speed was selected for the analysis (fig. 13.14).

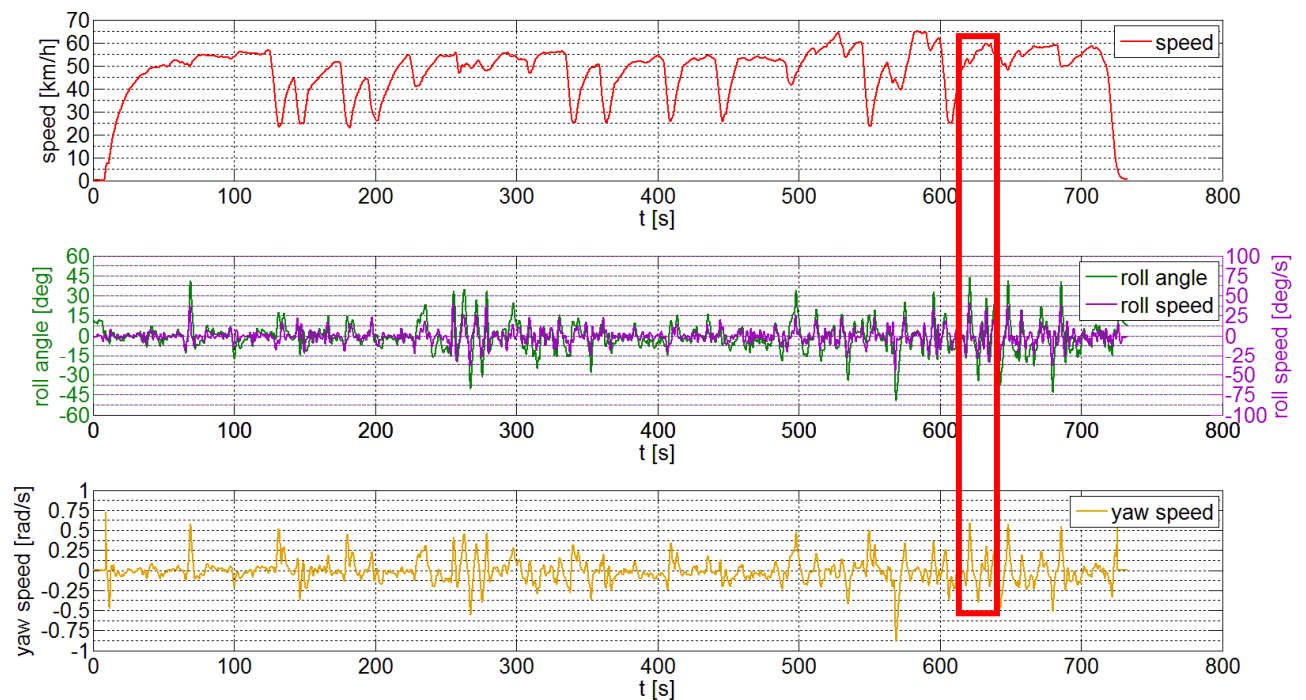


Fig. 13.13 Signals acquired or calculated for the entire test duration and selection of two consecutive curves.

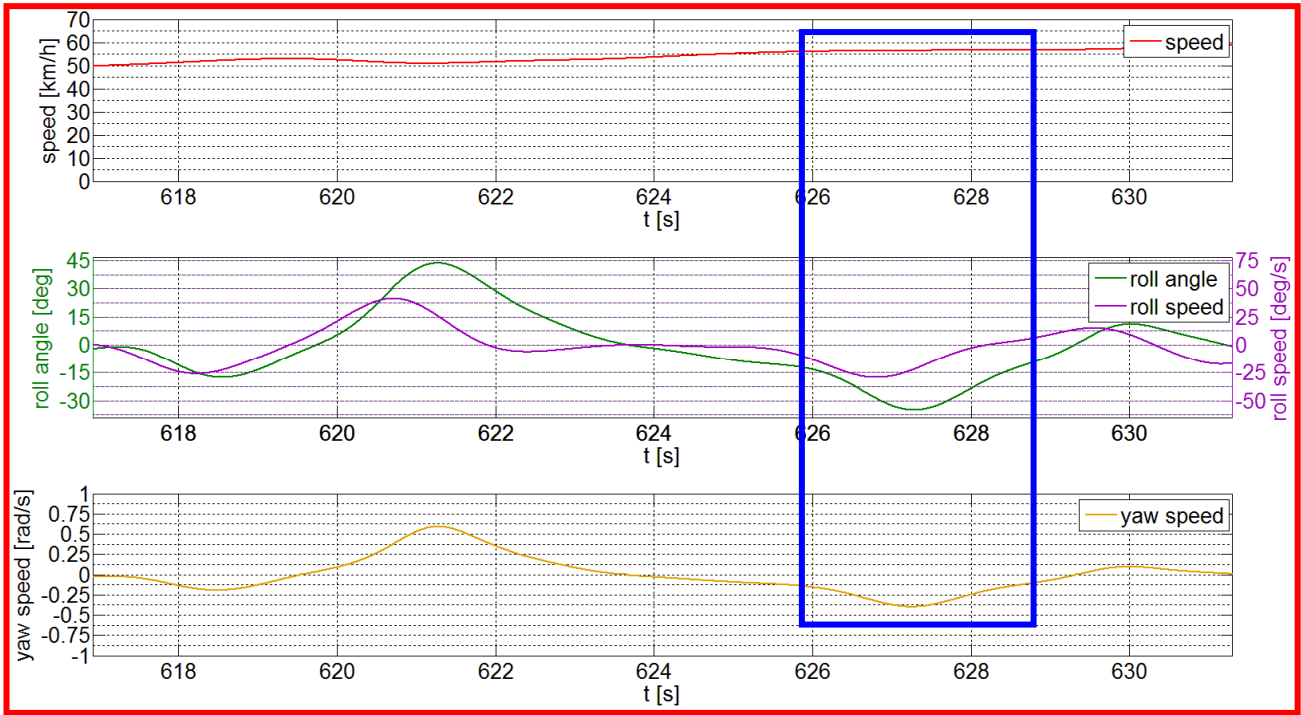


Fig. 1314. Selection of the analysed curve.

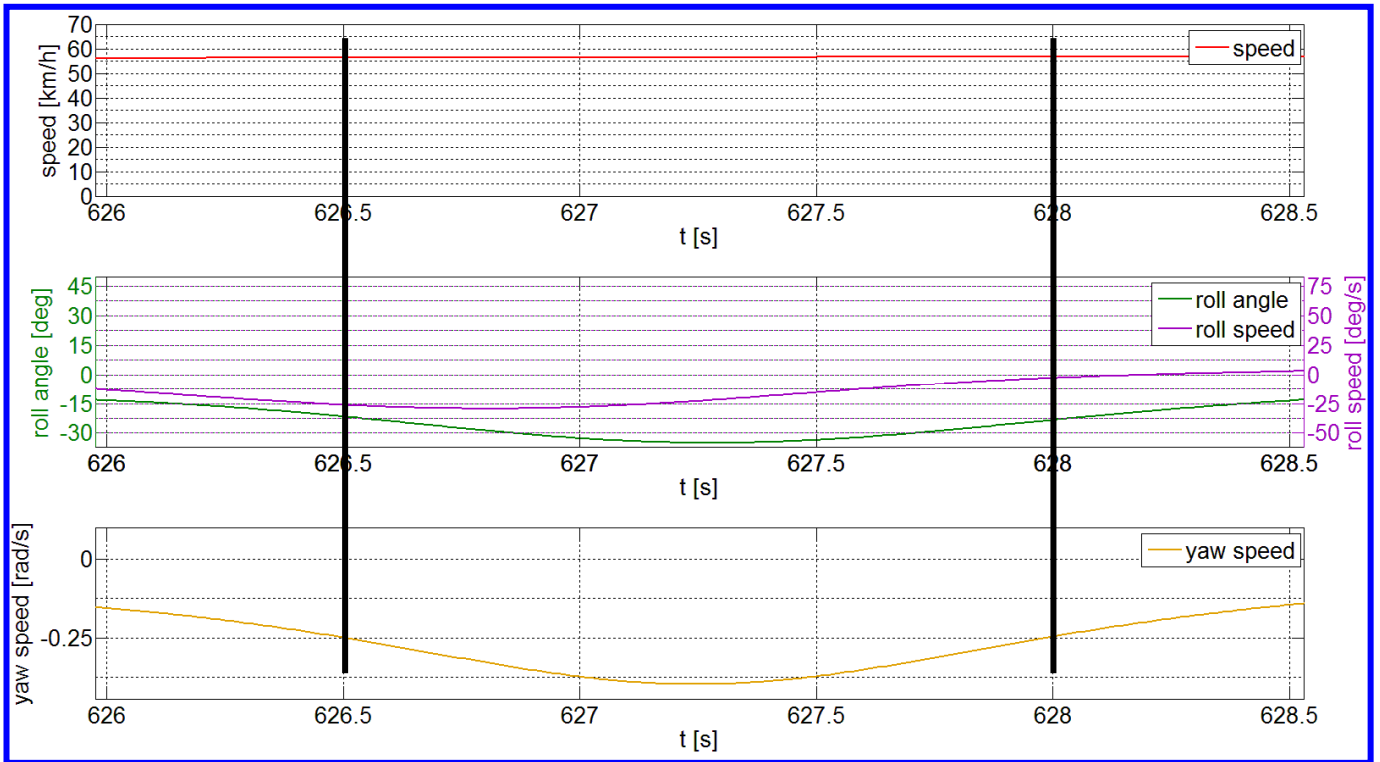


Fig. 13.15 Reference curve phase characterized by the maximum absolute value of yaw speed.

- **Calculation of  $\omega$ ,  $\psi$ , and  $\varphi$ .**

Referring to the figure 13.15, the curve phase around the highest absolute value of the yaw speed, was considered as reference for the computation of the data for the Road Holding Index. Since during the reference phase all parameters are variable, the mean value was calculated for each of them considering the reference turning phase. The duration of the reference turning phase is equal to 1.5 s.

**Summary of the data considered for the computation of the Road Holding Index**

The parameters considered for the computation of the Road Holding Index, and the respective values and source are summarized in the table 13.4.

| Parameter                          | Description                   | Source                      |
|------------------------------------|-------------------------------|-----------------------------|
| $\omega_{avg} = 48 \text{ rad/s}$  | Average forward rolling speed | Data analysis of field test |
| $\psi'_{avg} = 0.33 \text{ rad/s}$ | Total drive torque difference | Data analysis of field test |
| $\varphi_{avg} = 0.34 \text{ rad}$ | Average lateral roll angle    | Data analysis of field test |
| $v_{avg} = 56.48 \text{ km/h}$     | Average forward speed         | Data analysis of field test |

Tab. 13.4 Summary of the data considered for the computation of the road Holding Index.

**13.3.3 Road Holding Index validation**

The figure 13.16 shows the correlation coefficient calculated between the Road Holding Index and the Road Holding quality requirement (QR.6) evaluated by the cyclists during the subjective evaluation test. The correlation coefficient is equal to 0.903, greater than the threshold of 0.9 considered for the index validation. The Road Holding index results therefore validated, and we can say that it well expresses the perceived wheel influence on the precision of the bicycle in following the turning path.

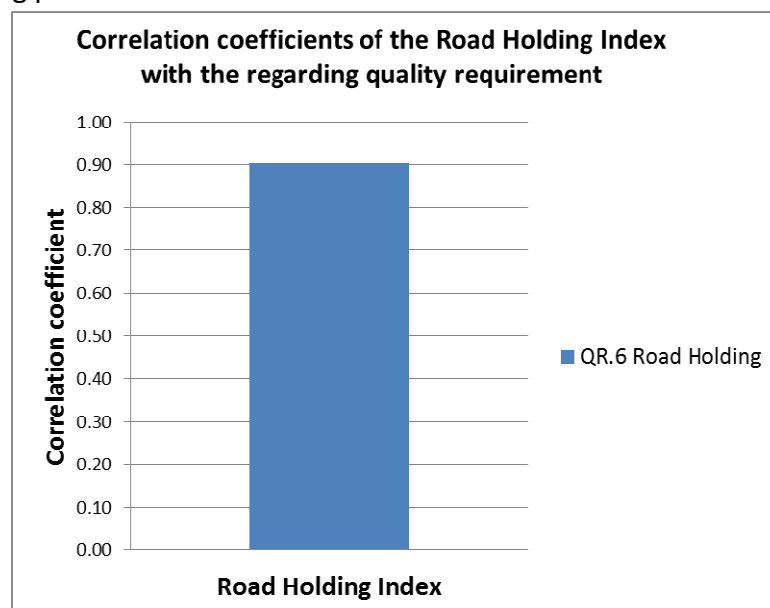


Fig. 13.16 Correlation coefficient calculated between the Road Holding Index and the Road Holding quality requirement (QR.6).



# Chapter 14

## Impulsive Comfort Index

### 14.1 Introduction

Comfort involves multiple aspects related to the different physical, thermodynamic, and physiological quantities perceived by the cyclist. Neglecting the thermodynamic and physiological quantities, comfort can be divided into five macro categories (see Chapter 3):

- vibrational comfort;
- impulsive comfort;
- contact pressure comfort;
- posture comfort.

In the part 2 of this thesis, concerning the evaluation of the basic engineering characteristics, the Vibrational and Impulsive Comfort properties of wheels and saddles were investigated. A Vibrational Comfort Index was introduced in the Chapter 6 with the aim to express the vibrational transmissibility of the saddles.

The radial stiffness of the wheels was measured during the static, the dynamic and the bump radial tests developed in the Laboratory of Machine Design of University of Padova (see § 4.3). The stiffness and damping behaviour showed during the bump tests were supposed to be correlated with the Impulsive Comfort properties. A test method for evaluating the Vibrational Comfort properties of wheels was also developed in the University laboratories (see § 5.2). Since the test methods were developed in a stage prior to the execution of the subjective evaluation test, there was not the possibility to apply these methods for measuring the three wheelsets used for the subjective evaluation tests. For this reason, a relationship between the engineering parameters measured through the two new testing methods, developed in University laboratories, and the quality requirements concerning the vibrational and impulsive comfort, could not be estimated, excluding the possibility to validate them. The conventional “Swinging arm laboratory test method”, developed in Campagnolo testing laboratories (see § 5.3), presented some limitations due to the characteristics of the equipment available for the test bench setup. The only basic engineering characteristic measured for the three wheelsets, that was supposed to be correlated with their comfort properties, is therefore the static radial stiffness measured through the new test bench developed in Campagnolo testing laboratories (see § 4.4).

The Impulsive Comfort Index developed in this work started from the analysis of the correlation between the static radial stiffness and the quality requirements represented by the Vibrational and Impulsive Comfort, and evaluated by the cyclists during the subjective evaluation tests.

## 14.2 Impulsive Comfort Index formulation

The correlation coefficients (see Chapter 10) calculated between the static radial stiffness  $K_{rad}$  of the wheels and the Vibrational and Impulsive Comfort, evaluated by the cyclists during the subjective evaluation tests, are lower than zero (fig. 14.1). This corresponds to an inverse correlation between the static radial stiffness and the comfort quality requirements, which testifies that an increase of the wheels radial stiffness negatively affects their perceived comfort properties.

The static radial stiffness shows a medium correlation with the Vibrational Comfort, for which the absolute value of the calculated correlation coefficient is lower than 0.9. A high correlation with the static radial stiffness is showed by the Impulsive Comfort, presenting a correlation coefficient greater than 0.9. We can say therefore that the radial stiffness well represents the Impulsive Comfort quality requirement.

On the base of these considerations, the **Impulsive Comfort Index ICI**, which expresses the wheels behaviour regarding the Impulsive Comfort, was calculated as the inverse of the static radial stiffness:

$$ICI_{w/r} = \frac{1}{K_{rad, w/r}} \left[ \frac{m}{N} \right] \quad (1)$$

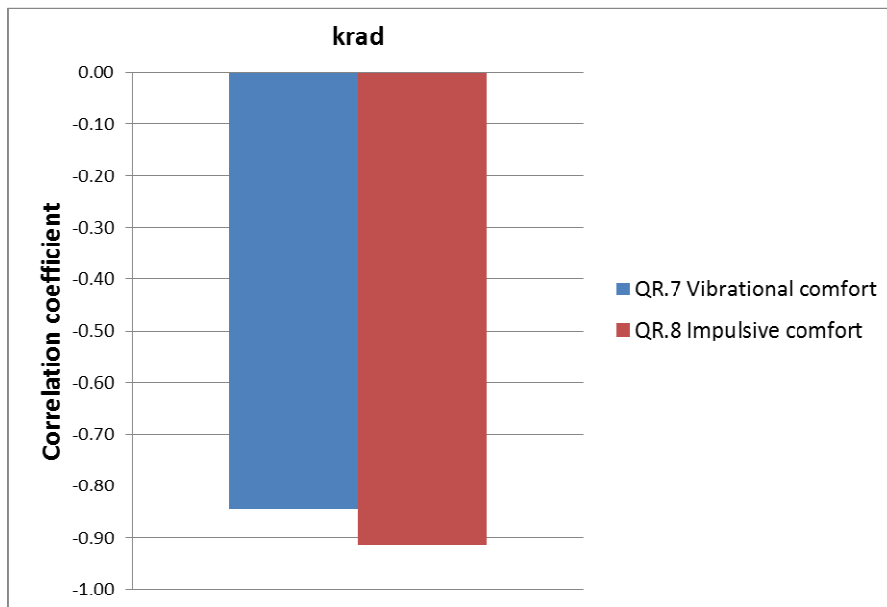


Fig. 14.1 Correlation coefficients calculated between the Radial Stiffness  $K_{rad}$  and the quality requirements represented by the Vibrational and the Impulsive comfort.

## 14.2 Validation of Impulsive Comfort Index and discussion

Since the only parameter included in the Impulsive Comfort Index formulation is represented by the static radial stiffness, which were found to be highly correlated to the Impulsive Comfort, the high correlation between the Impulsive Comfort Index and the quality requirement represented by the Impulsive Comfort (fig. 14.2) is obvious.

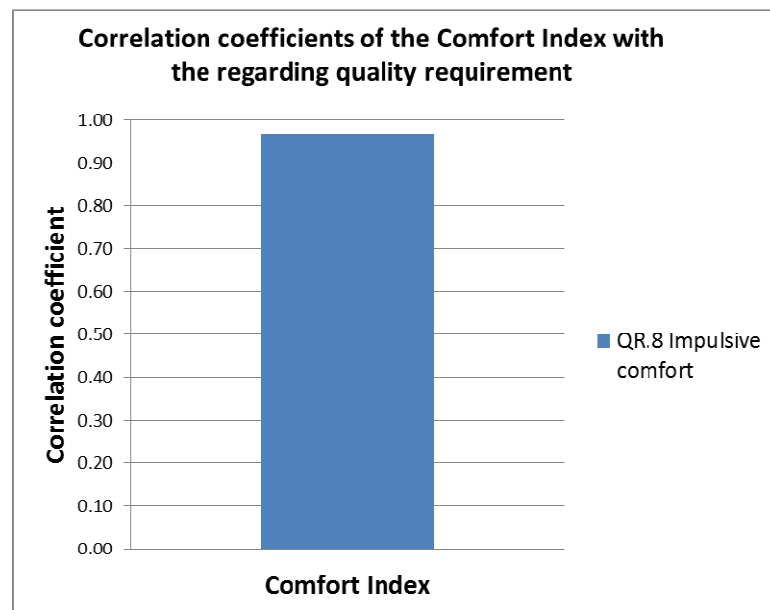


Fig. 14.2 Correlation coefficient calculated between the Impulsive Comfort Index, and the Impulsive Comfort quality requirement.

A further more detailed analysis of the correlation between the structural characteristics of the wheels, evaluated during radial bump tests, and the Impulsive Comfort, can represent the base for improving the Impulsive Comfort Index here developed. A Vibrational Comfort Index of the wheels can be developed following the same approach, namely studying the correlation of the quantities evaluated through the "Full bicycle laboratory test method" (University lab.) with the Vibrational Comfort perceived by the cyclists.





# Chapter 15

## Index of Forward Rolling Efficiency and Index of Stability to Crosswind

### 15.1 Introduction

The **Forward Rolling Efficiency** of a wheel is the quality requirement which summarizes the evaluation of the cyclist about the perceived influence of the wheel on the forces acting against the forward motion of the bicycle. The assessment of the cyclists concerning the influence of the wheels on the bicycle response to the presence of lateral wind, is sum up through the **Stability to Crosswind** quality requirement. Since both quality requirements just mentioned are directly connected to aerodynamic phenomena, the formulations of the respective two indexes, which aim to express a technical measurement of them, are both presented in this chapter. Because there was not the possibility to execute a dedicated study on the aerodynamics of the wheels, the parameters needed for the computation of the Index of Forward Rolling Efficiency, and of the Index of Stability to Crosswind, were estimated from the results of two works opportunely selected during the literature analysis.

In the first part of the chapter, the aerodynamic forces and moments, generated by the interaction between the wheels and the surrounding air flow, are presented together with a review of the literature regarding this topic. The formulation of the two indexes, the data considered for their computation, and their validation are exposed in the second part.

### 15.2 Aerodynamic loads acting on wheels

We consider a cyclist, riding in a straight direction, at a constant speed  $V$ , in absence of lateral wind, and without the drafting effect of other cyclists or vehicles (fig. 15.1). In these cycling conditions, the interaction of the front and the rear wheel with the frontal air flow generates the longitudinal drag force  $F_D$  and the aerodynamic moment  $M_{Yw,aero}$  around the hub axis, opposed to the forward rotation of the wheel (fig. 15.2). Both the longitudinal drag force and the aerodynamic moment represent two resistance loads that the cyclist has to overcome for keeping the forward motion of the bicycle. They depend mainly from the constructive characteristics of the wheel, such as the rim depth and shape, from the number, the shape, the length of the spokes, and from the spokes pattern. The bicycle frame and the cyclist movement affects the air flow, which encounters the wheels: this aspect has therefore to be kept in consideration during the study of the aerodynamic behaviour of the wheels.

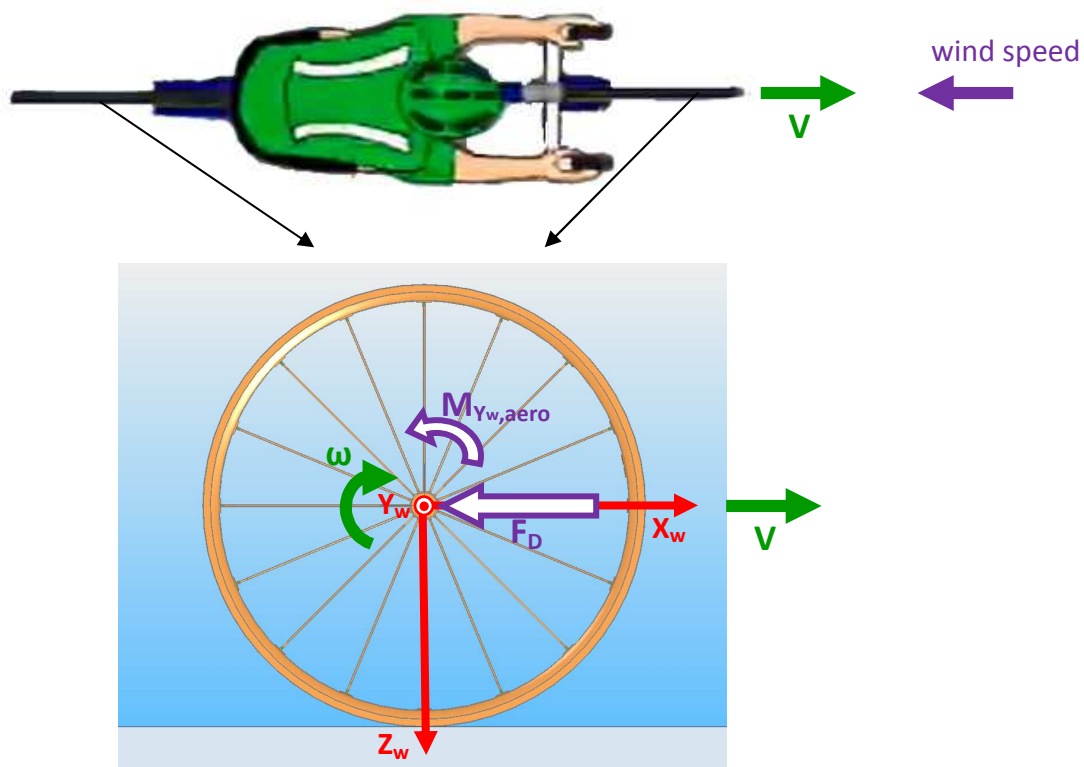


Fig. 15.1 Schematic of the aerodynamic loads acting on a wheel, during the straight bicycle motion in absence of lateral wind.

If the cyclists, while riding in a straight direction, at a constant speed  $V$ , encounters a lateral wind due to a wind gust or a turbulence generated, for example, by a car or a truck, the wheels, in addition to the loads presented above, are subjected also to an aerodynamic side force  $F_{S,aero}$  and twisting moment  $M_{tw,aero}$  (fig. 15.2). These two additional aerodynamic loads have the effect to reduce the bicycle stability, involving an action of the cyclist for their balancing. They directly depends by the, so named, yaw angle  $\psi$  between the wind and the bicycle speed directions. The aerodynamic side force  $F_{S,aero}$  mainly depends by the wheel lateral area, which, in turn, has a quadratic relationship with the rim depth. The effect of  $M_{tw,aero}$  regards mainly the front wheel, and it is directly related to the side force  $F_{S,aero}$ , while the pressure distribution of the air flow on the lateral wheel surface affects its magnitude and direction.

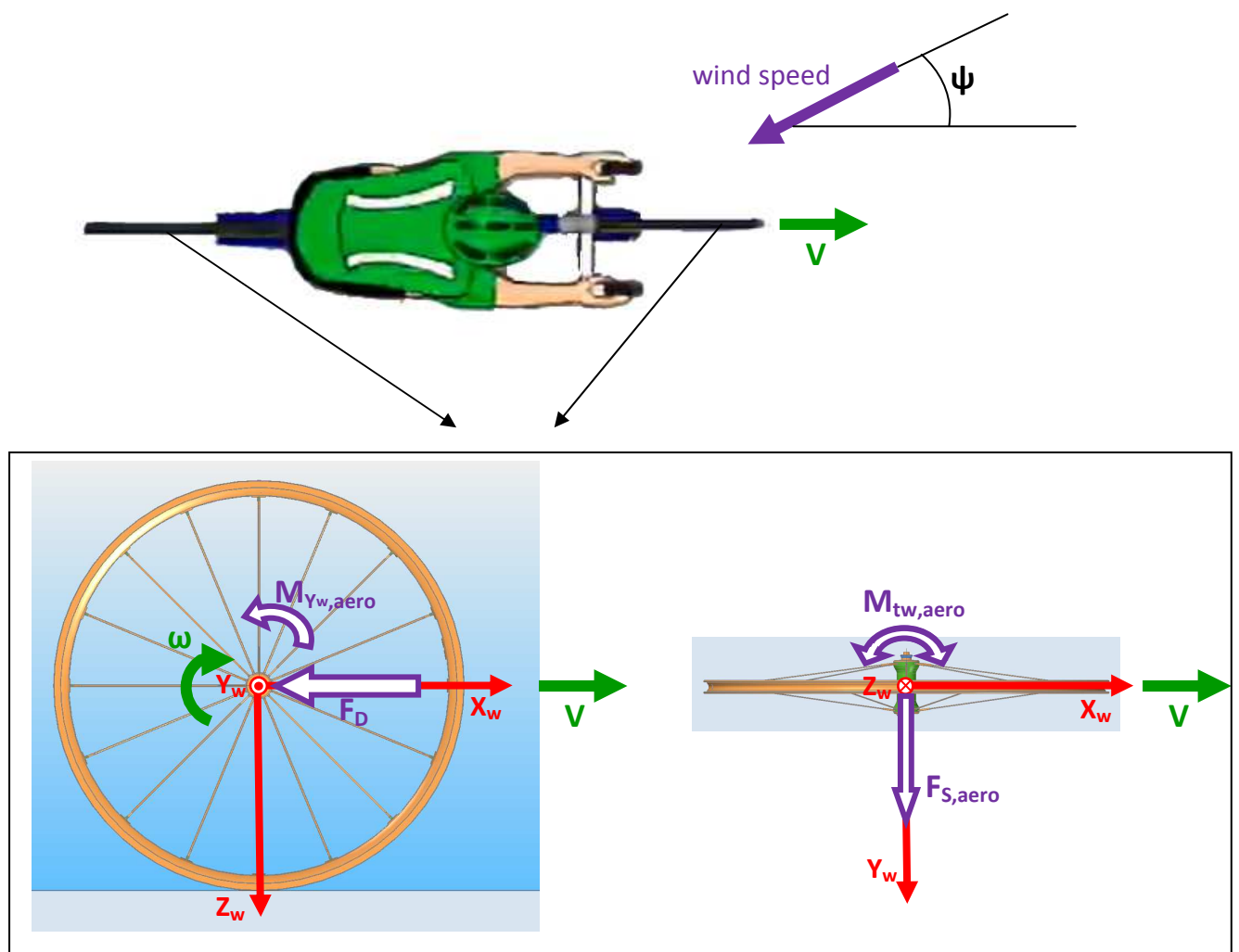


Fig. 15.2 Schematic of the aerodynamic loads acting on a wheel, during the straight bicycle motion in presence of lateral wind.

### 15.3 Review of the literature on aerodynamics of bicycle and wheels

Many works concerning the experimental or numerical analysis, the first one through wind tunnel tests, the second one through the CFD (Computational Fluid Dynamics), of the aerodynamic behaviour of the bicycle and of wheels can be found in literature.

Defraeye *et al.* [46] investigated the effect of the rider position on the total drag force acting on the bicycle. They tested the full bicycle, with the cyclist in static different positions, generating a frontal wind at three speed: 10, 15, and 20 m/s. During the tests, they measured the drag coefficient and compared the experimental results with the numerical CFD analysis. The results confirm that reducing the frontal area of the cyclist can significantly reduce his drag area. The aerodynamic drag of the cyclist is 60–70% of the total bicycle drag.

Similar tests were performed by Chowdhury *et al.* [47], in whose work a set of wind tunnel tests was performed on the full bicycle with the cyclist in different static positions. The effect of the

wind speed on the drag coefficient was also investigated, whereas its direction was always kept aligned with the symmetry plane of the bicycle. The drag coefficient  $c_D$  did not vary with the wind speed. The differences between the drag force, measured during the tests performed with the cyclist in different positions, increase with the wind speed due to the parabolic relationship between the drag force and the wind speed.

The wind tunnel tests executed by Tew & Sayers [48] concerned the single wheel. The different tested wheels were subjected to an air flow characterised by a different speed and a different yaw angle. The resulted side force coefficients showed a linear relationship with the yaw angle between the symmetry plane of the wheel and the wind direction.

Barry *et al.* [49] investigated the influence of the wheels on the drag and side force acting on the bicycle. With this purpose, they performed wind tunnel tests using a full bicycle with a mannequin in static position, with the forward rolling motion of the wheels, and an air flow with a constant speed of 50 km/h and different yaw angles. They performed different tests with and without the mannequin, and with the bicycle equipped with different wheel models. The addition of the mannequin to the testing setup greatly influenced the trend of the drag curves, highlighting the interference generated by the rider. For all wheels, side force was seen to be of similar magnitude to drag at 5° yaw and then increased linearly with yaw angle. The results presented in this paper highlight that to assess the performance of a bicycle wheel using only axial drag as the criteria is not sufficient, but rather consideration must be taken for the side force, roll and yaw moments imparted on the bicycle and rider.

Godo, Corson, and Legensky focused their study on CFD analysis of the wheels aerodynamic behaviour [50, 51, 52]. In the first two papers [50, 51] they modelled the wheel in a wheel-only configuration. The simulations were performed with the rolling wheel, subjected to an air flow with a speed of 32 and 48 km/h and different yaw angles. During the simulations, they evaluated the drag force, the side force, and the twisting moment. The comparison between the CFS results and the results obtained on previous wind tunnel tests agreed for what regards the drag force. The numerical results showed that the side force is one order of magnitude greater than the drag force. The authors improved their model in [52] simulating the front wheel together with the bicycle front assembly. The shape of the front fork resulted to highly influence the drag force, whereas it had a low effect on the twisting moment and on the aerodynamic moment around the hum axis. Contrarily, the aerodynamic moment was highly influenced by the rim depth.

Moore, in his M.Sc. thesis [53], analysed the aerodynamic behaviour of the racing bicycle wheels combining the wind tunnel tests with the CFD simulations. The wind tunnel tests were performed with the wheels positioned on a fixing device, without the presence of the bicycle and of the cyclist. The effect of the wheels characteristics, and of the wind speed and direction were investigated. During the tests, the drag force, the side force, and the aerodynamic moment were measured. Among the work analysed, this is the only work in which the aerodynamic moment was directly measured. Moore tested standard wheels with wire spokes, disc wheels, and wheels with three or five spokes. The results regarding the aerodynamic moment, showed higher differences between the disc wheels and the standard wheels than the differences obtained for the drag

force. Among the standard wheels with wire spokes, the rim depth affects more the drag force than the aerodynamic moment.

## 15.4 Index of Forward Rolling Efficiency

### 15.4.1 Index formulation

The Index of Forward Rolling Efficiency was formulated considering the cyclist, riding in a straight direction, at a constant speed  $V$ , without pedalling, in absence of lateral wind, and without the drafting effect of other cyclists or vehicles (fig. 15.3). In this configuration of motion, which can be analysed considering the bicycle dynamics on the vertical longitudinal plane, the equations of motion of a wheel are obtained through its translational and rotational equilibrium:

$$m_{\text{tot}} \cdot \ddot{x} - F_D = 0 \quad \text{translational equilibrium along } X_w \text{ axis} \quad (1)$$

$$I_p \cdot \dot{\omega} - M_{Y_w, \text{aero}} - F_V \cdot u_r - M_{H, \text{RR}} = 0 \quad \text{rotational equilibrium around } Y_w \text{ axis} \quad (2)$$

$m_{\text{tot}}$ : total mass of cyclist+bicycle [kg]

$\ddot{x}$ : bicycle acceleration [m/s<sup>2</sup>]

$$F_D = \frac{1}{2} \cdot \rho \cdot A_f \cdot c_D \cdot V^2 \quad \text{drag force [N].}$$

$\rho$ : air density [kg/m<sup>3</sup>].

$A_f$ : frontal area [m<sup>2</sup>].

$c_D$ : drag coefficient.

$V$ : bicycle speed.

$I_p$ : polar inertia of the wheel [kg\*m<sup>2</sup>].

$\dot{\omega}$ : forward rolling acceleration of the wheel [rad/s<sup>2</sup>].

$M_{Y_w, \text{aero}}$ : aerodynamic moment [Nm].

$F_V$ : vertical force at the ground/tire contact point [N].

$u_r$ : coefficient of rolling resistance of the tire [m].

$M_{H, \text{RR}}$ : rolling resistance torque of the hub [Nm].

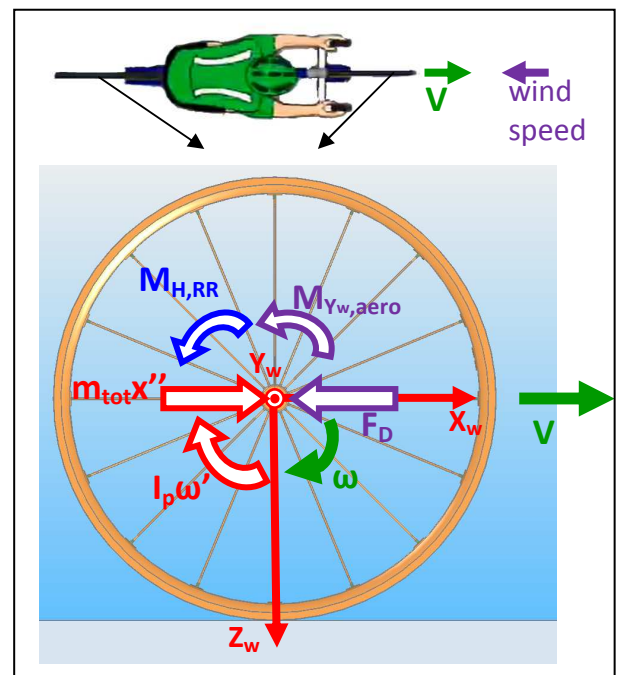


Fig. 15.3 Equilibrium of a wheel during the straight motion of the bicycle, in absence of lateral wind, with the cyclist that does not pedal.

The total resistant force of the wheel is represented by the drag force  $F_D$  (3).

$$F_{\text{res}, W} = F_D \quad (3)$$

The total torque, which acts against the forward rolling of a wheel is obtained through the sum of the aerodynamic moment, and of the tire and hub rolling resistance:

$$M_{res,W} = M_{Y_w,aero} + F_V \cdot u_r + M_{H,RR} \quad [Nm] \quad (4)$$

The contribution of each wheel, to the total resistant power that the cyclist has to balance for keeping the speed  $V$  of the bicycle constant, is expressed by the sum of the translational and the rotational power (5).

$$P_{res,tot,Wf/r} = F_{res,W} \cdot V + M_{res,W} \cdot \omega \quad [W] \quad (5)$$

The Index of Forward Rolling Efficiency  $IFRE_{Wf/r}$  of a wheel was defined as the inverse of the wheels contribution to the total resistant power that the cyclist has to balance for keeping the forward motion of the bicycle:

$$IFRE_{Wf/r} = \frac{1}{P_{res,tot,Wf/r}} \left[ \frac{1}{W} \right] \quad (6)$$

The subscript “f” or “r” indicates if the index is calculated for a front or a rear wheel. A lower contribution of a wheel to the total resistant power corresponds to higher Forward Rolling Efficiency of the wheel.

If we consider a wheelset, the index is calculated as the inverse of the sum of the resistant power of the front and rear wheels that compose the wheelset:

$$IFRE_w = \frac{1}{P_{res,tot,Wf} + P_{res,tot,Wr}} \left[ \frac{1}{W} \right] \quad (7)$$

#### 15.4.2 Data considered for the index computation

Because there was not the possibility to execute a dedicated study on the aerodynamics of the wheels, the draft force  $F_D$  and the aerodynamic moment  $M_{Y_w,aero}$  were estimated from the results obtained by Moore during the experimental analysis performed in his M.Sc. thesis [53]. The wind tunnel tests were performed with the tested wheel positioned on a fixing device, without the presence of the bicycle and of the cyclist. I have chosen the results regarding this work because among all works analysed, this is the only one in which the aerodynamic moment was directly measured in addition to the drag and the side force. The results obtained for two standard wheels with wire spokes (fig. 15.4), characterized by different rim depth, during a wind tunnel test performed with the wind speed at 50 km/h, and with a null yaw angle between the symmetry plane of the wheel and the direction of the air flow, were considered for the computation of the

Index of Forward Rolling Efficiency. The two wheels considered are the Zen Wire Spoke and the Zipp 808, whose rim depth is respectively equal to 40 mm and 82 mm.

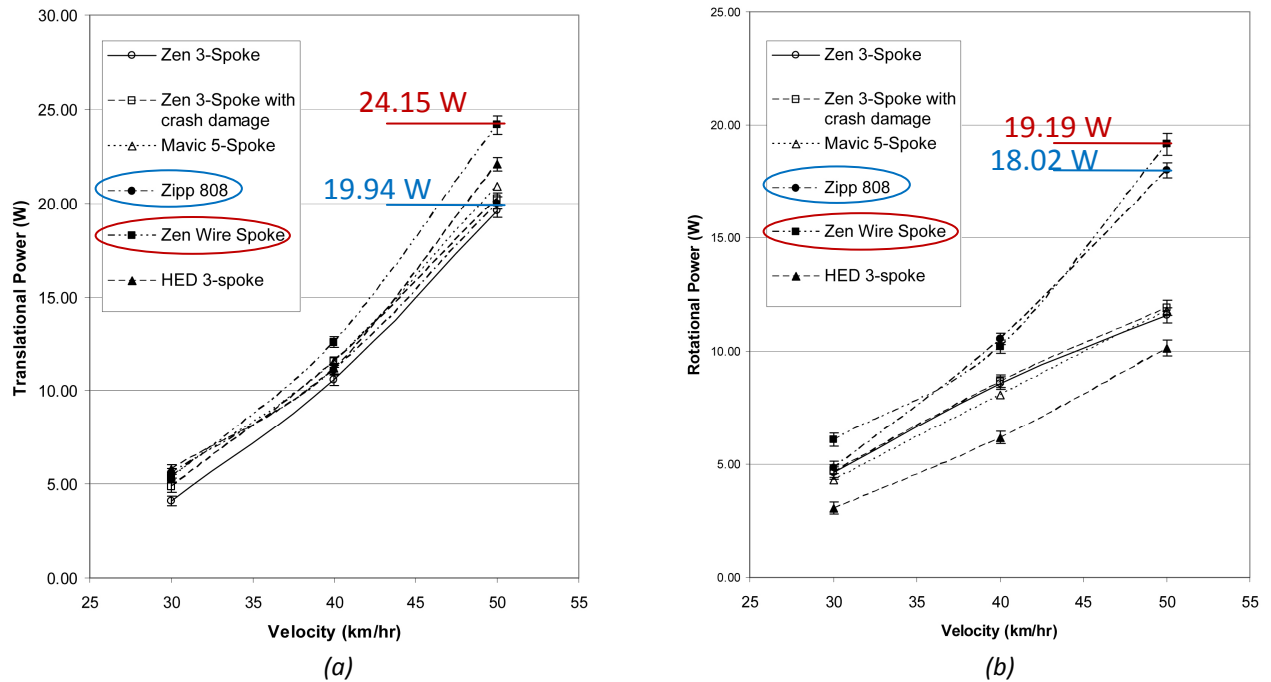


Fig. 15.4 Results obtained by Moore in his M.Sc. thesis [53] that were considered for the computation of the Index of Forward Rolling Efficiency.

The aerodynamic translational and rotational resistant power of the two considered wheels were respectively obtained from figure 15.4.a and 15.4.b. The relationship between the aerodynamic translational and rotational power and the rim depth was then calculated through the linear fitting of the experimental points (fig. 15.5):

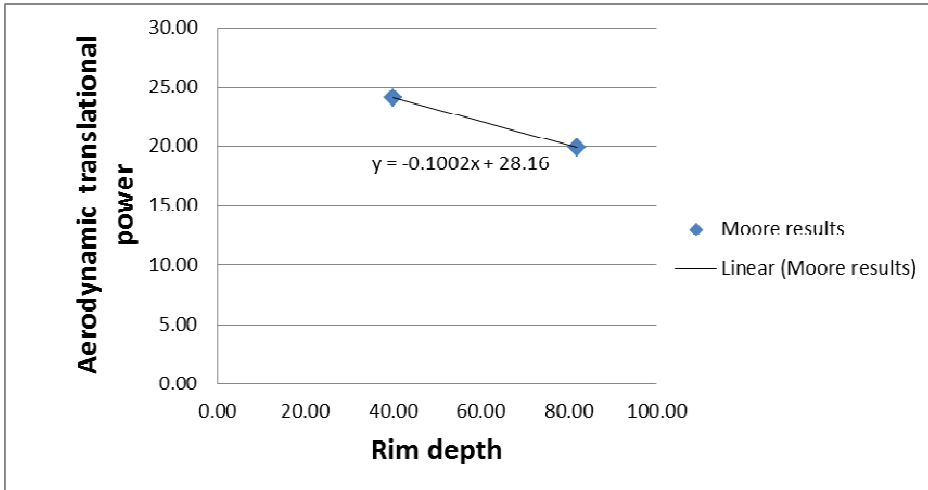
$$P_{res,transl,aero,W} = F_D \cdot V = -0.1002 \cdot h + 28.16 \quad [W] \quad (8)$$

$$P_{res,rot,aero,W} = M_{V_w,aero} \cdot \omega = -0.0279 \cdot h + 20.304 \quad [W] \quad (9)$$

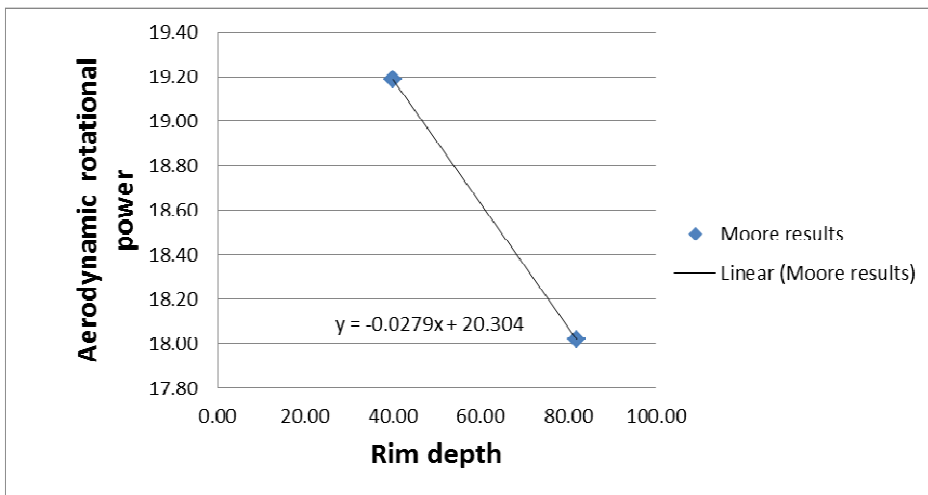
h: rim depth [mm].

With these two equations, the knowledge of the rim depth is enough for computing resistant power of the wheel due to the drag force and the aerodynamic moment.





(a)



(b)

Fig. 15.5 Relationship between the aerodynamic translational (a) and rotational (b) power and the rim depth.

The rolling resistance of the tires  $F_V \cdot U_r$  was not considered because the tire did not represent the object of the study.

The rolling resistance torque of the hub  $M_{H,RR}$  was measured by means of standard laboratory tests performed in Campagnolo laboratories. The data useful for the computation of the Index of Forward Rolling Efficiency are summarized in table 15.1.

| Parameter  | Description                          | Source                                     |
|--|--------------------------------------|--|
| $P_{res,transl,aero,W} = F_D \cdot V = -0.1002 \cdot h + 28.16$ [W]  | Aerodynamic translational power      | Literature: J. K. Moore [53]               |
| $P_{res,rot,aero,W} = M_{v_w,aero} \cdot \omega = -0.0279 \cdot h + 20.304$ [W]  | Aerodynamic rotational power         | Literature: J. K. Moore [53]               |
| $M_{H,RR} = 0.00884$ Nm -> ceramic bearings, w/o grease<br>$M_{H,RR} = 0.0397$ Nm -> ceramic bearings, w/grease<br>$M_{H,RR} = 0.0796$ Nm -> standard bearings | Rolling resistance torque of the hub | Standard test in Campagnolo laboratories   |
| $v=50$ km/h  | Bicycle speed                        | Literature: J. K. Moore [53]               |
| $\omega = 43.26$ rad/s   | Forward rolling speed of the wheel   | Calculated                                 |
| $r_W = 0.321$ m  | Wheel radius                         | Constructive characteristic of the bicycle |

Tab. 15.1 Summary of the data considered for the computation of the Index of Rolling Efficiency.

On the base of the data available, the contribution of each wheel, to the total resistant power that the cyclist has to balance for keeping the speed  $V$  of the bicycle constant, is expressed by the (10).

$$P_{res,tot,Wf/r} = P_{res,transl,aero,W} + P_{res,rot,aero,W} + M_{H,RR} \cdot \omega$$
 [W] (10)

The Index of Rolling Efficiency of a wheel was calculated as the (6).

### 15.4.3 Index validation

The figure 15.6 shows the correlation coefficient calculated between the Index of Forward Rolling Efficiency and the regarding quality requirement (QR.9) evaluated by the cyclists during the subjective evaluation test. The correlation coefficient equal to 0.965 testifies the high correlation between the index and the quality requirement that it aims to express. The Index of Forward Rolling Efficiency is therefore validated.

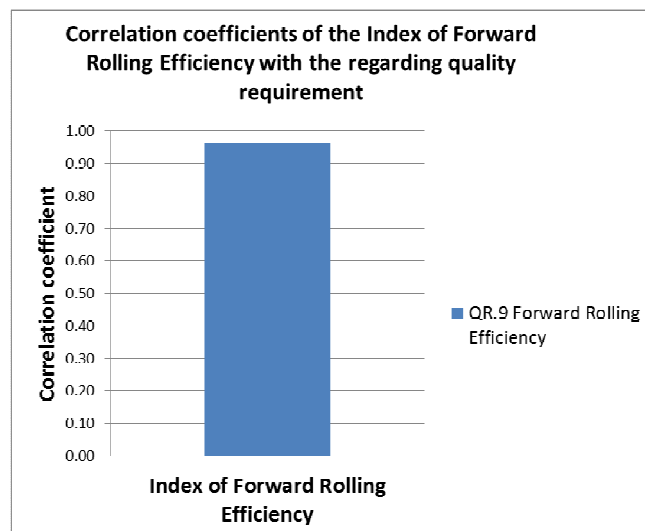


Fig. 15.6 Correlation coefficient calculated between the Index of Forward Rolling Efficiency and the Forward Rolling Efficiency quality requirement (QR.9).

## 15.5 Index of Stability to Crosswind

### 15.5.1 Index formulation

The Index of Forward Rolling Efficiency was formulated considering the cyclist, riding in a straight direction, at a constant speed  $V$ , without pedalling, **in presence of lateral wind**, and without the drafting effect of other cyclists or vehicles (fig. 15.2). In this configuration of motion, the effect of the crosswind, on the aerodynamic loads acting on the wheels, can be analysed considering the horizontal plane (fig. 15.7). As it was already explained in § 15.2, the lateral component of the wheel speed causes an aerodynamic side force  $F_{S,aero}$  and twisting moment  $M_{tw,aero}$  which act on each wheel. Since no data regarding the aerodynamic twisting moment  $M_{tw,aero}$  were available, only the negative effect of the aerodynamic side force on the bicycle stability was considered.

The Index of Stability to Crosswind  $ISC_{wf/r}$  of a wheel was defined as the inverse of the aerodynamic lateral force acting on the wheel:

$$ISC_{wf/r} = \frac{1}{F_{S,aero,Wf/r}} \left[ \frac{1}{N} \right] \quad (11)$$

The subscript “f” or “r” indicates if the index is calculated for a front or a rear wheel. If the boundary conditions are constant, a higher Index of Stability to Crosswind corresponds to a lower side force acting on the considered wheel, which less affects the global stability of the bicycle.

If we consider a wheelset, the index is calculated as the inverse of the sum of the side forces acting on the front and rear wheels that compose the wheelset:

$$ISC_w = \frac{1}{F_{S,aero,Wf} + F_{S,aero,Wr}} \left[ \frac{1}{N} \right] \quad (12)$$

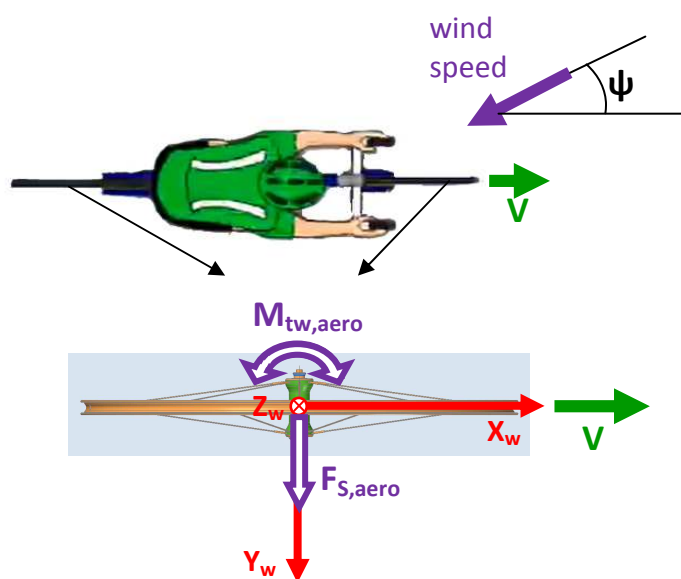


Fig. 15.7 Loads acting on a wheel caused by the lateral wind.

### 15.5.2 Data considered for the index computation

Because there was not the possibility to execute a dedicated study on the aerodynamics of the wheels, the side force  $F_{S,aero}$  was estimated from the results obtained by Godo et al. [50] in their work regarding the numerical analysis of the aerodynamic behaviour of racing bicycle wheels. The authors of this work performed a CFD analysis of different wheels adopting a wheel-only model. The results obtained for three standard wheels with wire spokes (fig. 15.8), characterized by different rim depth, after a CFD simulation performed with a wind speed of 48 km/h, and with a yaw angle equal to  $20^\circ$ , were considered for the computation of the Index of Stability to Crosswind. The side force resulted for the three wheels considered was obtained from figure 15.8.

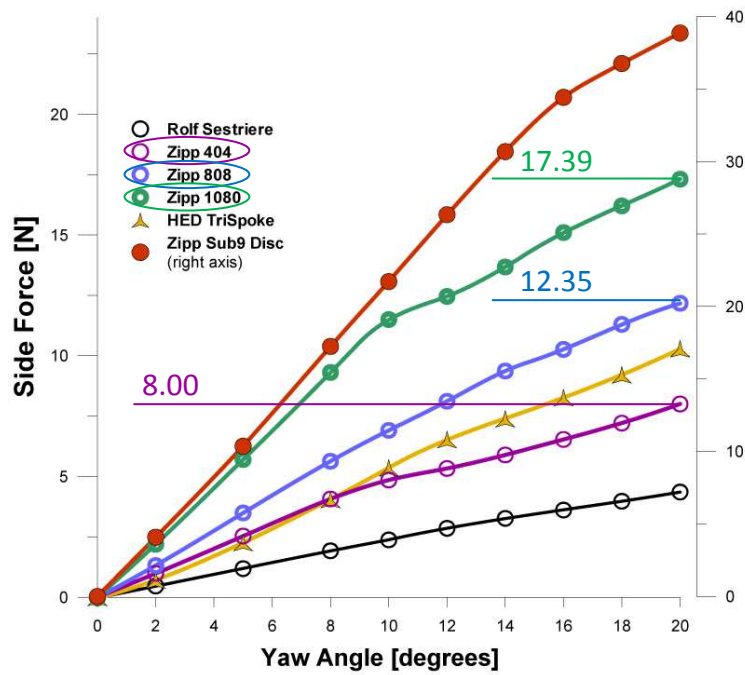


Fig. 15.8 Results obtained by Godo et al. [50] that were considered for the computation of the Index of Stability to Crosswind.

The relationship between the side force  $F_{S,aero}$  and the lateral area of the rim was then calculated through the polynomial interpolation of the experimental points (fig. 15.9):

$$F_{side,aero,Wr/r} = 3 \cdot 10^{-10} \cdot A_{side,rim} + 4 \cdot 10^{-5} \cdot A_{side,rim} + 0.2645 \quad [N] \quad (13)$$

$$A_{side,rim} = \pi \cdot [0.315^2 - (0.315 - h)^2] \quad [m^2] \quad \text{rim side area (fig 15.10)} \quad (14)$$

h: rim depth [mm].

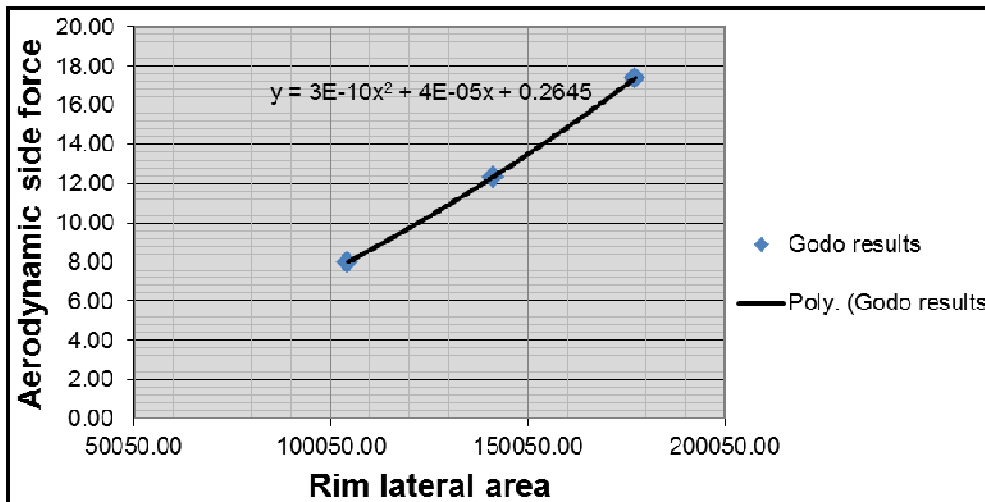


Fig. 15.9 Relationship between the aerodynamic side force and the rim side area.

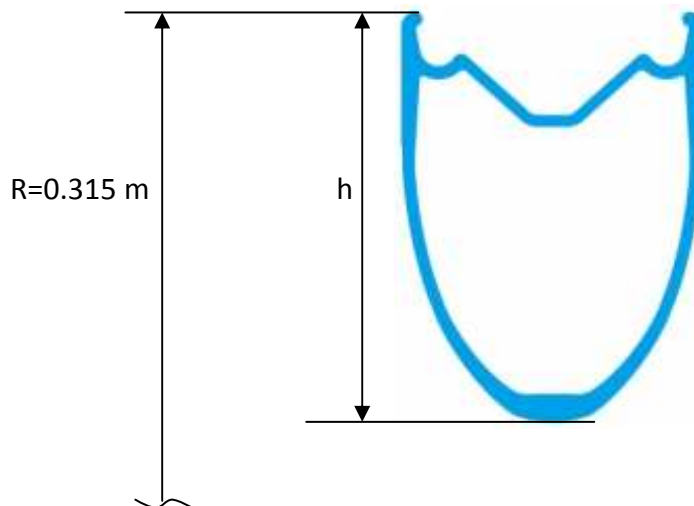
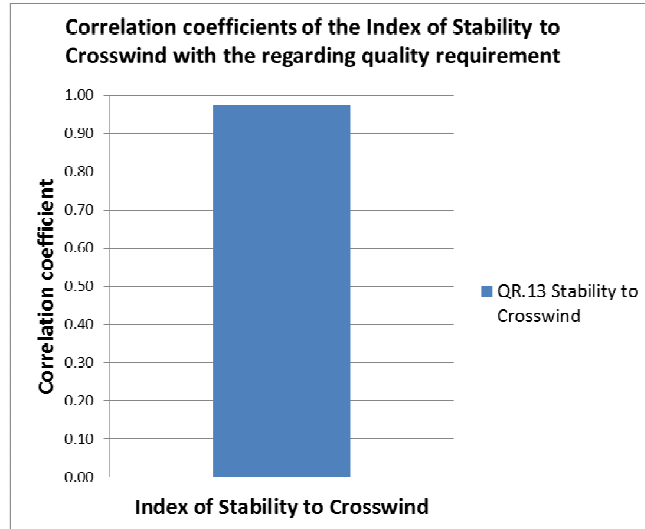


Fig. 15.10 Computation of the rim side area.

### 15.5.3 Index validation

The figure 15.11 shows the correlation coefficient calculated between the Index of Stability to Crosswind and the regarding quality requirement (QR.13) evaluated by the cyclists during the subjective evaluation test. The index was validated thanks to the high correlation coefficient, equal to 0.973. The index therefore expresses very well the influence of the wheels on the bicycle response to the presence of lateral wind.



*Fig. 15.11 Correlation coefficient calculated between the Index of Stability to Crosswind and the Stability to Crosswind quality requirement (QR.13).*



# Chapter 16

## Conclusions on the engineering complex indexes

### 16.1 Engineering complex indexes calculated for all Campagnolo wheelsets

The six developed engineering complex indexes were calculated for the whole range of wheels produced by Campagnolo in 2012 (fig. 16.1). For comparing all indexes in a single chart, the indexes were normalized in respect to the best value, adopting a decimal scale. The wheelsets are therefore classified through the **engineering complex indexes**, which represent a technical measurement of the quality requirements perceived by the cyclists. This chart can be useful for multiple purposes. It can be used for the management of wheels range, identifying the wheel models that have similar characteristics, or highlighting the quality requirements or the combination of them that are not enhanced by any wheelset currently produced, identifying the target characteristics that have to be achieved with potential new models. It can also represent a reliable guideline useful for customers in the choice of the wheelset, which meets their needs, or for marketing communication messages.

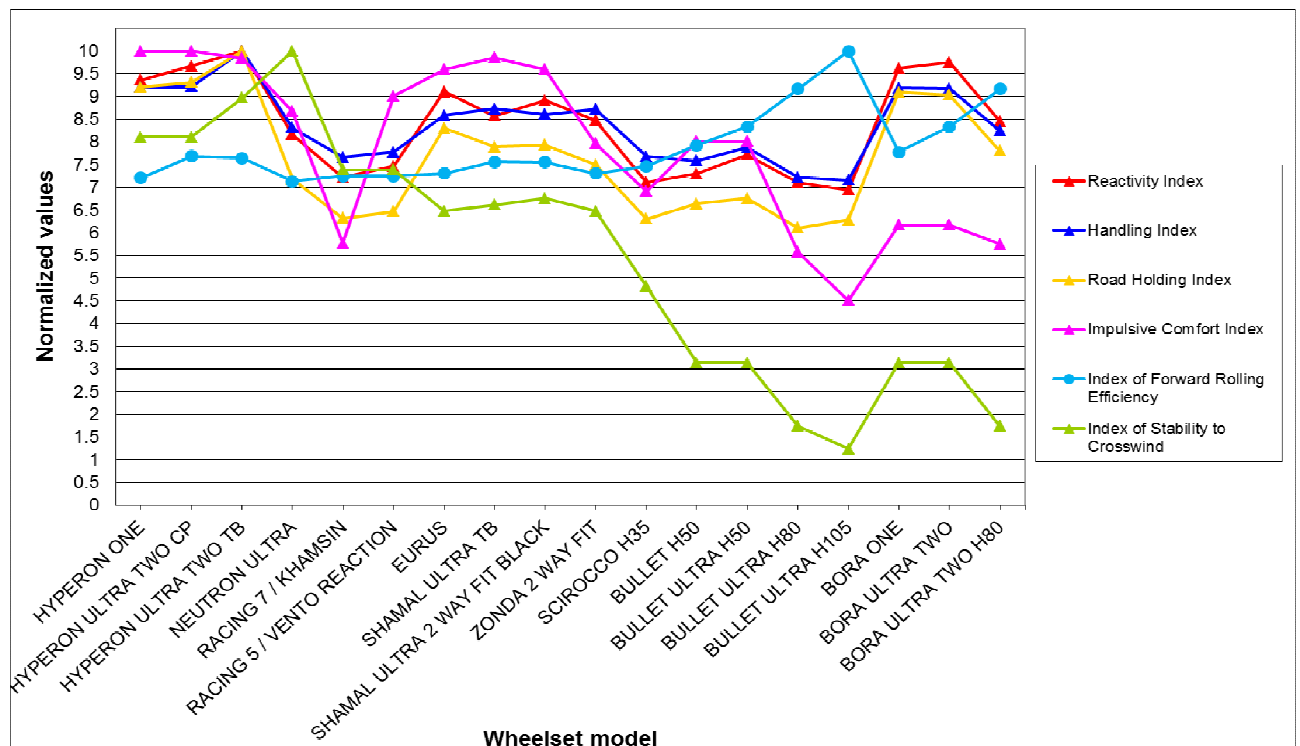


Fig. 16.1 Engineering complex indexes, calculated for all wheelsets produced by Campagnolo in 2012, represented through the normalised decimal scale.



## 16.2 Indexes of destination of use

In Chapter 8, 12 typical actions performed by the cyclist during racing bicycle riding were identified. The outcomes of the execution of the actions, and respective phases, are evaluated by the cyclists through a total of 35 metrics. The evaluation expressed through the 35 metrics is summarized through 13 quality requirements of the wheels. A set of 6 engineering complex indexes was then developed in order to express a technical measurement of the quality requirements evaluated by the cyclist (fig. 16.2). If we go back through the definition of the engineering complex indexes, we can find a direct relationship between them and the actions performed by the cyclist during racing bicycle riding (fig. 16.3). The engineering complex indexes of a wheel can therefore express its behaviour, perceived by the cyclist during the different fields of use. The 6 engineering complex indexes were therefore arranged in order to obtain a set of 5 indexes of destination of use, which maintain the technical source of the engineering complex indexes, whereas they result more user-friendly if used as guidelines for the costumers. The figure 16.4 shows the normalised values of the indexes of destination of use calculated for the whole range of Campagnolo wheels.

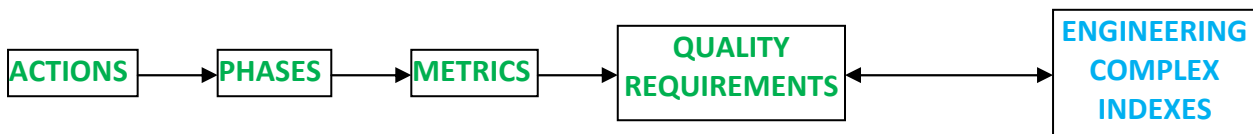


Fig. 16.2 Logical path followed for the definition of the engineering complex indexes.

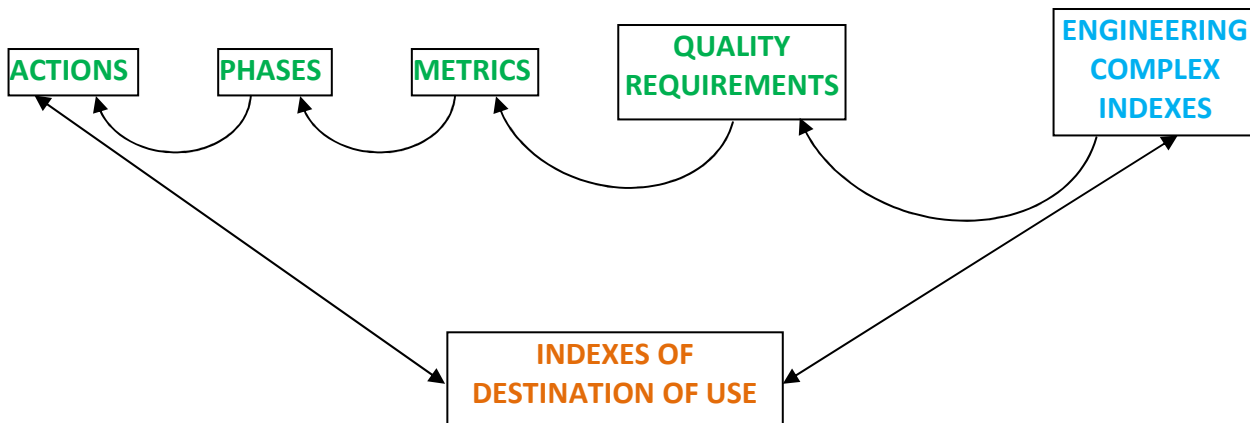


Fig. 16.3 Logical relationship between the engineering complex indexes and the indexes of destination of use.

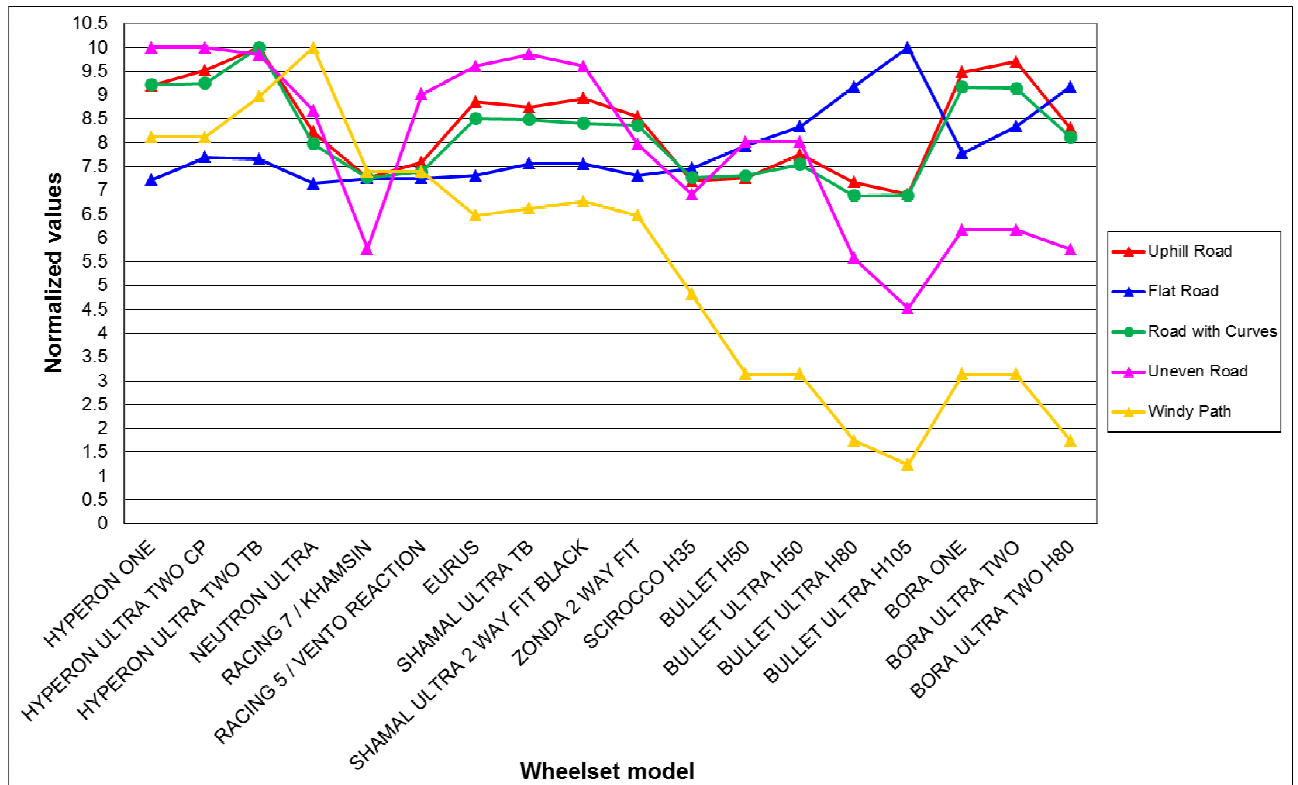


Fig. 16.4 Indexes of destination of use, calculated for all wheelsets produced by Campagnolo in 2012, represented through the normalised decimal scale.

### 16.3 Correlation between the engineering complex indexes and the user quality requirements

The correlation coefficients calculated between the user quality requirements and all engineering parameters, represented by the 5 basic engineering characteristics and the 6 engineering complex indexes, are reported in the “House of Quality” correlation matrix showed in table 16.1. This matrix represents the extension of the matrix showed in table 10.1, in which, among the engineering parameters, only the basic engineering characteristics were available. For the analysis of the correlation coefficients that regards the basic engineering characteristics, we can refer to § 10.4. Each engineering complex index was validated considering the calculated correlation coefficient with the quality requirement that it has to express. If the correlation coefficient was greater than 0.9, or lower than -0.9 (see § 10.3), the index was validated. The green highlighted correlation coefficients of tab. 16.1 allowed to validate the formulations developed for each engineering complex index. Because the engineering complex indexes resulted from a scientific processing of the basic characteristics, the high correlation that, in some cases, can be found between an engineering complex index and a quality requirement, different from the one that the index aims to express, is caused by the mutual relationship between the different basic characteristics of the wheels considered for this study.

These results could be improved if each basic engineering characteristic were independently varied.

|   | BASIC ENGINEERING CHARACTERISTICS |                       |                            |                         |                        | ENGINEERING COMPLEX INDEXES |                      |                           |                               |   |                                       |
|---|-----------------------------------|-----------------------|----------------------------|-------------------------|------------------------|-----------------------------|----------------------|---------------------------|-------------------------------|---|---------------------------------------|
|   | m [kg]                            | I [kgm <sup>2</sup> ] | K <sub>torx</sub> [Nm/rad] | K <sub>side</sub> [N/m] | K <sub>rad</sub> [N/m] | Reactivity Index [1/J]      | Handling Index [1/J] | Road Holding Index [1/Nm] | Impulsive Comfort Index [m/N] | Index of Forward Rolling Efficiency [1/W] | Index of Stability to Crosswind [1/N] |
| QR.1 Reactivity - low speed sprint (V<17 km/h)  | -0.883                            | -0.942                | -0.307                     | -0.647                  | -0.808                 | 0.925                       | 0.928                | 0.969                     | 0.893                         | -0.592                                    | 0.832                                 |
| QR.2 Reactivity - high speed sprint (V>30 km/h) | -0.260                            | -0.401                | -0.899                     | -0.262                  | -0.123                 | 0.357                       | 0.362                | 0.483                     | 0.283                         | 0.184                                     | 0.164                                 |
| QR.3 Reactivity - low speed uphill (V<17 km/h)  | -0.969                            | -0.994                | -0.076                     | -0.687                  | -0.924                 | 0.987                       | 0.990                | 0.998                     | 0.973                         | -0.765                                    | 0.939                                 |
| QR.4 Reactivity - high speed uphill (V>17 km/h) | -0.870                            | -0.933                | -0.333                     | -0.640                  | -0.792                 | 0.914                       | 0.917                | 0.962                     | 0.880                         | -0.570                                    | 0.817                                 |
| QR.5 Handling                                   | -0.999                            | -0.994                | 0.127                      | -0.690                  | -0.982                 | 0.997                       | 0.998                | 0.981                     | 0.999                         | -0.880                                    | 0.990                                 |
| QR.6 Road Holding                               | -0.980                            | -0.938                | 0.365                      | -0.655                  | -0.997                 | 0.953                       | 0.953                | 0.903                     | 0.974                         | -0.970                                    | 0.995                                 |
| QR.7 Vibrational comfort                        | -0.912                            | -0.962                | -0.245                     | -0.662                  | -0.845                 | 0.947                       | 0.950                | 0.983                     | 0.920                         | -0.643                                    | 0.866                                 |
| QR.8 Impulsive comfort                          | -0.962                            | -0.991                | -0.100                     | -0.684                  | -0.915                 | 0.983                       | 0.986                | 0.999                     | 0.968                         | -0.750                                    | 0.931                                 |
| QR.9 Forward Rolling Efficiency                 | 0.756                             | 0.649                 | -0.770                     | 0.462                   | 0.839                  | -0.684                      | -0.682               | -0.577                    | -0.739                        | 0.965                                     | -0.817                                |
| QR.10 Braking power                             | -0.836                            | -0.908                | -0.393                     | -0.622                  | -0.751                 | 0.886                       | 0.890                | 0.943                     | 0.848                         | -0.516                                    | 0.778                                 |
| QR.11 Braking regularity                        | 0.667                             | 0.770                 | 0.613                      | 0.523                   | 0.556                  | -0.738                      | -0.743               | -0.826                    | -0.684                        | 0.279                                     | -0.590                                |
| QR.12 Stability in Absence of Wind              | -0.987                            | -0.952                | 0.324                      | -0.665                  | -0.999                 | 0.965                       | 0.965                | 0.921                     | 0.983                         | -0.958                                    | 0.998                                 |
| QR.13 Stability to Crosswind                    | -0.946                            | -0.886                | 0.480                      | -0.621                  | -0.981                 | 0.906                       | 0.905                | 0.840                     | 0.937                         | -0.993                                    | 0.973                                 |

Tab. 16.1 House of quality matrix, which represents the correlation coefficients between the wheels quality requirements and all engineering parameters.

## **16.4 Discussion about the developed indexes**

Each developed index was validated through the computation of the correlation coefficient with the quality requirement that it has to express.

The Reactivity Index, the Handling Index, and the Road Holding Index were developed following a rigorous scientific approach, and the parameters needed for their computation were obtained from the analysis of dedicated field tests, performed with an instrumented bicycle opportunely equipped. The developed Reactivity Index does not express the wheels Reactivity evaluated by the cyclist during a sprint starting from high speed (QR.2). This highlighted that a study on the wheel aerodynamics is needed for the definition of an additional Reactivity Index, which can result highly correlated with this quality requirement. The consideration of the aerodynamic loads can also improve the formulation of the Handling Index.

The Impulsive Comfort Index was formulated starting from the high correlation obtained between the static radial stiffness of the wheel, and the quality requirement represented by the Impulsive Comfort. A further more detailed analysis of the correlation between the structural characteristics of the wheels, evaluated during radial bump tests, and the Impulsive Comfort, can represent the base for improving this index. A Vibrational Comfort Index of the wheels can be developed following the same approach, namely studying the correlation of the quantities evaluated through the “Full bicycle laboratory test method” (University lab.) with the Vibrational Comfort perceived by the cyclists.

The Index of Forward Rolling Efficiency and the Index of Stability to lateral wind are directly connected to aerodynamic phenomena. Since there was not the possibility to execute a dedicated study on the aerodynamics of the wheels, the parameters needed for the computation of these two indexes were estimated from the results of two works opportunely selected during the literature analysis. The study of the wheels aerodynamics is therefore the main activity to be carried out for using reliable data in the computation of these indexes.

No engineering complex indexes concerning the Braking Power and the Braking regularity were developed. A further specific activity, oriented on the improvement of the laboratory test methods and on the execution of dedicated subjective evaluation tests, is needed for the development of a set of indexes, which express the quality requirements that regard the braking action.



## ***Part 5***

### **Development of an instrumented racing bicycle**



# Chapter 17

## Development of the instrumented racing bicycle

### 17.1 Introduction

A racing bicycle was instrumented with two purposes:

- to characterize the phases of the braking actions performed during racing bicycle riding;
- to measure the parameters useful for the computation of the Reactivity Index, the Handling Index, and the Road Holding Index, during the actions in which the cyclist evaluates the quality requirements that the indexes are supposed to express.

Two brake levers were instrumented with strain gauges for measuring the cyclist command force, and two rotational potentiometers were used for the measurement of the levers rotation angle. The bicycle was also equipped with an inertial measurement unit provided with a GPS, with an instrumented crankset for measuring the bicycle drive torque at the bottom bracket, and with a speed meter.

Several works regarding the development of bicycles with instrumented components for the field data collection can be found in literature. Many of them were mainly focused on the loads acquisition for the structural analysis of bicycle components (Drouet & Champoux [43], Petrone *et al.* [38], Seragio *et al.* [39]) often carried out for the safety standard definition (Petrone *et al.* [37]). A second set of works regarded the kinematic analysis of the bicycle motion (Moore *et al.* [29], Peterson *et al.* [30]), or the analysis of bicycle dynamics (Wilson & Papadopoulos [27], Plöchl *et al.* [31], Schwalb *et al.* [34]). No studies have so far analysed the braking action during the downhill use of a racing bicycle.

The work here presented was carried out on the basis of a former experience in two works of which I was the co-author: the first one concerning the development of an instrumented downhill bicycle for field data collection (Petrone *et al.* [36]), and the second one regarding the development of instrumented bicycle saddles for the stress analysis of their structural components (Giubilato & Petrone [35]).

### 17.2 Characteristics of the instrumented bicycle

A racing bicycle (fig. 17.1) with a frame of medium size was chosen in order to be suitable for cyclists with medium total height (175-180 cm). The bicycle was equipped with instrumented brake levers, an instrumented crankset, an Inertial Measurement Unit, and a speed meter. The parameters measured through the sensors and the purposes of their measurement are listed in table 17.1.



| Symbols   | Description   | Sensor   | Purpose of the measurement   |
|---|---|--|--|
| $M_{BL,R}$ [Nm]                                 | <b>Command torque</b> of the cyclist at the right brake lever (rear brake).   | <b>Strain gauges</b> applied to the internal surface of the brake levers.                          | Characterization of the <b>braking actions</b> .   |
| $M_{BL,L}$ [Nm]                                 | <b>Command torque</b> of the cyclist at the left brake lever (front brake).   |  |  |
| $\vartheta_{BL,R}$ [deg]                        | <b>Angle of rotation</b> of the right brake lever.  |  |  |
| $\vartheta_{BL,L}$ [deg]                        | <b>Angle of rotation</b> of the left brake lever.   |  |  |
| $M_{D,BB}$ [Nm]                                 | Bicycle <b>drive torque</b> at the bottom bracket.  | <b>Spider arm</b> of the crankset instrumented with <b>strain gauges</b> (fig. 17.4).              | <b>Reactivity index:</b> measurement of the drive torque during a sprint.  |
| $A_{X_B}, A_{Y_B}, A_{Z_B}$ [m/s <sup>2</sup> ] | Bicycle <b>acceleration</b> along the orthogonal axis of the bicycle reference system ( $X_B, Y_B, Z_B$ ).            | Tri-axial <b>accelerometer</b> embedded in the Inertial Measurement Unit (fig. 17.6.a).            | - Characterization of the <b>braking actions</b> .<br>- <b>Reactivity, Handling and Road Holding Index</b> computation . |
| $G_x, G_y, G_z$ [deg/s]                         | <b>Angular velocity</b> of the bicycle along the orthogonal axis of the bicycle reference system ( $X_B, Y_B, Z_B$ ). | Tri-axial <b>gyroscope</b> internal to the Inertial Measurement Unit (fig. 17.6.a).                | - <b>Reactivity, Handling and Road Holding Index</b> computation.  |
| $\varphi$ [deg]                                 | Lateral <b>roll angle</b> of the bicycle.   | Computed by the Inertial Measurement Unit through a dedicated <b>algorithm</b> .                   | - Characterization of the <b>braking actions</b> .<br>- <b>Reactivity, Handling and Road Holding Index</b> computation.  |
| Lat Lon [deg min]                               | <b>Latitude</b> and <b>longitude</b> of the bicycle position.   | <b>GPS</b> inside of the Inertial Measurement Unit (fig. 17.6.a).                                  |  |
| V [km/h]  | Bicycle <b>speed</b> .  | <b>GPS</b> inside of the Inertial Measurement Unit and <b>magnetic speed sensor</b> (fig. 17.6.b). |  |

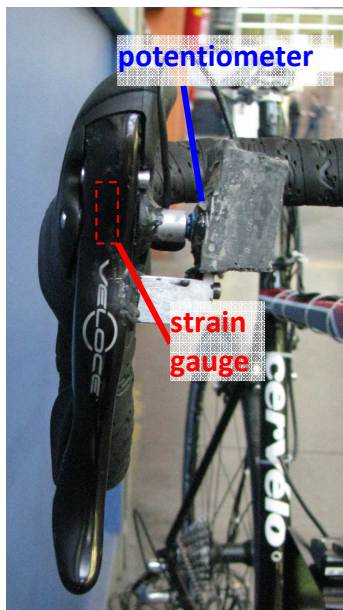
Tab. 17.1 List of the parameters measured through the sensors that equip the instrumented bicycle.

| Sensor   | Characteristics  |
|--|--|
| Inertial Measurement Unit:<br>E-SHARK by E-SHOCK srl | - Accelerations XYZ: $\pm 16g$<br>- Angular rates XYZ: $\pm 250^\circ/s$<br>- GPS: 10Hz fix update rate<br>- Attitude angles -3 dB @ 7Hz<br>- Accelerations -3 dB @ 15Hz<br>- Angular rates -3 dB @ 15Hz<br>- CAN Data transfer: Baudrate: 1 MBaud |
| Wireless transmitter: MicroStrain SG-Link            | - 2 channels; $f_{smax}=4096$ Hz; 0-3 V excitation   |
| Strain gauges  | - Uniaxial, 120 $\Omega$   |

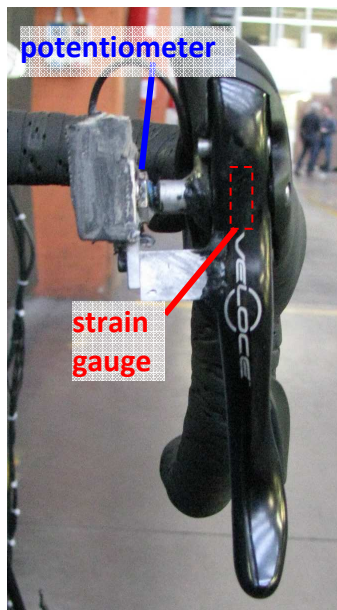
Tab. 17.2 Characteristics of the instrumentation.



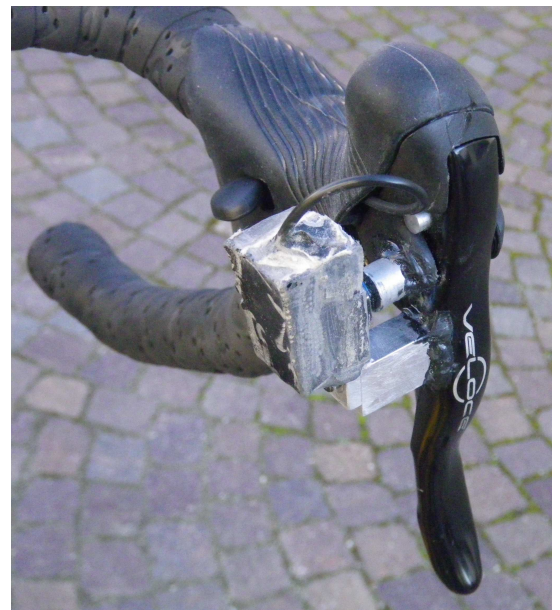
Fig. 17.1 Instrumented bicycle.



(a)



(b)



(c)

Fig. 17.2 Right (a) and left (b-c) instrumented brake levers.

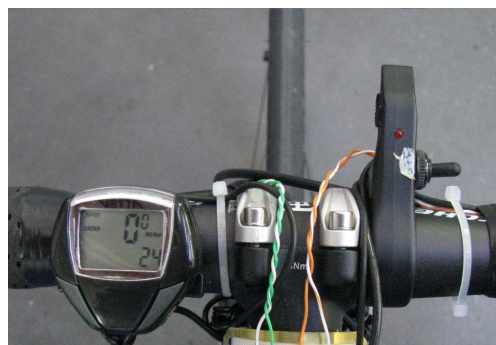


Fig. 17.3 Particular of the bicycle computer used for the field tests and of the trigger, positioned on the handlebar, of the data acquisition system.



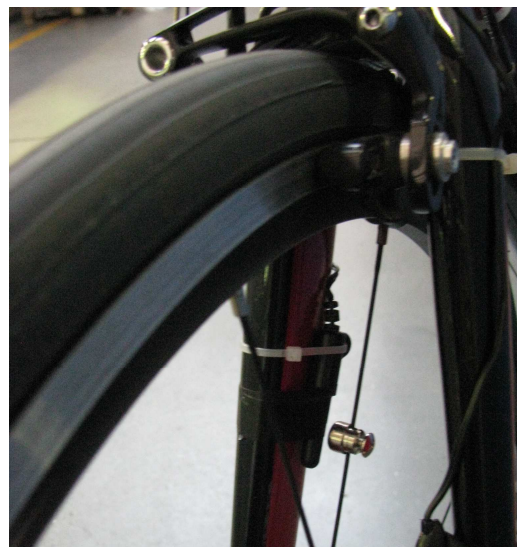
Fig. 17.4 Spider arm of the crankset instrumented with strain gauges.



Fig. 17.5 Wireless transmitter of the strain gauge signal of the spider arm.



(a)



(b)

Fig. 17.6. (a) Inertial Measurement Unit fixed on a support fastened on the frame at the bottle cage position; (b) magnetic speed sensor.

### 17.3 Setup of the data acquisition system

During the tests, all signals were simultaneously sampled by means of an IMC Cronos PL data acquisition system (fig. 17.7, A). The channels of the strain gauges, of the rotational potentiometers, and of the drive torque at the bottom bracket were defined as analogue channels. The signal of the instrumented spider arm of the crankset was sent, through a wireless communication protocol, from a transmitter positioned on the left crankarm (fig. 17.5) to a receiver (fig. 17.7, B) connected to an analogue channel of the data acquisition system. The Inertial Measurement Unit was connected to a CAN BUS port of the data acquisition system. A digital channel was created for sampling the signal of the speed magnetic sensor. During the field tests, the analogue channels were sampled at a sampling frequency of 1 KHz, the CAN BUS, and the digital channels were sampled at 100 Hz. A 15 V lithium battery was used for the voltage supply of the IMC data acquisition system (fig. 17.7, C). A second lithium battery (12 V) was used for the Inertial Measurement Unit (fig. 17.7, D).

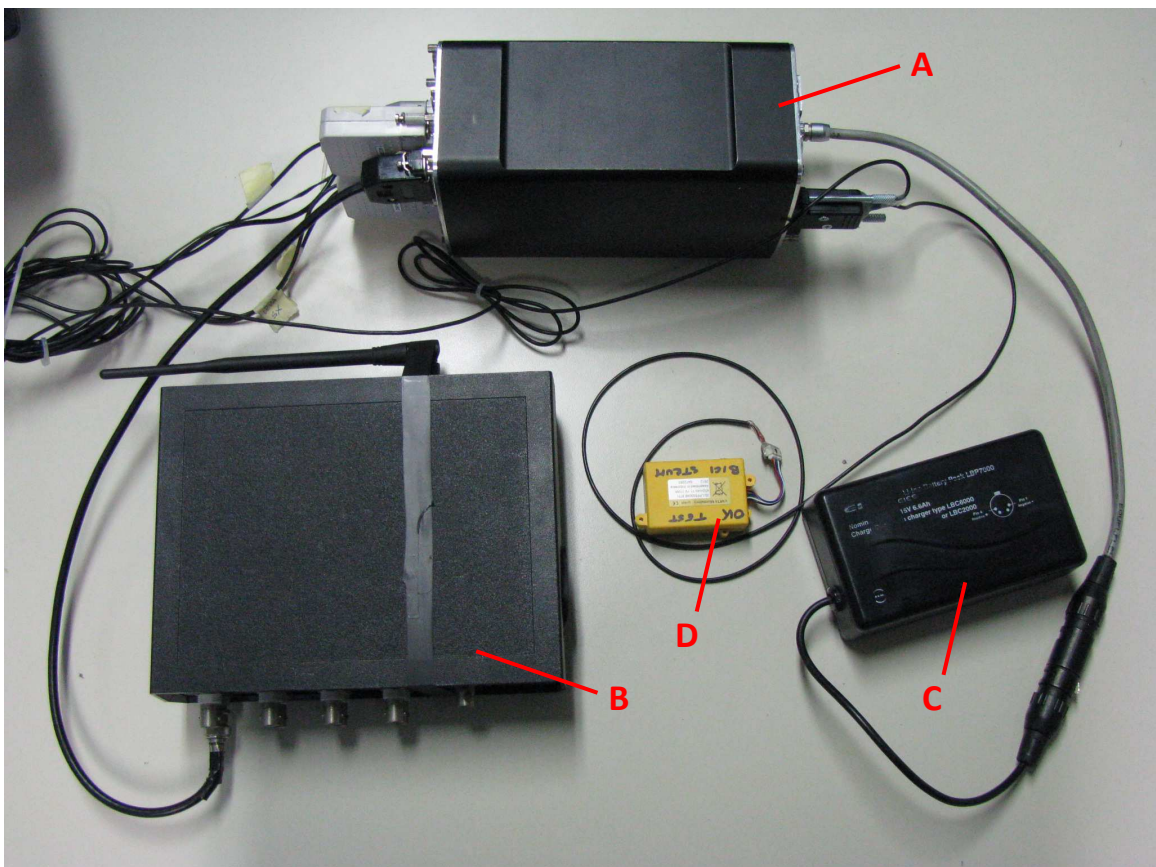
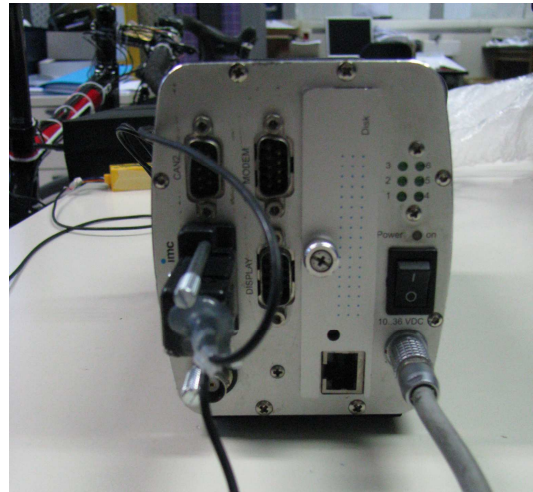


Fig. 17.7 Instrumentation used for the data acquisition: (A) IMC Cronos PL data acquisition system; (B) MicroStrain wireless receiver; (C) 15V battery of the data acquisition system; (D) battery of the Inertial Measurement Unit.



(a)



(b)

Fig. 17.8 Connection of the analogue and digital channels; (b) connection of the CAN BUS port.

## 17.4 Instrumented brake levers

### 17.4.1 Application of the strain gauges and positioning of the potentiometers

Each brake lever (fig. 17.2) was instrumented with a strain gauge placed on its internal surface, at a point close to the lever hinge, which corresponds to the lever section subjected to the maximum bending moment. The quarter-bridge connection scheme was adopted for each strain gauge channel. Two rotational potentiometers, as the one shown in figure 17.9, were used for measuring the angle of rotation of the brake levers during the braking action. The rotating shaft of each potentiometer was cut, aligned, and then glued to the axis of rotation of the brake lever. The body of the potentiometer was fixed on an aluminium support glued on the lateral surface of the lever. The solution adopted for the positioning of the potentiometers was chosen in order to not obstruct the movements of the cyclist's hands.



Fig. 17.9 Rotational potentiometer.

### 17.4.2 Calibration of the strain gauge channels

During the calibration tests of the each strain gauge channel, the brake lever was positioned horizontally (fig. 17.10.a), and a vertical load  $F_v$  was applied at a distance of 79 mm from the rotation axis of the lever. A threaded rod was used for pre-tensioning the brake wire and fixing the brake calliper (fig. 17.10.b) in order to not allow any movement of the brake lever during the test.

Additional tests were performed using a uniaxial load cell positioned between the brake pads (fig. 17.10.c) for measuring the relationship between the force on the lever, and the force orthogonal to the braking surface of the rim. Four known levels of bending moment  $M_{BL}$  were applied to the brake lever during each calibration test (fig. 17.11). The output signals were recorded at a sampling frequency of 10 Hz. Three calibration tests were performed for each instrumented brake lever, and the calibration constant was calculated as the average of the constants computed in the analysis of each test. An example of a calibration curve is showed in figure 17.12.

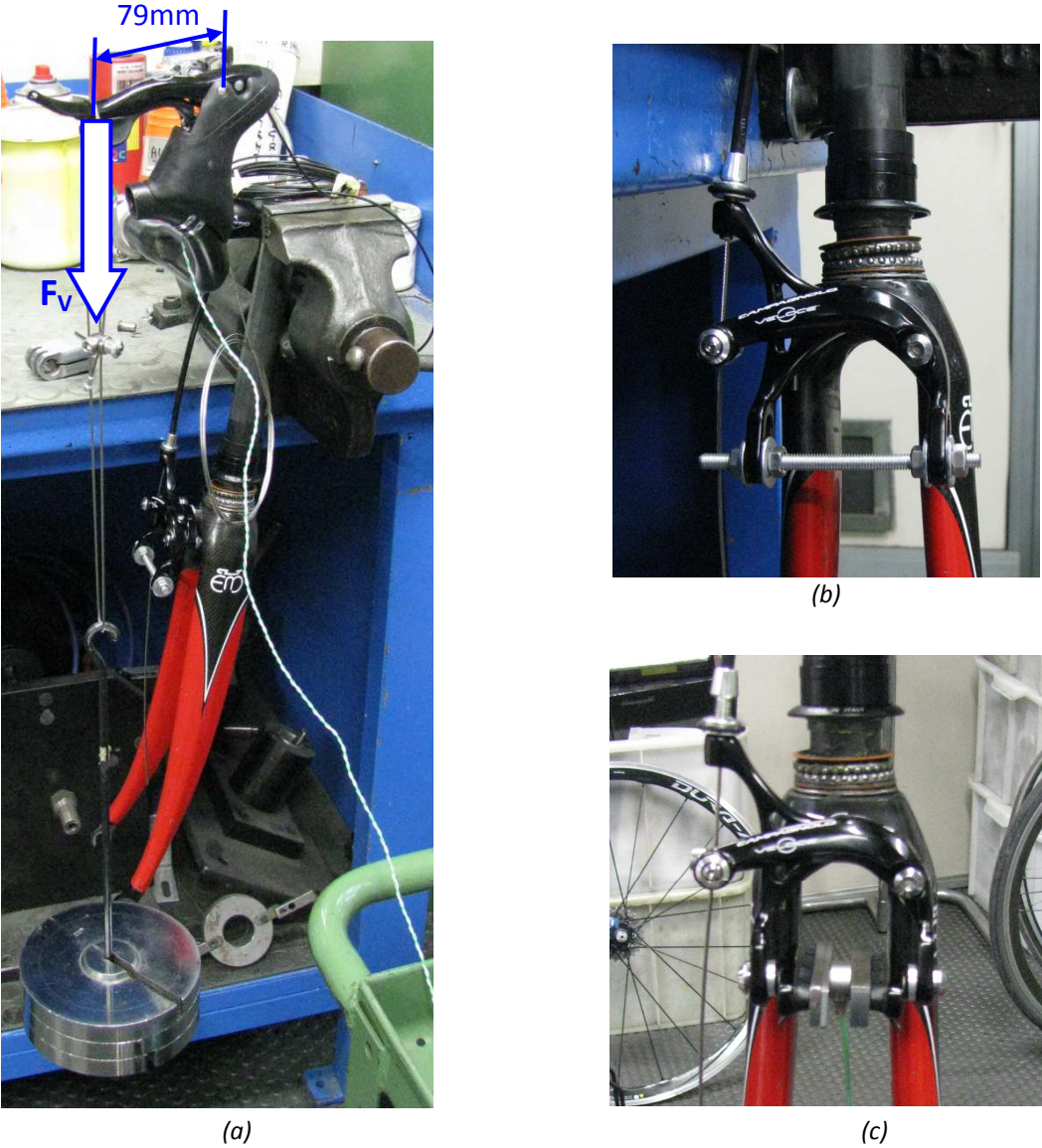


Fig. 17.10. (a) Setup of the brake lever calibration test; (b) solution adopted for fixing the brake calliper; (c) load cell positioned between the brake pads.

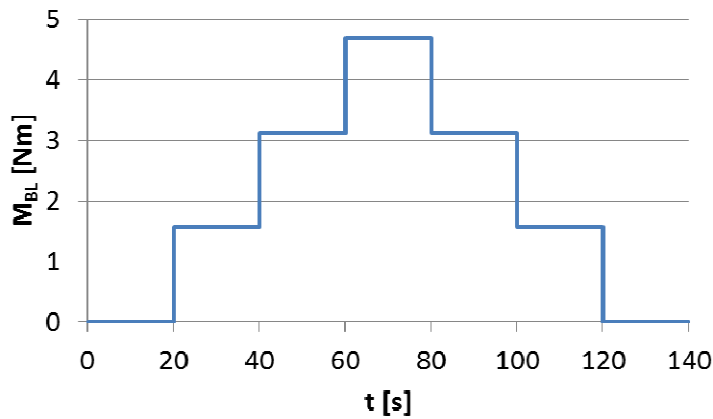


Fig. 17.11 Known bending moment applied on the brake lever during the calibration tests.

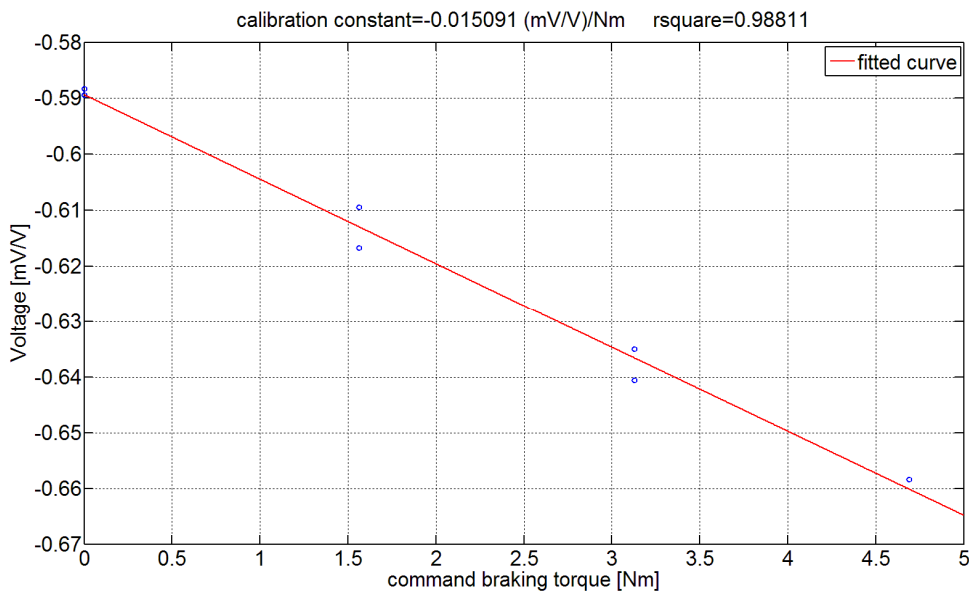


Fig. 17.12 Example of a calibration curve computed for a the strain gauge channel.

### 17.4.3 Calibration of the rotational potentiometers

Each rotational potentiometer was calibrated applying the following sequence of angles (fig. 17.13):  $0^\circ \rightarrow 90^\circ \rightarrow 180^\circ$ .

The voltage output of the potentiometer was recorded at sampling rate of 10 Hz. Three calibration tests were performed for each potentiometer, and the calibration constant was calculated as the average of the constants computed in the analysis of each test. An example of a calibration curve is showed in figure 17.14.

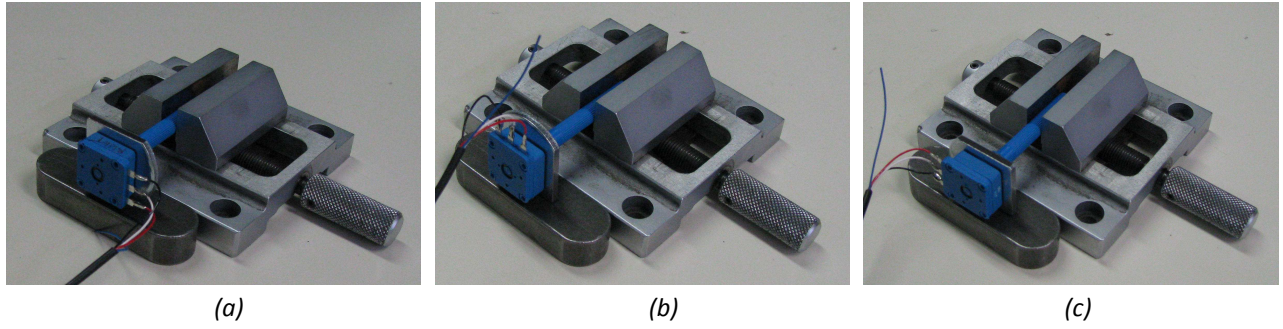


Fig. 17.13 Three orientations of a potentiometer during a calibration test.

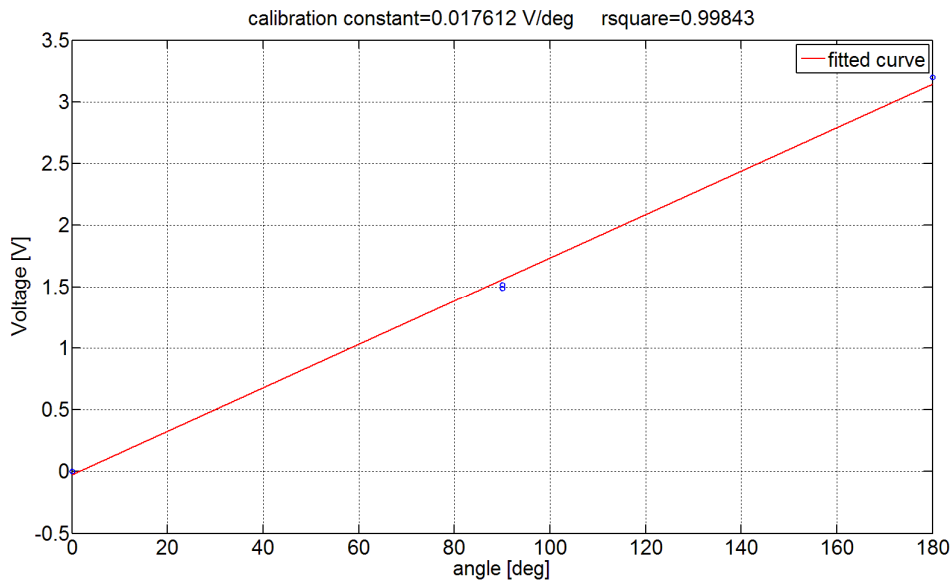


Fig. 17.14 Example of a calibration curve computed for a potentiometer.

### 17.5 Calibration of the instrumented spider arm of the crankset

The instrumented crankset was developed in previous works executed by the testing department of Campagnolo srl. It was calibrated for verifying the calibration constant, and its correct functioning. During the calibration tests the bicycle was fixed to a bike-support, the crankarms were positioned horizontally, and the rear wheel was blocked by means of the brake calliper (fig. 7.16). A vertical load was applied on the right crankarm at a distance of 172.5 mm from the bottom bracket. Four known levels of driving torque at the bottom bracket  $M_{D,BB}$  were applied on the right crankarm during each calibration test (fig. 17.15). The output signals were recorded at a sampling frequency of 10 Hz. Three calibration tests were performed, and the calibration constant was calculated as the average of the constants computed in the analysis of each test. An example of a calibration curve is showed in figure 17.17.



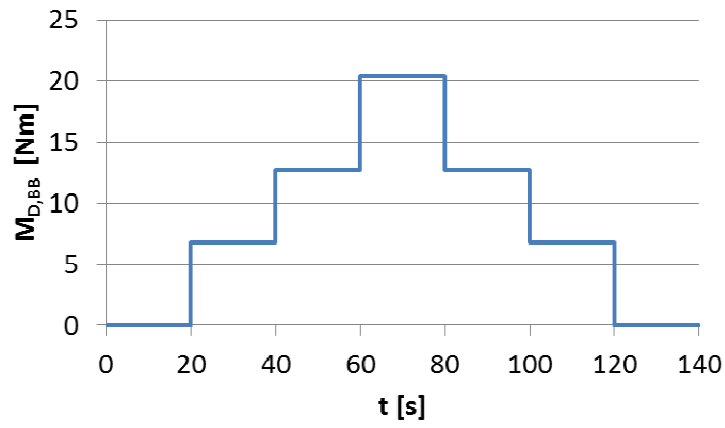


Fig. 17.15 Known drive torque applied on the crankarm during the calibration tests.



Fig. 17.16 Setup of the calibration test of the spider arm.

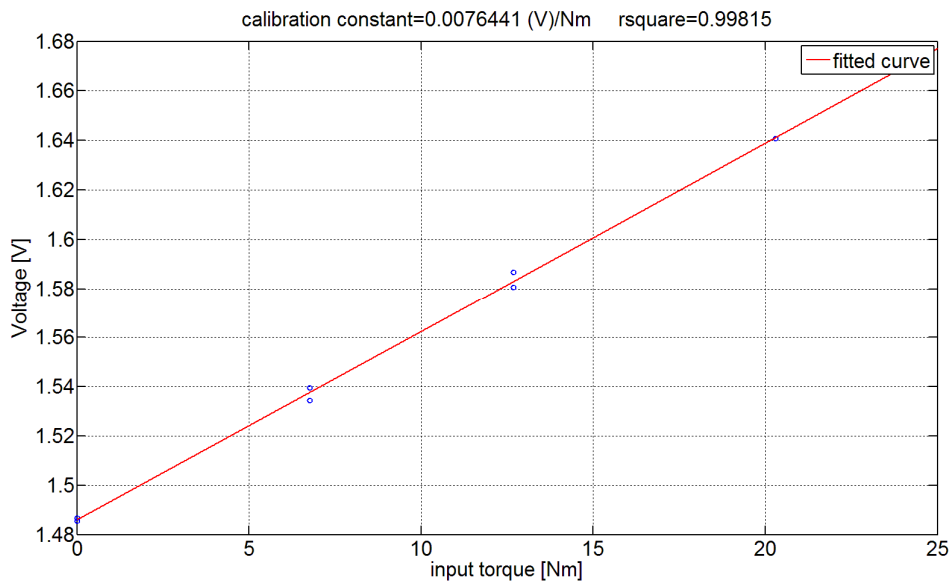


Fig. 17.17 Example of a calibration curve computed for the instrumented crankset.

## 17.6 Description of the field tests

### 17.6.1 Preparation of the equipment

During the field tests, the data acquisition system, its battery, the wireless receiver, and the battery of the Inertial Measurement Unit (fig. 17.7) were inserted into an Evoc™ Freeride backpack (fig. 17.18.a). The backpack has an integrated back protector, and an elastic waist belt, which ensures the maximum stability (17.18.b). Its total weight was equal to 7 kg.



(a)



(b)

Fig. 17.18. (a) Detail of the instrumentation inserted into the backpack; (b) tester A during a test.

### 17.6.2 Testers and workgroup

Two professional cyclists, of Trevigiani professional team, with the same height but different body weight, were selected for the tests. For the best management of the logistic and technical tasks, the tests were carried out with the support of Alan Beggin, which is the supervisor of the braking system testing activities of Campagnolo, and of Alessandro Stocco, the mechanic of Trevigiani professional team.

The characteristics of the testers are reported on tab. 17.3.

| Tester   | Name             | Category             | Cyclist type          | Age | Height | Weight |
|----------|------------------|----------------------|-----------------------|-----|--------|--------|
| Tester A | Liam Bertazzo    | Professional cyclist | Sprinter              | 21  | 180 cm | 75 kg  |
| Tester B | Gianluca Vecchio | Professional cyclist | Long-distance cyclist | 19  | 185 cm | 65 kg  |

Tab. 17.3 Characteristics of the testers.



Fig. 17.19 Picture of the workgroup. From the right: the author, Alessandro Stocco (mechanic of Trevigiani), Alan Beggin (Campagnolo test department), Liam Bertazzo (tester A), Gianluca Vecchio (tester B).

### 17.6.3 Characteristics of the performed tests

The field tests were executed on November 28<sup>th</sup> 2013 on the mountain roads close to Bassano del Grappa (VI), Italy. The weather conditions were the following:

- weather: sun;
- temperature: +4 °C;
- relative humidity: 57 %;
- wind speed: 0.9 km/h.

The asphalt was perfectly dry. Two types of tests were performed.

- **Sprint tests:** one of the two testers had to perform a sprint at his maximum power on roads with different slope (tab. 17.4). The gear ratio and the bicycle speed at the beginning of the sprint were different for each road slope. These tests were useful for the measurement of the parameters needed for the computation of the Reactivity Index.
  
- **Road downhill tests:** both the testers had to ride once through two road downhill presenting different characteristics (tab. 17.5). These tests were useful for characterizing the phases of the braking actions, and for measuring the parameters needed for the computation of the Handling Index and of the Road Holding Index.

| Test description                          | Testers  | Road slope | Start speed | Gear ratio |
|---|----------|------------|-------------|------------|
| sprint on flat road                       | tester A | 0 %        | 35 km/h     | 53/12      |
| sprint on an easy uphill                  | tester A | 6 %        | 20 km/h     | 53/15      |
| sprint on a road uphill with medium slope | tester A | 10 %       | 15 km/h     | 39/21      |
| sprint on a steep uphill road             | tester A | 16 %       | 10 km/h     | 39/25      |

Tab. 17.4 Description of the sprint tests.

| Testing path description                    | Testers                   | Length | Vertical drop | Number of curves                      |
|---|---------------------------|--------|---------------|---------------------------------------|
| Road downhill 1: winding, narrow, and steep | tester A<br>+<br>tester B | 5.6 km | 489 m         | 29 curves, including 10 hairpin turns |
| Road downhill 2: wide, with medium slope    | tester A<br>+<br>tester B | 9.6 km | 580 m         | 51 curves, including 10 hairpin turns |

Tab. 17.5 Description of the road downhill tests.

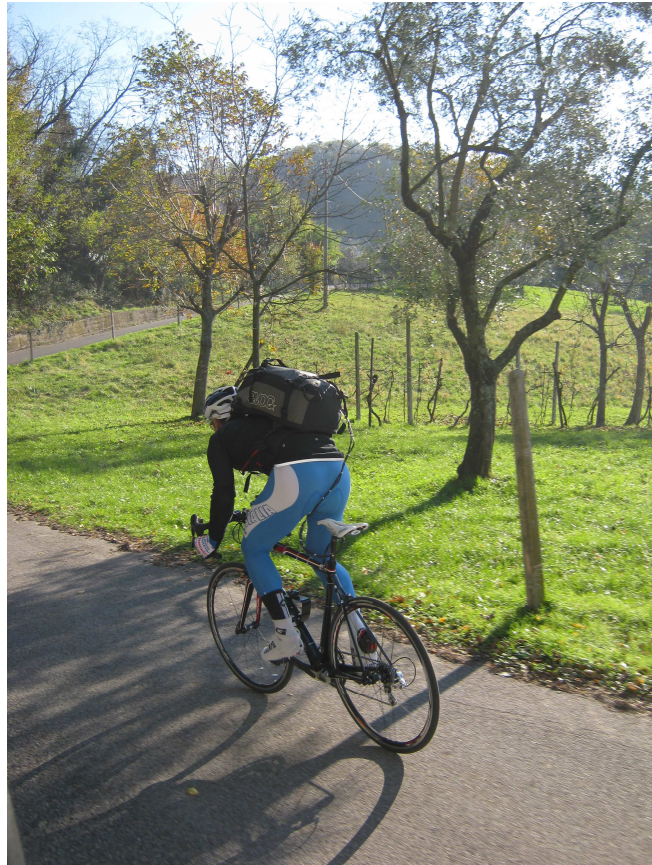


*Fig. 17.20 Tester in action during a sprint test.*



*Fig. 17.21 Tester in action during a road downhill test.*

# Chapter 18

## Analysis of the road downhill field tests

### 18.1 Introduction

The data analysis regarding the evaluation of the parameters useful for the computation of the Reactivity Index, the Handling Index, and the Road Holding Index, was presented in the chapters regarding the development of the indexes formulation (see § 12.5.1, 13.2.4, 13.3.2). In this chapter, the data analysis of the field tests concerning the road downhill is presented. This analysis is focused on the detailed study of the braking actions performed by the cyclist during road downhill cycling.

In literature, the bicycle braking systems were considered in few studies. Nakae *et al.* [54] have performed a laboratory analysis of disk brakes vibrations and noise phenomena, Lie & Sung [55] did a theoretical analysis of the bicycle braking action, whereas Oertel *et al.* [56] developed a test bench for bicycle brakes. No studies have analysed the braking action during road downhill use of the racing bicycle.

### 18.2 Data analysis

Among all parameters measured during the field tests (see tab. 17.1), five parameters were considered for the data analysis of the road downhill field tests (tab. 18.1). A dedicated Matlab® program was developed for the data analysis.

| Symbols                  | Description   | Sensor   | Purpose of the measurement                       |
|--------------------------|---|--|--|
| $M_{BL,R}$ [Nm]          | <b>Command torque</b> of the cyclist at the right brake lever (rear brake). | <b>Strain gauges</b> applied on the internal surface of the brake levers.                          | Characterization of the <b>braking actions</b> . |
| $M_{BL,L}$ [Nm]          | <b>Command torque</b> of the cyclist at the left brake lever (front brake). |  |  |
| $\vartheta_{BL,R}$ [deg] | <b>Angle of rotation</b> of the right brake lever.                          | <b>Rotational potentiometers</b> positioned at the rotation axis of the brake lever (fig. 17.2)    |  |
| $\vartheta_{BL,L}$ [deg] | <b>Angle of rotation</b> of the left brake lever.                           |  |  |
| $V$ [km/h]               | Bicycle <b>speed</b> .  | <b>GPS</b> inside of the Inertial Measurement Unit and <b>magnetic speed sensor</b> (fig. 17.6.b). |  |

Tab. 18.1 List of the parameters acquired during the field tests that were considered in the data analysis.

Starting from these quantities, the parameters listed in table 18.2 were computed in order to better characterize the bicycle braking actions.

| Symbols                 | Description  |
|-------------------------|--|
| $F_{BL,H,R}$ [N]        | <b>Command force</b> of the cyclist's hand on the right brake lever (rear brake).      |
| $F_{BL,H,L}$ [N]        | <b>Command force</b> of the cyclist's hand on the left brake lever (front brake).      |
| $F_{BP,N,f}$ [N]        | <b>Normal force</b> of the rear brake pads on the rim braking surface.                 |
| $F_{BP,N,r}$ [N]        | <b>Normal force</b> of the front brake pads on the rim braking surface.                |
| $BFD_{f/r}$             | The percentage <b>brake force distribution</b> at the front (f) and the rear (r) wheel |
| $a$ [m/s <sup>2</sup> ] | Bicycle <b>acceleration</b>  |

Tab. 18.1 List of the parameters acquired during the field tests that were considered in the data analysis of the road downhill tests.

### 18.2.1 Signals processing

A figure with three charts was created for the simultaneous analysis of the signals considered in this study (fig. 18.1). The bicycle speed  $V$  is reported in the upper chart, the middle one shows the command torque of the cyclist at the right and left brake lever ( $M_{BL,R}$ ,  $M_{BL,L}$ ), whereas the angles of rotation of both the brake levers are plotted in the lower one ( $\vartheta_{BL,R}$ ,  $\vartheta_{BL,L}$ ).

The raw data acquired during the field tests, an example is shown in figure 18.1, needed to be processed for the following reasons:

- since the speed signal derives from the digital conversion of a logic level channel, it is characterised by consecutive steps that affect the smoothness of the curve;
- the torque signals present an high noise and a drift;
- the signals regarding the angle of rotation of the brake levers presented a positive or negative offset from the zero level.

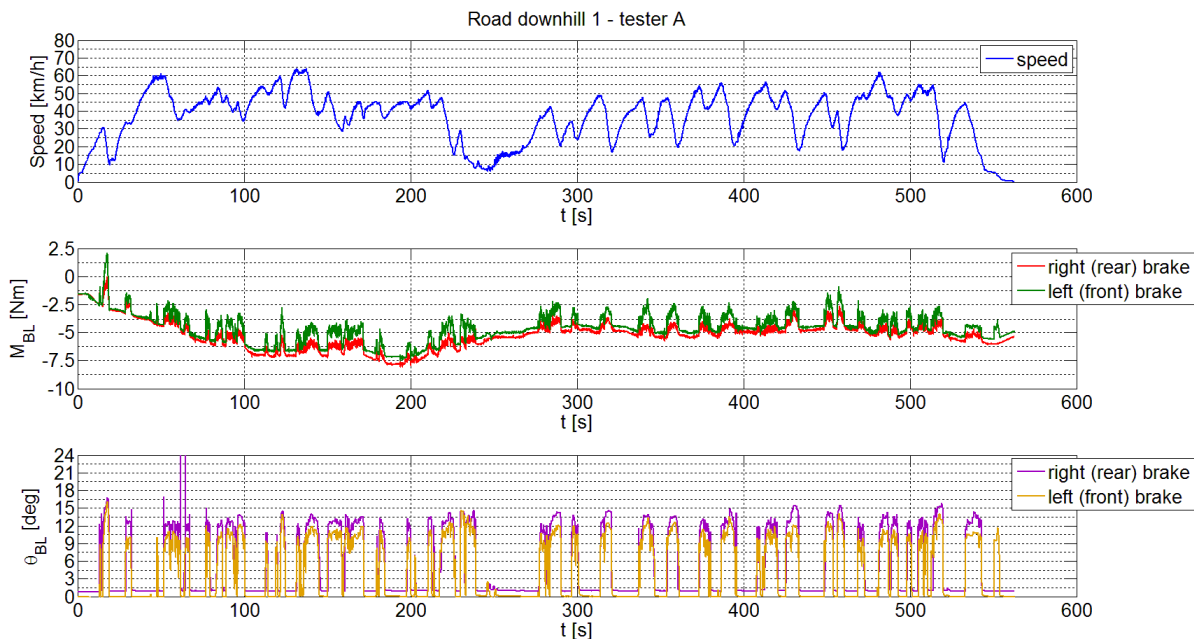
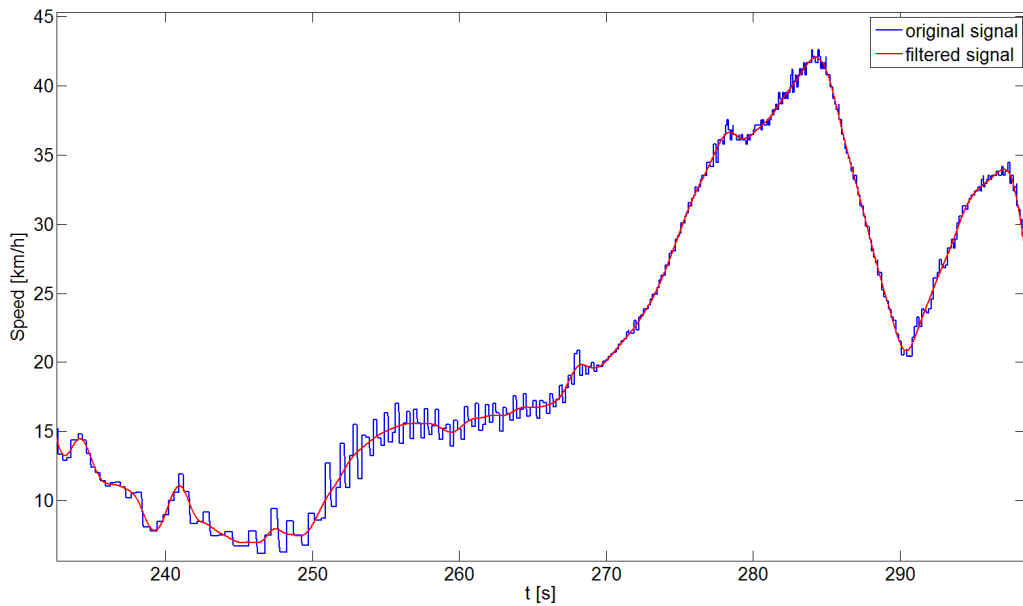


Fig. 8.1 Example of raw signals acquired during a road downhill test.

The signals were therefore processed through the operation listed in the points below.

- **Signals filtering**

A 4 poles Butterworth lowpass filter was used for smoothing the speed signals, and for deleting the noise of the torque signals. A cutoff frequency of 0.5 Hz and 5 Hz was adopted for the respective filtering of the speed and torque signals. Two examples of the effect of the lowpass filter on the signals are visible on figure 18.2 and 18.3.



*Fig. 18.2 Effect of the speed signal filtering.*

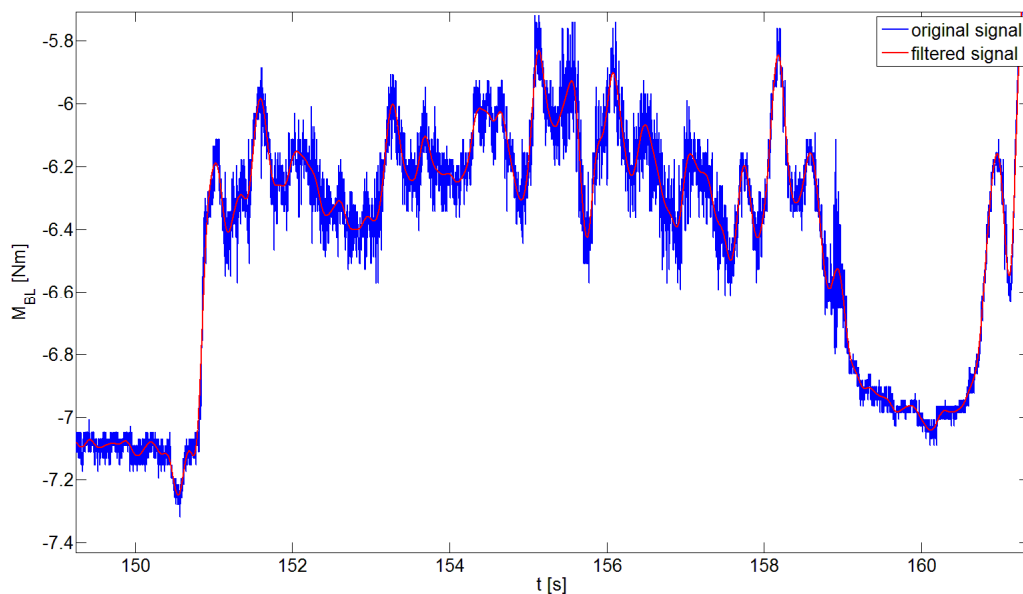


*Fig. 18.3 Effect of the torque signal filtering.*



- **Signals offset correction**

The offset of the signals regarding the angle of rotation of the brake levers, was adjusted for each of them, subtracting from all samples the relative difference between a reference flat curve portion and the zero level.

- **Signals drift correction**

The drift phenomenon showed by the torque signals is due to the temperature effect on the deformation signals measured by means of the strain gauges. This phenomenon was corrected through the development of a dedicated algorithm, based on the identification of the beginning and of the end of each braking action.

The enlarged view of figure 18.4 shows the effect of the executed signal processing operations: the speed curve became smooth, the noise and the drift of the torque signals were deleted, and the offset of the angles signals was eliminated.

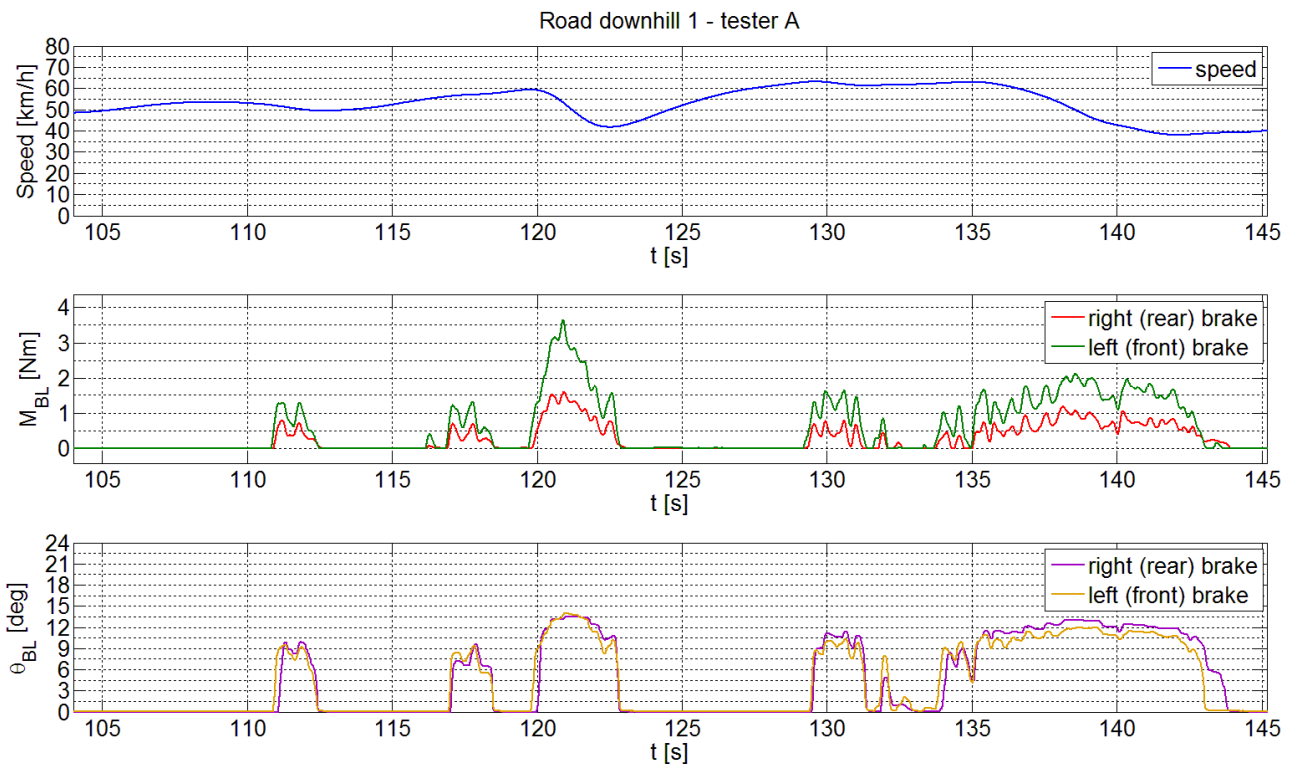


Fig. 18.4 Enlarged view of the signals obtained after their processing.

### 18.2.2 Parameters computations

After the signal processing, the parameters listed on table 18.2 were then computed.

- **Acceleration  $a$  [m/s<sup>2</sup>]**

The acceleration of the bicycle was calculated performing a numerical differentiation of the speed signal  $V$ .

- **Command force  $F_{BL,H}$  [N]**

The resultant force that the cyclist applies on the brake lever was assumed to be coincident with a point at a distance of 79 mm from the axis of the brake lever hinge (fig. 18.5). This assumption derives from an analysis of the ergonomics of the brake lever. The force applied by the hand of the cyclist was then calculated as follows:

$$F_{BL,H} = \frac{M_{BL}}{0.079\text{ m}} \quad [\text{N}] \quad (1)$$

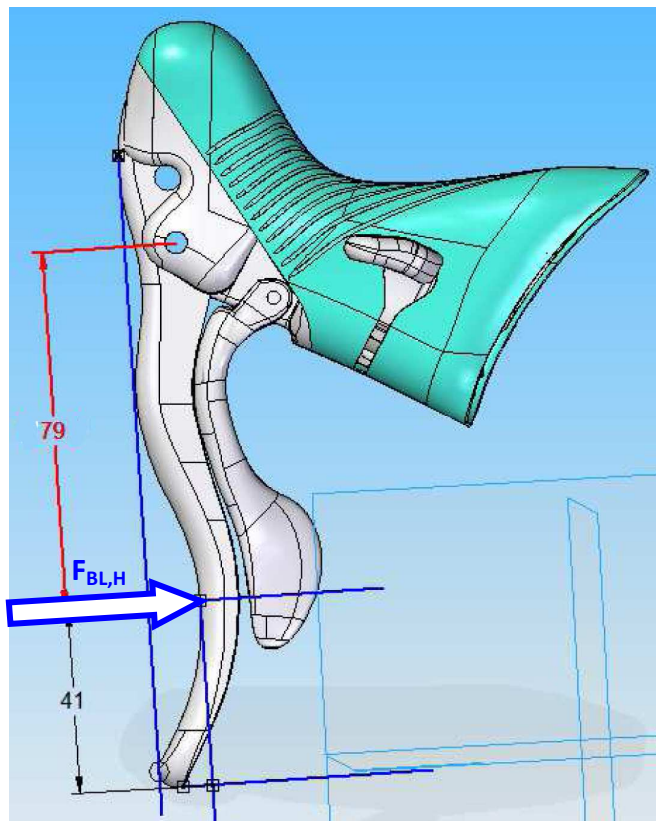


Fig. 18.5 Position of the resultant force applied on the brake lever.

- **Normal force of the brake pads  $F_{BP,N}$  [N]**

During the calibration of the strain gauge channels of the brake levers (see § 17.4.2), some tests were performed using an uniaxial load cell positioned between the brake pads (fig. 17.10.c) for measuring the relationship between the load on the lever, and the force orthogonal to the braking surface of the rim  $F_{BP,N}$ . The resultant constants allowed to calculate the normal force to the rim braking surface, starting from the measurement of the command torque applied at the brake levers (2,3).

$$F_{BP,N,f} = M_{BL,L} \cdot 39.43 \quad [\text{N}] \quad (2)$$

$$F_{BP,N,r} = M_{BL,R} \cdot 35.43 \quad [\text{N}] \quad (3)$$

• **Brake Force Distribution BFD**

During a braking action, the equilibrium of a wheel can be represented as in figure 18.6. For the equilibrium of the moments in respect to the wheel axis, the tangential force  $F_{rim,T}$  on the rim braking surface, which is due to the friction between it and the brake pad, is equal to the longitudinal braking force  $F_L$  at the contact point between the tire and the road surface. Since the rim tangential force is related to the normal force  $F_{BP,N}$  through the friction coefficient of the rim, and if we assume that the friction coefficients of the front and the rear rims were the same, the ratio between the longitudinal braking force of the front and the rear wheel can be expressed as it follows:

$$\frac{F_{L,f}}{F_{L,r}} = \frac{F_{rim,T,f}}{F_{rim,T,r}} = \frac{\mu_{rim,f} \cdot F_{BP,N,f}}{\mu_{rim,r} \cdot F_{BP,N,r}} = \frac{F_{BP,N,f}}{F_{BP,N,r}} \tag{4}$$

The percentage brake force distribution at the front and the rear wheel was then calculated as showed below:

$$BFD_f = \frac{F_{BP,N,f}}{F_{BP,N,f} + F_{BP,N,r}} \cdot 100 \tag{5}$$

$$BFD_r = \frac{F_{BP,N,r}}{F_{BP,N,f} + F_{BP,N,r}} \cdot 100 \tag{5}$$

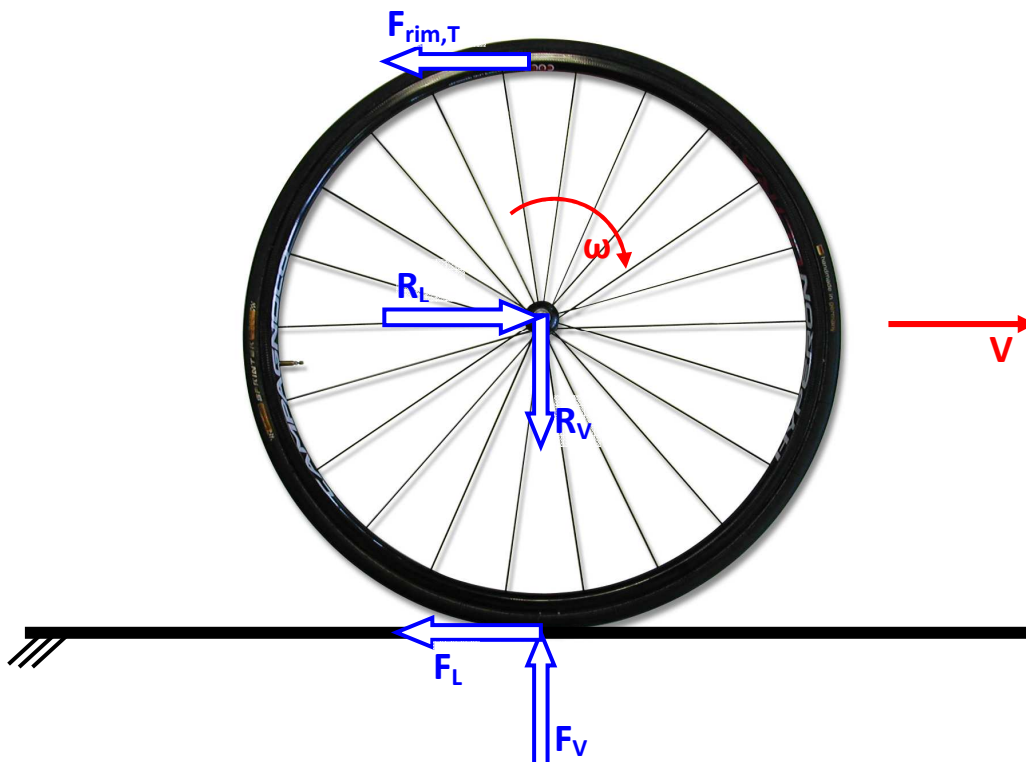


Fig. 18.6 Equilibrium of a wheel during the braking action.

### 18.3 Results

The characteristics of the performed tests are shown in table 18.2. The highest average speed was calculated for the Tester B in all tests performed. This could be correlated with its lower body weight (tab. 17.3), which probably facilitates him in the bicycle handling. Both the testers had reached the highest maximum speed, and the highest deceleration during the Road Downhill 1, which presented the steepest road sections.

| Testing path description                    | Length | Vertical drop | Number of curves                      | Tester   | V <sub>MAX</sub> | V <sub>avg</sub> | max decel.             | test time |
|---|--------|---------------|---------------------------------------|----------|------------------|------------------|------------------------|-----------|
| Road downhill 1: winding, narrow, and steep | 5.6 km | 489 m         | 29 curves, including 10 hairpin turns | tester A | 63.1 km/h        | 35.2 km/h        | -3.11 m/s <sup>2</sup> | 9' 32''   |
|   |        |               |                                       | tester B | 70.3 km/h        | 44.4 km/h        | -3.53 m/s <sup>2</sup> | 7' 34''   |
| Road downhill 2: wide, with medium slope    | 9.6 km | 580 m         | 51 curves, including 10 hairpin turns | tester A | 65 km/h          | 47.6 km/h        | -2.65 m/s <sup>2</sup> | 12' 6''   |
|   |        |               |                                       | tester B | 63.2 km/h        | 49.8 km/h        | -2.75 m/s <sup>2</sup> | 11' 34''  |

Tab. 18.2 Characteristics of the performed road downhill tests.

The figures 18.7 and 18.8 show the signals of speed, acceleration, command forces, and angle of rotation of the brake levers, that regards the Road Downhill 1 respectively performed by the Tester A and the Tester B. We can firstly observe that for both the tests, during each braking action, the maximum command force is always applied to the left brake lever, which contrarily presents the minimum angle of rotation. Since the left brake lever represents the command device of the front brake, we can deduce that, as expected, the main brake is the front, and the lower length of the brake wire and hood is the cause of their lower deformation. A comparison between the two figures highlights the higher number of braking actions and the higher peak values of the command forces resulted from the test performed by the Tester A. This confirms the lower average speed calculated for this tester. The figure 18.9 shows the signals acquired during the Road Downhill 2 performed by the tester B. If we compare these results with the signals measured during the road Downhill 1 performed by the same tester (fig. 18.8), we can observe that the Road Downhill 1 shows a closer time interval between two consecutive braking actions and huge number of speed variation and of decelerations. This agrees with the differences between the characteristics of the two testing paths (tab. 18.2).

A reference braking action was selected and analysed in details in the following paragraph.

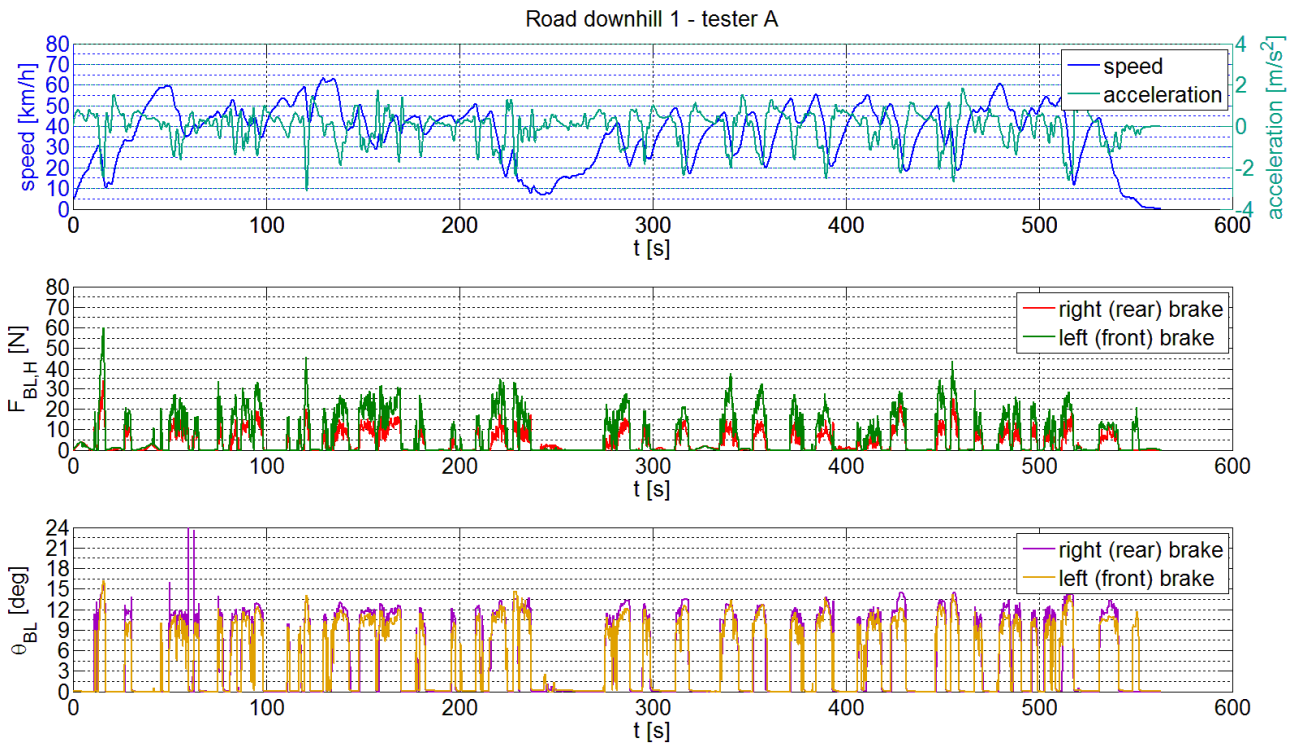


Fig. 18.7 Signals regarding the Road Downhill 1 performed by the Tester A.



Fig. 18.8 Signals regarding the Road Downhill 1 performed by the Tester B.

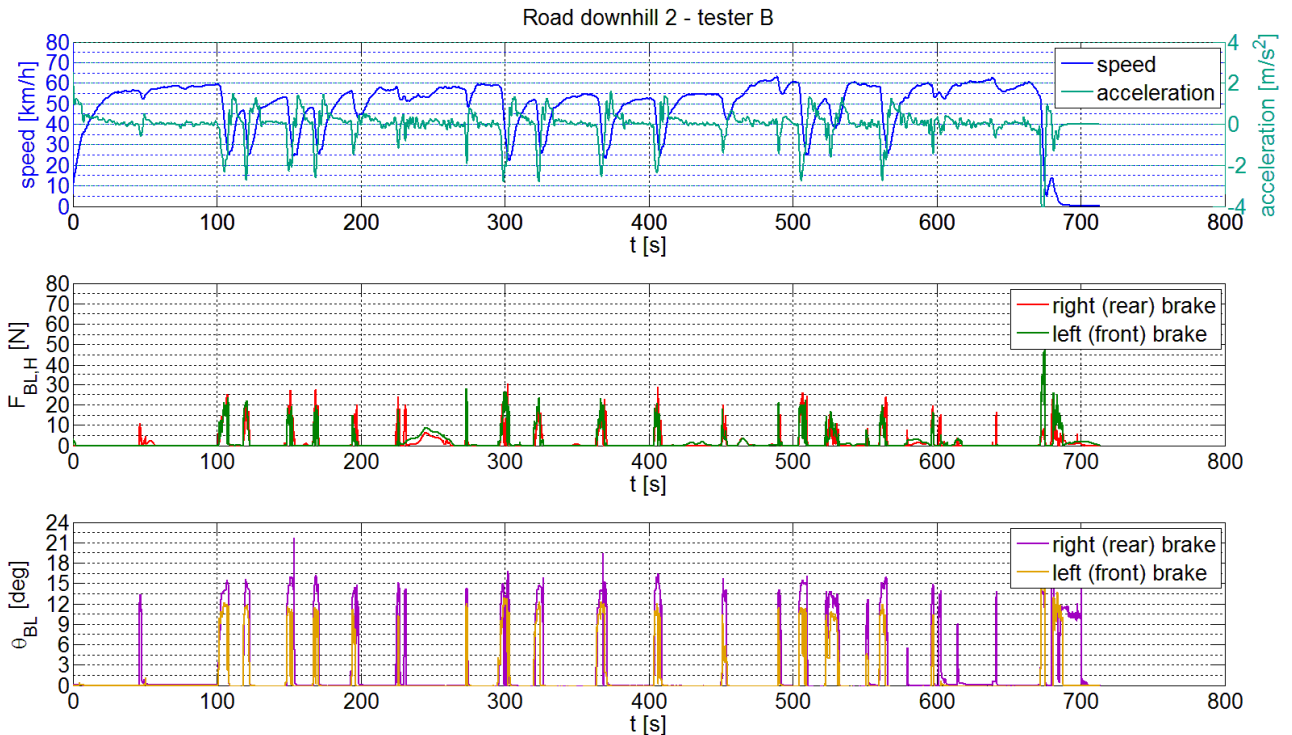


Fig. 18.9 Signals regarding the Road Downhill 2 performed by the Tester B.

### 18.3.1 Analysis of a reference braking action

It was considered the Road Downhill 1 performed by the tester A (fig. 18.10). The selected reference braking action is represented by the one, which presents the maximum deceleration and the maximum peak of the command force (fig. 18.11). The braking action is characterised by an initial section, during which the command forces, and the lever angles increases, and the deceleration increases (decrease of acceleration). The command force of the front brake lever is always greater than the command force of the rear one. It reaches a peak of 45 N, which is more than the double of the peak reached by the command force of the rear brake lever. The maximum value of the bicycle deceleration corresponds to the peak of the command force. In the second section the deceleration and the command forces slowly decreases. The first transient phase is visible in figure 18.12. It is characterised by an initial linear increasing of the command forces, and of the levers angles. This corresponds to the approach of the brake pads to the rim braking surface. At the beginning of the contact between the brake pads and the rim braking surface, the lever angle decreases its slope, and the command force shows an irregular trend, due to the friction phenomena at the pad/rim interface. The figure 18.13 shows the percentage brake force distribution at the front and the rear brake. At the beginning of the braking phase, the cyclist used only the front brake. During the central main phase, the ratio between the braking force of the front and the rear brake is kept approximately constant: the 70 % of the braking force is distributed to the front brake, the remaining 30 % to the rear one. At the end of the braking phase the front brake was released, and the rear brake was used for the last speed control.



Fig. 18.10 Signals regarding the Road Downhill 1 performed by the Tester A and selection of the reference braking action.

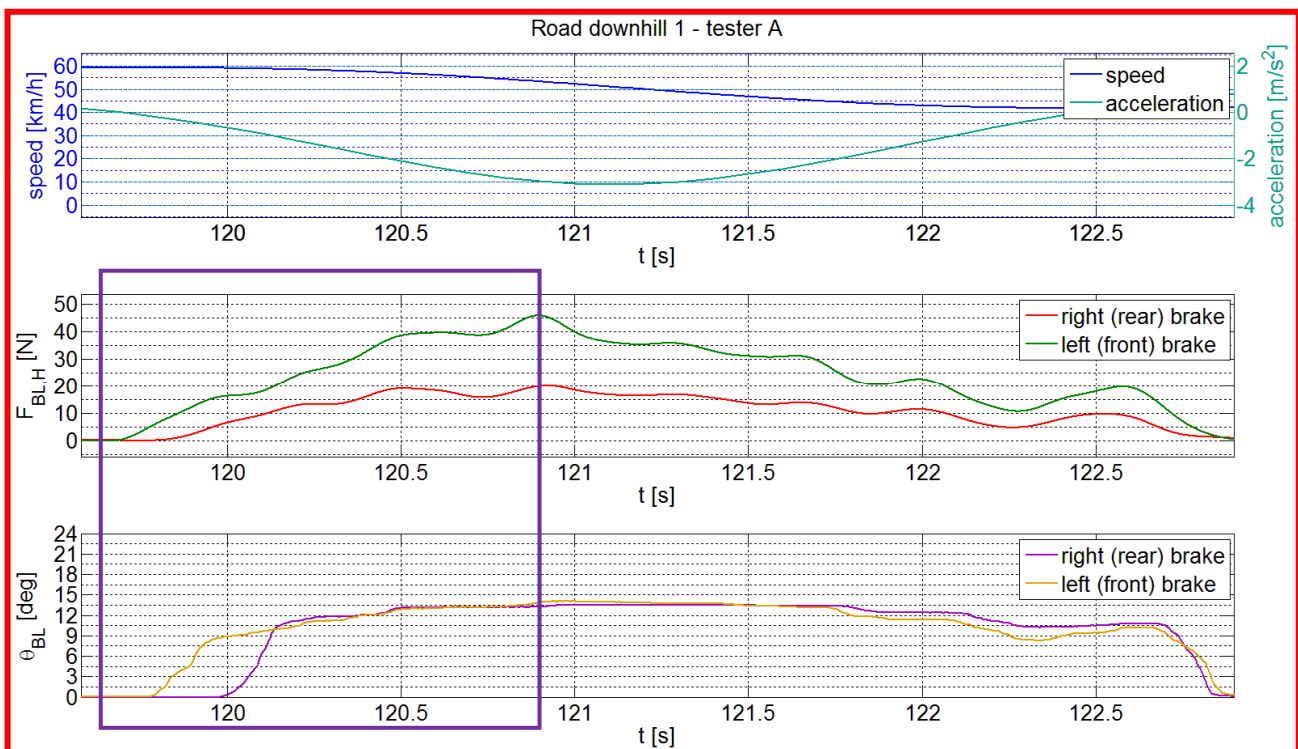


Fig. 18.11 Selected braking action reference.

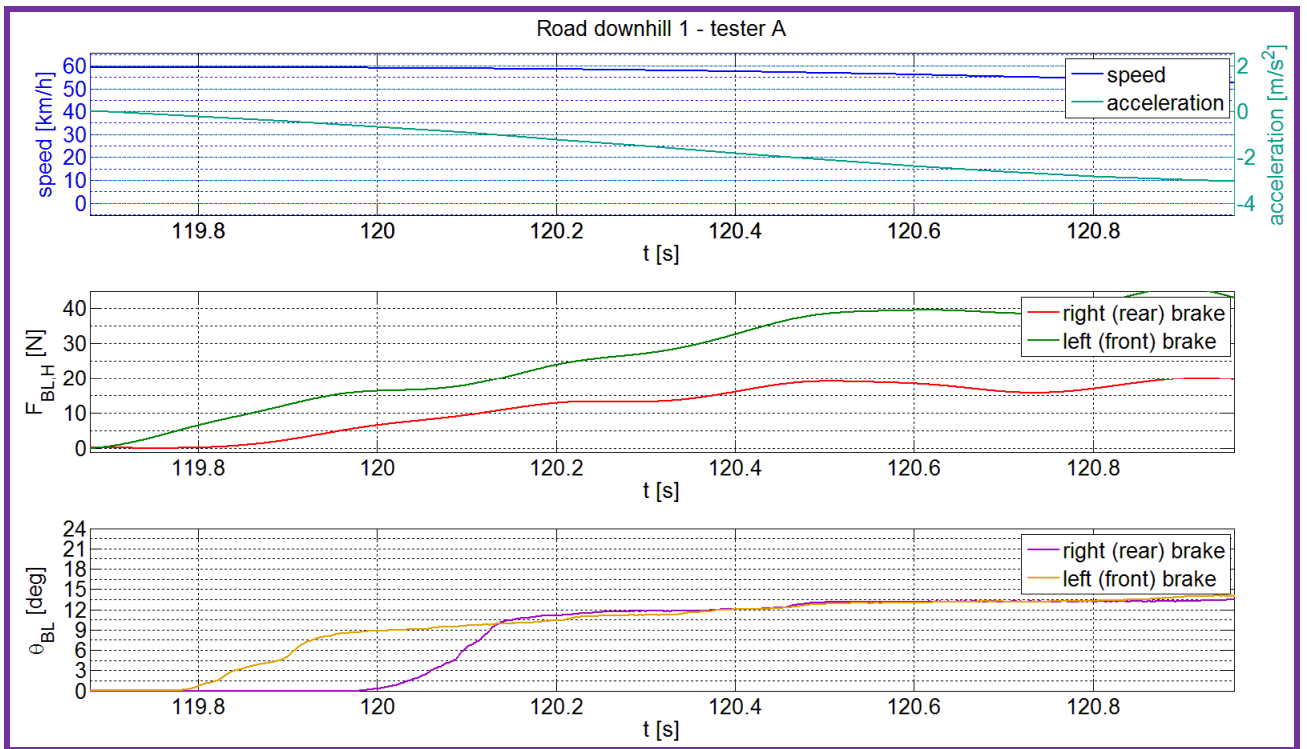


Fig. 18.12 Initial transient phase of the braking action reference.

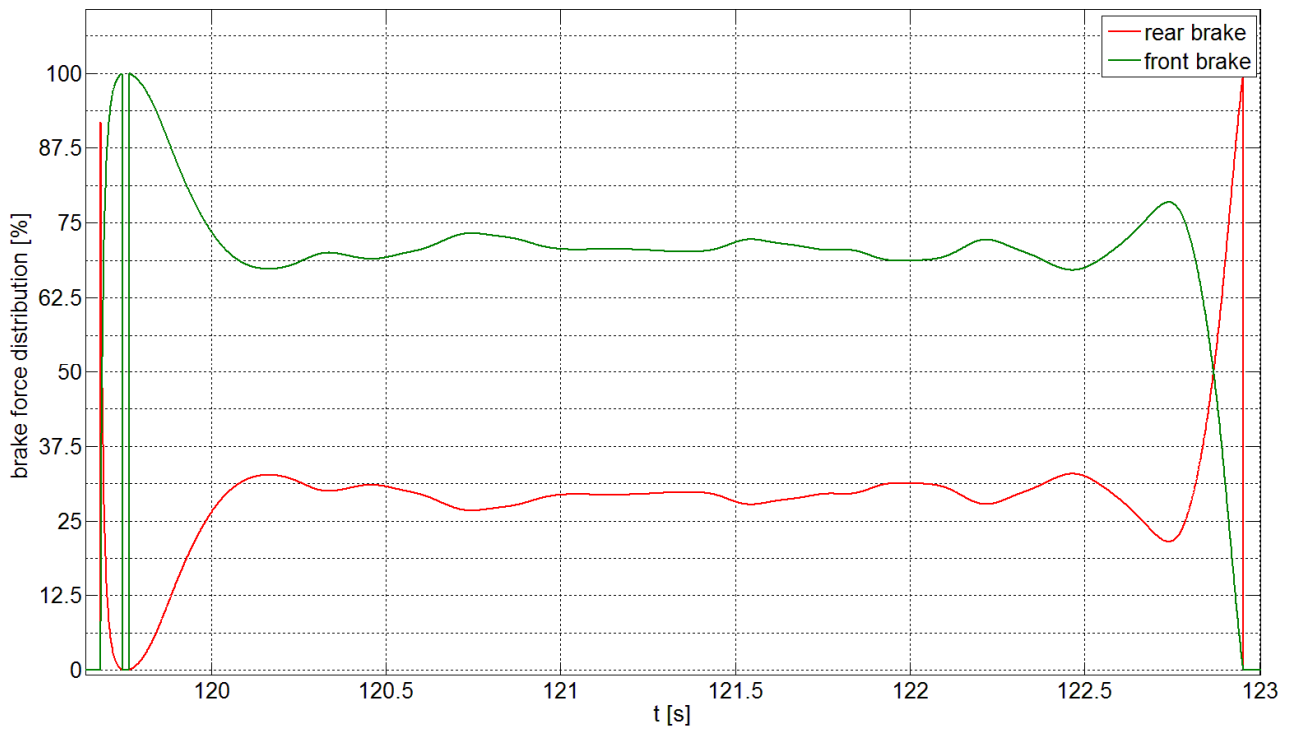


Fig. 18.13 Brake force distribution during the braking action reference.



## 18.4 Conclusions

The sensors used for equipping the instrumented bicycle, the solutions adopted for their fixation, and the data acquisition system resulted suitable for the field tests performed. The developed instrumented bicycle allowed the measurement of the parameters needed for the computation of the Reactivity Index, the Handling Index, and the Road Holding Index, and for the characterization of the braking actions performed during the racing bicycle riding. The differences, among the riding style of the two testers and between the characteristics of the two selected testing paths, were recognizable through the data analysis. Each phase of a reference braking action was analysed in details, highlighting the possibility of using this instrumented bicycle as a tool for a deep analysis of the influence that each component of the braking system has on its perceived quality requirements. Dedicated field tests, together with a subjective evaluation tests session, could represent the first stages of an activity concerning the integrated characterization of the braking systems, in which the perceived quality requirements can be correlated to the measurable engineering characteristics adopting the same structured approach developed in this thesis, considering the racing bicycle wheels. The data collected through the field tests can be useful for the definition of the laboratory testing protocol. The used sensors can be easily transferred to other racing bicycles, allowing the measurement of the influence of the structural components on the bicycle dynamics and on the braking performance of the bicycle.

# Chapter 19

## Conclusions

An integrated method was developed for the engineering characterization of bicycle components. This method was obtained through five stages. The first stage concerned the development of new measurement methods for evaluating the engineering characteristics that were not yet measured before. Comfort properties of bicycle wheels and saddles were studied in this stage. With this purpose, new laboratory testing methods were developed for the characterization of the wheels radial structural behaviour, and of the vibration transmissibility of wheels and saddles. Two testing methods developed for the evaluation of the radial stiffness and the vibration transmissibility of the wheels were developed in the University laboratory and then implemented in the laboratories of Campagnolo srl. During the second stage of the work, a structured and objective method was developed for the collection and organization of the wheels perceived quality requirements, evaluated by the cyclists during road cycling. The assessments of the cyclists, among the identified quality requirements, were obtained through dedicated subjective evaluation tests, and the correlation between them and the basic engineering characteristics of the wheels was calculated through the adoption of a mathematic method. The high differences obtained among the evaluated quality requirements of three different wheelsets suggested the development of the engineering complex indexes. Six engineering complex indexes were formulated in the fourth stage, through a scientific and rigorous approach, with the aim of expressing a technical measurement of the regarding quality requirements. In the fifth stage, an instrumented racing bicycle was developed for measuring, through dedicated field tests, the parameters needed for the computation of the indexes, and for characterizing the braking actions performed by the cyclists during road downhill riding.

The developed method for the evaluation of the radial structural behaviour of wheels, and of the vibration transmissibility of wheels and saddles, regards the study of the impulsive and vibrational comfort properties. With the adopted approach, the global system represented by the bicycle and the cyclist was divided into subsystems. The developed testing methods are therefore suitable for evaluating the contribution of each bicycle component to the global vibration or to the transmissibility of impulsive loads. Starting from this work, the development of a tests bench, which allows the vibrational test of the full bicycle with a real cyclist (fig. 19.1), regards the on-going activity of the research group of the Laboratory of Machine Design of University of Padova.

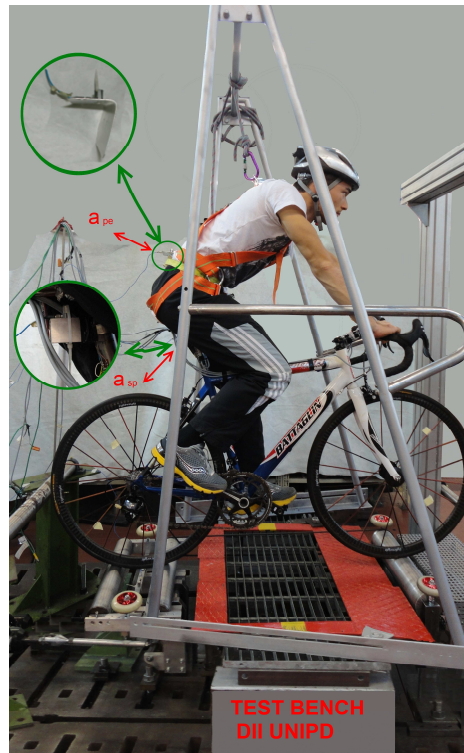


*Fig. 19.1 Test bench developed during the on-going research activity on the comfort properties of bicycle components.*

The structured features of the user-centred method developed for collecting and organizing the wheels quality requirements, minimize the influence of the analyst, and enhance the characteristics of repeatability. The identification and organization of the user quality requirements, united to a subjective evaluation test session, can represent the starting stages in the definition of a methodology for the systematic collection of the subjective evaluation during the product development. The method developed for the computation of the correlation coefficients allows obtaining a quantitative correlation, based on statistics and experimental evidence, between the quality requirements and the engineering characteristics of racing bicycle wheels. This aspect represents a significant improvement of the widely used method proposed by QFD [16]. The results highlighted also the interdependence between the different basic engineering characteristics, and suggested to the additional engineering characteristics to be measured for a complete characterization of the wheels.

The engineering complex indexes were formulated combining the analysis of the subjective evaluation of the cyclists with the analysis of the bicycle dynamics. Each developed engineering complex index was validated through the computation of the correlation coefficient with the quality requirement that it has to express. The engineering complex indexes are the final result of the overall method developed. Since they give a technical measurement of the cyclist feelings, they represent the integrated engineering characterization of the wheels. The indexes are a tool

that can be used for the product development based on a user-centred approach, or for the management of the products range. They can also represent a reliable guideline for customers in the product choice, or a tool for marketing communication messages.

The low correlation coefficients calculated, between the Forward Rolling Efficiency and all basic engineering characteristics that were available during this study, and the lacks of measured parameters useful for the computation of the Index of Forward Rolling Efficiency and the Index of Stability to Crosswind, suggested the need to characterize the aerodynamic behavior of the wheels. These results represent the base of a new PhD program, focused on the study of the wheels aerodynamics, born from the partnership between the Department of Industrial Engineering of the University of Padova and the Campagnolo srl company.

The developed instrumented bicycle allowed the measurement of the parameters needed for the computation of the Reactivity Index, the Handling Index, and the Road Holding Index, and for the characterization of the braking actions performed during the racing bicycle riding. It can be further used for multiple activities. It can represent a tool for the integrated characterization of the braking systems, in which the perceived quality requirements can be correlated to the engineering characteristics measured during the field tests, adopting the same structured approach developed in this thesis, considering the racing bicycle wheels. The data collected through the field tests can be useful for the definition of the laboratory testing protocol. Since the used sensors can be easily transferred to other racing bicycles, an activity concerning the measurement of the influence of the structural components on the bicycle dynamics and on the bicycle braking performance can be carried out.

The overall developed methodology, represents an innovative structured approach for the user-centred characterization of sports equipment. Despite the fact that it was developed mainly considering the racing bicycle wheels, it can be applied to other bicycle components or to other sports equipment.



## ***Part 6***



## References

### Bicycle Comfort

- [1] A.Z. Hastings, K.B. Blair, F.K. Culligan, D.M. Pober, *Measuring the effect of transmitted road vibration on cycling performance*, The Engineering of Sport 5, Davis, (2004).
- [2] S. Richard, Y. Champoux, *Modal analysis of road bike's front components*. Proceedings of IMAC-XXII – 2004. Ed. Curran Associates, Inc. ISBN:9781604238020 (2007).
- [3] M. Olieman, R. Marin-Perianu, M. Marin-Perianu, (2012). *Measurement of dynamic comfort in cycling using wireless acceleration sensors*. In: -. Procedia Engineering. PROCEEDIA ENGINEERING, vol. 34, p. 568-573, ISSN: 1877-7058, Lowell, Massachusetts, 9-13 July 2012, doi: 10.1016/j.proeng.2012.04.097.
- [4] G Marcolin, A Paoli, FA Panizzolo, G Biasco, N Petrone, *A method for the analysis of cyclist shorts with different pads for perineal area protection: comparison between drum and road tests*. Procedia Engineering, Volume 2, Issue 2, June 2010, Pages 2831-2835.
- [5] J. Vanwalleghem, F. Mortier, I. De Baere, M. Loccufier, W. Van Paepegem, *Design of an instrumented bicycle for the evaluation of bicycle dynamics and its relation with the cyclist's comfort*, 9th Conference of the International Sports Engineering Association (ISEA), Procedia Engineering 34 ( 2012 ), pp. 485 – 490.
- [6] F. Giubilato, *Development of a methodology for the quantitative comparison of performance and comfort of wheels for racing bicycles*, M.Sc. thesis in Mechanical Engineering, Department of Mechanical Engineering, University of Padova.
- [7] F. Giubilato, N. Petrone (2012). *A method for evaluating the vibrational response of racing bicycles wheels under road roughness excitation*. In: -. Procedia Engineering. PROCEEDIA ENGINEERING, vol. 34, p. 409-414, ISSN: 1877-7058, Lowell, Massachusetts, 9-13 July 2012, doi: 10.1016/j.proeng.2012.04.070.
- [8] C. Hölzel, F. Höchtl, V. Senner, *Cycling comfort on different road surfaces*, In: -. Procedia Engineering. PROCEEDIA ENGINEERING, vol. 34, p. 479-484, ISSN: 1877-7058, Lowell, Massachusetts, 9-13 July 2012.
- [9] A. Doria, L.Taraborrelli, *On the structural vibrations of bicycles: influence of materials and construction technology on the modal properties*, Proceedings, International Cycling Safety Conference 2013 20-21 November 2013, Helmond, The Netherlands.



- [10] J. L. Wojtowicki, Y. Champoux, J. Thibault, *Modal properties of road bikes vs ride comfort*, Acoustics and Vibration Group of Universite de Sherbrooke (GAUS).
- [11] Y. S. Liua, T. S. Tsayb, C. P. Chenc, H. C. Panc, *Simulation of riding a full suspension bicycle for analyzing comfort and pedaling force*, *Procedia Engineering* 60 ( 2013 ) pp. 84 – 90, 6th Asia-Pacific Congress on Sports Technology (APCST).
- [12] ISO 2631-1, *Evaluation of human exposure to whole-body vibrations*.
- [13] ISO 5349, *Measurement and evaluation of human exposure to hand-transmitted vibrations*.
- [14] ISO 13473-1, *Characterization of pavement texture by use of surface profiles*.
- [15] K. Shin, J. K. Hammond, *Fundamentals of signal processing for sound and vibration engineers*, Wiley.

### **Analysis of User Quality Requirements**

- [16] Y. Akao, *QFD: Quality Function Deployment - Integrating Customer Requirements into Product Design*. Productivity Press, 2004, Portland. p 1-83, 147-181.
- [17] A. W. Ulwick, *An Introduction to Outcome-Driven Innovation*, Strategyn Inc.
- [18] A. W. Ulwick, L. A. Bettencourt, *Giving costumers a fair hearings*, MIT Sloan Management Review.
- [19] J. Darques, R. Carreira, A. De La Mettrie, D. Bruyant, *Quality Function Deployment - A means for developing adequate skis and snowboards*, 2004, The Engineering of Sport 5 - Conference Proceedings of the Engineering of Sport, pp. 428-434. Davis, USA.
- [20] P. Clifton, *Investigation and Customisation of Snowboard Performance Characteristics for Different Riding Styles*, 2011, PhD thesis School of Aerospace, Mechanical and Manufacturing Engineering, College of Science, Engineering and Health, RMIT University.
- [21] P. Clifton, M. Burton, A. Subic, T. Perret-Ellena, A. Bedford, A. Schembri, *Identification of performance requirements for user-centered design of running shoes*, 2011, 5th Asia-Pacific Congress on Sports Technology - *Procedia Engineering* 13, pp. 100-106.
- [22] W. J. Vincent, *Statistics in Kinesiology*, California State University, Northridge; Human Kinetics
- [23] A. Subic, P. Clifton, J. Beneyto-Ferre, *Identification of innovation opportunities for snowboard design through benchmarking*, *Sports Technology*.
- [24] J. A. Carnevalli, P. C. Miguel, *Review, analysis and classification of the literature on QFD—Types of research, difficulties and benefits*, *Int. J. Production Economics*.
- [25] L. K. Chan, M. L. Wu, *Quality function deployment: A literature review*, *European Journal of Operational Research*.

- [26] C. C. Usma-Alvarez, A. Subic, M. Burton, F. K. Fuss, *Identification of design requirements for rugby wheelchairs using the QFD method*, *Procedia Engineering* 2 (2010) pp. 2749–2755, 8th conference of the International Sports Engineering Association.

### **Dynamics of Two Wheeled Vehicles**

- [27] D. G. Wilson, J. Papadopoulos, *Bicycling Science*, third edition, 2004, Massachusetts Institute of Technology.
- [28] V. Cossalter, *Motorcycle Dynamics*, 2008.
- [29] J. K. Moore, M. Hubbard, A. L. Schwab, J. D. G. Kooijman, D. L. Peterson, *Statistics of Bicycle Rider Motion*, *Procedia Engineering* 2 (2010) pp. 2937–2942.
- [30] D. L. Peterson, J. K. Moore, D. Fintelman, M. Hubbard, *Low-power, modular, wireless dynamic measurement of bicycle motion*, *Procedia Engineering* 2 (2010) pp. 2949–2954.
- [31] M. Plöchl, J. Edelmann, B. Angrosch, C. Ott, *On the wobble mode of a bicycle*, *Vehicle System Dynamics* Vol. 50, No. 3, March 2012, pp. 415–429.
- [32] P. Basu-Mandal, A. Chatterjee, J. M. Papadopoulos, *Hands-free circular motions of a benchmark bicycle*, *Proc. R. Soc. A* (2007) 463, 1983–2003 doi:10.1098/rspa.2007.1849.
- [33] J. P. Meijaard, J. M. Papadopoulos, A. Ruina, A. L. Schwab, *Linearized dynamics equations for the balance and steer of a bicycle: a benchmark and review*, *Proc. R. Soc. A* (2007) 463, 1955–1982 doi:10.1098/rspa.2007.1857.
- [34] A. L. Schwab, P. D. L. de Lange, R. Happee, J. K. Moore, *Rider control identification in bicycling using lateral force perturbation tests*, *Proc IMechE Part K: J Multi-body Dynamics* 227(4) 390–406.

### **Structural Analysis of Bicycle Components**

- [35] F. Giubilato, N. Petrone, *Stress analysis of bicycle saddles structural components during different cycling conditions*, The 2014 conference of the International Sports Engineering Association.
- [36] N. Petrone, F. Giubilato, A. Giro, N. Mutinelli, *Development of instrumented downhill bicycle components for field data collection*, *Procedia Engineering* 34 (2012), pp. 514 – 519, 9th Conference of the International Sports Engineering Association (ISEA).
- [37] N. Petrone, L. Susmel, *Biaxial Testing and Analysis of Bicycle-Welded Components for the Definition of a Safety Standard*, *Fatigue and Fracture of Engineering Material and structures*, 26, 491-505, Blackwell Publishing Ltd., UK, 2003.

- [38] N. Petrone, A. Tessari , R. Tovo, *Acquisition and analysis of service load histories in mountain-bikes*, XXV° Convegno Nazionale AIAS, International Conference on Material Engineering, Gallipoli - Lecce, 4-7 September 1996, pp. 851-858.
- [39] E. Seragio, N. Petrone, M. Marchiori, 2004, *Design and calibration of a dynamometric saddle support for racing and mountain bikes* , Proceedings of 5th International Conference on the Engineering of Sport, University of California, Davis, 13-16 September 2004, Vol. 2, pp. 187-193, ISBN 0-9547861-1-4.
- [40] A. Callens, A. Bignonnet, *Fatigue design of welded bicycle frames using a multiaxial criterion*, 9th Conference of the International Sports Engineering Association (ISEA), Procedia Engineering 34 ( 2012 ), pp. 640 – 645.
- [41] M. L. Hull, D. Wootten, *An improved accuracy six-load component pedal dynamometer for cycling*, Journal of Biomechanics, Vol. 29, pp. 1105-1110, 1996.
- [42] R. R. Biniab, P. A. Humea, A. Cerviric, *A comparison of cycling SRM crank and strain gauge instrumented pedal measures of peak torque, crank angle at peak torque and power output*, Procedia Engineering 13 (2011) pp. 56–61, 5th Asia-Pacific Congress on Sports Technology (APCST).
- [43] J. M. Drouet, Y. Champoux, *A novel dynamometric hubset design to measure wheel loads in road cycling*, 2010 , 8th Conference of the International Sports Engineering Association (ISEA)
- [44] Henri P. Gavin, *Bicycle-wheel spoke patterns and spoke fatigue*, Journal Of Engineering Mechanics. August 1996.
- [45] Robin C. Redfield, Cory Sutela, *Mountain bike wheel endurance testing and modeling*, 9th Conference of the International Sports Engineering Association (ISEA), Procedia Engineering 34 (2012), pp. 658 – 663.

## **Bicycle Aerodynamics**

- [46] T. Defraeye, B. Blocken, E. Koninckx, P. Hespel, J. Carmeliet, *Aerodynamic study of different cyclist positions: CFD analysis and full-scale wind-tunnel tests*, Journal of Biomechanics, Vol 43 (2010) pp. 1262–1268
- [47] H. Chowdhury, F. Alam, D. Mainwaring, *A full scale bicycle aerodynamics testing methodology*, 5th Asia-Pacific Congress on Sports Technology (APCST), Procedia Engineering 13 (2011), pp. 94–99.
- [48] G.S. Tew, A.T. Sayers, *Aerodynamics of yawed racing cycle wheels*, Journal of Wind Engineering and Industrial Aerodynamics 82 (1999), pp. 209-222.

- [49] N. Barry, D. Burton, T. Crouch, J. Sheridan, R. Luescher, *Effect of crosswinds and wheel selection on the aerodynamic behavior of a cyclist*, 9th Conference of the International Sports Engineering Association (ISEA), Procedia Engineering 34 ( 2012 ), pp. 20 – 25.
- [50] M. N. Godo, D. Corson, S. M. Legensky, *A Comparative Aerodynamic Study of Commercial Bicycle Wheels using CFD*, American Institute of Aeronautics and Astronautics 2010.
- [51] M. N. Godo, D. Corson, S. M. Legensky, *An Aerodynamic Study of Bicycle Wheel Performance using CFD*, 47th AIAA Aerospace Sciences Meeting Including The New Horizons Forum and Aerospace Exposition, 5 - 8 January 2009, Orlando, Florida.
- [52] M. N. Godo, D. Corson, S. M. Legensky, *A Practical Analysis of Unsteady Flow Around a Bicycle Wheel, Fork and Partial Frame Using CFD*, American Institute of Aeronautics and Astronautics 2011.
- [53] J. K. Moore, *Aerodynamics of high performance bicycle wheels*, M.Sc thesis in Mechanical Engineering, University of Canterbury.

### **Bicycle Braking Systems**

- [54] T. Nakae, T. Ryu, A. Sueoka, Y. Nakano, T. Inoue, *Squeal and chatter phenomena generated in a mountain bike disc brake*, Journal of Sound and Vibration 330 (2011) 2138–2149.
- [55] D. Lie, C. K. Sung, *Synchronous brake analysis for a bicycle*, Mechanism and Machine Theory 45 (2010) 543–554.
- [56] C. Oertel, H. Neuburger, A. Sabo , *Construction of a test bench for bicycle rim and disc brakes*, 8th Conference of the International Sports Engineering Association (ISEA), Procedia Engineering 2 (2010), pp. 2943–2948.
- [57] A. Caya, Y. Champoux, J. M. Drouet, *Dynamic behaviour and measurement accuracy of a bicycle brake hood force transducer*, 9th Conference of the International Sports Engineering Association (ISEA), Procedia Engineering 34 ( 2012 ), pp. 526 – 531.

### **Safety Standard**

- [58] EN 14781, *Racing bicycles – Safety requirements and test methods*.



## List of publications

The following is a list of publications arising from this research:

- F. Giubilato, N. Petrone, V. Franch, *Engineering evaluation of "reactivity" of racing bicycle wheels*, The 10th Conference of the International Sports Engineering Association (ISEA 2014), Sheffield UK.
- F. Giubilato, N. Petrone, V. Franch, *A method for the quantitative correlation between quality requirements and product characteristics of sport equipment*, the 6th Asia-Pacific Congress on Sports Technology (APCST), 2013, Hong Kong
- N. Petrone, F. Giubilato, *Development of a test method for the comparative analysis of bicycle saddle vibration transmissibility*, the 6th Asia-Pacific Congress on Sports Technology (APCST), 2013, Hong Kong
- N. Petrone, F. Giubilato, *Comparative analysis of wheels vibration transmissibility after full bicycle laboratory tests*, AIAS 2011
- N. Petrone, F. Giubilato, *Methods for evaluating the radial structural behaviour of racing bicycle wheels*, The 5th Asia Pacific Congress on Sports Technology (2011)



## Acknowledgements

The first acknowledgement for my research work goes to Professor Nicola Petrone, my supervisor, for his valuable suggestions and contributions, his on-going support and his much appreciated availability.

I acknowledge the company Campagnolo s.r.l. for the financial and technical support of my research work, especially the Engineer Valentino Franch, my supervisor at Campagnolo s.r.l., for his assistance with my work and his valuable technical contribution. A grateful thanks goes to the employees of the test department of the company for their availability and much appreciated inputs and suggestions.

I also wish to extend a big thanks to the colleagues of the laboratory of machine design of the University of Padova for their much-valued technical support and their availability.

Special thanks must be given to the 33 testers who took part in the subjective evaluation tests and the two testers who took part in the road downhill field tests. Their valuable contribution has been very important for my work.

I warmly thank my family who accompanied and supported me in this project, for their support and for the confidence they have always had in me.

A special and big thanks goes to Marta for her constant support, patience and tolerance especially during the drafting of this work and in the days of hardest work.

I thank Barbara for the language review of this thesis and my sister for the final support to the review.

No pain no gain!

Federico



